Tactile Based Active Perception of Structural Members in Truss Structures

by Lili Bykerk

Thesis submitted in fulfilment of the requirements for the degree of

Doctor of Philosophy

under the supervision of Distinguished Professor Dikai Liu and Professor Kenneth Waldron

University of Technology Sydney
Faculty of Engineering and Information Technology

March 2020

Certificate of Original Authorship

I, Lili Bykerk, declare that this thesis is submitted in fulfilment of the requirements for the award of Doctor of Philosophy in the School of Mechanical and Mechatronic Engineering, Faculty of Engineering and Information Technology at the University of Technology Sydney.

This thesis is wholly my own work unless otherwise referenced or acknowledged. In addition, I certify that all information sources and literature used are indicated in the thesis.

This document has not been submitted for qualifications at any other academic institution.

Production Note:
Signature: Signature removed prior to publication.

Date: 21/02/2020

Tactile Based Active Perception of Structural Members in Truss Structures

by

Lili Bykerk

A thesis submitted in partial fulfilment of the requirements for the
degree of Doctor of Philosophy

Abstract

Complex Three-Dimensional (3D) truss structures such as power transmission towers require regular inspection and maintenance during their service life. Developing a robot to climb and explore such complex structures is challenging. Changing lighting conditions can render vision sensors unreliable; therefore, the robot should be endowed with a complementary sensory modality such as touch for accurate perception of the environment, including recognising a structural beam member and its properties of cross-sectional shape, size and the grasping Angle-of-Approach (AoA).

The research presented in this thesis addresses three questions related to grasping and touch based perception of beam members in truss structures. (1) Methods for designing adaptive grippers for grasping a wide variety of structural beam member cross-sectional shapes and sizes; (2) Sensing for data collection and methods for classifying beam member properties; and (3) Efficient methods for selecting the next best grasping action to confidently recognise a beam member.

A stiffness constrained topology optimisation design method is developed and applied in designing a soft gripper for grasping a variety of cross-sectional shapes of beam members. The gripper design is verified through both simulation and experiments. It is found that the gripper is proficient in grasping different shapes and sizes of beam members, with adequate contact points.

A comparative study of commonly used machine learning classifiers is conducted to analyse the effectiveness of recognising a structural beam member and its properties. Using data collected during grasping with a soft gripper, the cross-sectional shape, size and grasping AoA of a beam member are classified. Evaluation of the various classifiers revealed that a Random Forest (RF) classifier with 100 trees achieved high classification accuracies, with short training and classification times.

An information-based method for selecting the next best grasping AoA to confidently recognise a beam member is developed. This method is verified through simulation using grasping data collected with a soft gripper. The results show that this method can correctly recognise a structural beam member and its properties, typically with fewer than four grasping actions. This method can be generally used with many different gripper designs and sensor arrangements.

Acknowledgements

First and foremost, I would like to thank my supervisor Professor Dikai Liu for his support during the past four years. Thank you for giving me direction throughout this journey, and for giving me the opportunity to pursue a research degree before the TEPCO project was secured. I appreciate the independence I have had during the course of this research and I have thoroughly enjoyed having the freedom to chase after the research topics which have interested me most.

Thank you to those from the CAS TEPCO project team over the years who facilitated interesting meetings with creative inputs, particularly at the inception of the project. This creativity encouraged me to pursue my growing passion and interest in soft robotics as a research topic.

I am grateful to have had the time to enjoy so many hours playing futsal with a great group of core people from UTS in the RMSH. A special mention must go out to both Krzysztof Komsta and Leigh Monahan for their dedication with organising multiple weekly futsal games. Clocking up the hours in the sports hall has been an important part of my work-life balance while I've been studying at UTS, so I am very thankful that this once sporadic booking arrangement grew into regular weekly events. Thank you to all of those who have joined our games over the last few years. Without the right number of players, these games never would have happened.

Thanks must also go out to all my friends who have provided words of wisdom and lent their ears when I have needed it most. To my dear friend, Em, thank you for being there for me through some tough times during the course of this research degree. Your support means so much to me and I couldn't have got to the end without you. In fact, I couldn't have got to where I am today without you. I am so grateful to have you in my life. I promise that I will eventually get around to building you that robot you have been asking me about for years.

I am very lucky to have met a very important person during this research journey. To my partner, Craig, your itemised thank you list is immeasurable. Thank you for everything you have done on a daily basis to help me push forward and get to this finish line. I've

been so fortunate to be able to spend so much time with you, discussing all manner of topics. Your knowledge and wittiness has helped me to overcome many hurdles along the way; both in research and in life.

Last, but certainly not least, thank you to my family for your ongoing encouragement and support during this degree. To mum and dad, you have both been amazingly supportive. Thank you for nurturing me and fostering my passion for learning from a young age. You have both undoubtedly given me the confidence I've needed to get through to this point in life. I simply cannot thank you both enough. To my brother, Tamás, thank you for being there to talk all things PhD research with me. It's funny to think that after all these years of combined studies, we will both be doctors of engineering. Thank you for sharing many German biers, laughs and plane spotting sessions with me, it's often been just the thing I've needed at the end of a week (or day).

To my dear cousin Amy, I miss you immensely.

Contents

Appendices   185

A Grasping Simulation Results   185

B Classifier Comparison: Results   191

Bibliography   195

List of Figures

List of Tables

Acronyms & Abbreviations

2D   Two-Dimensional

3D   Three-Dimensional

ANN   Artificial Neural Network

AoA   Angle-of-Approach

AoAs   Angles-of-Approach

BN   Bayesian Network

CAS   Centre for Autonomous Systems

CAD   Computer Aided Design

CC   Constant Curvature

CCD   Charge-Coupled Device

CCW   Counterclockwise

COTS   Commercially Available Off-The-Shelf

CO$_2$ Carbon Dioxide

CPR   Cardiopulmonary Resuscitation

CW   Clockwise

DES   Dielectric Elastomer Sensor

DOF   Degrees Of Freedom

ECOC   Error-Correcting Output Codes

EGaIn   Eutectic Gallium-Indium

EP   Exploratory Procedure

e-3DP   Embedded 3D Printing

FEA   Finite Element Analysis

FSR   Force Sensitive Resistor

KLD   Kullback Leibler Divergence

k-NN   k-Nearest Neighbours

LDA   Linear Discriminant Analysis

LVDT   Linear Variable Differential Transformer

MEMS   Microelectromechanical Systems

NZ   New Zealand

OC   Optimality Criteria

OOB   Out-of-bag

PAM   Pneumatic Artificial Muscle

PCC   Piecewise Constant Curvature

PDMS   Polydimethylsiloxane

PPE   Personal Protective Equipment

PCB   Printed Circuit Board

RF   Random Forest

RVDT   Rotational Variable Differential Transformer

SA   South Australia

SIMP Solid Isotropic Material with Penalisation

SVM Support Vector Machine

TEPCO Tokyo Electric Power Company

ToMBot Tower Maintenance Robot

UK United Kingdom

USA United States of America

UTS University of Technology Sydney

WHS Workplace Health and Safety

Nomenclature

General Notations

$[\cdots]^T$	Transpose
$f(\cdots)$	A scalar valued function
$\mathbf{f}(\cdots)$	A vector valued function
$max(\cdots)$	Maximum value

Stiffness Constrained Topology Optimisation Method

$\tilde{\mathbf{x}}_{\text{stiffer}}$	The density of elements in the regions of the design domain to stiffen
$\tilde{\mathbf{x}}_{\text{rest}}$	The density of elements in the remainder of the design domain
α	A user defined stiffness multiplier
N_i	The neighbourhood of an element
x_i	An element in the design domain
x_e	The design variable
v_i	Volume of an element in the design domain
$\bar{v}$	The prescribed volume limit of the design domain
H_{ij}	A weight factor
$\mathbf{L}$	A unit length vector with all zeros at all degrees of freedom except at the output point where it is one
n	The number of elements used to discretise the design domain
$\mathbf{F}$	A vector of nodal forces
$\mathbf{U}(\tilde{\mathbf{x}})$	A vector of nodal displacements
$\mathbf{K}(\tilde{\mathbf{x}})$	Global stiffness matrix

Information-based Method

Bm	Number of beam members
N_{AoA}	Number of Angles-of-Approach (AoAs)
N_{ba}	Number of beam-angle pairs
N_g	Number of grasps performed for data collection
N_{grasps}	Number of grasps executed for beam member identification
β	Angle shift increments
F	Force Sensitive Resistor (FSR) data
I_a	Information for a candidate Angle-of-Approach (AoA)
N_{FSR}	Number of individual FSR sensors
N_{enc}	Number of encoder readings
n	Number of predicted beam member AoAs after a haptic glance
μ_i	Average of FSR data for a given sensor number and AoA
σ_i^2	Variance of FSR data for a given sensor number and AoA
τ	Threshold value above which to count the Random Forest (RF) classifier votes as valid

Glossary of Terms

Autonomous	Without human intervention.
Compliance Match	The principle that contacting materials should share similar mechanical rigidity in order to evenly distribute internal load and minimise interfacial stress concentrations.
Effector	An organ or cell that acts in response to a stimulus.
Extensor Digitorum Communis	A muscle of the posterior forearm present in humans and other animals. It extends the medial four digits of the hand.
Exteroception	By which one perceives the outside world.
Haptic Glance	A brief, spatially constrained contact that involves little or no movement of the fingers.
Haptic Perception	The ability to identify something by active exploration of surfaces by a moving subject.
Interphalangeal Joint	Hinge joints between the phalanges of the fingers that provide flexion towards the palm of the hand.
Metacarpophalangeal Joint	Hinge joints between the metacarpal bones and the proximal phalanges of the digits.
Modulus of Elasticity	A quantity that measures an object or substance's resistance to being deformed elastically when a stress is applied to it.

Papillae | A small rounded protuberance on a part or organ of the body. Associated with nerve endings, they are able to relay sensory information.

Phalanges | Finger or toe bones.

Proprioception | The ability to sense the position, location, orientation and movement of the body and its parts.

Tactile Pattern | A distribution of tactile sensor readings collected during grasping.

Chapter 1

Introduction

Since the inception of the field of robotics, it has been envisaged that robots would be used to complete jobs that fell within the categories of the three D's of robotisation: *dirty*, *dangerous* and *dull*. A recent prediction [1] suggests that it is only a matter of time before a fourth 'D' will be added, with robots also starting to take over *dear* (expensive) jobs. The concept of robotic workforces and artificial intelligence is often despised, with people feeling threatened by the "robot uprising" when it directly impacts their job security. Many people would prefer working **with** robots, instead of robots working **in place of** them [2].

When considering the robotic workforce, it is often neglected that these "new workers" might be able to fill a void that cannot currently be filled by human workers. In certain industries, there is a lack of workforce, resources or funding to keep up with high demand. One such example is in the inspection and maintenance of complex steel structures such as bridges, ship hulls, radio and power transmission towers. These jobs fall within the categories of *dirty*, *dangerous* and *dull* and are ideal for robotic substitutes (or collaborative platforms) to be developed. However, one redeeming feature preventing robots from completely taking over is that humans are very proficient in completing these jobs, since they have the manoeuvrability in their limbs to gain access to hard to reach or confined spaces. Humans also have the advantages of incredible hand dexterity, perception and

decision making capabilities which allow them to seamlessly climb complex structures and perform a variety of inspection and maintenance tasks.

There are many different types of climbing robots which have been developed over the years to climb walls or vertical surfaces [3–12], vertical poles [13–16], trees [17] or complex Three-Dimensional (3D) man-made structures [18–22]. A majority of these systems have been designed for very specific applications; mostly for accessing places which cannot physically be reached by humans or where human access is too costly or dangerous [23].

Developing a robotic platform which matches the capabilities of humans in these jobs is challenging, especially when considering the dexterity of the human hand and the need for controlled tool manipulation in maintenance operations. The robot's ability to complete the tasks of climbing, inspection and maintenance is directly linked to its perception of the environment. For a robot to successfully plan and execute the next action in its climbing process during inspection, or to manoeuvre to the next location for maintenance operations, it must have a good understanding of its current location and surroundings in the structure.

This thesis focuses on the application environment of truss structures, with a focus towards power transmission towers. The motivation behind this work stems from a research project partially funded by Tokyo Electric Power Company (TEPCO) to develop climbing robots for the inspection and maintenance of power transmission towers (Tower Maintenance Robot (ToMBot)). Using a climbing robot in this application environment will reduce or entirely eliminate the multitude of safety concerns for humans who currently work at heights and near live high voltage power lines. The goal of the overall robot development is ultimately to reduce the risk to human operators, but also to eventually reduce the inspection and maintenance time, as well as assisting with the backlog of scheduled jobs as the demand for inspection and maintenance increases.

Outdoor environments bring about many challenges in vision sensing, due to constantly changing illumination conditions which can either help or hinder the robots operation. For the robot to have a confident perception of its environmental surroundings, it can be extremely useful for the robot to utilise the sense of touch, either as a standalone or complementary sensory modality.

To date, climbing robots for truss structures have been designed for the simple scenarios where all structural beam members are of consistent cross-sectional shape and size. Consequently, the design of their grippers has concentrated on achieving the strength required to support the full weight of a robot during climbing. Due to the homogeneous structural beam members in the application environment, these grippers have no need to consider adaptiveness or compliancy in design, as these features limit the grasping strength. Furthermore, due to the uniformity of the structures, the grippers do not require sensing to determine features of the environment such as the beam member shapes or sizes.

In reality, assuming that a truss structure is constructed from uniform beam members is invalid. Many truss structures—such as power transmission towers—are composed of structural beam members with varying cross-sectional shapes and sizes. Grippers designed for climbing robots in recent literature are not capable of adapting to this wide range of structural beam members; however, grippers designed for the manipulation of household objects may meet this requirement. In the truss structure environment, adaptability is a necessity, both for reliable grasping and data collection to be performed. Methods for distinguishing between objects of similar cross-sectional shapes using touch have not been explored well in recent literature. Researchers have either focussed on achieving such tasks with vision systems or have looked to the touch based identification and recognition of (usually uniquely shaped) household objects instead. From an application environment standpoint, it is critical that a gripper can be designed to adapt to various beam member shapes and sizes to achieve sufficient points of contact.

This thesis presents methods developed to facilitate tactile based active perception of structural beam members in truss structures. In this research, three research questions are addressed. Sections 1.1 and 1.2 present the motivations for the research and the research questions. Section 1.3 outlines the proposed approaches to the research questions, including any assumptions made. Section 1.4 outlines the contributions made in this thesis. Section 1.5 lists the publications resulting from this research. The final section in this chapter provides a succinct outline of the remainder of the thesis.

1.1 Background and Motivation

Steel truss structures such as power transmission towers require inspection and maintenance at regular intervals during the lifetime of the structure to maintain safe operation. This background study delves into the specific application environment of power transmission towers; structures which are present across the globe in enormous numbers. However, many of the issues motivating this research generalise to other steel truss structures comprised of beam members with varying cross-sectional shapes and sizes, such as radio towers, water towers and bridges, amongst others.

1.1.1 Motivating Factors

There are several key factors that motivate the development of a robotic system for the inspection and maintenance of power transmission towers. Broadly, they can be categorised into three main topics: (1) Scale of required work, (2) Constraints preventing ongoing inspection and maintenance and (3) Safety issues surrounding this work.

1.1.1.1 Scale

In Australia, there are just over 50 000 km of transmission lines [24], with 6 500 km of transmission lines and 13 000 transmission towers in Victoria alone [25]. By comparison, in Japan, there are about 125 000 km of transmission lines, 28 000 km of which is supported by 50 369 power transmission towers maintained by TEPCO [26]. The national grid of New Zealand (NZ) has a total of about 25 000 transmission towers on the network [27], and in the United States of America (USA), there are hundreds of thousands of transmission towers, operated by more than 3 200 electrical utilities [28].

Considering that many power transmission towers were installed in Australia in the 1960s and 1970s, with a standard expected life of about 55 years [29], a significant influx of inspection and maintenance is forecast for the near future to ensure continued safe operation of assets in the transmission grid. Worldwide, it is difficult to quantify the sheer number

TABLE 1.1: Transpower NZ unpainted tower life expectancy. Source: [27]

Corrosion Zone	Typical Exterior Environment	Life Expectancy (Years)
Extreme	Geothermal/exposed	18
Very Severe	Sea-shore (surf)	25
Severe	Sea-shore (calm)	44
Moderate	Sheltered/coastal with low salinity	62
Low	Arid/rural/inland	86
Benign	Dry, rural/remote from coast	120

of transmission towers and the required maintenance scheduling to ensure continued safe operation.

Since the main cause of the deterioration of steel truss structures is corrosion, the maintenance scheduling is further complicated by the location of the structures. Prolonged exposure to harsh environments such as coastal and heavy industrial regions can expedite the degradation of the structures — see Table 1.1. One major concern in tower maintenance is that once the corrosion of a galvanised transmission tower begins, it advances exponentially. For example, a tower with less than 5% rust at age thirty can oxidise to the point of failure within ten years. As the corrosion of the tower accelerates, so too can the time, labour and material costs to repair it [28]. If these towers are not inspected and maintained to regular scheduling, the results can be disastrous.

1.1.1.2 Constraints

Factors such as lack of available funding or personnel, weather conditions and the extent of required maintenance can create challenges for ongoing scheduling of inspection and maintenance works.

Often, financial allocation is the major constraint for the scheduling of tower maintenance. Considering the increasing cost of preparing and painting a tower as it deteriorates, the optimal solution would be to conduct repairs as early as possible in the early phase of corrosion, when it is less costly. However, due to budget constraints, this is often not possible for many companies. Instead, the most effective way to minimise maintenance

expenditures is to repair towers which are closest to transitioning from one stage of corrosion to the next. In the short term, this approach can save several thousands of dollars per repair, but also allows companies to plan ongoing repairs in the most efficient and systematic way possible [28].

It is vital that thorough tower inspections are conducted, to ensure that the correct number of workers can be allocated to maintenance tasks, to keep on track with the maintenance schedule. Depending on the tower condition, cleaning (paint and rust removal) is often required prior to painting. Current methods of cleaning involve workers using either an angle grinder brush or abrasive blaster (see Figure 1.1a). The poorer the tower condition, the more aggressive and time consuming the cleaning methods need to be to ensure the structural members are suitably prepared for painting.

After cleaning the tower and once the structure is dry, the freshly cleaned areas will be primed and painted. To achieve the best coverage of paint, workers typically use paint tins and thick paint brushes (see Figure 1.1b) or giant mitts [28] which are hoisted up from the base of the tower. Between three and four painters can paint a 345 kV tower in about 5 hours and often, up to two towers can be single coated in a day [28].

Factors such as a lack of resources or personnel create challenges for ongoing maintenance scheduling. For example, Transpower NZ's tower painting schedule was constrained by financial allocation until 2005, after which time the schedule became constrained by resource availability—specifically the number of available certified painters [27]. Between 2005 and 2013, the number of towers painted was significantly lower than the scheduled number, resulting in towers being painted later than ideal, with increased lifecycle costs.

Delays due to natural causes such as poor weather conditions can also hinder the progress of tower maintenance. In 2012, workers from one particular maintenance company in the United Kingdom (UK) were struggling to catch up with vital maintenance work after a particularly wet year delayed their work schedule [32].

If these constraints are not considered and managed appropriately, catastrophic failures can result, as was brought to light in the supercell storms and cyclonic winds in South Australia (SA) in 2016 [33, 34]. Twenty-two transmission towers were ripped out of the

(A)

(B)

FIGURE 1.1: Maintenance workers on power transmission towers performing: (A) Abrasive blasting. Source [30], (B) Painting. Source: [31].

(A)

(B)

FIGURE 1.2: Transmission tower failures in SA during storms in 2016: (A) Tower ripped out of the ground due to foundation degradation [33], (B) Tower failed due to bending of corroded beam members [34].

ground (Figure 1.2a) and others failed due to bending of structural members (Figure 1.2b), bringing down three major transmission lines and causing an automatic shutdown of the system. ElectraNet was first warned in 2005 of the risk that 43 of its towers were prone to collapse in windy conditions because of corrosion and degradation of their foundations.

1.1.1.3   Human Safety Issues

The transmission lines of power transmission towers must remain live while inspection and maintenance works are completed, otherwise there may be significant disruption of the power supply and power outages may occur further down the transmission line. Depending on the transmission voltage of a particular tower (which usually ranges from 66 kV to 500 kV), workers must keep a safe operating boundary from the live wires; with increasing voltage, the safe boundary increases in size. Areas of the towers which are encompassed by the safe operating boundaries must be scheduled for maintenance when the transmission lines are out of service and the towers have been de-energised.

Inspection and maintenance of a single tower proves to be very time consuming, costly and dangerous for the workers and they are usually required to be fully trained [28] in:

- High voltage electrical safety
- Certified tower climbing
- Tower safety and aerial rescue
- Fall protection
- Cardiopulmonary Resuscitation (CPR)

- First aid
- Workplace Health and Safety (WHS)
- Hazard identification
- Safe work habits and climbing practices
- Emergency rescue

1.1.2   Robotic Solutions

Robots have already been considered for the **inspection** of power transmission towers, with human controlled or autonomous drones emerging as viable solutions [35, 36]. Drones have several advantages over humans climbing the structures; most notably, they are safer, faster, cheaper, more thorough (taking high definition photos for condition reporting) and are not limited by the weather conditions (with the exception of high winds and precipitation). The use of drones can lead to more frequent inspection of the structures and closer monitoring of deterioration and structural issues. One of the current main limitations of drones is their limited battery life, resulting in the need for efficient inspection paths to maximise tower coverage and minimise flight time [37]. Additionally, the risk of crashing, especially due to strong electromagnetic fields prevents drones from flying inside

the tower structure to collect data. A recent development in the area of collision tolerant drones [38] may however prove promising for a future solution.

Other methods of inspection exist, which include the use of full-sized helicopters with workers suspended during flight for close examination of power lines, connections and other equipment. This technique is not typically used for transmission tower structural inspection, but rather power line inspection. Robotic power line inspection solutions have also been recently developed [39–41].

It is currently impossible for these airborne inspection methods to also be viable for **maintenance** procedures. The required cleaning equipment can be a bulky payload for drones and the required proximity to structural beam members for cleaning and painting also rules out the prospect of maintenance from helicopters.

Considering the work that human workers currently complete, any robotic platform designed for this application environment needs to have many complex elements to achieve sufficient work outputs. The multifaceted nature of the inspection and maintenance procedures creates a significant challenge for a robotic platform. The robot must excel in many areas, requiring:

- Adequate sensing platforms for climbing and structural condition assessment (such as analysis of rust and paint thickness),

- Payload capabilities for cleaning and painting tools,

- Intelligent sensing, perception, planning and control algorithms to execute cleaning procedures and to ensure that freshly painted surfaces are not interacted with (i.e. climbed on), and

- A safety harness for tethering the robot to the tower—which complicates the path planning—to ensure that the robot does not become tangled within the structure.

The need for intelligent climbing robots for the inspection and maintenance of power transmission towers has been identified by TEPCO and this thesis forms part of the ongoing project to create an intelligent climbing robot for truss structures, such as power

transmission towers. This project aims to eliminate many of the issues surrounding the scale of required maintenance, resource management, scheduling and the safety issues posed to human workers who currently complete the inspection and maintenance works. The robot must be capable of climbing complex truss structures, performing a condition assessment, mapping the environment and planning a path for cleaning and painting. The robot design must cater for a number of climbing and grasping scenarios as the robot manoeuvres through the tower. The specific research topics discussed in this thesis are motivated by the need for suitable robotic grasping mechanisms incorporating sensing and active perception capabilities.

There are many complex elements of truss structures which make climbing complicated, even for highly trained human inspection and maintenance workers. One major challenge is the ability to reliably grasp the structural beam members during climbing. Truss structures can have great variation in beam member sizes and orientations. However, beam members are typically of similar cross-sectional shapes, especially from particular grasping Angles-of-Approach (AoAs) e.g. "T", "L", "I". During climbing, humans are required to constantly use touch in both their upper and lower extremities along with vision and hearing to safely and efficiently navigate throughout the structure.

A climbing robot will also require similar methods of environmental awareness and localisation. Climbing outdoor structures has challenges, however, as the use of vision sensors might not always be viable due to occlusions, poor illumination conditions, excessive reflection or shadowing. In these situations, the robot may have to rely on the use of other sensory modalities such as touch for the recognition of structural beam members and localising itself within the structure. Thus, it is expected that the grippers can adapt to the various shapes and sizes of beam members at any given Angle-of-Approach (AoA) for reliable grasping. The robot's grippers should also incorporate adequate sensing capabilities for data collection during climbing. For practicality when relying on touch sensing, the robot should not exhaustively explore the environment without a strategy. Efficient and intelligent actions should be planned and executed so as to not compromise the climbing efficiency.

1.2 Research Questions

Existing research into the development of robots for climbing in complex 3D truss structures has focussed on structures composed of beam members with consistent cross-sectional shape and size (typically round or box sections). Considering this structural consistency, climbing robot grippers have been designed to perform high strength, repeatable and reliable grasps on fixed cross-sectional shapes, with no compliancy or adaptability in the grasping mechanism. In reality, truss structures can be comprised of a range of cross-sectional shapes and sizes of structural beam members. Therefore, a gripper designed for a robot to climb truss structures is required to have design features of adaptability and compliancy, as well as suitable sensory capabilities to recognise a beam member and its properties during grasping.

Adaptive and compliant gripper designs are becoming of broad and current interest, with the emergence of soft robotics and advanced additive manufacturing fabrication methods. Adaptive and compliant grippers typically lack grasping strength and are designed for grasping highly irregular cross-sectional shapes which are commonly present in household environments. Due to the contradiction of strength and compliancy, designing an adaptive gripper for climbing robots must find a suitable compromise to be able to adapt to varying cross-sectional shapes and sizes of structural beam members with suitable grasping strength. An opportunity then arises for a hybrid design of a rigid exoskeleton with soft, adaptive surfaces to achieve the desired grasping capabilities.

Collecting useful and reliable data from sensors embedded within or retrofitted to soft grippers has its challenges. Compliancy can cause changes to gripper morphology during interaction with structural beam members which can, in turn, affect sensor readings. With rigid grippers, information about a structural beam member being grasped can be easily obtained by combining finger joint angles and tactile sensor readings with the gripper kinematics. With soft grippers, however, accurate kinematic models can be difficult to obtain and sensors are less reliable in measuring the motion of the soft structures, resulting in uncertain representations of the structural beam member being grasped. A suitable method to translate raw sensor data (obtained during grasping with a soft gripper) to structural

beam member properties is therefore required. To date, similar problems have been addressed through the use of machine learning methods, although the target object sets have typically been comprised of uniquely shaped objects, allowing for accurate classifications with a single grasping action.

Considering the task of climbing within truss structures, executing a series of complex exploratory motions to gain a perception of the immediate surroundings is impractical. Desired features and properties of the environment can be extracted by using the most efficient method of haptic exploration (a *haptic glance*). This method of exploration is desirable for climbing in a complex truss structure, performing data collection and beam member recognition simultaneously.

Ideally, a simple strategy to minimise the number of *haptic glances* and maximise the amount of information extracted would be developed. Similarities in the structural beam members and their properties (cross-sectional shape and size), however, increases the difficulty of the problem and beam members may be erroneously recognised if only a single *haptic glance* is executed. Therefore, further *haptic glances* at favourable locations are required in order to correctly recognise the beam member and its properties. Strategic selection of the next best grasping action is an important question to address.

Considering the limitations in the current research of grasping and touch based perception of truss structures, three main research questions arise: (1) How can methods for designing adaptive grippers for grasping a wide variety of structural beam member cross-sectional shapes and sizes be developed and implemented? (2) What sensing and classification methods are suited to the problem of recognising a beam member and its properties? and (3) How can efficient methods for selecting the next best grasping action to confidently recognise a beam member be produced?

1.3   Scope

This thesis aims at addressing three questions:

1) Methods for designing adaptive grippers for grasping a wide variety of structural beam member cross-sectional shapes and sizes,

2) Sensing for fast data collection and methods for classifying beam member properties such as cross-sectional shape, size, and grasping AoA, and

3) Efficient methods for selecting the next best grasping action to confidently recognise a beam member.

First, a stiffness constrained topology optimisation method is developed for the design of an adaptive, compliant gripper. A gripper designed using this method is developed and tested in both simulation and experiments. During experiments, grasping data was collected for the research in this thesis. Incorporation of this soft gripper design with a rigid exoskeleton mechanism to provide the grasping strength for a climbing robot gripper falls out of the scope of this research.

Next, machine learning algorithms are used for classifying a structural beam member's cross-sectional shape, size and grasping AoA, using a classification model trained with raw sensor data. A number of commonly used classifiers are evaluated for the application of tactile based active perception of structural members.

Finally, an information-based method for selecting the next best grasping AoA to confidently recognise a structural beam member and its properties is developed. This method uses a database of sensor data collected during grasping at various discrete AoAs to a variety of structural beam members of similar cross-sectional shape and size.

The research presented in this thesis makes a number of assumptions. Since the designed gripper is intended only for structural beam member recognition and not for the final application of a climbing robot system, the strength of the gripper design is beyond the scope of this thesis. In this thesis, a method for designing a soft gripper capable of grasping various cross-sectional shapes and sizes of beam members from any AoA is developed, for the purpose of beam member recognition. The AoA is assumed to lie within a Two-Dimensional (2D) plane, as the gripper is assumed to approach a structural beam member perpendicularly (co-incident with the cross-section of a beam member). This assumption is based on the premise that grasping perpendicular to the structural beam member will

provide a high surface area of grasped surfaces, with sufficient points of contact along the proximal phalanges (rather than the distal, which would result in a pinch grasp) and therefore stability in grasping. In this research, data was collected by manually positioning the gripper at a set distance from a structural beam member and at a desired AoA. It is expected that for practical applications, the robot has adequate sensors to align the gripper in such a configuration. Research into developing an active touch based recognition method assumes that a soft, compliant gripper with simple force sensors is used. However, it is envisaged that this method generalises well to other hardware setups, including gripper designs, tactile sensors and their arrangements.

1.4   Contributions

The main contributions of this thesis are:

- A stiffness constrained topology optimisation method for designing soft grippers for grasping and adapting to beam members of varying cross-sectional shapes and sizes,

- A comparative study of machine learning classifiers to analyse the effectiveness of classifying a structural beam member's shape, size and grasping AoA using grasping data collected with a soft gripper, and

- An information-based method for selecting the next best grasping AoA for recognition of beam members with similar cross-sectional shape and size. Case studies evaluating the method in a truss structure such as a power transmission tower were conducted. This method is not limited to a particular hardware set up and can generalise well to other applications where the objects being grasped are of similar shape at particular AoAs.

1.5   Publications

[1] **L. Bykerk**, D. Liu and K. Waldron, "A Topology Optimisation Based Design of a Compliant Gripper for Grasping Objects with Irregular Shapes", *2016 International Conference on Advanced Intelligent Mechatronics (AIM)*, pages 383–388, 2016.

[2] **L. Bykerk** and D. Liu, "Experimental Verification of a Completely Soft Gripper for Grasping and Classifying Beam Members in Truss Structures", *2018 International Conference on Advanced Intelligent Mechatronics (AIM)*, pages 756–761, 2018.

[3] **L. Bykerk**, P. Quin and D. Liu, "A Method for Selecting the Next Best Angle-of-Approach for Touch-Based Identification of Beam Members in Truss Structures", *IEEE Sensors*, vol. 19, no. 10, pages 3939–3949, 2019.

1.6   Thesis Outline

Chapter 2 provides a comprehensive literature review of the related state of the art work in the research topics. The review covers the topics of gripper design, the use of sensors, object identification and recognition methods and strategies for tactile based active perception.

Chapter 3 presents a stiffness constrained topology optimisation method for designing soft grippers. Verification of the method is presented; where various grippers are designed for grasping a range of cross-sectional shapes of structural beam members. A prototype gripper is manufactured and used for data collection during grasping.

Chapter 4 discusses a comparative study of machine learning classifiers conducted to analyse the effectiveness of classifying a structural beam member's shape, size and grasping AoA from a single set of grasping data. The results of this study are analysed across a number of criteria and the effectiveness of the classifiers are evaluated.

Chapter 5 presents an information-based method for selecting the next best grasping AoA for confident recognition of beam members with similar cross-sectional shape and size. Case studies of the method are also analysed.

Chapter 6 summarises the outcomes and contributions of the research in this thesis. The advantages, disadvantages and limitations of the methods are discussed. Conclusions are drawn and further research work is discussed.

Appendix A contains the results from grasping simulations discussed in Chapter 3.

Appendix B contains a summary of the classifier comparison results discussed in Chapter 4.

Chapter 2

Review of Related Work

This chapter presents a brief overview of the related work. Section 2.1 reviews gripper designs, with a focus towards underactutated and soft grippers.

Section 2.2 reviews the current state of the art sensing technology which may be utilised in the gripper design for haptic perception. There are many sensing options, depending on whether exteroceptive sensing and/or proprioceptive sensing is desired. A comparison of sensory options is discussed and sensing applications for soft grippers are reviewed.

Section 2.3 reviews exploration methods for data collection using touch alone. In many scenarios during climbing in the application environment, non-ideal lighting conditions are expected to be encountered, resulting in poor outcomes from vision sensing alone. It is therefore desirable to explore the environment using a complementary sensory modality such as touch. Humans are highly adept at haptic perception and exploration, thus in this section, methods of human haptic exploration are reviewed.

Section 2.3.2 reviews methods for object identification using the sensory modality of touch. It is highly desirable for the robot to collect information about the beam members being grasped as it navigates and climbs throughout the truss structure.

Finally, Section 2.4 provides a summary of the related work and the limitations of current state of the art approaches are identified.

2.1   Robot Grippers

In the last 50 years of robotics research and development, many different methods of grasping and manipulating objects have been explored. Depending on the target application, wide variations in gripper designs exist to meet specific requirements. This is also reflected in nature, where the anatomy of the manipulator of an animal (including its softness and adaptability) varies depending on its habitat. It is common for robotics researchers to take inspiration from nature and create bio-inspired designs as they can take advantage of very efficient designs which have been developed over long periods of environment-specific evolution.

The human hand is one of the most fascinating examples of natural engineering—it is impressive in many aspects of its "design", including the anatomy, sensing and control. As such, robotics researchers have naturally turned to the human hand for inspiration in developing robotic grippers. The versatility of the hand can be attributed to the fully opposable thumb, which makes it possible for both powerful and precise grasps to be performed.
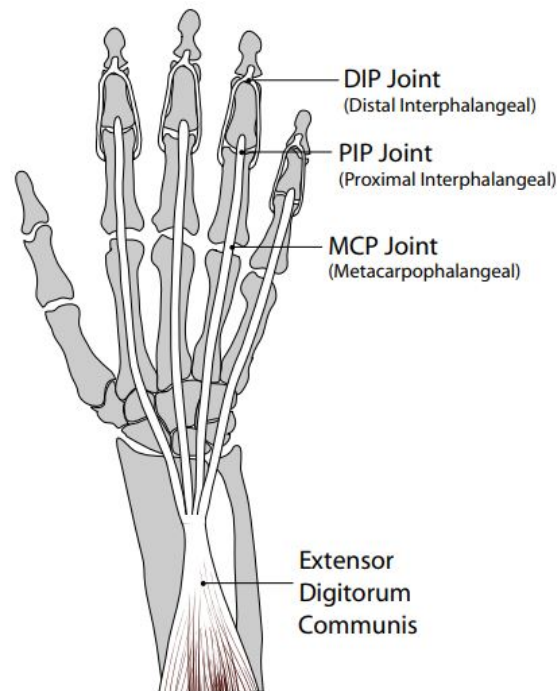
FIGURE 2.1: Bones and joints of the human hand and the Extensor Digitorum Communis.
Source: [42].

Dissection of the human hand reveals how the incredible dexterity and strength of the hand is possible. Muscles in the forearm connect to the finger bones via long tendons (*Extensor Digitorum Communis*) which pass through a flexible wrist—see Figure 2.1. This gives the fingers movement and strength that wouldn't be possible if all of the muscles were directly attached to the fingers. It is claimed that through habitual use and training, even a single finger can support the entire body weight [43]. At the other end of the spectrum is the finesse provided by the intrinsic muscles in the hand, some of which directly control the thumb and little finger and others which indirectly control subtle movements of the fingers.

Clearly, there are many desirable features of the human hand that could be practically implemented in robotic systems. Especially given that humans have a history of performing many of the jobs that robotic grippers are typically tasked with—production line pick and place, assembly, loading and unloading of industrial machine tools, amongst others.

Early work in robotics research and development focused on low compliancy, low Degrees Of Freedom (DOF) (rigid) gripper designs which are very precise in their motions and capable of exerting large forces. Most of these designs are manufactured from materials such as metals and hard plastics which have a modulus of elasticity greater than 10^9 Pa (see Figure 2.2). Due to the manufacturing materials, these designs are limited in their ability to elastically deform and adapt their shape to external constraints and obstacles [44]. Additionally, complex control strategies are required; however, due to their reliability and repeatability, these systems are still used in industrial robotics applications today.
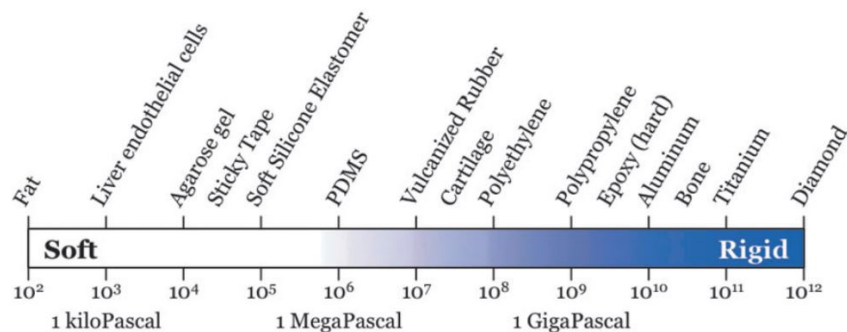
FIGURE 2.2: Young's modulus for various materials. Source: [44].

More recent robotics research has looked to bio-inspired, underactuated and soft gripper designs with almost entirely opposite features to rigid grippers. Soft robots are mostly manufactured from easily deformable materials such as silicones and polyurethanes and contain few, or no rigid components. Soft robots are designed to be able to *compliance match* with natural organisms such as skin and muscle tissue. As such, soft robots are manufactured from materials with a modulus of elasticity between 10^2 and 10^6 Pa (see Figure 2.2). Durometer (measure of softness/hardness of a material) is another important consideration when designing a soft robot. Durometer is measured by the Shore Hardness Scale as shown in Figure 2.3, with soft robots in literature mostly being manufactured from materials belonging to Shore 00 or the lower spectrum of the Shore A category.
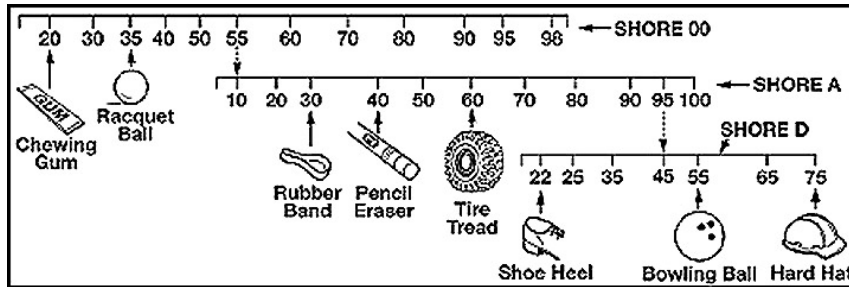
FIGURE 2.3: Shore Hardness Scale. Source: [45]

Figure 2.4 provides a summary of design features for both rigid and soft robotic grippers and how the human hand fits in relation with these two distinct designs. With both rigid (skeletal) and soft (flesh) components, the human hand is a very impressive design that reaps the benefits of both soft and rigid features. Depending on the application environment, hybrid (rigid-soft) grippers like the human hand could be highly desirable. In this section, some examples of gripper designs will be discussed, with applications in industrial robotics, climbing robots and manipulation of household objects (using underactuated or soft grippers).

2.1.1   Industrial Robot Grippers

For industrial robotics, it is vital that the robot end effector can repeatedly and reliably grasp a certain set of objects, depending on the application. Early work in industrial
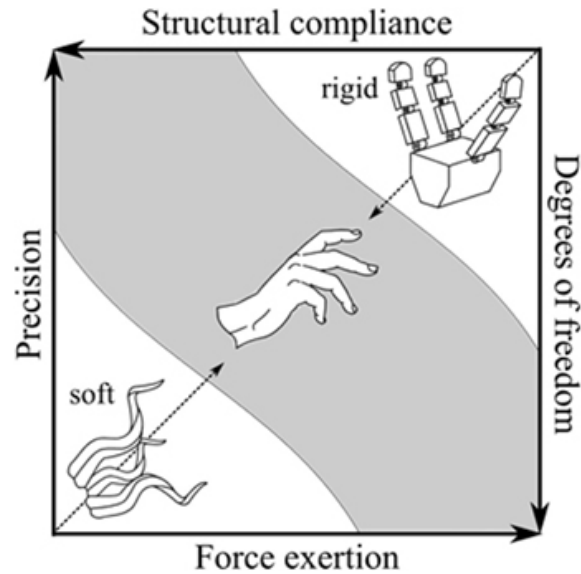
FIGURE 2.4: The position of soft and rigid manipulators in the 2D design space. Four key parameters: precision, structural compliance, DOF, and force exertion define the manipulator design. The axes only show quantitative change. Human hands lie on the diagonal line (gray coloured) of the whole design space which combines soft and hard materials. Source: [46].

robotics proposed a multitude of gripper designs, which covered a versatile range of applications and objects to be handled [47]. Nowadays, by virtue of their reliability, two types of grippers have commonly been used in industrial applications:

1) **Mechanical parallel grippers** use frictional forces between parallel plates and the target object to pick up and release objects (Figure 2.5a). They can be actuated electrically, pneumatically or hydraulically, and

2) **Vacuum grippers** use suction cups and air to hold and release objects (Figure 2.5b).

These two main grippers are suitable for grasping objects with simple geometrical shapes; however, adaptive grippers are needed for grasping irregular shaped objects. Modern industrial grippers such as the Robotiq Adaptive 2 (Figure 2.5c) and 3 fingered (Figure 2.5d) grippers are capable of grasping a wider variety of target objects, often by executing different grasping modes (such as enveloping or pinching). Depending on the gripper design and grasping mode, the payload capability ranges from 2.5 kg to 10 kg.

(A)   (B)   (C)   (D)

(E)   (F)
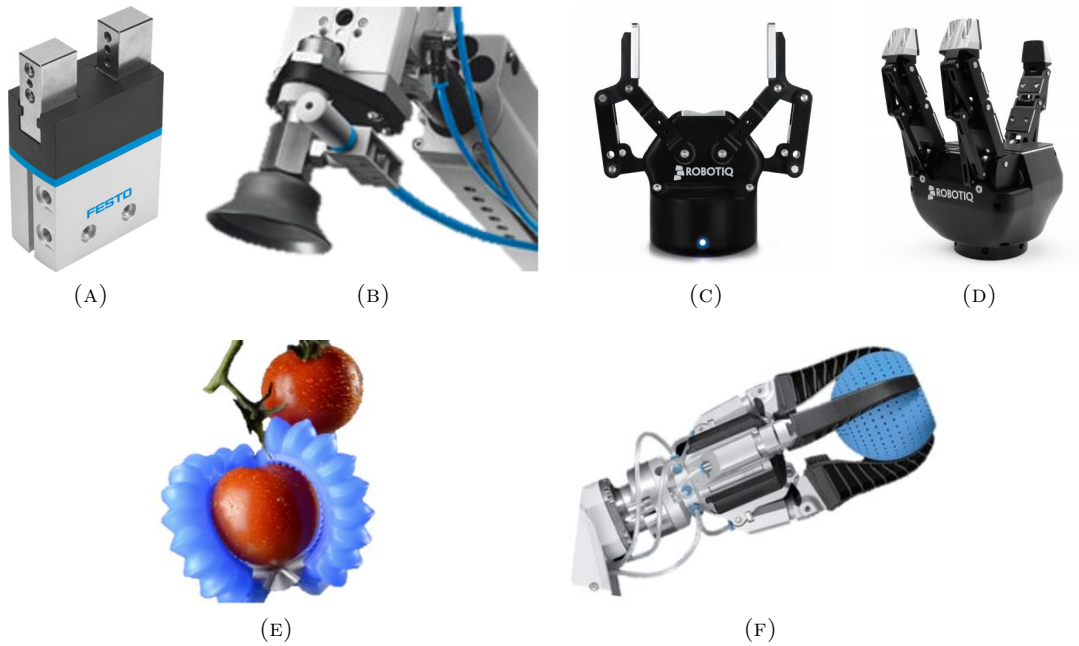
FIGURE 2.5: Various industrial robot grippers: (A) Festo parallel gripper [48], (B) Festo vacuum gripper [49], (C) Robotiq 2 fingered gripper [50], (D) Robotiq 3 fingered gripper [50], (E) Soft Robotics Inc. gripper [51], (F) Festo Fingripper [52].

Soft and compliant industrial robot grippers (Figure 2.5e and Figure 2.5f) have also recently been developed for grasping (often delicate and lightweight) objects with greatly varying geometrical shape and size on production lines. Another form of vacuum gripper which has the features of adaptability and compliancy applies the principle of granular jamming [53]. These grippers consist of an outer membrane which is filled with a gritty substance. The grasping procedure for this type of gripper is outlined in Figure 2.6.

gripper approaches   gripper deforms   air is evacuated   object can be
   in soft state   around object   from gripper   manipulated
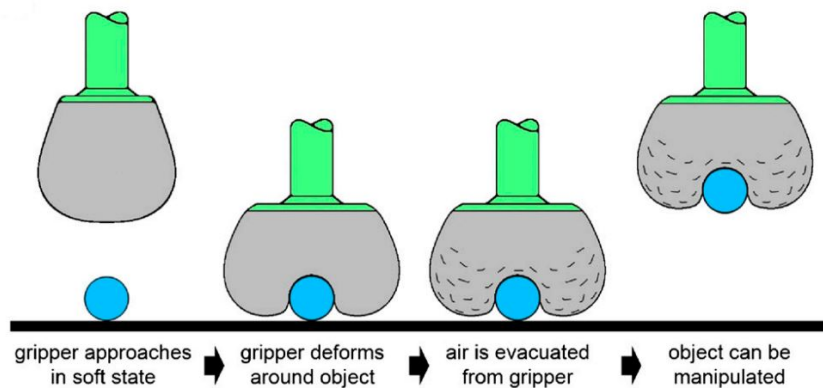
FIGURE 2.6: Operational procedure of a granular jamming gripper. Source: [53].

These grippers are effective solutions for grasping and manipulating objects on production lines, mostly for pick and place applications. These gripper designs, however, would not be viable for a climbing robot application due to their payload capabilities.

2.1.2 Climbing Robot Grippers

Robots developed to climb man made structures such as truss structures or bridges have commonly used mechanical adhesion in the form of parallel grippers (similar in design to industrial parallel grippers), magnetic adhesion or vacuum suction to adhere to the target surface. For brevity, this subsection reviews only the mechanical forms of adhesion, since this has been identified as the most feasible option for climbing in a truss structure.

The required grasping strength of a climbing robot gripper is determined by the size and mass of the climbing robot and its payload. For a climbing robot to be practically deployable for inspection and maintenance, the grasping strength needs to be large enough to support the full weight of the robot (including the factor of safety) and consider any reaction forces due to maintenance operations.

TABLE 2.1: Climbing robot grippers and their target grasping objects.

Climbing Robot	Target Object Shape	Target Object Dimensions (mm)
Climbot [13]	Circular or cylindrical	ø50-110
Pole-like Tree Climbing Robot [14]	Cylindrical	ø100
Electrical Pole Climbing Robot [15]	Cylindrical	ø100-140
RiSE V3[1] [16]	Cylindrical	ø250
Treebot[2] [17]	Cylindrical	ø64-452
ROMA I [18]	Square	Unknown
Shady3D [19]	Square	19x19
Raupi [20]	Cylindrical	Unknown
3DCLIMBER [21]	Cylindrical	ø200-350

Robots designed for climbing in truss structure environments composed of beam sections most commonly employ parallel gripper designs. Depending on the target beam cross-sectional shape and size, parallel grippers for climbing robots are configured in a specific fixed shape designed for safe and secure grasping, using either power or precision (pinch)

---

[1]Designed for climbing wooden telephone poles, the robot uses sharp claws that penetrate the wood.
[2]Designed for climbing trees, the robot uses claws that penetrate into the gripping substrate, even if it has an irregular shape.

grasps [54]. These grippers are usually controlled by a single actuator to open and close the fingers. These grippers could be applied to the research work in this thesis; however, the main limitation of these grippers in the practical application environment is their lack of compliancy. This design feature limits their usability to grasping only a specific type and size of target object (see Table 2.1 for a summary of recent climbing robot gripper designs and their target object shapes and sizes). In general, with these gripper designs, it is assumed that the robotic system is able to accurately align its end effectors with the target beam members to prevent large torques from being generated on the arm of the robot during a poorly aligned grasp.

Due to its "V" shape (with self-centering properties), the gripper in Figure 2.7g has the advantage that the grippers do not have to be accurately positioned before a grasp can take place. Similarly, the gripper in Figure 2.7e is somewhat compliant and robust to misalignment and tilt in the approaching angle to the target beam members. Partial compliance is achieved mechanically, through sloped edges on the inner sections of the gripper housing, which provide a means for guiding and locating the gripper as it envelops the beam members.

Little research has been conducted in the design of robotic grippers for climbing truss structures with target beam members of varying cross-sectional shapes and sizes. Designing a gripper for this environment brings about many challenges, as the gripper needs to be adaptive and compliant to accommodate the various target beam members, but also strong and reliable for supporting the weight of a climbing robot during inspection and maintenance procedures.

2.1.3   Underactuated Grippers for Manipulation of Household Objects

Underactuation in robotics refers to having fewer actuators than DOF. Applying the concept of underactuation to gripper designs results in reduced system complexity and the ability for the gripper to automatically adapt to the shape of the target object being grasped. However, depending on the configuration of the rigid links comprising the fingers (in discrete or serpentine type designs—see Figure 2.8), the gripper's adaptability to a wider range of sizes of more irregular shapes is limited. Underactuated grippers in

(A)

(B)

(C)

(D)

(E)

(F)

(G)
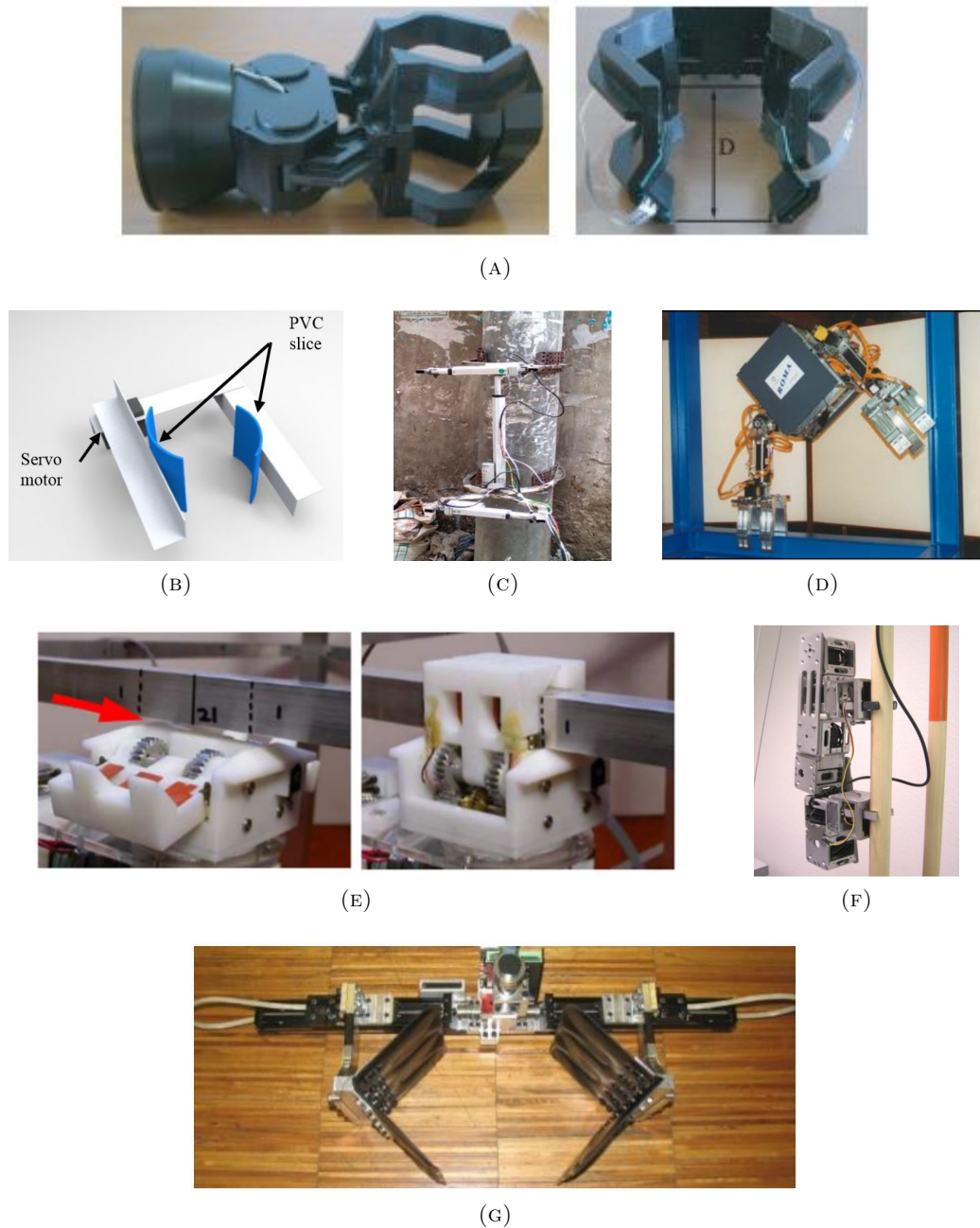
FIGURE 2.7: Various parallel climbing robot grippers: (A) Climbot [13], (B) Pole-like tree climbing robot gripper [14], (C) Electrical Pole Climbing Robot [15], (D) ROMA I [18], (E) Shady3D [19], (F) Pipe-like climbing robot "Raupi" [20], (G) 3DCLIMBER [21].

literature have typically been designed for the application of grasping a wide variety of household items. Continuum mechanism type designs are common in soft robotics and will be discussed in further detail in the following section.
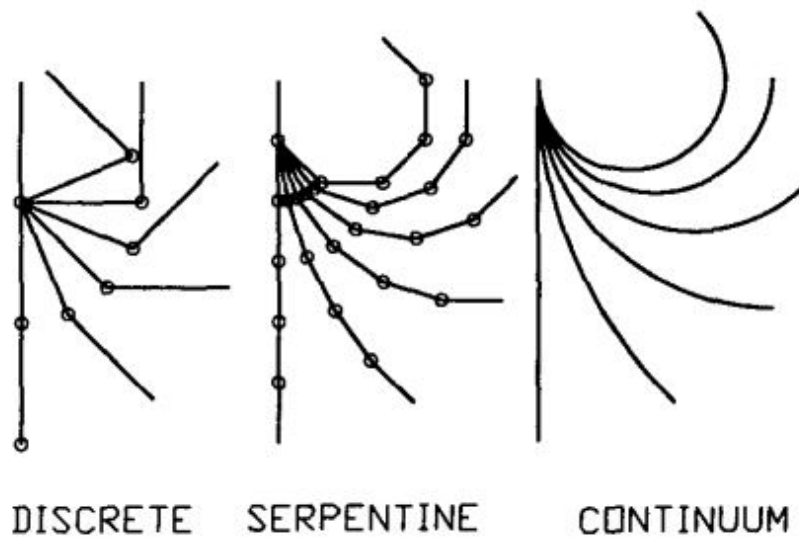
FIGURE 2.8: Robot mechanism types and their motions. Source: [55].

2.1.3.1   Rigid Underactuated Grippers

Traditional robotic grippers (parallel or vacuum grippers as discussed in Section 2.1.1) function well when grasping regular shapes, however struggle to achieve stable, reliable grasps when the object shape is irregular as they cannot obtain sufficient points of contact. Real world applications involve grasping objects of many different shapes and sizes, with uneven surfaces and irregularities. Designing a gripper to adapt to these irregularities is a great challenge, with rigid underactuated grippers arising as a possible solution.

Underactuated rigid grippers generally provide a lighter weight solution than fully actuated rigid grippers due to the use of fewer actuators. The inherent adaptiveness of the gripper design means they are also capable of grasping a wider range of target objects than parallel grippers. Comparing to fully actuated rigid grippers, underactuated grippers also have the advantage of not requiring complex control systems to grasp objects of irregular shape.

Perhaps the first documented underactuated system exhibiting passive compliance was presented in 1978 by Shigeo Hirose [56], where a multi link (serpentine type) gripper was simply actuated by a pair of wires routed through the structure via pulleys as shown by Figure 2.9. Pioneering this field of research, the development of this gripper generated further interest in underactuated grippers due to their simplicity and versatility. As a

result of this research, several smaller scale robotic grippers have been recently developed which employ the design concepts of underactuation.
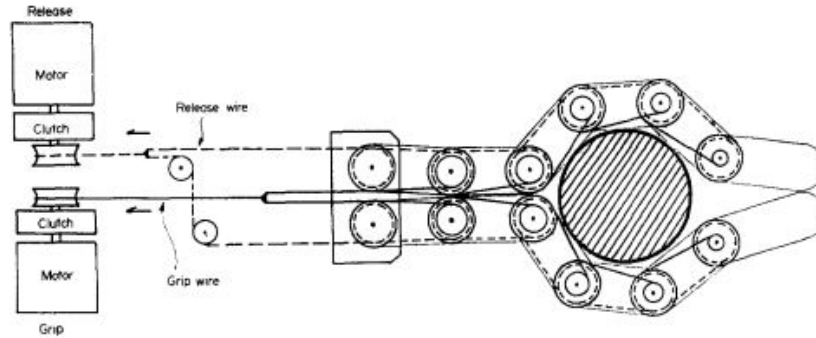
FIGURE 2.9: Mechanism of the soft gripper designed by Shigeo Hirose. Source: [56].

Many underactuated gripper designs follow a typical discrete mechanism structure (similar to the human hand), with variations possible in each of the necessary components. Table 2.2 provides a summary of recent underactuated gripper designs and their features. A range of underactuated grippers are also shown in Figure 2.10. Common designs are comprised of rigid phalanges (of either two links [proximal and distal], or three links [proximal, middle and distal]) connected in a serial chain mounted to the grippers' palm. Actuation methods typically use active tendons routed through the palm and fingers and to a drive motor via a pulley system. These grippers are generally designed for grasping and manipulating household items in different orientations and positions.

Some continuum inspired underactuated grippers such as the Flexirigid Gripper [61] have been designed. The gripper is similar in concept to other underactuated grippers and is designed for grasping cylindrical objects, but has the flexibility to grasp other shapes. The gripper design, as shown in Figure 2.11 consists of two trunks, each containing several small links fixed to an elastomer belt. The gripper is actuated by a steel wire tendon which passes through each of the links and to a wire pulley attached to a servomotor at the base. Actuating these tendons results in the fingers closing and approaching each other until the magnetic locking mechanism connects the tips of the fingers together. The elastomer belt is connected to a belt pulley attached to a servomotor, also at the base of the gripper. Driving the belt pulleys results in the object being squeezed between the gripper palm and the trunks—caging the object and securing tightly. The gripper itself weighs 2.61 kg and is capable of grasping objects of varying size and shape up to 4 kg. This type of gripper

(A)   (B)

(C)   (D)
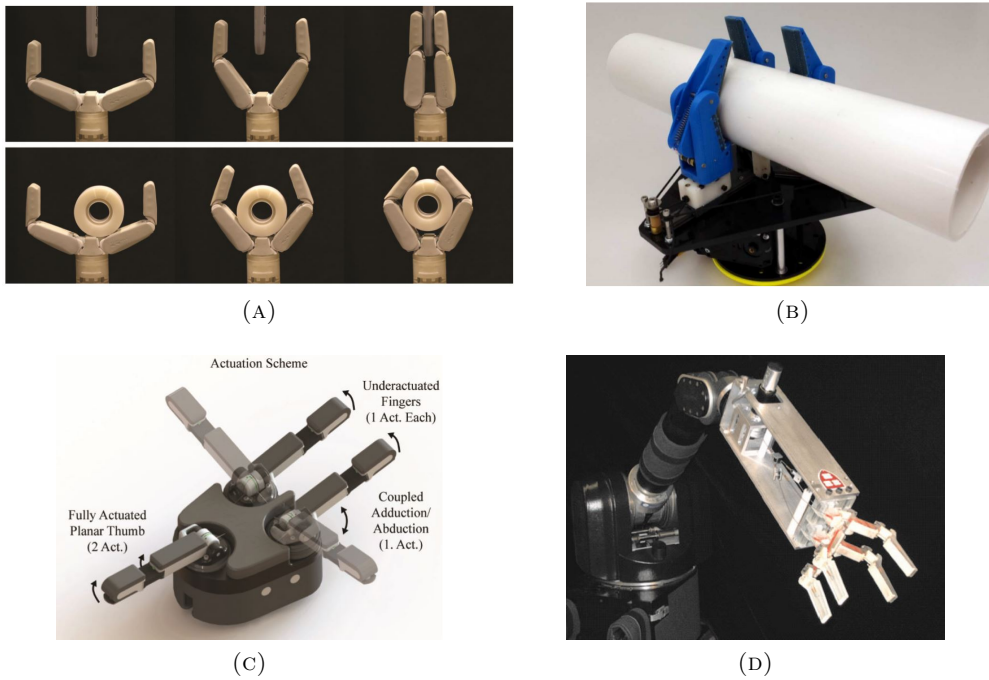
FIGURE 2.10: Various underactuated gripper designs: (A) Velo Gripper [57], (B) Model S Hand [58], (C) iHY Hand [59], (D) SDM Hand [60].
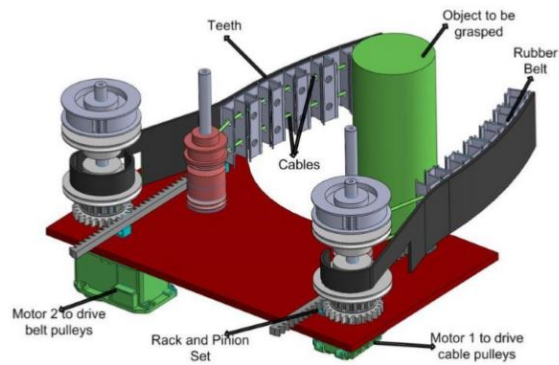
FIGURE 2.11: The Flexirigid gripper. Source: [61].

design could be considered a hybrid (rigid-soft) gripper, due to the choice of materials for its design. Its semi-continuum deformation style has features of both rigid and soft grippers.

TABLE 2.2: Various underactuated discrete mechanism gripper designs.

	Gripper Name			
	Velo Gripper [57]	Model S Hand [58]	iHY Hand [59]	SDM Hand [60]
Design Components				
Number of Phalanges	2	2	2	2
Number of Fingers	2	3	3	4
Inter-phalangeal Joints	Pin with return torsional springs	Pin	Compliant Tendon Flexure	Compliant Tendon Flexure
Metacarpo-phalangeal Joints		Pin with flexion spring	Pin with return torsional spring	Pin
Actuation Methods	Tendon driven Single actuator	Tendon driven Single actuator	5 actuators: Thumb fully actuated Remaining 2 fingers: - underactuated with single tendon each - coupled adduction/ abduction	Tendon driven Single actuator
Design Features				
Target Objects	Typical household items	Round and flat objects of varying dimensions, tools	Typical household items	Typical household items, Simple geometric extrusions
Grasping Modes	Parallel, Enveloping	Spherical, Cylindrical	Spherical Pinch/Power, Cylindrical Pinch/Power, Opposed Pinch, Lateral	Enveloping, Pinch
Special Features	-	Actuated prismatic joint in the palm with return spring for passive adaptation to the principal axis of the object	Capable of performing in-hand repositioning tasks. Able to adjust the force exerted on grasped objects.	Novel manufacturing method, gripper can reliably grasp objects spanning a wide range of shapes, sizes, positions, orientations.

2.1.3.2   Soft Underactuated Grippers

Like rigid underactuated grippers, soft grippers are ideal for conforming to object varia-
tions in size and shape due to their adaptability. Compliance is the fundamental attribute
of soft robotics that allows for adaptability and robustness when interacting with the envi-
ronment. Soft grippers take inspiration from nature and are typically manufactured from
soft, flexible and compliant materials such as silicones or polyurethanes. Soft grippers
typically do not have a limited number of DOF, as they are continuum robot mechanisms.

One advantage of soft grippers over rigid underactuated grippers is their "gentle" touch,
allowing them to grasp and manipulate delicate objects without the possibility of dam-
age. This is achieved by conforming to the object and distributing grasping forces across
the contact surface/s. This advantage, however, brings about a major disadvantage; the
payload capacity is very limited and is highly dependent on the stiffness of the chosen
soft material. Additionally, due to these features, soft grippers have an inherent lack of
repeatability and precision. Depending on the application, these grippers can be highly de-
sirable over conventional rigid grippers and have applications in areas requiring compliancy
and soft interactions. One further advantage is their low cost and simple manufacturing
procedures which take advantage of additive manufacturing methods such as 3D printing.
This can result in rapid transitions from design to prototype to the final product.

Many soft grippers presented in recent literature have focused on grasping small, household
objects which don't generally require strong grasping forces due to the physically light
weight of the objects being grasped. The focus of soft robotic gripper designs has generally
been on the compliancy and the ability for the gripper to adapt to various object shapes and
sizes. Actuation techniques vary, depending on the gripper design, with common actuation
methods including pneumatics, hydraulics, linear actuation and cable driven mechanisms.
Table 2.3 provides a summary of recent soft gripper designs and their features (also shown
in Figure 2.12).

One of the more viable soft gripper design choices uses topology optimisation and the
Optimality Criteria (OC) method [64, 70]. An initial gripper topology was obtained from
models described in literature [71] and [72]. The gripper was designed through iterative
finite element optimisation using a kinematic approach. This final topology was then

successfully simulated with a range of both convex and concave objects, then manufactured and tested with physical objects. Another similar design of topology optimised gripper is found in [73].

(A)

(B)

(C)

(D)

(E)

(F)

(G)

(H)
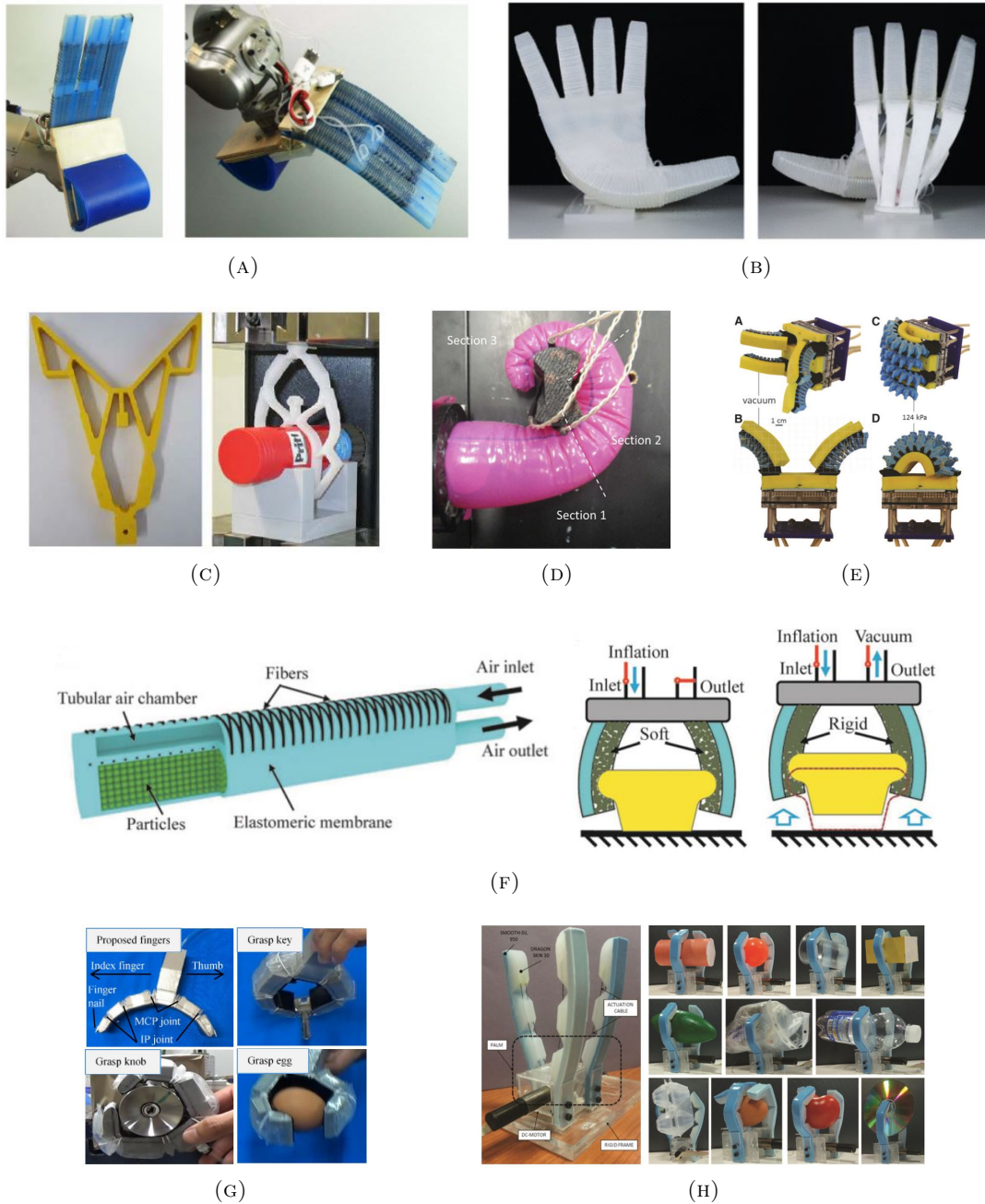
FIGURE 2.12: Various soft gripper designs: (A) RBO Hand [62], (B) RBO Hand 2 [63], (C) Passively Adaptive Compliant Gripper [64], (D) Variable Compliance Soft Gripper [65], (E) Soft Robotic Gripper for Underwater Sampling [66], (F) Variable Stiffness Gripper [67], (G) Lightweight Underactuated Pneumatic Fingers [68], (H) Bio-inspired Under-actuated Soft Gripper [69].

TABLE 2.3: Various underactuated discrete, serpentine & continuum mechanism gripper designs.

Soft Robot Gripper	Number of Fingers	Gripper Material	Actuation Method	Target Objects
RBO Hand [62]	3	Silicone (EcoFlex 50)	Pneumatic	Objects ranged from a tissue to a full water bottle
RBO Hand 2 [63]	5	Silicone	Pneumatic	Objects ranged from a rectangular plate to a lead ball
Passively Adaptive Compliant Gripper [64]	2	Silicone (Elastosil R420/70)	Linear Actuator	Convex and concave objects
Variable Compliance, Soft Gripper [65]	1	Polyurethane outer shell	Cable Driven	Square, round, irregular
Soft Robotic Gripper For Underwater Sampling [66]	4	Silicone (M4601) + memory foam	Hydraulic	Coral (irregular shapes)
Lightweight Underactuated Pneumatic Fingers [68]	2	Polyurethane foam + rubber material.	Pneumatic	Objects include a tennis ball, banana, tofu, screw and bottle.
Bio-inspired, Under-actuated Soft Gripper [69]	3	Silicone	Cable Driven	Objects include a cylinder, a sphere, an egg, a tomato and a CD.
Variable Stiffness Gripper [67]	3	Silicone + small particle	Pneumatic Pressure & Vacuum	Objects of different shapes, sizes, weights and rigidities

Improving the payload capacity, stability and strength of grasping with soft grippers has looked to adding tunable stiffness components which can be activated during different stages of the grasping process. Examples in recent literature have used the concept of granular jamming [68, 74–76] and rigidity tunable elastomer strips activated by resistive heating [77] to achieve higher grasping strength, whilst still maintaining adaptability to an object's shape.

Other methods of increasing the grasping strength of soft grippers have incorporated rigid components; transforming soft grippers into hybrid (rigid/soft) designs. One design is bio-inspired by lobsters [78] and is comprised of a soft pneumatically actuated chamber embedded within a rigid shell. The rigid shell regulates the bending into multi-link configurations, effectively transforming the soft continuum fingers into multiple discrete DOF structures. Through experimental verification, this gripper is reported to achieve both high compliance and good controllability. A hybrid pneumatic network design of finger incorporating both soft and rigid components [79] showed dramatic improvements in the fingertip force (1.5–2 times greater than) and actuation speed (1.3 times faster than) other soft pneumatic actuators.

2.2   Sensing Technology for Grippers

Generally speaking, the sensory elements comprising a robotic system are critical to its effective performance. Similar to humans, robots can use the senses of vision, touch, hearing and even smell to complete a given task. These "robot senses" are made possible through the use of many different types of sensors. For object identification and recognition, vision and touch are the most practical senses as the greatest amount of information can be collected.

Directly comparing the sensory modalities of vision and touch in robotics, however, shows that vision systems are more commonly used and more reliable in given scenarios. Object identification and recognition in laboratory settings have been performed using vision

systems. These systems are generally reliable in controlled environments, since ideal environmental conditions can be maintained. When considering a practical outdoor application environment such as climbing a complex truss structure, however, there are many limitations for sensing with vision alone. Some of these limitations include:

- **Illumination and Background**

    - Camera pointing directly into the sun

    - Excessive reflection from the surface of beam members

    - Cluttered background (containing many beam members) with low contrast

- **Occlusions**

    - Due to the robot not being able to physically manoeuvre the camera to a desired position

    - Due to beam members which prevent direct line of sight from the camera to a beam member for grasping

- **Scale**

    - Given that the environment is comprised of similar cross-sectional shapes and sizes of beam members, it might be difficult to determine the true scale, especially given the proximity to beam members.

In these identified scenarios, the sensory modality of touch can be utilised to collect information about the beam members surrounding the robot during climbing. Additionally, there are certain features of the structural members that cannot be determined through the use of vision systems alone. Some examples may include surface texture and condition. By physically interacting with the environment, touch based object identification has the advantage of gleaning details that other sensory modalities fail to determine.

For proper control and to collect data during grasping, a gripper needs to incorporate sensing (both proprioceptive, to sense the positions of the grippers fingers and exteroceptive sensing, to sense the interactions with the environment). This section will review the

current state of the art proprioceptive and exteroceptive sensing technologies for robotic grippers; rigid, underactuated and soft.

Sensing technologies for rigid grippers are comprised of Commercially Available Off-The-Shelf (COTS) solutions that can be easily integrated into the gripper. Sensing for conventional rigid grippers has been well refined over the course of many years of research and development. Equipping rigid grippers with sensors for proprioception (e.g. to measure finger joint positions) and exteroception (e.g. to measure forces exerted on objects and points of contact) are essential for repeatable and reliable system functionality. Having knowledge of the joint positions and contact locations during grasping can also provide the robot with geometric information for manipulation and further exploration.

Sensing for soft grippers, however, is predominantly in the research phase, with very few COTS solutions currently available. Soft robotics, wearable electronics and human/machine interfaces have gained recent attention and interest as areas of research. There have been significant efforts invested in the research of soft sensors and sensing technologies which can be embedded into or retrofitted to these various systems. The field of soft sensing looks away from conventional "rigid" sensors such as force-torque sensors and encoders and more towards "soft" and flexible materials with sensing elements embedded within. Solutions for soft sensors do not use circuitry in the conventional sense, but instead, conductive materials embedded within elastomeric structures.

To date, research in soft sensing has looked into pressure, strain and tactile sensing using combinations of hyperelastic materials, conductive liquids such as liquid metals, 3D printed viscoelastic inks, resistive and capacitive substances, electro-conductive yarn, flexible circuitry and barometers. Most soft robots are comprised of separate sensing and actuation systems, with very few examples having integrated soft sensors. Manufacturing soft robots with integrated soft sensing is challenging to achieve and there are several requirements for integrating sensing elements in soft robots [80]:

- They must be sufficiently compliant to not restrict or dramatically modify the properties of the soft device,

- They must be resilient and extensible to avoid failure over many cycles of motion, and

- They cannot possess features that act as stress concentrators and cause damage.

The choice of sensors is highly dependent on both the hardware platform and the intended application. As the selection of sensors is predominantly application driven, a theoretical and mathematical analysis of the application scenarios should be conducted when evaluating a sensing option.

2.2.1 Proprioception

Fundamentally, all robots must have sensors to measure their own state; otherwise, their motions are simply incalculable. Originating from rigid robotics, the most common way to measure a robot's state is to measure its actuator's positions. This method is effective for rigid grippers, where an unambiguous number of DOF are able to be individually measured. As discussed in Section 2.1.3.2, soft grippers are continuum type mechanisms with no distinguishable number of finite DOF. This results in a challenging sensing problem, where a one-to-one pairing of sensor to DOF is not possible, and alternative methods and approaches of sensing must be developed [46].

With soft robotic systems, the dynamics are not as simple as rigid robotics and compliancy makes accurate position sensing and control difficult. Under unknown loads and as the system dynamics change over time, this problem only becomes more challenging. For each unique soft robotic system, new methods specific to the system need to be developed to accurately describe how the system behaves when actuated. Examples in recent literature have shown that planning for elastomeric actuators is possible by using dynamic and Constant Curvature (CC) kinematic models [81–83].

2.2.1.1 Sensing in Rigid Grippers

Well-established technologies for measuring the joint positions of rigid grippers exist, as low level system dynamics are well developed. These technologies rely on measuring an

actuators position—either rotary or linear, depending on the actuator type—and is generally achieved through the use of an encoder, potentiometer, resolver, hall effect sensor, Linear Variable Differential Transformer (LVDT) or Rotational Variable Differential Transformer (RVDT). The most common sensor for measurement of rotation is the encoder.

Two main types of encoders exist; absolute encoders and incremental encoders. Absolute encoders have a unique reading for each mechanical position which is not affected by power-cycling the system. Incremental encoders measure the current position, relative to the last position sensed, providing information about the motion by processing the output signals. Therefore upon power-cycling the system, the position of the encoder is not known. Properties such as speed, position and distance travelled can be calculated. These types of sensors are highly accurate, particularly when used in conjunction with a reduction gear which allows for accuracies in the thousandths of radians to be achieved.

Resistive sensors such as potentiometers are similar to absolute encoders and provide a cheap analogue alternative. They operate by moving a contact along a resistor to produce a voltage proportional to the position. These sensors encounter more wear during use and are thus limited to applications in low-use actuators. Because they are incrementally resistive in nature, absolute readings can be obtained without any data processing.

2.2.1.2   Sensing in Soft Grippers

Depending on the gripper design, including its structure and manufacturing materials, different methods of proprioception may be required. A wide variety of gripper designs utilise highly flexible materials that can bend or stretch when actuated. Therefore, soft sensors to measure changes in pressure and strain have been developed in an attempt to gain insight into the motion of soft grippers during their operation.

Simple resistive sensors with high stretch capabilities can be manufactured by embedding resistive micro/nano particles, such as carbon black into silicone rubbers [84]. A similar approach for creating stretch sensors uses a conductive paste film deposited on a rubber surface [85]. These sensors are simple to manufacture, however, they suffer the effects of large hysteresis and exhibit unpredictable behaviours [86, 87] which are not ideal for

collecting accurate and repeatable measurements. Similar to resistive sensors, Dielectric Elastomer Sensors (DESs) are capacitive stretch sensors that consist of a thin elastomer film that is coated on both sides with compliant electrodes. They can be configured as single-axis sensors [88], or as multi-axis sensors [89, 90]. The change in resistance or capacitance of these types of sensors can be measured and related back to an input displacement; with capacitive sensors generally showing better performance in accuracy and repeatability than resistive-based sensors.

Another common type of strain and pressure sensor design consists of conductive liquids embedded within a soft material such as silicone. When these sensors have a force (or pressure) applied to their surface, or are stretched (either uniaxial strain or bending), the conductive liquid changes resistance dependent on the loading situation. While much of the current research focus is towards different manufacturing methods for these types of sensors, it is envisaged that they could be used as soft sensory skins to determine the pose of soft robotic systems and the nature of their interactions with the environment. There are many examples of these types of sensors in literature, which use different manufacturing methods and materials to achieve the same sensing result. Eutectic Gallium-Indium (EGaIn) (a liquid metal at room temperature) is a popular choice of sensing element as it has high surface tension and conductivity and can be easily embedded into soft materials.

An early research example of a soft sensor manufactured using liquid metal uses a multi-layered sensor circuit comprised of thin elastomer layers with a micro-channel filled with EGaIn [91]. The combination of the signals from the three sensor layers (as shown in Figure 2.13) enables the device to detect and distinguish three different stimuli: x-axis strain, y-axis strain and z-axis pressure. Applying pressure or stretching the structure changes the resistance of the EGaIn by the relationship: $R = \rho\frac{l}{A}$, thus enabling pressure and strain sensing by monitoring the change in resistance.

The emergence of advanced manufacturing methods such as Embedded 3D Printing (e-3DP) and laser-based fabrication have greatly improved the ease and accuracy of manufacture for these types of sensors. Using e-3DP, conductive viscoelastic ink can be printed into an uncured elastomeric reservoir, which is then capped by filler fluid and finally, cured to
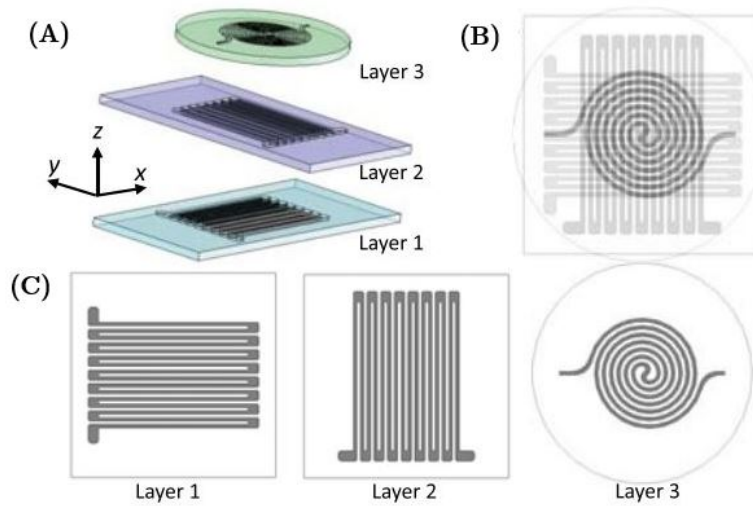
FIGURE 2.13: Design of a soft sensor composed of three sensor layers with embedded microchannels: (A) Exploded view, (B) Assembled view, (C) Each sensor layer design (Layer 1: x-axis strain sensing, Layer 2: y-axis strain sensing, and layer 3: z-axis pressure sensing). Source: [91].

complete the strain sensor [92]. Laser-based manufacturing methods include the use of Carbon Dioxide (CO_2) lasers to pattern thin films of Polydimethylsiloxane (PDMS) which are then embedded with liquid-phase EGaIn to produce elastic, soft strain sensors [93, 94]. A method utilising masked deposition and selective wetting has also been investigated to produce hyperelastic strain sensing components composed of EGaIn embedded within thin elastomer films [95].

While many of these sensor designs focus on measuring axial strain, few designs using liquid metals embedded in elastomers look to measuring the curvature of bending. An example of a stretchable thin-film bend sensor is manufactured using soft lithography [96]. Other methods of curvature sensing employ electro-conductive yarn which is capable of measuring bending behaviour as well as elongation when wrapped helically around a soft continuum manipulator [97].

Few examples of the practical application of these sensors exist in literature, however, examples of sensing axial contraction using Pneumatic Artificial Muscles (PAMs) have employed varying sensing designs and methods. One example [98], consists of a double-layered elastomer tube with Kevlar thread reinforcement on the inner layer and the outer layer contains an embedded helical EGaIn microchannel. When compressed air is injected

into the air inlet, the chamber expands radially and contracts axially. The radial expansion causes elongation of the EGaIn microchannel, resulting in a change of resistance that can be related back to the distance of axial contraction. Another example [99], uses insulated wire braid in the PAM fibre mesh to measure contraction and force output of the actuator. This is achieved through monitoring the change in inductance and resistance during elongation and contraction motions. A roughly linear relationship existed between the measured inductance and the contraction length (resolution of 0.5 mm) and there was a strong correlation between measured resistance and the actuator force (resolution of 5 N).

An example of a soft robotic bending actuator embedded with a complex network of soft sensors is manufactured using e-3DP [100]. Proprioceptive and haptic feedback is achieved through monitoring the state of the embedded ionically conductive curvature, inflation and contact sensors.

The sensing technologies discussed in this section use similar hardware, where the sensors change resistance or capacitance under a specific type of load (e.g. stretch, pressure, twist or bend). Each of these sensors shows promise for measuring the deformation of continuum type soft robots for proprioception. Pressure sensors could also be utilised for exteroception, however, they have their limitations. One current limitation of these sensors is their configuration; they are typically not manufactured as an array, therefore in pressure sensing scenarios, they are not capable of determining **where** on the sensor a load was applied, only the **magnitude** of the load. This is a critical requirement for object identification.

2.2.2 Exteroception

Tactile sensing is critical in robotic systems to enable the robot to sense interactions with the environment. For robotic manipulation, it is particularly important to collect data during grasping, as object properties such as cross-sectional shape, size and surface condition can be identified. This information can then be used to determine the grasp stability, detect slip and to adjust the grasping pose as required. Furthermore, this data

can be used to determine features of the object being grasped, therefore aiding in the identification of the object.

Researchers and industry are developing tactile sensing systems to meet a range of applications within the automotive, medical, dental and robotics industries, amongst others. Whilst many of these technologies could be integrated into soft systems, the rigid components that comprise their designs are often the limiting factor in their practicality for a given application.

2.2.2.1   Sensing for Rigid Grippers

As with proprioceptive sensing methods for rigid grippers, exteroceptive sensing technologies are well-established systems that do not warrant extensive discussion in this literature review. Exteroceptive sensing for rigid grippers has focused on measuring the actuator effort during grasping, as well as sensing the physical points of contact the gripper makes with an object during grasping, manipulation and exploration tasks.

For estimation of the force and torque exerted by or on an end effector such as a wrist joint, multi-axis load cells, or force/torque sensors can be utilised. The data collected from these sensors provides insight into the actuator effort under loading, which can be essential for determining the grasp success rate.

To determine the points of contact during grasping, it is common for rigid grippers to incorporate simple force sensors on the surfaces of their fingers, either as individual sensors or arrays. These sensors are generally comprised of resistive or capacitive elements which change resistance or capacitance as the force or pressure applied to them changes. Many force sensors, commonly referred to as FSRs using flexible circuitry have been developed by companies such as Tekscan [101], Spectra Symbol [102], Interlink [103] and Pressure Profile Systems [104]. Whilst these systems utilise flexible components, they still contain rigid parts which are prone to stress and ultimately failure over extended usage periods.

Individual FSRs are effective in determining the magnitude of a force applied at a particular position during grasping. Variations in sensor shapes and active area sizes exist, depending on the application. If the exact location of the sensor placement on the gripper

is known, along with the joint sensor readings, the geometrical shape of an object can be determined during grasping. These COTS sensors are the most common, simplest and readily available method of incorporating tactile sensing into a system. Users can create arrays by utilising many individual FSRs, however wiring and circuitry requirements become demanding with larger scale systems. Despite being flexible, these sensors are susceptible to bending fatigue and delamination of the individual sensor layers under excessive shear force loading. These sensors also require a rigid mounting surface to ensure repeatable and reliable readings and protection to ensure that the active areas of the sensors do not become kinked or dented.

Similar to FSRs, tactile arrays are comprised of many small sensing nodes configured in a set number of rows and columns, which can be customised. These sensors have the added advantage of being able to detect contact points with an object across many sensing elements as well as the magnitude of the force exerted at each element, which may provide a more complete representation of the object being grasped. Additionally, such sensors can be used to detect slip during grasping, although vibration sensors and accelerometers have proved more sensitive to slip detection [105, 106]. An advantage of these sensors is the wiring and processing requirements. Their array configuration means that the rows and columns of the array can be scanned at a high frequency, which results in fewer wires being required, as compared to an array of individual FSRs.

2.2.2.2 Sensing for Soft Grippers

Exteroceptive sensing for soft grippers has mostly focused on the need to determine the points of contact during grasping. Thus, arrays of force sensors, or tactile arrays using soft and conformable materials have been developed. Typically, these sensors are still comprised of some rigid components such as Printed Circuit Boards (PCBs) and wires, although a shift towards flexible electronics has been a recent development.

Soft COTS sensors developed by PPS [104] include the Stretchable TactArray Sensor (STS) and the Conformable Tactarray Sensor (CTS). The features of the CTS and STS sensors enable them to be easily retrofitted into many robotic applications. Since they are soft and flexible (constructed from conductive cloth (CTS) and conductive silver-metalised

Spandex (STS)), they can be wrapped around simple geometries or moulded to more complex shapes without compromising data quality. Both sensors are highly sensitive (the CTS can measure pressures as low as 10 Pa) and repeatable in their measurements. These COTS sensors are sold with visualisation software for ease of data analysis and integration into existing robotic systems.

The Tekscan I-Scan System [101] is another example of a soft tactile array sensor. This sensory system is advertised as being capable of "pressure mapping". The system measures and analyses the interface between two surfaces, using over 200 flexible, thin film tactile pressure sensors. These sensors are available in a range of different sizes, shapes, resolutions, temperature and pressure ratings which are customisable.

These types of sensors could be retrofitted to many existing robotic systems, however cable management would be a problematic design factor. An alternative approach for tactile sensing looks to embedding sensing elements directly within soft material structures and routing cables throughout the structure, eliminating the need for cable management systems.

An example of an embeddable tactile sensing system is the Takktile sensor [107]. This sensor utilises a Microelectromechanical Systems (MEMS) barometer embedded within soft rubber to produce tactile sensing elements (see Figure 2.14 for manufacturing process). Once the rubber has cured, a direct force applied to the rubber is transmitted through to the diaphragm of the sensor. MEMS barometers can detect gentle contacts (1 gram sensitivity) in a small, inexpensive package, whilst also being tolerant up to 25 lbs of static weight and durable enough to handle an impact from a hammer. The sensors can be configured in an array and can also be integrated with flexible PCBs to provide flexible contact sensing capable of tolerating elongations of about 25% [108]. These features of sensitivity, robustness, flexibility and low-cost make the tactile sensors ideal for many applications in robotics and human-interface applications [109].

The BioTac [110] is an entire tactile sensing fingertip which can be retrofitted to existing robot hands. Its biologically inspired design (based on the human fingertip) is comprised of a rigid, bone-like core surrounded by an elastic fluid filled skin to achieve a compliance remarkably similar to the human fingertip (see Figure 2.15). Within the rigid core of the
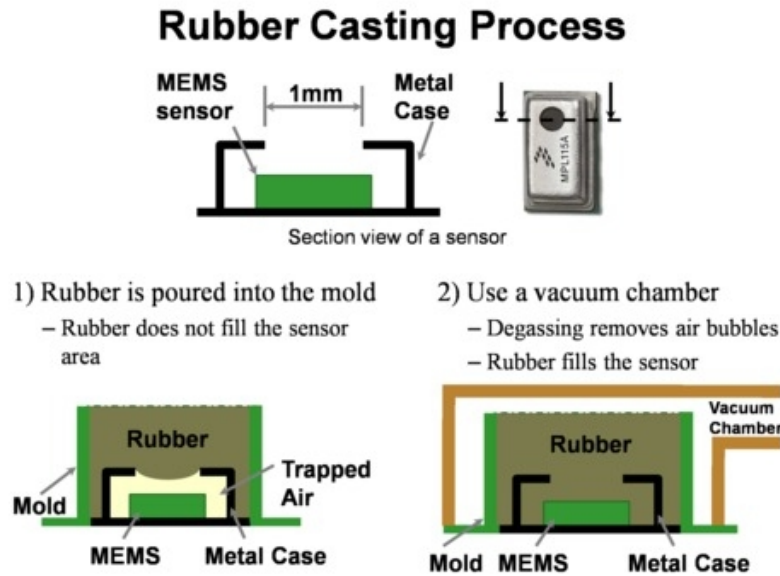
FIGURE 2.14: Tactile sensors from MEMS barometers: rubber casting process. Source: [107].

fingertip, force, vibration and temperature sensors are incorporated, allowing the sensor to mimic the sensing capabilities of human fingers. The sensor, in conjunction with a Bayesian exploration method is particularly proficient in identifying textures (using the lateral motion *Exploratory Procedure (EP)*) [111].
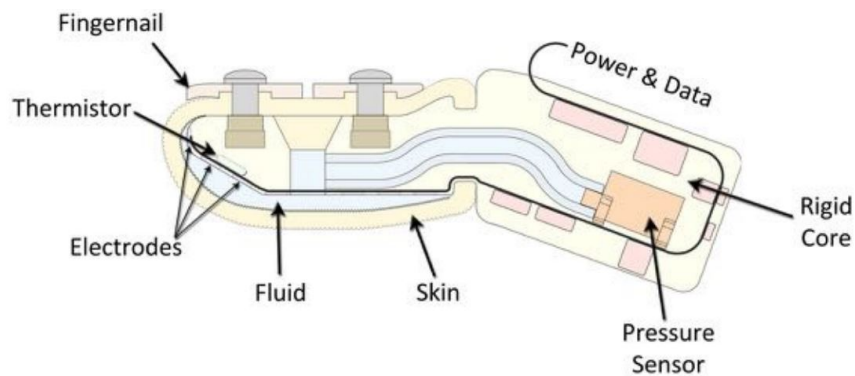
FIGURE 2.15: BioTac sensor schematic. Source: [110].

An alternative tactile sensor, the TacTip [112], is based on theories of the functional morphology of the human fingertip. The sensor mimics the layered macro-structure of fingertip skin and is composed of a thin flexible rubber skin. Encased within this rubber skin is an array of artificial *papillae* which deflect during grasping actions. These deflections are detected by a Charge-Coupled Device (CCD) camera (see Figure 2.16). The sensor

has proven to be highly sensitive and practical, especially for extracting edge information. Further research using this sensor for tactile exploration of surface features such as edges or ridges [113, 114], has shown promising results for object shape recognition.
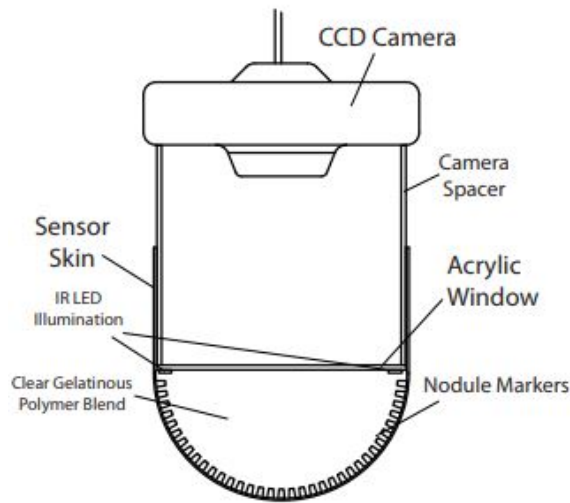
FIGURE 2.16: TacTip sensor design. Source: [112].

2.3   Object Identification and Recognition Using Touch Based Exploration

Touch based exploration is frequently performed in nature in situations where sensing with vision alone is either not ideal or not possible. Exploration typically involves using the arms, hands or any other tactile *effectors* to touch and manipulate objects. During object interaction, the multitude of sensors in the tactile *effector* provides the ability to extract object features.

Some examples in nature include animals who reach for food in high clutter and low visibility during foraging. Raccoons, like primates, typically use vision to identify and reach for objects. However, they also make extensive use of haptically controlled movements, which may relate to the use of their forepaws in foraging for food in swampy areas at night. In some instances, raccoons were even observed to have turned their heads 180° from the position of the hand as they reached [115].

Moles are small fossorial mammals who live in dark underground tunnels and feed on earthworms and other small invertebrates found in soil. Their small eyes and tiny optic nerves limit their sensing capabilities for finding sustenance and create a major survival challenge. To compensate for their lack of vision, many moles of the family Talpidae have incredible senses of smell, which can detect changes in air pressure and vibrations. The star-nosed mole has a snout surrounded by twenty-two fleshy and mobile appendages, which, despite its appearance and location is not an olfactory organ. Instead, the star is devoted to the sense of touch as its appendages are covered with thousands of small mechanoreceptive Eimer's organs. Behavioural studies have found that the star acts like a "tactile eye" and is used for detailed explorations of objects of interest [116].

Humans often use the sense of touch for object exploration and identification. Some situations include reaching into cupboards and feeling for an object which is out of sight, navigating through spaces in the dark and feeling for obstacles, reaching for a mouse whilst looking at the computer screen, amongst others.

This literature review section naturally flows on from robotic gripper designs and sensing options as it looks at the integration of the two and the development of strategies for object identification, recognition and touch based exploration. In this section, human touch based exploration, object identification and recognition methods are reviewed and an analysis of how these methods translate to the robotic domain is conducted. The remaining review of literature relates to robotic touch based exploration, with a focus on underactuated rigid and soft grippers.

2.3.1 Human Haptic Perception

Touch, by nature, is an interactive behaviour which humans exploit to perceive features of their surroundings. The human skin is highly sensitive to touch and humans rely on the forces experienced during touch to perform a multitude of everyday tasks. By physically contacting objects, features which cannot be detected by other senses, such as compliancy, texture, temperature and specific geometric details can be determined. The process of feature extraction involves the co-ordination of the human hands, with sensors and their feedback to the brain for control.
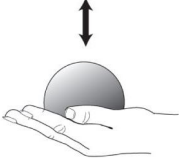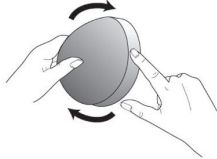
Haptic perception ("the process of perceiving the characteristics of objects through touch" [117]) refers to active exploration of surfaces and objects by a moving subject such as a human hand. Humans are capable of making informed decisions to select a sequence of movements to extract sufficient information for object identification. Context awareness allows for actions to be selected based on prior knowledge extracted from exploratory motions in conjunction with the current belief of the identity of an object. Humans also execute these motions with the knowledge that particular actions will yield certain information.

In 1987, Lederman and Klatzky first described a set of specialised patterns of haptic exploration, called *Exploratory Procedures (EPs)* [118]. In experiments, blindfolded participants were instructed to explore objects and attempt to identify them using touch alone. It was deduced that *EPs* executed by participants were specific to particular properties of the object. This was especially demonstrated when participants were asked feature specific questions about an object. It was found that a two-stage sequence was executed to gain a global understanding of the object followed by a more specific *EP* for more detailed analysis of object features. A basic set of *EPs*, along with their associated properties and behaviours are listed in Table 2.4.

Each of the six identified *EPs* vary in duration, from the fastest (static contact), followed by enclosure (grasping), to the slowest (contour following). The *EPs* which provide the most information regarding an object are enclosure (grasping) and contour following. Performing all *EPs* to identify objects by touch can be very impractical and time-consuming.

Depending on the task, it may be favourable to learn the greatest amount of information about an object as quickly as possible, expending minimal effort. In further research by Lederman and Klatzky, it was found that a brief, spatially constrained contact involving little or no movement of the fingers ("haptic glance") was sufficient for blindfolded humans to extract a number of features which were critical in identifying objects [120]. It was also speculated that the current hand position relative to the object could be extracted, and thus, the hand and arm movements required to gain an appropriate arm and hand pose for successfully manipulating the object. It was claimed that all of this could possibly be completed without even seeing the target object.

TABLE 2.4: *Exploratory Procedures (EPs)*, adapted from [118, 119]

Exploratory Procedure	Associated Property	Behaviour
	Surface texture	The skin is passed laterally across an object's surface, producing shear force. Typically, the fingers rub back and forth across a small homogeneous area of the surface; interior surfaces are explored, rather than edges.
	Compliance or hardness	A normal force or torque is applied to one part of the object, while another part is stabilised or a resisting force is applied. For example, pressing into the surface, bending the object, or twisting.
	Apparent temperature	The skin surface is held in contact with the object surface, without motion; typically, a large surface (like the whole hand) is applied.
	Weight	The object is lifted away from any supporting surface and maintained in the hand without any effort to mould the hand to the object. Typically, there is some lifting, hefting or wielding of the object.
	Volume/global shape	The hand maintains contact with as much of the object as possible. Often there is an effort to mould the hand more precisely to object contours. Periods of static enclosure may alternate with shifts of the object in the hand(s).
	Exact shape	The hand maintains contact with a contour of the object. Typically, the movement is smooth and non-repetitive within a segment of object contour, stopping or shifting direction when a contour segment ends.

2.3.2 Robotic Haptic Perception

When designing a robotic system capable of grasping and performing haptic perception, researchers have often looked for inspiration in one of the most highly advanced species known in the niche of manual manipulation—Homo sapiens. The human hand is extremely dexterous, contains millions of nerve endings and is controlled by a very complex biological

neural network—the brain. All able-bodied humans possess the capability of performing basic exploratory motions for object recognition and feature extraction; skills which were mastered by years of practise throughout childhood. These exploratory motions are so naturally executed that they are often performed without even thinking about each individual step in the overall process. Robotics researchers can apply lessons learned from human haptic perception when developing efficient methods for robotic haptic perception. In fact, many robotics researchers have attempted to replicate human haptic perception using various forms of robotic grippers.

2.3.2.1   Haptic Perception Using Rigid Grippers

Literature relating to object identification and recognition in robotics has predominantly focused on vision sensing in controlled, indoor environments. However, in outdoor environments, sensing with vision alone can be unreliable due to variable lighting conditions and occlusions, amongst other reasons. For situations where vision sensing is unreliable, the sense of touch can be used as either a standalone or complementary sensory modality. Robotic touch-based object recognition has naturally looked to mimic human EPs to extract as much information about a target object as possible [121].

Whilst humans are extremely proficient in haptic perception, the concept in robotics is challenging and current state of the art robots are still not capable of recognising objects and their properties with similar accuracy to a human. It can be difficult to install dense tactile arrays in a robot's grippers and in order to execute EPs, complex control systems are typically required with active hand control. Errors in actuation and sensing, with motion restrictions due to hand and arm dexterity further complicate the procedure. In many cases, passive sensing is not sufficient to determine certain features of objects. For example, small features often can't be sensed accurately through static touch and require motion, or active sensing procedures [122].

Early research on active touch and robotic perception looked to directly translate the EPs described by Lederman and Klatzky into the robotic domain [123–126]. One early example was a Utah-MIT hand fitted with Interlink tactile sensors on the distal links of each finger [127]. This hand was mounted on a PUMA 560 arm and was used to carry

out three different *EP*s to extract the shape of different objects. These procedures were lengthy to execute and still required some human aid to function correctly. Different types of robotic *EP*s have been attempted by several research groups [122, 128–130] with similar time consuming outcomes. In one such example of early robotic haptic exploration methods, "tactile subroutines" [131] were developed in an attempt to mimic human tactile perceptual functions. Each subroutine was targeted at extracting a specific feature from an object being explored. Experimental results demonstrated the feasibility and usefulness of the method in robotic exploratory operations.

Researchers over the years have continued to implement *EP*s in robotics—usually on a set of household objects—with greatly improved results as technology has also improved. A multitude of sensing configurations and hardware platforms can be combined with data collection techniques to achieve object recognition and identification. Some methods use rigid grippers endowed with multiple sensory modalities and the ability to perform multiple *EP*s [132–139]. Others focus on executing a single *EP* such as contour following [114, 122, 140], or repeatedly probing a target object to collect local "tactile images" [141–147]. Whilst improvements in this field have been made, robots are still not able to exceed the capabilities of humans performing object classification using haptic perception alone.

Due to the simplicity of the concept, the *haptic glance* [120] is much more easily appropriated to robotics—where it is much simpler to practically implement. By using a *haptic glance* as a method of exploration, the hardware set-up, including the actuation method can be simple and sensors can be sparse. Rigid grippers performing *haptic glances* for object recognition are of particular interest in this literature review. Early implementations used superquadric model-based methods to determine the shape of objects, using proprioceptive and tactile data [127, 148]. Recent developments have identified objects from a defined set using classifiers trained with data from grasping with anthropomorphic hands—using only joint sensor data [149] or both joint sensor and tactile data [150–152].

Methods of object identification from *haptic glances* have been developed through the use of supervised machine learning classifiers. Popular classifiers include Support Vector Machines (SVMs), k-Nearest Neighbours (k-NN), Artificial Neural Networks (ANNs), Bayesian Networks (BNs) and Decision Trees, amongst others. Each classifier has its own

advantages and disadvantages for given problems, with common comparison features being classifier training time, classifier accuracy and classifier storage space requirements. For example, SVMs and ANNs tend to perform much better when dealing with multi-dimensions and continuous features. In contrast, logic-based systems such as Decision Trees tend to perform better when dealing with discrete or categorical features [153].

Ensemble classifiers, such as Random Forests (RFs) are commonly chosen in object identification applications as they can achieve higher classification accuracies if configured correctly. RFs are particularly beneficial for object identification as they do not overfit (because of the Law of Large Numbers) and are typically known as accurate classifiers due to their randomness [154].

2.3.2.2   Haptic Perception Using Soft and Hybrid Grippers

The concept of haptic perception using soft grippers is in its early stages of development, with much research focus in soft robotics being directed towards actuator and sensor design methods. Since soft gripper mechanisms are typically designed to bend in a plane during actuation, modelling their kinematics assumes either a Constant Curvature (CC) approximation [155] or a reduced kinematic Piecewise Constant Curvature (PCC) model [156]. Due to structural compliancy, knowledge of a the specific configuration of a gripper at any given time is difficult. To further complicate the problem, as a gripper interacts with the environment, unconstrained and unpredictable deformations can arise which limit the accuracy of these models. Sensor selection is therefore highly dependent on the gripper design, actuation method and grasping application. Recent literature in soft sensing has focused on sensor design, with few integrations in grippers for object recognition purposes.

Early methods of equipping soft robotic grippers with sensors has involved either retrofitting or embedding flexible or soft sensors (many of which were discussed in Section 2.2) within the structure of a gripper during manufacture—a process which has become more viable as a result of additive manufacturing technologies. By assuming CC, many different methods of proprioceptive sensing in soft robotics have emerged—where sensors typically change resistance with respect to an input force or strain. Some examples include the use of soft stretch and bend sensors embedded with liquid metals [157–159] or conductive elastomers

[100, 160–162]. Flexible bend sensors are also a popular COTS solution for proprioceptive sensing in soft grippers [163, 164], along with flexible force sensors for measuring point loads.

A number of factors prevent object recognition methods using rigid grippers from being directly translated to the soft robotic domain. Uncertainty in kinematic models and interactions with target objects has generally resulted in the use of machine learning methods with sparse sensory inputs. Object identification methods using soft robotic grippers reported in recent literature have mostly used proprioceptive sensing only. For example, a soft pneumatic gripper with two embedded sensors—an air pressure sensor and a bend sensor—was able to recognise different sizes of spherical objects by monitoring the inflation pressure and bend sensor curvatures during pneumatic actuation [165]. A topology optimised, passively compliant gripper with embedded conductive silicone rubber elements [160] has been used for rudimentary object size and orientation discrimination, albeit with a very limited object set. A soft gripper with embedded resistive bend sensors [166] was designed to classify (using a k-NN classifier) objects of unique shape and size from a known set. During grasping, bend sensor readings were used to predict the hand configuration and classify the target object.

Few soft robotic grippers have incorporated both proprioceptive sensing and exteroceptive sensing for object recognition. Some recent examples include a custom sensor skin (similar in design to the soft sensors of [91]) for measuring deformation and contact, with the ability to construct 3D tactile object models [167]. Another design uses a four fingered gripper [168] with resistive bend sensors along the fingers and a force sensor in each of the fingertips for contact detection. The configuration of both hand and object can be detected and objects are identified using a k-NN classifier. A similar soft four fingered pneumatic gripper uses an embedded multi-layered arrangement of curvature and pressure sensors [169]. Objects are identified using a trained SVM classifier, although only trained with curvature sensor data. A related example uses an underactuated hybrid (rigid/soft) robot hand equipped with an array of barometric pressure sensors distributed along the grippers phalanges [170]. Object identification is performed with a RF classifier trained with grasping data from force sensors and actuator positions.

There has been a seemingly significant lack of soft or hybrid grippers possessing **only** an array of tactile sensors for object recognition. One identified example is a Fin Ray® style semi-rigid gripper with a retrofitted thin, flexible tactile sensor pad on the inner side of **only one** of the two fingers [171]. During grasping, pressure images were collected, with a total of 50 tactile images collected for each of the 15 target objects (of unique shapes and sizes). A Deep Convolutional Neural Network was trained with this data and objects were reported to be recognised with high accuracies from a single tactile image.

2.3.2.3   Selecting the Next Best Action for Object Identification and Recognition

Depending on factors such as the gripper design, sensors, the types of target objects and how they are constrained in the application environment, the amount and quality of information obtained during a single *haptic glance* can vary. Often, several touches or grasps are required to gain confidence in the objects identity, pose and/or location in the environment.

Various methods exist for selecting the next best action for object identification or feature extraction using rigid robotic grippers. To identify an object from a set of household and industrial objects, a two fingered hand equipped with tactile sensors was used to collect low-resolution intensity images during grasping at various object heights [172]. In this application, to simplify the classification, detailed images were not required. Therefore, a sparse tactile array was used with this gripper. Classification was performed on the local image patches by applying a "bag-of-features" approach and maintaining a probabilistic belief about the current object being grasped. Histogram intersection was used to find the next action (height at which to grasp the object) that would provide the highest expected information gain. Across the 21 industrial and household objects, a classification accuracy of 84.6% was achieved.

An alternative method for object recognition uses a three fingered robotic hand to actively explore objects [173]. Active behaviours, similar to human *EP*s, are executed using a Bayesian approach to explore object locations that will reduce uncertainty. Simple objects of varying cross-sectional shapes and sizes were used for data collection (position

and orientation data from the robot hand), training and testing of the perception and exploration methods. The hand, which was equipped with tactile and strain sensors, was actively controlled to explore familiar and novel locations to improve perception until a threshold was exceeded, then a decision was made about the objects identity.

A texture discrimination algorithm using a process called Bayesian exploration was used to determine a texture from a candidate set, using the BioTac fingertip sensor [111]. The algorithm adaptively selected the next optimal exploratory movement, based on previous experience by calculating the Bhattacharyya coefficient for two probability distribution functions. A decision to execute a movement is dependent on the potential information gained and if a higher level of confidence is worth the time and energy expenditure. By using Bayesian exploration, a classification accuracy of 99.7% (better than human capabilities) was achieved when choosing between two difficult textures. Classification from a database of 117 textures had an accuracy of 95.4%.

To localise an object in its environment, a tactile method for an autonomous robot was developed [174]. The next best touching action was determined using an information gain metric calculated by the Kullback Leibler Divergence (KLD), based on measurements from tactile and force-torque sensors. Once the action which maximised the information gain was executed, the state of the objects pose was updated using an estimator (Bayes filter) and the uncertainty. The uncertainty was then checked against a threshold to determine if further actions were required for localisation. Both simulation and experiments showed that the proposed methods produced reasonable plans and the uncertainty was reduced.

By introducing the computational and motion costs as additional terms in the decision making process, a methodology to localise a solid object in 3D was proposed [175]. The robot was equipped with a force-torque sensor coupled with a spherical end effector. A case study was conducted where the robot was given two different time constraints for action execution, with the results being different candidate actions, given the time constraints.

2.4   Summary

Truss structures are comprised of structural beam members of varying cross-sectional shapes, sizes and orientations. For a robot to successfully, reliably and safely climb a truss structure, its grippers need to meet several design requirements.

These design requirements mainly relate to the grippers' ability to execute firm, enclosing grasps. This requirement is somewhat trivial to achieve when the target beam members are of consistent cross-sectional shape and size. In truss structures, however, the structural beam members vary in cross-sectional shape and size, complicating the ability to meet the design requirement. Particularly, in order to execute a stable and reliable grasp, the gripper needs to deform to the cross-sectional shape of a beam member from any grasping AoA to achieve sufficient points of contact. Finally, the robotic system requires sensory feedback for data collection and beam member recognition during grasping.

Depending on the intended application, when designing a robotic gripper, a compromise between structural compliance, degrees of freedom, force exertion and precision must be made. For example, some pick and place applications for delicate items such as fruits require low force exertion, to ensure the item is not crushed. Additionally, having many degrees of freedom can result in reliable grasping from many approach angles, due to a high number of points of contact. On the other hand, considering the application of an industrial, or climbing robot gripper, large force exertion, and therefore mechanical rigidity is imperative to support a large payload. Due to the rigidity of such grippers, however, during grasping, they must be precisely controlled and aligned with a target object, due to a lack of compliancy.

As a result of these often-complicated trade-offs, gripper designs in early robotics literature predominantly focussed on simple rigid mechanisms which could exert large forces, assisting in assembly line automation at the time. In more recent literature, as the prospect of robotic solutions for new environments emerge, there has been a focus towards investigating compliant and soft materials which are capable of gently adapting themselves to the contours of objects. Employing this concept in grippers has resulted in a multitude of soft robotic grippers which are typically capable of manipulating common household objects.

Grippers for climbing robots presented in literature have focussed on application environments composed of consistently shaped (usually box or pipe sections) and sized (with some slight variations) structural beam members. Whilst these grippers can achieve strong and reliable grasps, capable of supporting large loads, they have little adaptability. On the other hand, gripper designs incorporating adaptive and compliant features (underactuated and soft grippers) lack the grasping strength required for safe climbing, however they can effectively conform to the variable cross-sectional shapes of structural members. Ideally, a hybrid rigid/soft gripper would be developed to have both strength and adaptability.

Considering the recent literature, it appears that grippers for climbing robots are yet to be developed for grasping structural beam members of varying cross-sectional shapes and sizes. Furthermore, adaptive grippers in literature have predominantly focused on grasping a wide range of shapes and sizes of household objects. In this thesis, the problem of adaptive and compliant gripper design to accommodate grasping a range of structural beam member cross-sectional shapes and sizes is addressed. The scope is limited by only addressing the adaptability requirement. The grasping strength requirement therefore falls out of the scope of this thesis.

Adding suitable sensors to a robotic gripper—for data collection during grasping—is imperative for determining grasp stability and reliability as well as features and properties of beam members. Many different types of sensing technologies have been discussed in this literature review. Proprioceptive and exteroceptive sensors for rigid grippers are well established and reliable, with the ability to measure individual DOF in a robotic system. Sensing for soft grippers is more challenging, due to the continuum and deformable nature of soft structures which lack discrete and distinguishable DOF. Few COTS sensing solutions are available for integration into a soft gripper. Furthermore, solutions to sensing with soft grippers typically assume CC models, which are limited in practice because interactions with the environment can cause unpredictable and unconstrained deformations.

Many proprioceptive and exteroceptive sensing solutions exist for robotic grippers. The sensing methods used depend highly upon the actuation method and materials used to construct the gripper. For example, rigid robotic grippers, whose finger joints are directly coupled to motors, can have their joint angles measured using motor encoders.

This method of proprioceptive sensing does not, however, directly translate to continuum mechanisms, which lack the required discrete links to their fingers for this form of sensing to function. Many COTS sensing solutions exist for rigid robotic grippers, however, due to the field of soft robotics being in its infancy, sensing in soft robotic grippers is highly experimental and lacking in reliability and robustness by comparison.

By reviewing the literature, COTS sensing technologies for simple integration in soft robotic grippers were identified. Tactile sensors such as flexible PCB FSRs can provide the required data to determine grasp stability and contact points during grasping. Flexible bend sensors can be retrofitted to the outer finger surfaces of a soft gripper for proprioceptive sensing, although such methods are limited in their accuracy. Depending on the actuation method, encoders could provide a more reliable means of proprioceptive sensing, although the repeatability of such sensing techniques could be affected by the hyperelasticity of soft materials. In this thesis, the designed soft gripper is retrofitted with an array of FSRs. By actuating the gripper with a custom linear actuator, proprioception is achieved through monitoring the state of the motor encoder.

In certain situations, object identification using vision alone may not be achievable. In these cases, an alternative or complementary sensory modality such as touch can be used to explore and identify an object based on the tactile feedback received. This method of touch-based exploration is commonly used by animals foraging for food, but also by humans executing everyday tasks. Like humans, touch-based exploration in robotics relies on a hardware platform (i.e. gripper) endowed with exteroceptive and/or proprioceptive sensing capabilities.

Research into human haptic perception revealed that humans perform six possible EPs when haptically exploring an object. These six procedures vary in duration and the amount of information obtained during each action; the most efficient EP being a *haptic glance*. Taking inspiration from humans, any combination of EPs may be performed to glean object properties during object exploration with a robotic gripper.

Feature extraction techniques presented for rigid grippers in recent literature have looked to human haptic perception for inspiration. Thus, many robotic grasping systems mimic

human EPs, often resulting in the need for multiple sensory modalities and complex control systems. Simpler methods exploit the use of a single EP, such as a *haptic glance* to achieve rapid recognition. Examples of touch-based robotic object identification and recognition have generally focused on a pre-defined set of (typically unconstrained household) objects. It is common for these target objects to vary greatly in their properties of size, stiffness and cross-sectional shape. By implementing machine learning methods, unique and distinguishable properties often result in reliable classifications using few data samples. Many soft grippers in literature incorporate bend sensors into their structures for proprioceptive approximations. One example has been identified where a soft gripper utilises only a tactile array for feature extraction, where its finger coverage is limited by the physical sensor array dimensions.

Complex truss structures are considerably different in nature to the application environments discussed in recent literature. In this thesis, the target object sets contain beam members with similar (or even identical) cross-sectional shapes at certain AoAs. To be practically implemented during climbing, data collected from a single *haptic glance* is used for beam member recognition. Recognition of these beam members using a single grasp, however, is hindered by similarities in the properties of structural beam members. The soft gripper used in this research uses an array of FSRs as the sensory input for beam member recognition—a setup that has only been reported in a recent publication in soft robotics [171].

Although the most efficient EP for humans, a single *haptic glance* does not always provide sufficient information for unambiguous object recognition. Excessively grasping an object at varying AoAs can be time consuming and impractical. Therefore, multiple strategic executions of a *haptic glance* could be carried out to maximise the information obtained during exploration. The question then arises of how to select the next best action for object identification and recognition. Methods presented in literature have relied on machine learning, combined with probabilistic methods and calculating expected information gain. By choosing the next best action which maximises the information gain, a minimum number of actions for confident object identification and recognition can be inherently achieved. Some examples in the reviewed literature employ these strategies for rigid robotic grippers

for object recognition and texture identification. However, there is limited information on implementing such strategies in exploration using soft robotic grippers.

Instead of using probabilistic methods for selecting the next best grasping AoA, in this presented work, an information-based method is proposed. The information-based method is based on a case where a gripper approaches a structural beam member that is unknown but known to be present in its collected dataset. Since all possible structural members are from a known set, the obtainable information from a new grasping AoA is known a priori. Therefore, based on the estimate of the initial position, the robotic system doesn't need to reason about unobserved areas of the structural member, or occlusions. For the case presented in this thesis where all structural members being grasped are known, a simple, computationally efficient information-based method can be used. For the more practical application of the robotic system, whereby all structural members and the data extracted at their various AoAs (including variations in roll, pitch, yaw) cannot be completely known a priori, the use of probabilistic methods for information gain would need to be explored.

This method is designed for grasping scenarios where the beam members in the target beam member set have similar cross-sectional shape and size. The next best AoA is selected (in a 2D plane), based on the sum of the variance of collected tactile sensor data for a known set of structural beam members. This method is not limited to a specific case of robotic manipulation and can therefore be used for other adaptive robotic grippers fitted with suitable tactile sensors.

Chapter 3

Stiffness Constrained Topology Optimisation Method

This chapter presents a stiffness constrained topology optimisation method for designing a soft gripper capable of grasping a variety of structural beam members (e.g. those shown in Figure 3.1b, amongst others) which may be encountered in a truss structure such as a power transmission tower (Figure 3.1a). The design method discussed in this chapter is focussed on designing a soft gripper by including stiffness constraints into a topology optimisation model.

3.1   Overview

In order to be an effective solution for grasping in a truss structure environment, the robot's grippers need to meet several key design requirements. To simplify the actuation requirements of the practical robotic grasping system, a single actuation input is desirable. Then, basic requirements for safe climbing dictate that the robot's grippers should be able to:

- Reliably grasp and deform to the cross-sectional shapes and sizes of beam members possibly found in truss structure from any AoA,
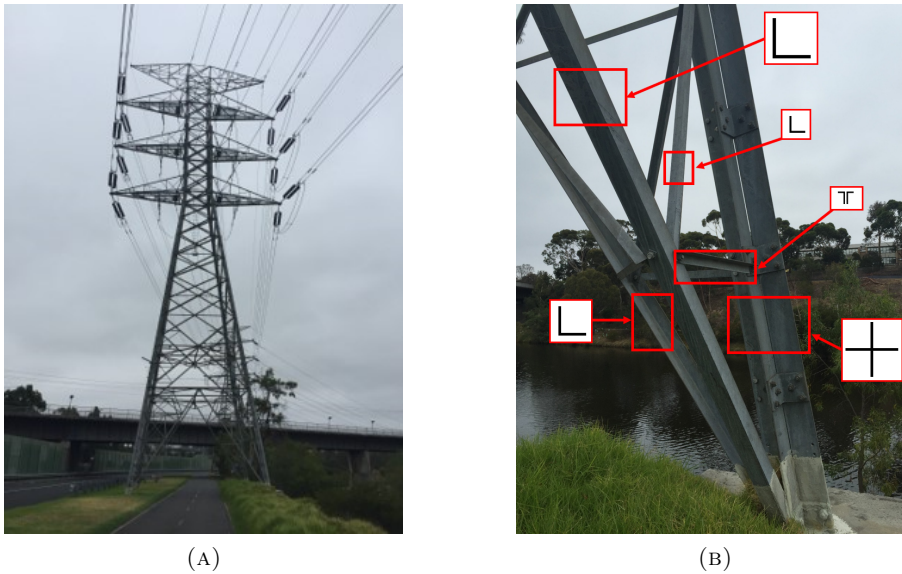
FIGURE 3.1: Power transmission tower examples: (A) A power transmission tower in Melbourne, Australia, (B) Structural beam members in the tower with cross-sectional shapes and relative sizes shown.

- Firmly grasp beam members to support the weight of the robot during climbing and maintenance procedures, and

- Incorporate sensing technology to **reliably** collect data (which can be used to classify properties such as the cross-sectional shape, size and grasping AoA) of a beam member during a grasp.

Truss structures may be constructed from a variety of cross-sectional shapes and sizes of structural beam members. Power transmission towers, for example, can be comprised of combinations of predominantly "L" and "O" (pipe) shaped beam members of varying sizes, which are highly dependent on the transmission voltage and height of a tower. For clarity in this research, the structural beam members have been categorised into three target beam member sets (as shown in Figure 3.2), chosen to represent samples of structural beam members which are likely to be found in power transmission towers. This chapter concentrates on the design of a soft gripper which is able to deform to each of the target beam member sets shown in Figure 3.2. Each target beam member set contains structural beam members of:

#1: Similar cross-sectional shapes of a fixed size—see Figure 3.2a.
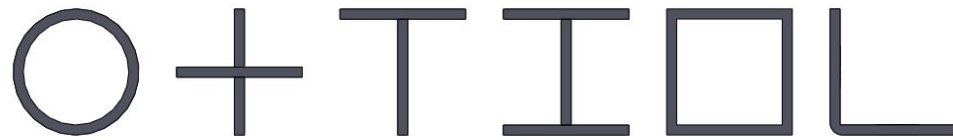
(A)

(B)
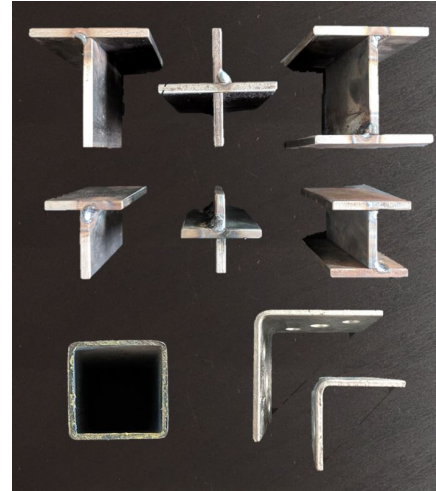
(C)

FIGURE 3.2: Target beam member sets: (A) #1: Beam members with similar cross-sectional shapes of a fixed size. (B) #2: Beam members with unique cross-sectional shapes and sizes, (C) #3: Beam members with similar cross-sectional shapes and sizes.

#2: Unique cross-sectional shapes and sizes—see Figure 3.2b.

#3: Similar cross-sectional shapes and sizes—see Figure 3.2c.

Soft gripper designs in the literature were reviewed for their viability as a solution in a truss structure environment. Soft grippers, with their inherent compliancy are capable of deforming to the shape of an object being grasped, whilst also resulting in a small reaction force at the joints of the robot body during grasping (as the gripper can deform to the shape of the object as opposed to forcing the robots joints). It was determined that a gripper design based on a topology optimisation model would provide the required compliancy in grasping to adapt to the beam members possibly found within a truss structure. The topology optimisation method was chosen since it could produce an optimised gripper, based on the estimated contact locations that would occur during grasping of structural beam members. To increase the grasping strength of the gripper and produce

firm grasps—where the gripper also effectively deforms to the shape of the beam member being grasped—a stiffness constraint-based topology optimisation method was developed.

This chapter is composed of three sections; Section 3.2 presents the stiffness constrained topology optimisation method; Section 3.3 details the verification of the stiffness constrained topology optimisation method; and Section 3.4 details the verification of a prototype soft gripper. In this chapter, two sets of grippers corresponding to each verification section are designed, analysed and discussed.

The first set of grippers described in Section 3.3.1 are designed using the stiffness constrained topology optimisation method presented in Section 3.2.1. Three grippers of identical size, each with different stiffness constraints are designed, with the aim of grasping structural beam members from target beam member set #1, as shown in Figure 3.2a. By comparing the simulated grasping results of the grippers in this set, it is verified that effective use of the stiffness constrained topology optimisation method can result in the increased grasping strength of a gripper.

The second set of grippers described in Section 3.4.1 are designed for the practical application of grasping structural beam members from target beam member sets #2 and #3, as shown in Figures 3.2b and 3.2c respectively. The prototype soft grippers are based on stiffness constrained, topology optimised grippers, with some design modifications to enable controlled grasping and data collection.

3.2   Design Method

A compliant mechanism is defined as a 'morphing structure that undergoes elastic deformation to transform force, displacement or energy' [176]. The design approach presented in this section is based on a compliant mechanism synthesis using a 3D topology optimisation model [177] to design a soft gripper. The topology optimisation problem can be defined as 'a binary programming problem in which the objective is to find the distribution of material in a prescribed area of volume referred to as the *design domain*' [177]. In a 2D topology optimisation problem, the design domain is discretised by a number of

square elements of identical size. For 3D problems, as presented in this thesis, a number of eight-noded cubic elements are used to discretise the design domain.

For the compliant mechanism synthesis design approach, structural compliancy (the inverse of stiffness) is desired to maximise an output displacement due to an input displacement. As a result, the produced mechanism is highly deformable and inherently lacks the grasping strength required for a climbing robot gripper. A stiffness constrained topology optimisation method has been developed to produce a strengthened soft gripper that is able to adapt to various cross-sectional shapes of beam members from differing AoAs. By introducing the stiffness constraints into strategic regions in the design domain, the gripper can achieve stronger grasps (than the un-stiffened gripper topology) when actuated. The grasping strength is evaluated by calculating the input-to-output force ratio of a grasp. When performing grasping of structural members, the output forces are the contact forces applied to the member during grasping.

This type of gripper is acceptable for grasping in a truss structure environment due to its compliancy, adaptability and simple control using a single linear input displacement. By virtue of its adaptability, the gripper is proficient in grasping a variety of cross-sectional shapes of structural beam members. Considering these features of the gripper, it is not strictly limited to grasping applications in truss structures. For the practical application, it is envisaged that the final soft gripper designed and prototyped in this chapter could be placed within a rigid mechanical frame to achieve a further increase in grasping strength—the design of a rigid frame, however, falls out of the scope of this thesis.

3.2.1   Topology Optimisation Method

Based on a topology optimised soft gripper obtained using the Optimality Criteria (OC) method [64], a similar approach has been taken in this thesis to design a soft gripper. The design method presented in Section 3.2.1.2 has modified an existing topology optimisation model [177] (summarised in Section 3.2.1.1) to impose stiffness constraints on a set of discrete 3D elements in a design domain.

3.2.1.1 Core Topology Optimisation Algorithm

For the compliant mechanism synthesis, a typical goal is to maximise the output port displacement. The optimisation problem [177] for this goal is given as:

$$
\begin{aligned}
\text{find} \quad & \tilde{\mathbf{x}} = [x_1, x_2, \ldots, x_e, \ldots, x_n]^{\mathrm{T}} \\
\text{minimise} \quad & c(\tilde{\mathbf{x}}) = -u_{\text{out}}(\tilde{\mathbf{x}}) = -\mathbf{L}^{\mathrm{T}}\mathbf{U}(\tilde{\mathbf{x}}) \\
\text{subject to} \quad & v(\tilde{\mathbf{x}}) = \tilde{\mathbf{x}}^{\mathrm{T}}\mathbf{v} - \overline{v} \leq 0 \\
& \mathbf{x} \in \mathcal{X}, \quad \mathcal{X} = \{\mathbf{x} \in \mathbb{R}^n : \mathbf{0} \leq \mathbf{x} \leq \mathbf{1}\},
\end{aligned}
$$

where

- x_e is the design variable

- $\mathbf{L}$ is a unit length vector with zeros at all degrees of freedom except at the output point where it is one

- $\mathbf{U}(\tilde{\mathbf{x}}) = \mathbf{K}(\tilde{\mathbf{x}})^{-1}\mathbf{F}$ is the nodal displacement vector

- $\mathbf{F}$ is the vector of nodal forces and is independent on the physical densities $\tilde{\mathbf{x}}$

- $\mathbf{K}(\tilde{\mathbf{x}})$ is the global stiffness matrix

- $\mathbf{v} = [v_1, ..., v_n]^{\mathrm{T}}$ is a vector of element volume

- $\overline{v}$ is the prescribed volume limit of the design domain

- n is the number of elements used to discretise the design domain

Note that for brevity of notation, the dependence of physical densities $\tilde{\mathbf{x}}$ on the design variables $\mathbf{x}$, $\tilde{\mathbf{x}} = \tilde{\mathbf{x}}(\mathbf{x})$ has been omitted.

The physical densities $\tilde{\mathbf{x}}$ are defined by the basic filter density function

$$
\tilde{\mathrm{x}}_i = \frac{\sum_{j \in N_i} H_{ij} v_j x_j}{\sum_{j \in N_i} H_{ij} v_j}, \tag{3.1}
$$

where

- N_i is the neighbourhood of an element x_i with volume v_i, and H_{ij} is a weight factor.

- A mesh with equally sized cubic elements of unit volume is used, thus $v_i = v_j$

- The neighbourhood is defined as $N_i = j : \text{dist}(i, j) \leq R$, where the operator $\text{dist}(i, j)$ is the distance between the centre of element i and the centre of element j, and R is the size of the neighbourhood or filter size.

- The weight factor H_{ij} may be defined as a function of the distance between neighbouring elements, for example $H_{ij} = R - \text{dist}(i, j)$, where $j \in N_i$

The filtered density $\tilde{x}_i$ defines a modified (physical) density field that is now incorporated in the topology optimisation formulation and the Solid Isotropic Material with Penalisation (SIMP) model as

$$\text{E}_i(\tilde{\text{x}}_i) = \text{E}_{\min} + \tilde{\text{x}}_i^p(\text{E}_0 - \text{E}_{\min}), \quad \tilde{\text{x}}_i \in [0, 1], \tag{3.2}$$

where

- E_i is an element's Young's Modulus

- E_0 is the elastic modulus of the solid material

- p is the penalisation power $(p > 1)$

- $\text{E}_{\min}$ is the elastic modulus of the void material, which is non-zero to avoid singularity of the finite element stiffness matrix

3.2.1.2   Stiffness Constrained Topology Optimisation Algorithm

By constraining the stiffness of elements in a strategic region in the design domain, it was expected that the output gripper topology would be capable of stronger grasps, as compared to a gripper produced using the topology optimisation without imposing stiffness constraints. Through strategically implementing these constraints in certain regions (based on desired gripper design) in the design domain, theoretically the gripper is still able to

deform to the cross-sectional shape of the beam member being grasped whilst providing a strengthened grasp.

With each iterative step in the optimisation loop, the stiffness constrained set of elements are assigned a higher stiffness value than the rest of the elements in the design domain by implementing the stiffness multiplier, α, which affects the physical stiffness of the chosen design domain elements. In order to effectively increase the stiffness of the desired elements, the stiffness multiplier, α, must be greater than 1. Selecting a large value of α will result in faster convergence of the solution in the stiffness constrained region. This method is undertaken in three steps:

1) The maximum stiffness value is determined by considering the stiffness of each discrete element in the design domain.

2) The maximum stiffness value is multiplied by a user defined value, α (> 1), to create the stiffness constrained value.

3) The stiffness constrained value is allocated to the discrete elements in the desired 'stiffer' region of the design domain.

Mathematically, the stiffness constraints are given by Equation 3.3.

$$\mathbf{K}(\tilde{\mathbf{x}}_{\mathrm{stiffer}}) - \mathbf{K}(\tilde{\mathbf{x}}_{\mathrm{rest}}) > 0, \tag{3.3}$$

where

- α is a user defined stiffness multiplier

- $\mathbf{K}(\tilde{\mathbf{x}}_{\mathrm{rest}})$ is the stiffness of elements in the remainder of the design domain

- $\mathbf{K}(\tilde{\mathbf{x}}_{\mathrm{stiffer}}) = \alpha * \max(\mathbf{K}(\tilde{\mathbf{x}}_{\mathrm{rest}}))$ is the stiffness of elements in the regions of the design domain to be stiffened (e.g. highlighted in yellow in Figure 3.4b)

Adding this constraint, the optimisation problem becomes:

$$\text{find} \quad \tilde{\mathbf{x}} = [x_1, x_2, \ldots, x_e, \ldots, x_n]^{\mathrm{T}}$$

$$\text{minimise} \quad c(\tilde{\mathbf{x}}) = -u_{\text{out}}(\tilde{\mathbf{x}}) = -\mathbf{L}^{\mathrm{T}}\mathbf{U}(\tilde{\mathbf{x}})$$

$$\text{subject to} \quad v(\tilde{\mathbf{x}}) = \tilde{\mathbf{x}}^{\mathrm{T}}\mathbf{v} - \overline{v} \leq 0$$

$$\mathbf{k}_j = \alpha * \max(\mathbf{K}_1(\tilde{x}_1), \ldots, \mathbf{K}_{k-1}(\tilde{x}_{k-1}), \mathbf{K}_{m+1}(\tilde{x}_{m+1}), \ldots, \mathbf{K}_n(\tilde{x}_n))$$

$$\mathbf{x} \in \mathcal{X}, \quad \mathcal{X} = \{\mathbf{x} \in \mathbb{R}^n : \mathbf{0} \leq \mathbf{x} \leq \mathbf{1}\},$$

where

- j is an element in the stiffened region of the design domain bounded by the elements 'k' and 'm', i.e. $k \leq j \leq m$

- $\alpha > 1$

3.2.2 Optimal Design

There are many optimisation algorithms which can be used to solve this topology optimisation problem. For this optimisation problem, the algorithm and code [177] for compliant mechanisms can be used. In this algorithm, a SIMP method is used with the OC method to update design variables. Density filtering, sensitivity filtering and a gray-scale filter can be used together to achieve a purely black (solid) and white (void) topology solution. The working principle of the sensitivity filter is to replace the real sensitivities by the filtered sensitivities by modifying the element sensitivity during every iteration by the following [178]

$$\widehat{\frac{\partial c(\mathbf{x})}{\partial x_i}} = \frac{1}{\max(\gamma, x_i) \sum_{j \in N_i} H_{ij}} \sum_{j \in N_i} H_{ij} x_j \frac{\partial c(\mathbf{x}))}{\partial x_j} \tag{3.4}$$

where $\gamma = 10^{-3}$ is a small number in order to avoid division by zero.

The gray-scale filter is used to further achieve black-and-white topologies. This filter functions by changing the OC update scheme as the following [179]

$$x_i^{\text{new}} = \begin{cases} \max(0, x_i - m), & \text{if } x_i B_i^\eta \leq \max(0, x_i - m), \\ \min(1, x_i + m), & \text{if } x_i B_i^\eta \geq \min(1, x_i - m), \\ (x_i B_i^\eta)^q, & \text{otherwise.} \end{cases} \tag{3.5}$$

The OC method is a classical approach to structural optimisation problems, and is formulated on the grounds that if the constraint $\mathbf{0} \leq \mathbf{x} \leq \mathbf{1}$ is inactive, then convergence is achieved when the Karush–Kuhn–Tucker (KKT) condition [177]:

$$\frac{\partial c(\tilde{\mathbf{x}})}{\partial x_e} + \lambda \frac{\partial v(\tilde{\mathbf{x}})}{\partial x_e} = 0,$$

is satisfied for $k = 1, \ldots, n$, where λ is the Lagrange multiplier associated with the constraint $v(\tilde{\mathbf{x}})$. This optimality condition can be expressed as $B_e = 1$, where

$$B_e = -\frac{\partial c(\tilde{\mathbf{x}})}{\partial x_e} \left(\lambda \frac{\partial v(\tilde{\mathbf{x}})}{\partial x_e} \right)^{-1}.$$

The OC updating scheme [180] is used to update design variables:

$$x_e^{\text{new}} = \begin{cases} \max(0, x_e - m), & \text{if } x_e B_e^\eta \leq \max(0, x_e - m), \\ \min(1, x_e + m), & \text{if } x_e B_e^\eta \geq \min(1, x_e - m), \\ x_e B_e^\eta, & \text{otherwise.} \end{cases} \tag{3.6}$$

Where m is positive move-limit, and η is a numerical damping coefficient. The choice of $\eta = 0.3$ is recommended for compliant mechanisms, which improves the convergence of the algorithm. The only unknown in Equation 3.6 is the value of the Langrange multiplier λ, which satisfies that $v\left(\tilde{\mathbf{x}}(\mathbf{x}^{\text{new}}(\lambda)) \right) = 0$.

Numerically, λ is found by a root-finding algorithm such as the bisection method. Finally the termination criteria are satisfied when a maximum number of iterations is reached, or

$\parallel \mathbf{x}^{\text{new}} - \mathbf{x} \parallel_{\infty} \leq \epsilon$. Where the tolerance ϵ is a relatively small value, for example $\epsilon = 0.01$ [177].

The design domain is sized with $x \times y \times z$ 1mm^3 cubic elements—each with 8 nodes (one on each corner of the cubic element). Each node in the structure has three DOF corresponding to linear displacements in the xyz directions (i.e. one element has 24 DOF). These node descriptions are used to accurately define the boundary and loading conditions.

3.3 Verification of Stiffness Constrained Topology Optimisation Method

In this section, a study is conducted to verify that the stiffness constrained topology optimisation method can be used to meet the gripper requirements laid out in Section 3.1. In particular, this study focusses on meeting the requirement of reliable grasping, through gripper adaptability to the various cross-sectional shapes of beam members in target beam member set #1 (Figure 3.2a). In this study, the stiffness constraint based 3D topology optimisation method (as described in Section 3.2.1) was used to design three grippers capable of performing enclosure grasps.

3.3.1 Gripper Design

In this study, three grippers are designed using the compliant mechanism synthesis, with varying stiffness constraints and identical design domains. The complete gripper design domain is defined in Figure 3.3. A single input force, $\mathbf{F}_{in}$, is applied at the base of the design domain (and gripper), which is converted to the output forces, $\mathbf{F}_{out}$, of the gripper, resulting in the closing motion of the gripper's "fingers" through the elastic deformation of the structure. Pin 1 (green) represents the fixed point of the gripper which is present in the design to produce movement of the gripper's fingers when the input force is applied. Pins 2_1 and 2_2 (orange) act as dummy supports which represent potential contact points when grasping a beam member.
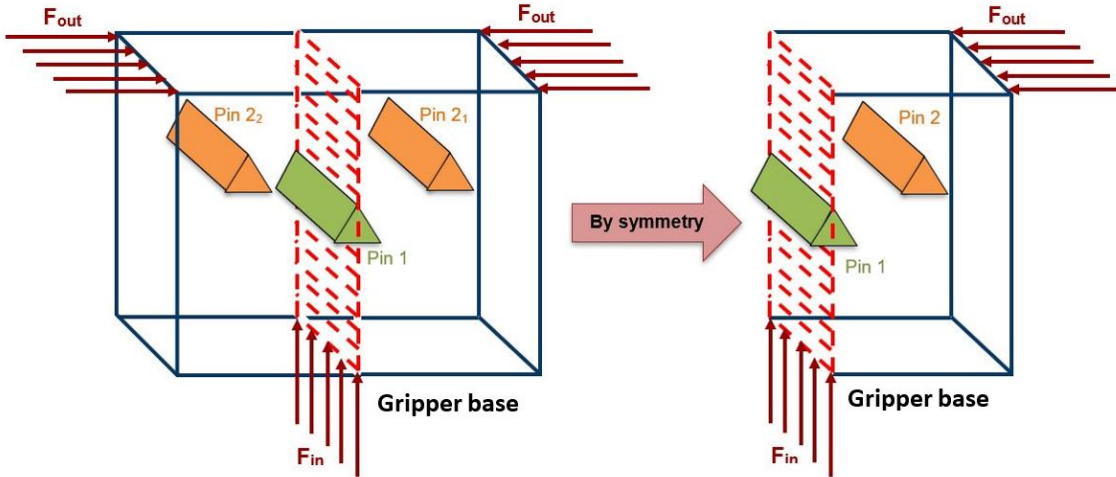
FIGURE 3.3: 3D design domain for soft gripper.

To reduce the complexity of the computation and obtain a simplified topology for testing, the 3D optimisation was used to generate a 2D solution by selecting a design domain depth of $z = 1$ discrete elements. The optimisation problem can be further simplified by taking advantage of the symmetrical nature of the design domain, where the complete design domain can be halved (as shown in Figure 3.3) for the topology optimisation procedure.

In total, three individual gripper topologies were designed to analyse the viability of the stiffness constrained topology optimisation method. The design domains were set up as shown in Figure 3.4 and summarised by Table 3.1.

The number of elements—and therefore the dimension of the design domains—were selected to ensure that the gripper was sufficiently large to grasp the beam members in target beam member set #1. The volume fraction limit of the design domain was defined as $\bar{v} = 0.3$, resulting in an upper limit of 30% of the total design domain being filled with elements which form the topology of the gripper. 30% was chosen to ensure the overall mass of the gripper was kept relatively low. If this upper limit were increased, the gripper would increase in mass, which is undesirable. Additionally, for compliant mechanisms, a volume limit of 30% improves the convergence of the algorithm [177]. A filter size of 1.4 was chosen. In order to avoid the presence of checkerboard patterns in the gripper topology, the filter size must be greater than the grid size (1mm^3) [181]. Increasing the
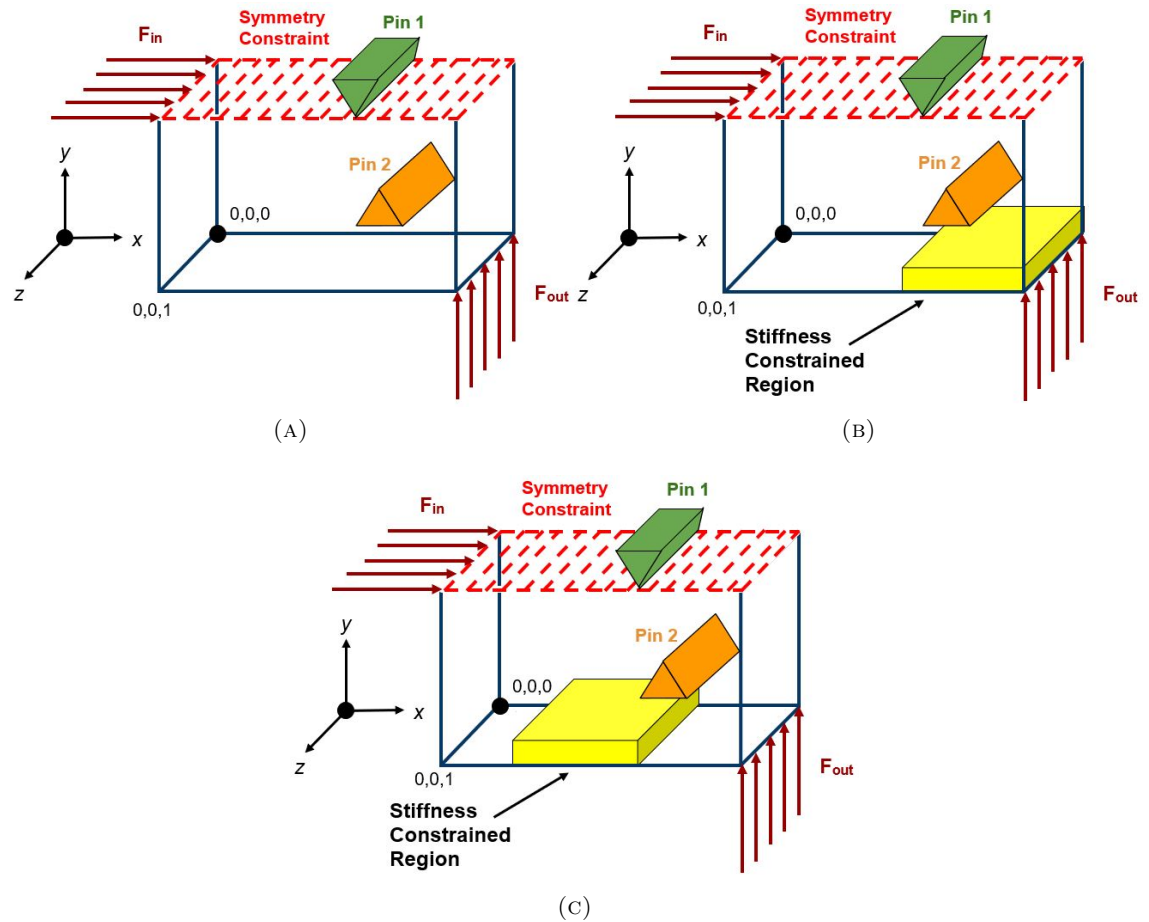
FIGURE 3.4: 3D gripper design domain with: (A) No stiffness constraints, (B) Stiffness constraints applied in strategic region (highlighted region), (C) Stiffness constraints applied in poorly chosen region (highlighted region).

filter size further above the grid size results in the space of feasible effective designs reducing in size. After brief experimentation, a filter size of 1.4 was chosen, however, further experimentation with the filter size setting can achieve certain curvatures or widths of topological structures in the design domain.

The input forces were applied at the axis of symmetry of the gripper (0, 84) and the output dummy force at the far end of the design domain (183, 0), to achieve maximum displacement of the gripper's fingertips during grasping. Pin 1 was placed along the axis of symmetry of the gripper, at a distance that would result in the gripper's "fingers" being long enough to fully enclose around the beam members from target beam member set #1 during grasping. Pin 2 was placed half way along a virtual diagonal line that can be drawn

between fixed pin 1 and the output force location. This pin was positioned to simulate contact between the gripper and the beam members half way along the grippers "fingers".

For effective application of the stiffness constraints, it is necessary to have an understanding of the desired gripper topology and the position of the output force. As a guideline, the stiffness constraints should be placed in a region as close to the output force location as possible, and along the path where it is expected that the material will be distributed in the optimisation procedure. This will ensure that the output force is sufficiently increased, whilst maintaining overall compliancy in the inner parts of the gripper where the "fingers" make contact with the surfaces of the structural beam members. In this study, the stiffness constraints for grippers #2 and #3 are applied over an arbitrarily dimensioned region (60×13 discrete elements) at differing starting x-coordinates in their respective design domains (see Table 3.1).

TABLE 3.1: Individual gripper design domain settings summary; grippers #1 – #3.

Gripper Number	Design Domain Dimensions (mm)		Fixed Pins				Stiffness Constrained Region	
			1		2			
	x	y	x	y	x	y	x	y
#1 - see Figure 3.4a	183	84	120	84	152	42	N/A	N/A
#2 - see Figure 3.4b							123:183	0:13
#3 - see Figure 3.4c							63:123	

Figure 3.5 shows the resultant half-gripper topologies which correspond to the design domains in Figure 3.4. Figure 3.5c demonstrates the need for an understanding of where to place the stiffness constraints within the design domain, as an undesirable topology has been produced which is not expected to significantly increase the grasping strength. Specifically, there are a number of elements generated in the design domain which are away from the direction of the force transformation from the input to the output, which will have little to no effect on re-enforcing the output force from the gripper.

3.3.2　Simulations

This section presents the verification of the three grippers described in Section 3.3.1. Each of the grippers are compared in simulation, using the Finite Element Analysis (FEA)
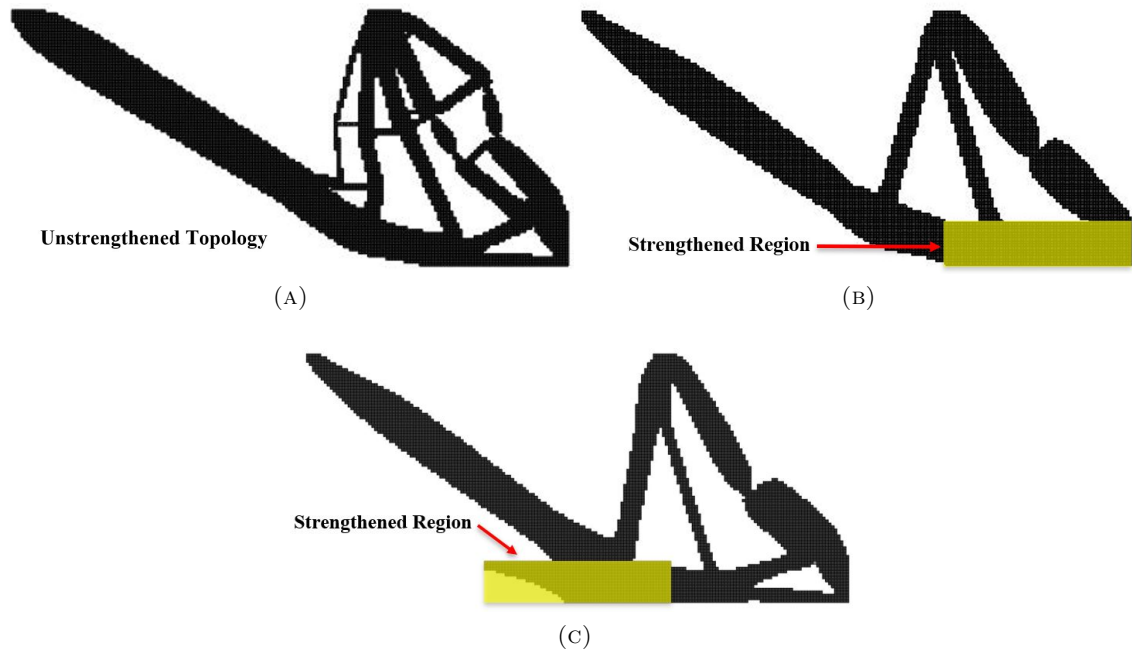
FIGURE 3.5: Output of topology optimisation with: (A) No stiffness constraints, (B) Stiffness constraints applied in strategic region (highlighted region), (C) Stiffness constraints applied in poorly chosen region (highlighted region).

software ABAQUS/CAE. This section details the two simulations which were conducted to compare the three gripper designs; (1) empty grasping, and (2) grasping beam members from target beam member set #1.

After obtaining the three topology optimised designs, the half gripper topologies were imported into Computer Aided Design (CAD) software and spline sketches were used to smooth the vertices of the grippers and therefore remove the pixelation due to the discrete elements used in the topology optimisation procedures. To offset the grippers' fingers, a centre extrusion of 25 mm was added to each gripper and the structure was mirrored about the axis of symmetry. Finally, the sketch was extruded to a thickness of 22.5 mm to reduce the effects of out of plane bending. Figure 3.6 shows the final gripper topologies which were used in simulation.

The gripper models shown in Figure 3.6 were imported into ABAQUS/CAE as 3D deformable parts with solid homogeneous sections. A hyperelastic material (Polyurethane Shore A 60) was allocated to the grippers for simulation; material data was downloaded from Solidworks Materials Web Portal. The material had a density of 1225 kg/m^3 and
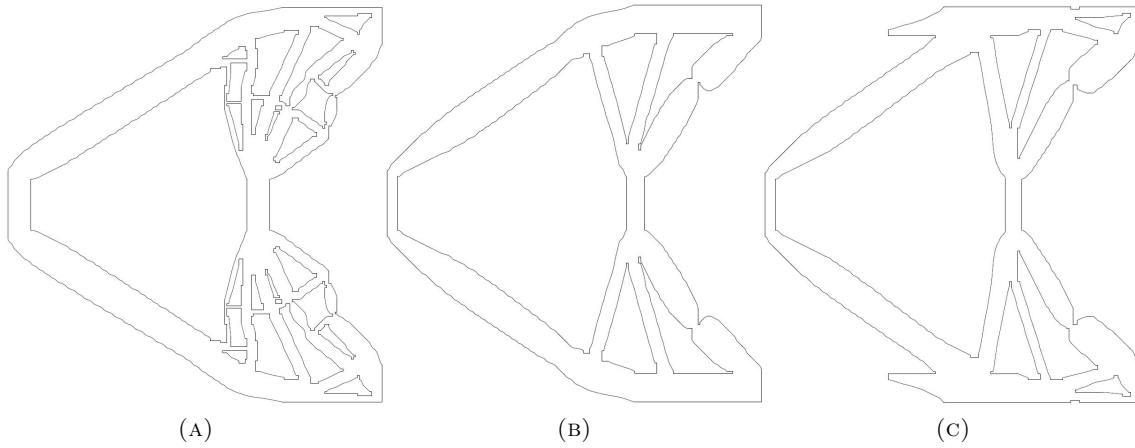
FIGURE 3.6: Three final gripper topologies: (A) Gripper #1: No stiffness constraints, (B) Gripper #2: Stiffness constraints in strategic region, (C) Gripper #3: Stiffness constraints in poorly placed region.

Poisson's Ratio of 0.498. The stress-strain curves of the material are shown in Figure 3.7, which were imported into ABAQUS/CAE and a Mooney-Rivlin hyperelastic material model was fitted. A mesh comprising of standard 3D stress elements with quadratic geometric order and hybrid formulation (C3D10H: A 10-node quadratic tetrahedron, hybrid, constant pressure), with an approximate global size of 2.5 mm was applied.
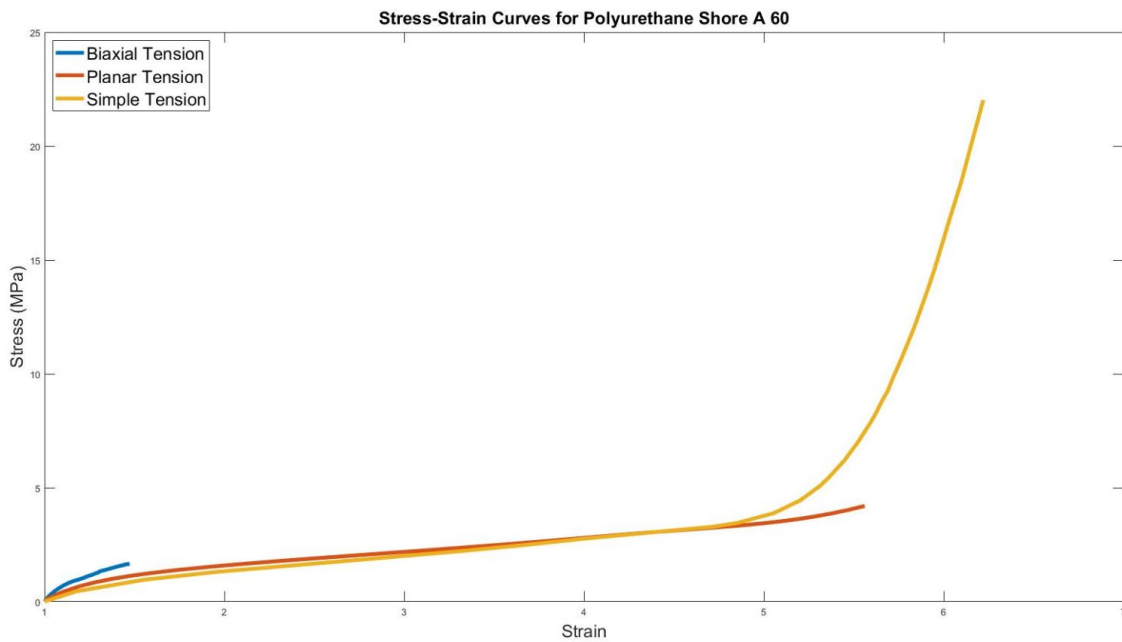
FIGURE 3.7: Polyurethane Shore A 60 stress-strain curves.

3.3.2.1 Simulation 1

Simulation 1 consisted of performing empty grasps with each of the three grippers. The grasping motion was achieved by applying displacement boundary conditions at the base of the grippers to simulate linear actuation by 85 mm along the x-axis only. In these simulations, no structural beam members were present. The aim of this simulation was to quantitatively compare the grippers' x-y displacements and input-to-output force ratio, thus the following parameters were measured during grasping simulations:

- Input and output displacements, defined as the positions where the forces $\mathbf{F}_{in}$ and $\mathbf{F}_{out}$ were applied in the design domains shown in Figure 3.4,

- Reaction forces from the input displacement actuation, measured at the input surface at the base of the gripper, and

- Contact forces generated at the fingertips of the gripper during closure.

In order to measure the contact forces at the grippers fingertips, contact interactions were required. Self-contact interactions were setup using a tangential penalised friction formulation with a friction co-efficient $\mu = 0.6$ and a normal pressure-overclosure with "hard" contact. These properties were applied to surfaces of the gripper which touched as the gripper deformed during actuation.

3.3.2.2 Simulation 2

Simulation 2 consisted of performing grasps on the structural beam members from target beam member set #1, using each of the three grippers. The aim of this simulation was to qualitatively compare the grippers' compliancy and adaptability to a range of beam member cross-sectional shapes.

Models of 30×30 mm beams from target beam member set #1 with 2.5 mm wall thicknesses were created as 3D discrete rigid shell extrusions. The finite element type assigned was a 4-node 3D bilinear rigid quadrilateral (R3D4) with an approximate global mesh size of 1 mm. The beam members were positioned in the simulation environment such that during

actuation, the gripper would grasp the beam member, making contact at the approximate points of the fixed pins 2_1 and 2_2 shown in Figure 3.3.

Similar to simulation 1, gripper self contact interactions were defined. Interactions between the gripper and the target beam member for grasping were setup using a tangential penalised friction formulation with a friction co-efficient $\mu = 0.64$ and a normal pressure-overclosure with "hard" contact. These properties were applied to surfaces of the gripper which made contact with the beam member during actuation, with the master surfaces being the structural beam member outer faces and the slave surfaces being the inner portions of the grippers fingers.

3.3.3   Results

3.3.3.1   Simulation 1

The simulated empty grasp results for each of the three grippers are presented below, with Figure 3.8 showing each of the grippers in two states, before actuation and after linear actuation by 85 mm.

The input and output displacements for each of the three grippers are shown in Figure 3.9, where the output paths of curvature resulting from linear input displacements can be observed. Comparing the three plots, gripper #2 has the smallest radius of curvature at the output, settling at a steady-state position of $(37.05, 85.70)$ when fully actuated. It should also be noted that there is a slight translation of the output in the positive x-direction at the end of gripper #2's curve, which can be attributed to the frictional contact at the fingertips.

By comparing the displacement plots in Figure 3.9 with the gripper final positions in Figure 3.8, it can be confirmed that the force applied at the input of gripper #2 is most efficiently transformed to an output force. This behaviour can be attributed to the effective placement of the stiffness constrained region, which aids in directing the output force towards the fingertips during actuation, rather than away from them. This can also be observed with gripper #3, but to a lesser extent, as the stiffness constrained region was not as effectively positioned.
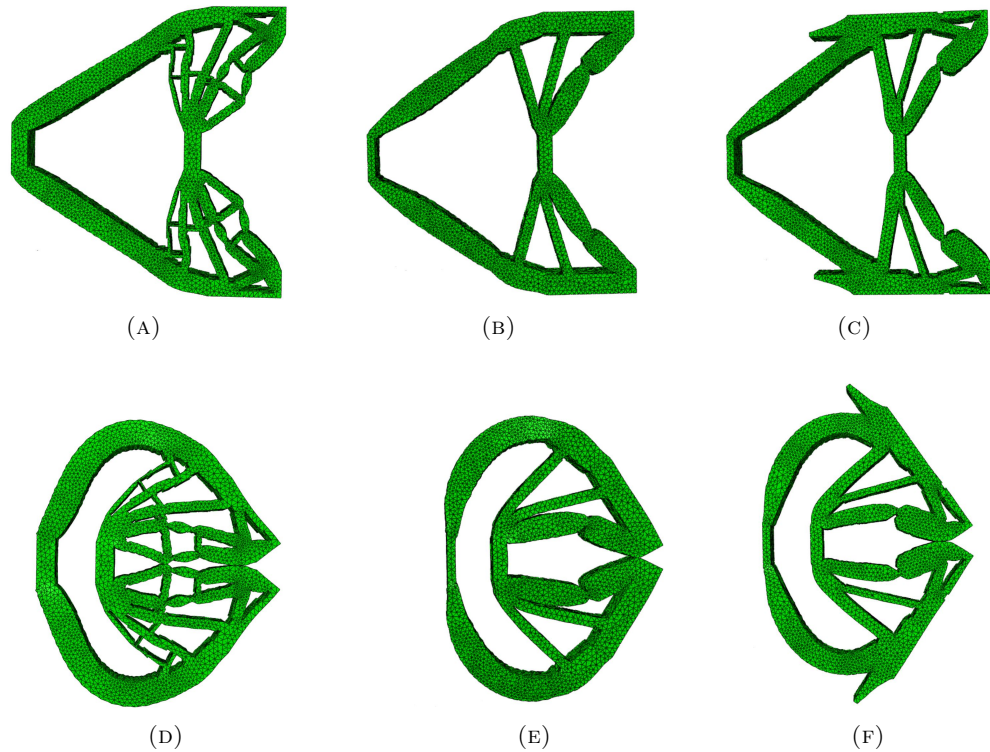
FIGURE 3.8: Grippers #1 – #3 in two positions during an empty grasp: fully opened position and fully closed position (linearly actuated 85 mm): (A),(D) Gripper #1; (B),(E) Gripper #2; (C),(F) Gripper #3.

To further analyse the grippers' performance, a force analysis was also conducted. Specifically, the monitored forces were the input reaction forces at the input surface as a result of the input displacement, as well as the contact forces generated at the fingertips of the grippers during actuation. Plots of the input and output forces are presented in Figure 3.10, where the average input surface reaction force is calculated by averaging the total force readings across a number of elements where the input displacement was applied. For ease of comparison, the input-to-output force ratio at the end of the linear actuation stroke can be calculated for each gripper, as summarised by Table 3.2. Gripper #1 is clearly not effective in transferring the applied input force to an output force, as the input-to-output force ratio is the highest out of the three topology optimised gripper designs. This demonstrates the need for the stiffness constrained topology optimisation method which can be observed as achieving much lower input-to-output force ratios, regardless of the effective placement of the stiffness constrained region, in this study. Intuitive and strategic placement of the stiffness constraints within the design domain has demonstrated in simulation,
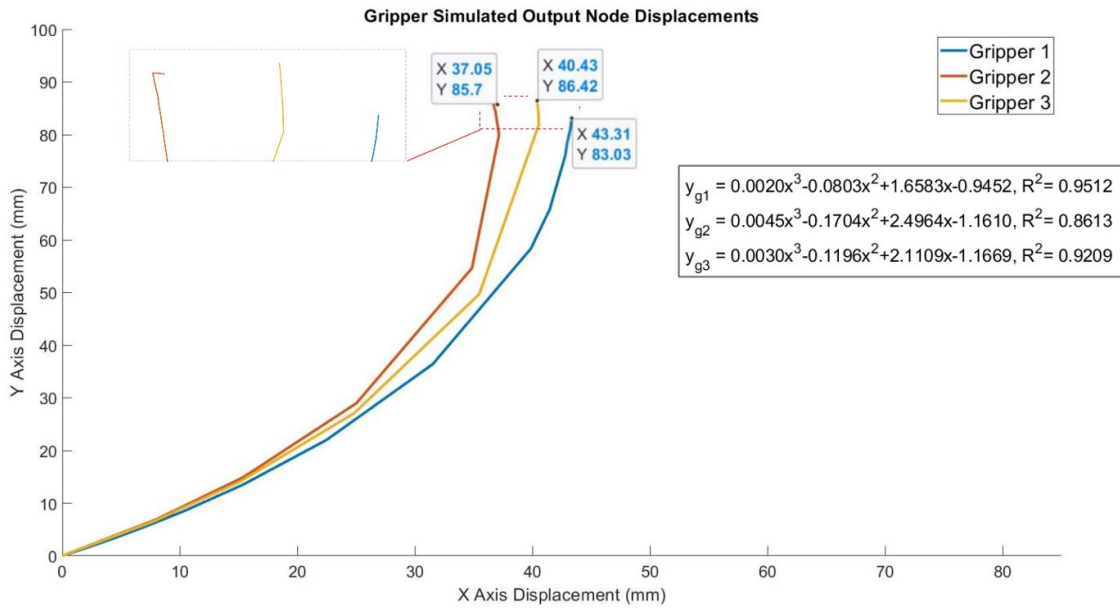
FIGURE 3.9: Grippers #1 – #3 empty grasp data: output x-y displacements.

to produce the lowest input-to-output force ratio of the three grippers.
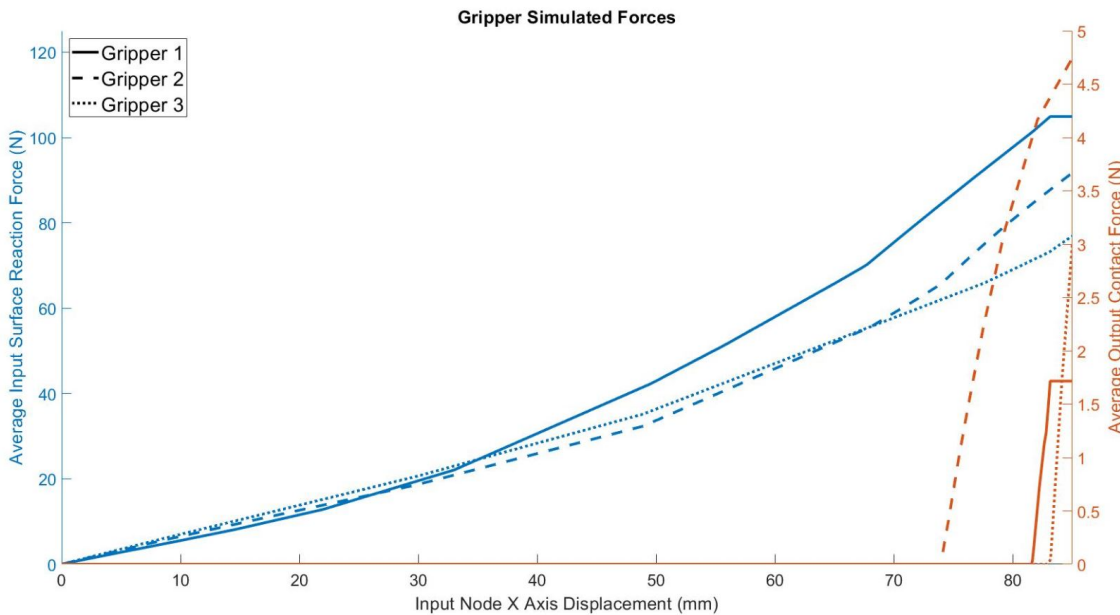
FIGURE 3.10: Grippers #1 – #3 empty grasp data: input and output forces.

An overall comparison of the contact forces as a result of input surface displacement is shown in Figure 3.11. Also shown in this plot is the output displacement of one of the gripper's fingertips with respect to the input displacement applied at the base of the gripper. The output displacement vector lines show that when the fingertips make contact with one

TABLE 3.2: Input and output forces and input-to-output force ratios for grippers #1 – #3 at 85 mm linear input displacement.

Gripper Number	Input Reaction Force (N)	Output Contact Force (N)	Input-to-Output Force Ratio
#1	104.91	1.72	60.99
#2	91.72	4.75	19.31
#3	76.94	3.01	25.56

another, there is little change observed in the output displacement, as the displacement is transformed into fingertip forces. In this plot, it is clear that the un-stiffened topology of gripper #1 has a significantly lower output contact force capability than that of the stiffened topologies, over the same input linear actuation distance. Moreover, gripper #2, with its strategically placed stiffness constrained region, produced the highest contact forces out of all of the gripper designs, and made self-contact at the fingertips earlier in the actuation stroke than the other two gripper designs. It can therefore be deduced that by strategically applying stiffness constraints to specific regions in the design domain, an effectively stronger gripper can be produced for grasping. One limitation of this gripper design that remains to be discussed further, however, is its severely limited output forces, as compared to rigid grippers.
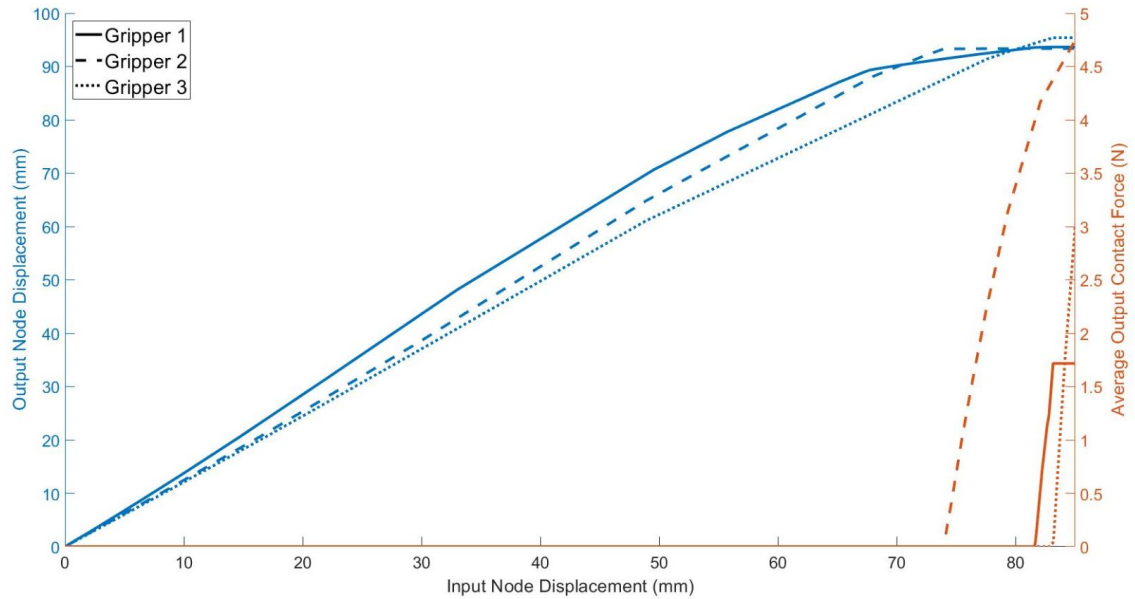
FIGURE 3.11: Comparison of grippers #1 – #3 output contact forces and output displacements.

3.3.3.2   Simulation 2

Due to the qualitative nature of this simulation, the results presented are brief, with the purpose of visually verifying the grippers' adaptability to a range of beam member cross-sectional shapes from target beam member set #1.

Detailed simulation results are shown in Appendix A. Figures A.1, A.2 and A.4 show that generally, each of the three grippers demonstrated some compliancy and adaptability to conform to the various beam cross-sectional shapes of target beam member set #1, given that the gripper contacted the beam members at the approximate points of contact defined by pins 2_1 and 2_2 in the topology optimisation design domain of Figure 3.3.

The material distribution of gripper #1's fingers results in a pinch style grasp being executed in simulation. This type of grasping is less reliable and stable than enclosing grasps, particularly for climbing applications, as typically fewer points of contact are made. Despite showing promise as an adaptive gripper, gripper #1 is less adaptive to the varying cross-sectional shapes of target beam member set #1 than grippers #2 and #3.

Grippers #2 and #3 show much more reliable performance in adapting to the range of cross-sectional beam member shapes. Each of the grasps executed typically resulted in full closure of the fingers of the grippers and therefore full enclosure of the beam members within the gripper. Furthermore, multiple points of contact have been achieved, which increases the stability and reliability of grasping. Grippers #2 and #3 would be considered suitable candidates for an adaptive climbing robot gripper, purely from an adaptability standpoint.

To further analyse the performance of gripper #2, beam grasps at varying AoAs to a 30×30 mm "L" shaped beam member from target beam member set #1 were conducted in simulation. Detailed figures are available in Appendix A. Figure A.3 shows the gripper's ability to conform to the 30×30 mm "L" beam regardless of position and orientation, so long as the gripper approaches the structural beam member perpendicularly.

3.4   Verification of a Prototype Soft Gripper

Section 3.3 verified that use of the stiffness constrained topology optimisation method with the design domain shown in Figure 3.4b produced a desirable topology. However, this design domain was sized such that the gripper would be able to grasp beam members from target beam member set #1. To enable grasping of a wider range of **sizes** of beam members (from target beam member sets #2 and #3), a larger gripper design domain is needed. Additionally, to meet the requirement of data collection during grasping, appropriate sensors are required to be integrated into the grasping platform. This section describes the design and verification stages for producing a prototype soft gripper, gripper #6, which is used for all subsequent research in this thesis.

3.4.1   Gripper Design

3.4.1.1   Gripper #2

Based on results presented in Section 3.3.3, gripper #2 was manufactured. The prototype gripper was moulded from Polyurethane elastomer F–180 A/B, Shore Durometer A 80 ± 5. A mould was assembled from five 4.5 mm thick laser cut sheets of acrylic with the topology of the gripper, which were stacked and secured together as shown in Figure 3.12 to achieve a gripper depth of 22.5 mm. Release agent was applied to the inner surfaces of the mould and the Polyurethane material was mixed and poured into the mould. Due to a lack of a suitably sized vacuum chamber, the material was not vacuum degassed during manufacture, resulting in visibly noticeable air bubbles throughout the structure. The presence of air bubbles would alter the material properties reported in the material datasheet, however the degree of this effect is unknown. After allowing to cure for 7 days, the mould was disassembled and the gripper prototype was extracted.

A linear actuator consisting of a geared micro DC motor coupled to a lead screw was mounted to the gripper as shown in Figure 3.13. During experimental testing of the gripper, the motor was driven Clockwise (CW) and Counterclockwise (CCW) to achieve the desired linear motion to open and close the gripper's "fingers".
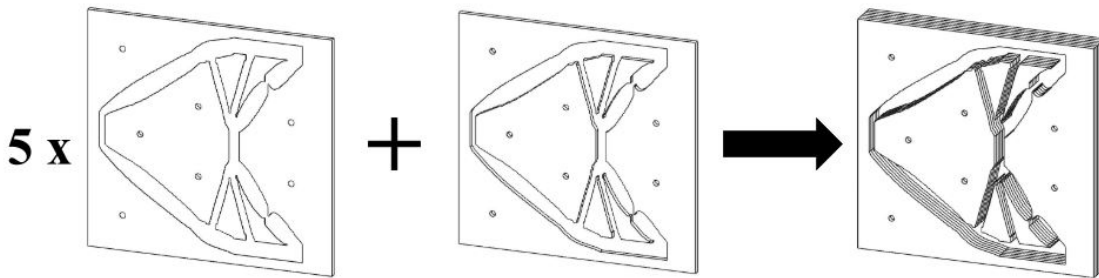
FIGURE 3.12: Gripper #2 mould assembly: five 4.5 mm through cut sheets stacked and mounted on a base plate etched with the gripper topology.
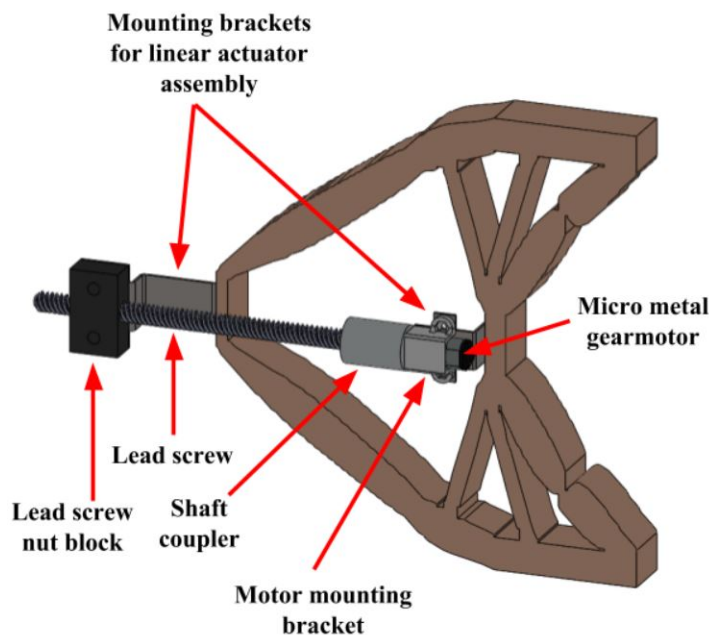
FIGURE 3.13: CAD model of gripper #2 with mounted linear actuator.

First, the motion of the gripper was observed without any beams present as shown by Figure 3.14a. Next, a length of a 30×30 mm "L" shaped beam member was clamped to a benchtop and several grasps at different AoAs were performed. The adaptability of each grasp was observed and the qualitative results were compared to those obtained from the simulations. Figure 3.14b shows the gripper grasping an "L" shaped beam member in two different orientations. The physical test results were similar to the ABAQUS/CAE simulations, despite simulation with a different Shore A Hardness of the Polyurethane material.

(A)   (B)
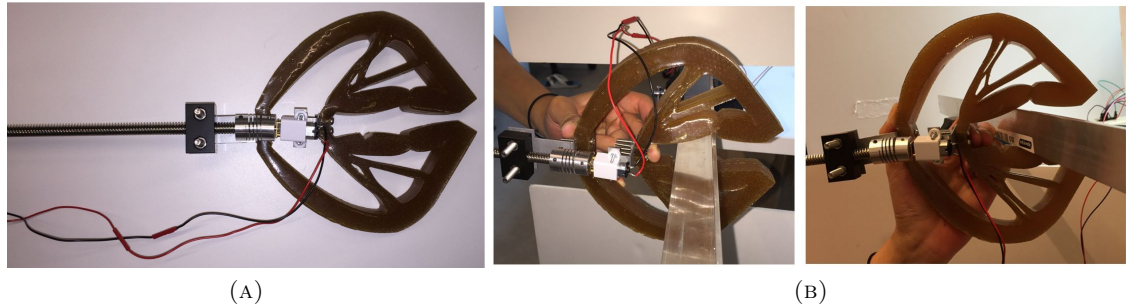
FIGURE 3.14: Prototype gripper #2 performing grasping actions: (A) An empty grasp, with input actuation displacement at approximately 80 mm, (B) A grasp at two AoAs (left: -90° and right: ±180°) to a 30 × 30 "L" shaped beam member.

3.4.1.2 Gripper #4

From the brief experiments discussed in Section 3.4.1.1, it was found that the finger surfaces of gripper #2 were stiffer than desired and therefore required a significant input force to actuate. To overcome this issue and to increase the compliancy of the gripper, a modified gripper (gripper #4), based on the topology of gripper #2 was designed. A comparison of the two grippers is shown in Figure 3.15. To produce gripper #4, gripper #2 was modified by creating more defined proximal and distal phalanges (based on the approximate dimensions of the existing finger sections) and increasing the gripper compliancy through addition of thin "joint" sections.
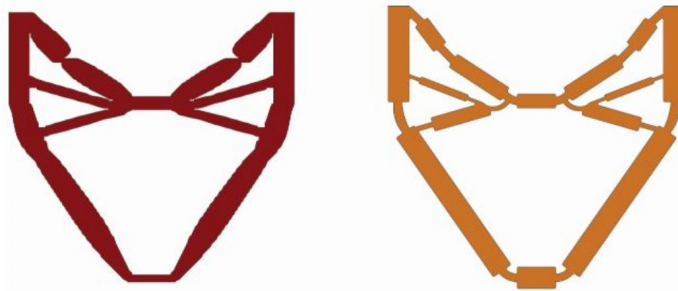
FIGURE 3.15: CAD model comparison of gripper #2 (red) and gripper #4 (orange).

A direct comparison of grippers #2 and #4 was briefly analysed. Gripper #4 performing an empty grasp can be seen in Figure 3.16a, where an input linear displacement of 85 mm was applied. Comparing the plots for grippers #2 and #4 in Figure 3.16b, it can be observed that the fingertips of gripper #4 make contact with one another as a result of an input displacement of 60.91 mm; as opposed to gripper #2, where 73.88 mm input

displacement was required before contact was initiated. Also shown in this plot is the output displacement of one of the gripper's fingertips with respect to the input displacement applied at the base of the gripper. This change in required actuation displacement can be attributed to the addition of the thin flexible joints, which have increased the overall compliancy of the grasping structure. This increase in compliancy, however, causes a decrease in output contact force (as demonstrated in Figure 3.16b), where a lower fraction of the force has been transferred to the output.
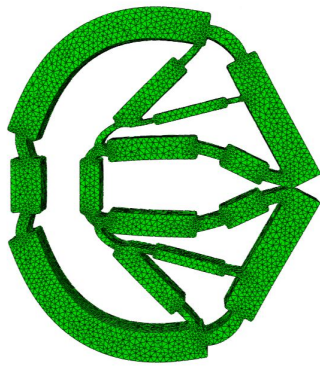
(A)
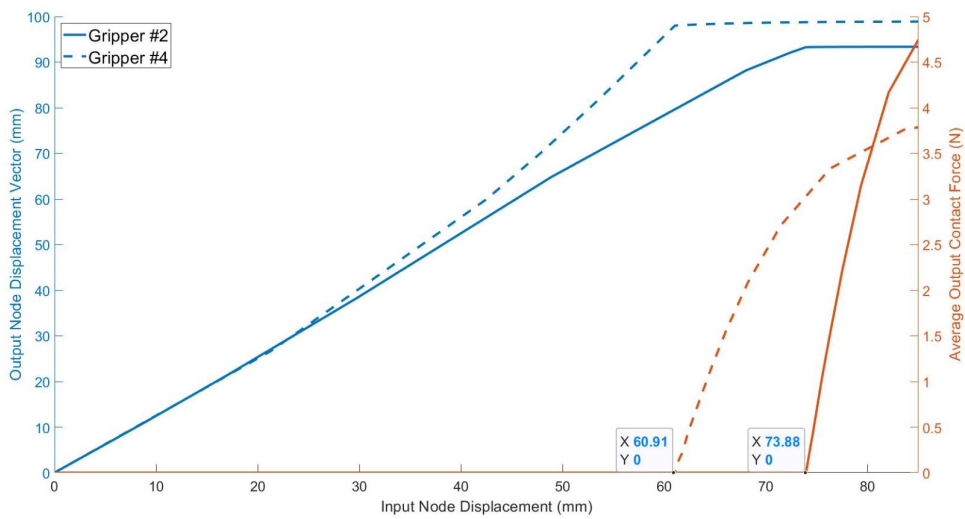
(B)

FIGURE 3.16: Gripper #4 empty grasping results: (A) Gripper deformation as a result of an empty grasp, (B) Comparison of gripper #2 and #4 contact forces and locations.

3.4.1.3 Gripper #5

To meet the functional requirements (as listed in Section 3.1) for the application environment, the design of gripper #5 is similar to the topology optimised material distribution of gripper #2 in Section 3.3. In order to grasp a wider range of sizes of structural beam members, however, the design domain for the topology optimisation method is scaled. Based on the sample of structural beam members listed in Table 3.4, the gripper must be able to grasp a maximum cross-sectional dimension of 75×75 mm, or 250% of the size of 30×30 mm beam members in target beam member set #1. Therefore, the design domain presented shown in Figure 3.4b is scaled by 250% and all dimensions are rounded up to produce the design domain for gripper #5. The gripper design domain settings, comparing to gripper #2 are summarised in Table 3.3.

TABLE 3.3: Individual gripper design domain settings summary; grippers #2 and #5.

Gripper Number	Design Domain Dimensions (mm)		Fixed Pins				Stiffness Constrained Region	
			1		2			
	x	y	x	y	x	y	x	y
#2	183	84	120	84	152	42	123:183	0:13
#5	458	210	300	210	380	105	308:458	0:33
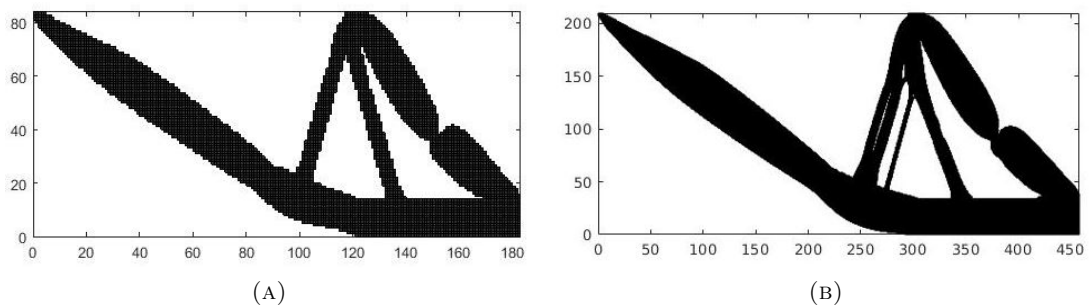
FIGURE 3.17: Stiffness constrained topology optimisation outputs: (A) Gripper #2, (B) Gripper #5.

The results of the stiffness constrained topology optimisation method with a scaled design domain can be seen in Figure 3.17b. One disadvantage to gripper #5 is its physical size and the large actuation stroke length required to achieve full closure of the gripper's fingers. To reduce the overall dimension of the gripper, the distance between the input actuation

port and pin 1 could be reduced, therefore reducing the overall x-dimension of the gripper and thus the required actuation stroke length.

3.4.1.4   Gripper #6

The final gripper (gripper #6) used for all subsequent research presented in this thesis—and which will be verified through simulations and experiments in the following section—was based on the design of gripper #5. Similar to gripper #4, however, some design modifications were made, considering the practical use of the gripper:

- Structural changes to increase "joint" compliancy and create more defined proximal and distal phalanges,

- Reduction of linear distance between input force and pin 1 to decrease the required linear actuation stroke length,

- Addition of a linear actuator for controlling the grasping motions of the gripper, and

- Retrofitting simple force sensors on the surfaces of the gripper's "fingers" for data collection during grasping.

In order to meet requirement of data collection during grasping, the prototype gripper needs to be appropriately equipped with reliable sensors. By using flexible and elastomeric materials, soft grippers have the benefits of inherent compliancy and adaptability, making a soft gripper ideal for adapting to a variety of cross-sectional shapes and sizes of beam members. This is beneficial from a sensing point of view, since the gripper can make sufficient surface contact with the beam members to determine the point/s of contact during a grasp. On the other hand, these soft gripper properties also make it very difficult to measure joint angles, calculate finger positions and achieve strength in grasping.

Soft grippers are continuum type mechanisms which inherently lack distinguishable, finite DOF. Due to structural compliancy, knowledge of a gripper's specific configuration at any given time is difficult. To further complicate the problem, as a gripper interacts with the environment, unconstrained and unpredictable deformations can arise. Sensor selection is

therefore highly dependent on the gripper design, actuation method and grasping application. In recent literature (see Sections 2.2.1.2 and 2.2.2.2), equipping soft robotic grippers with sensors has involved either retrofitting or embedding flexible or soft sensors within a gripper's structure during manufacture. By assuming CC, many different methods of proprioceptive sensing in soft grippers have emerged—where sensors typically change resistance with respect to an input force or strain. The accuracy of CC models is however limited by the nature of a soft gripper's interactions with the environment.

To meet the sensing requirement for reliable data collection, the prototype gripper does not incorporate any form of proprioceptive "joint position" sensing, as commonly seen in soft robotic grippers to date. Instead of relying on potentially erroneous proprioceptive sensing data, the effectiveness and suitability of using only exteroceptive force sensing (using an array of simple force sensors (FSRs)) and linear distance sensing (using a motor encoder and limit switches) are studied. This analysis is further conducted in the following chapters.

Figure 3.18 shows the complete soft gripper design, which incorporates a linear actuator for actuation and an array of FSRs for exteroceptive tactile sensing. The gripper was manufactured from Polyurethane elastomer F–180 A/B, Shore Durometer A 80 ±5, using the same manufacturing method as gripper #2 in Section 3.4.1.1.

An actuator is required to actuate the gripper for grasping a structural beam member. In this design, a linear actuator consisting of a Maxon A-max DC motor with planetary gearhead and Avago HEDS–5540 quadrature encoder, coupled to a lead screw is used. The motor enables the system to drive back and forth along the linear rail to open and close the gripper's fingers. At the extremities of the linear actuator stroke are two limit switches which prevent the gripper from opening and closing too far.

The exteroceptive sensing consisted of an array of 18 small, COTS Interlink FSRs (FSR 400 Short—Figure 3.19) each connected to an analog pin of a Teensy 3.6 microcontroller in the voltage divider configuration shown by Figure 3.20a. In this configuration, the output voltage increases with increasing force according to:

(A)

(B)
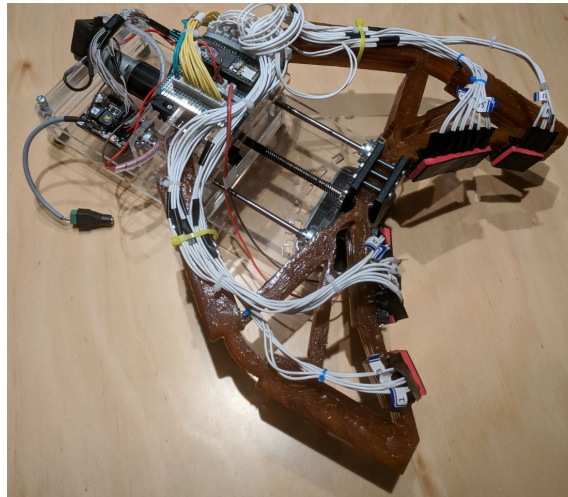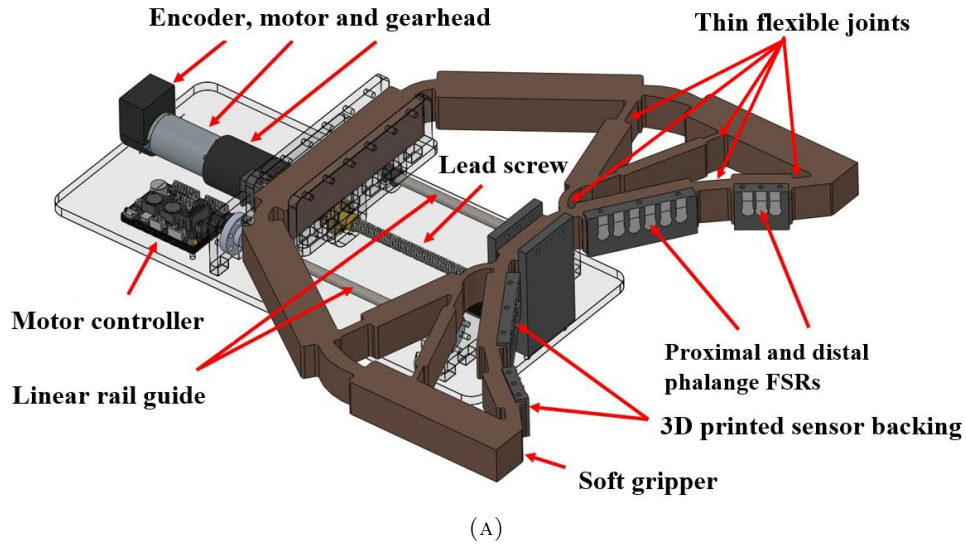
FIGURE 3.18: Gripper #6 prototype design: (A) CAD design of gripper with actuator and sensors. (B) Physical gripper with controller, actuator and sensors wired.

$$V_{out} = 3.3 \times \frac{R_{FSR}}{R_2 + R_{FSR}} \tag{3.7}$$

Scaling this voltage from the maximum voltage of 3.3 V to 5 V and cross-referencing with the typical force vs voltage curve for the $R_2 = 10k\Omega$ resistor shown in Figure 3.20b, the force applied to an individual sensor can be determined. It should be noted that these FSRs were only intended for contact detection, therefore only the raw analog values were interpreted for feature extraction purposes. Should the output forces be required for
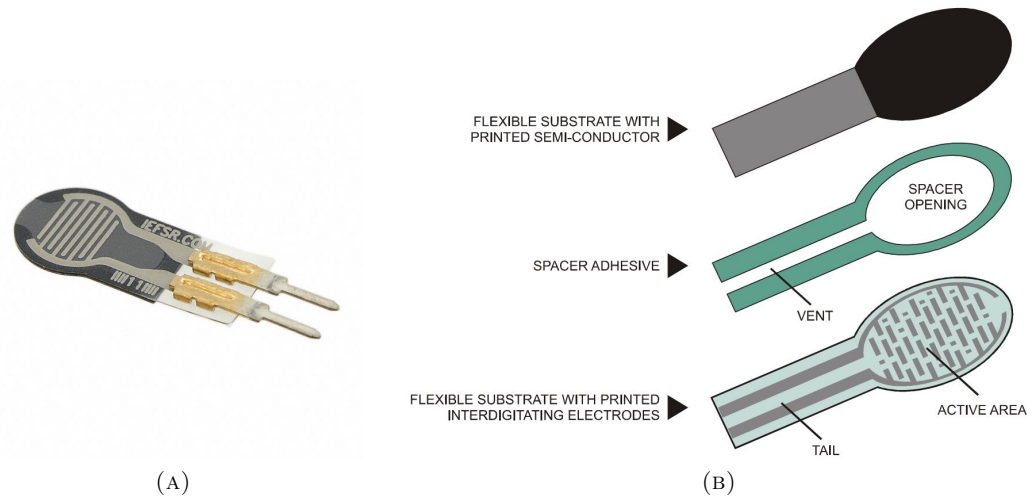
FIGURE 3.19: Interlink FSR 400 Short details: (A) Sensor, (B) Sensor construction showing individual layers [182].

analysis, force vs voltage curves would be generated and averaged across each of the 18 FSRs used for varying force inputs. This would allow for an accurate system representation that is specific to the sensors used, instead of adapting a generic curve response as provided by the product datasheet.
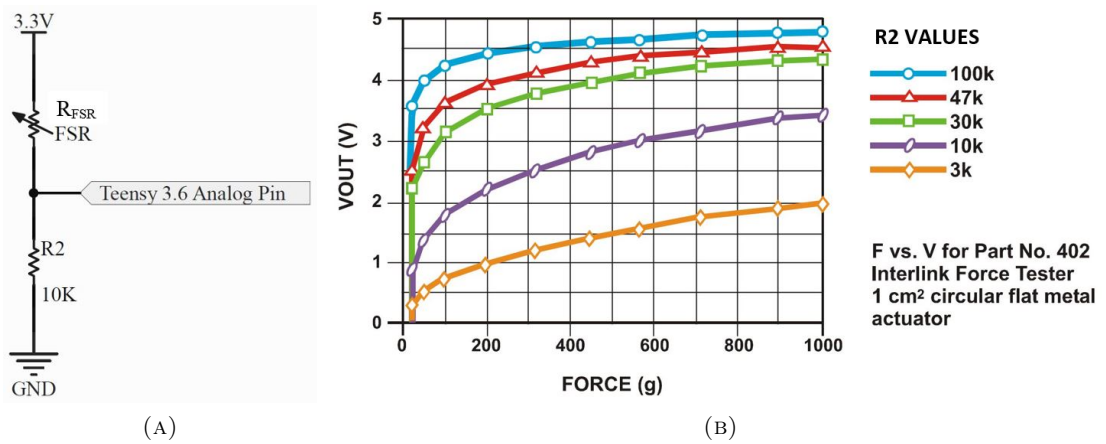
FIGURE 3.20: FSR connection and performance details: (A) Electrical schematic for connection to Teensy 3.6 microcontroller, (B) Typical force vs voltage curves for a voltage divider configuration [182].

Six sensors were placed on each of the proximal phalanges and three on each of the distal phalanges of the two fingers as shown in Figure 3.18a. These FSRs were selected as they could be easily retrofitted to the soft gripper in an arrangement that was anticipated would

provide sufficient grasping data. The arrangement of sensors and their numerical labels can be found in Figure 3.21.
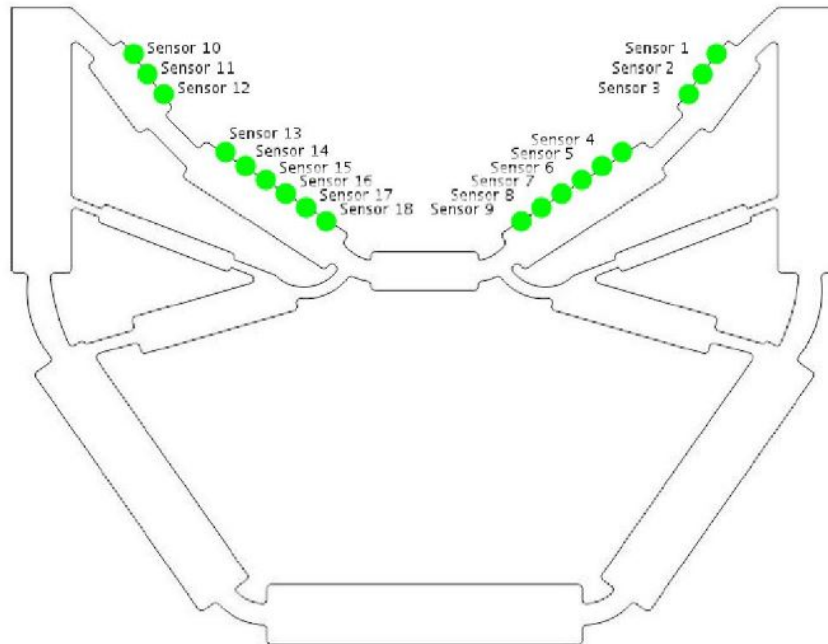
FIGURE 3.21: Gripper #6 FSR arrangement.

Typically, FSRs do not function reliably without a firm, flat and smooth mounting surface. Additionally, to protect the device from sharp objects, such as the edges of structural beam members during grasping, it is recommended to use an elastomer to prevent gouging of the FSR device [182]. In the design of this prototype soft gripper, 3D printed sections were used to both secure the sensors to the inner finger surfaces and to ensure that the sensors were evenly spaced along the surface of the fingers. The 3D printed sensor backing also allowed for reliable and repeatable readings due to its rigidity.

Due to the sparseness of the sensor distribution, in certain scenarios during grasping it was possible for a contact to occur directly between two sensors. In this scenario, the sensors on either side of the contact would not register a force. This is represented by the red markers in Figure 3.22a, which show the FSRs which would be expected to register a force under normal operation. To aid in force distribution to overcome this issue, the FSRs were covered with a 3 mm layer of PE–180 foam and covered with a 1 mm thick rubber sheet. All layers were adhered together using 3M clear double sided tape. A cross-section

of the final assembly is shown in Figure 3.22b, where it can be seen that —- in this new configuration — the FSRs are able to correctly register forces.
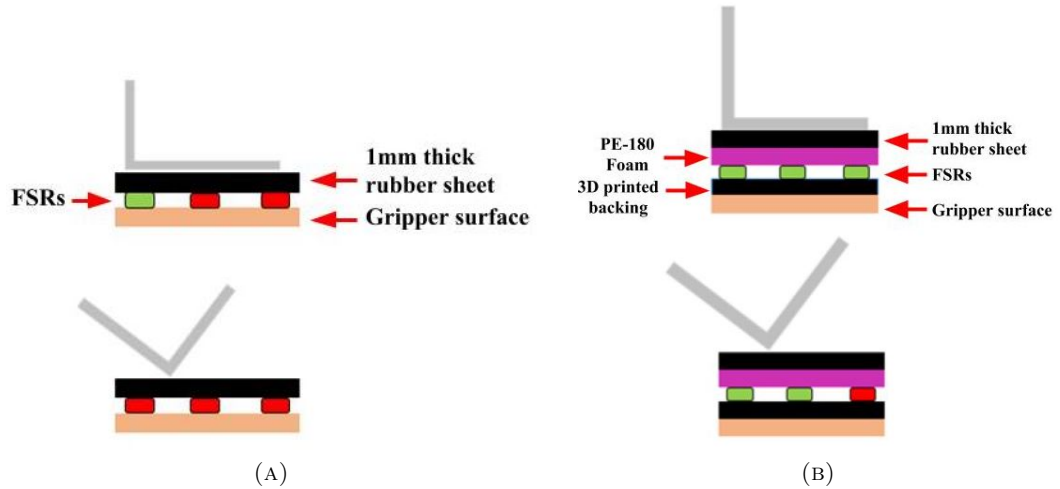
FIGURE 3.22: : Sensor design layout for gripper #6 (sensors able to register a force are denoted by the green markers, sensors unable to register a force are marked as red): (A) Original design with poor pressure distribution (B) Final design with improved pressure distribution.

3.4.2 Simulations and Experiments

In this section, the simulations and experiments conducted to verify the design of gripper #6 are presented. Gripper #6 was first verified through simulation by observing its adaptability to the 250% scaled beam members from target beam member set #1. Then, the gripper was manufactured for physical experimental verification. This involved grasping beam members from target beam member sets #2 and #3 and recording grasping data at each of the AoAs shown in Table 3.4 for further analysis. The entries marked "N/A" in Table 3.4 refer to the structural members that were only grasped in simulation.

3.4.2.1 Simulation 1

Simulation 1 consisted of performing an empty grasp simulation with gripper #6 to qualitatively record the required input displacement for actuation, as well as the input and output forces, similar to the simulations conducted in Section 3.3.2.1.

TABLE 3.4: Target beam member sets and their structural beam member shapes, sizes and AoAs for data collection. This listing represents an *example of* possible structural beam members which may be found in a truss structure.

Structural Beam Member Shape	Cross-sectional Dimensions (mm)	Included in Target Beam Member Set (#)	AoAs for Data Collection
"L"	30×30	1	N/A
	50×50	2,3	$0° \rightarrow \pm 180°$
	75×75	2,3	$\pm 180° \rightarrow -10°$
	100×100	2	
"O"	ø 30	1	N/A
	ø 63	2	$0°$
"+"	30×30	1	N/A
	50×50	3	$0° \rightarrow -80°$
	75×75	3	
"T"	30×30	1	N/A
	50×50	3	$0° \rightarrow \pm 180°$
	75×75	3	$\pm 180° \rightarrow -10°$
"I"	30×30	1	N/A
	50×50	3	$0° \rightarrow -170°$
	75×75	3	
Square	30×30	1	N/A
	51×51	2,3	$0° \rightarrow -80°$
Rectangular	81×25	2	$0° \rightarrow -170°$

3.4.2.2 Simulation 2

Simulation 2 consisted of beam member grasping simulations to verify that gripper #6 would be able to adapt to a scaled ($250\% \times 30\text{mm} = 75\text{mm}$) range of the structural beam members in target beam member set #1.

3.4.2.3 Experiment 1

Experiment 1 was conducted using the manufactured prototype of gripper #6 which had been verified through simulation in the previous experiment. The grasping platform used for this experiment consisted of the soft gripper, FSRs and linear actuator as shown in Figure 3.18b. In this experiment, data was collected by performing *haptic glances* (enclosing grasps) of structural beam members from target beam member set #2, at the AoAs listed in Table 3.4.

First, the experimental rig was set up to enable repeatable grasps of target beam members at a variety of AoAs and set distances, depending on the beam member dimensions. The experimental rig consisted of a beam member from the target beam member set, gripper with linear actuator and angle measurement tool as shown by Figure 3.23.

The angle measurement tool was fixed to the target beam member and was used to perform repeatable grasps at a given AoA and distance from the surface of the beam members. This tool consisted of a circular structure with alignment holes at $\beta = 10°$ increments, located at varying radii from the centre of the target beam members. These holes were used to lock the linear actuator to the angle measurement tool at the desired AoA for data collection.
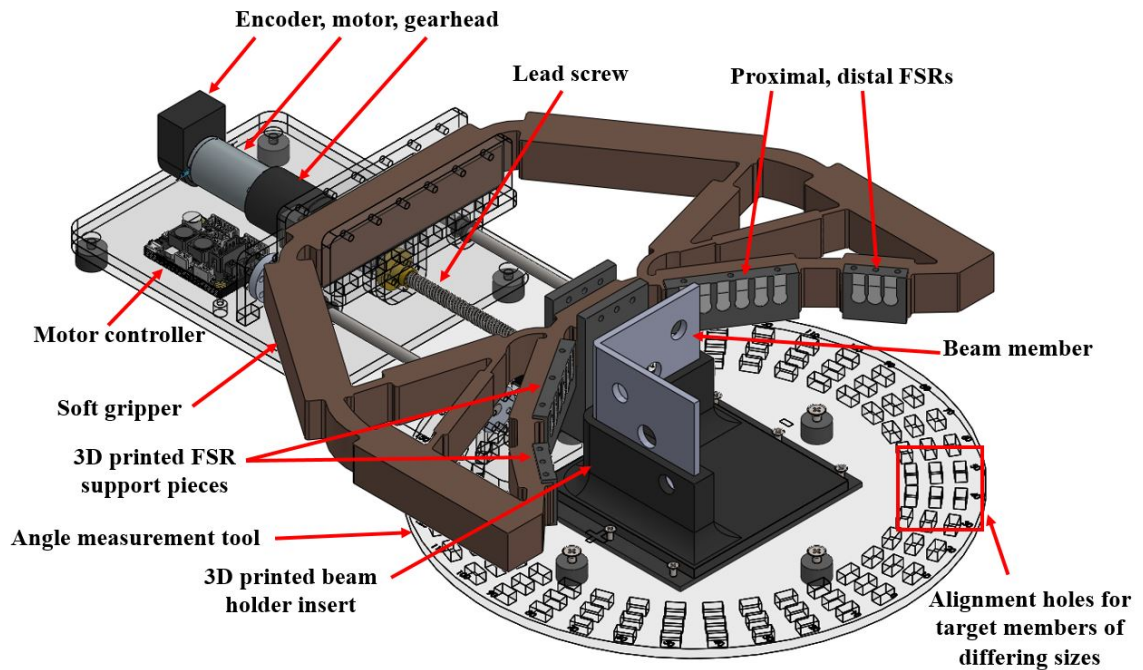
FIGURE 3.23: CAD model of data collection rig setup with gripper #6.

Depending on the cross-sectional shape and symmetry of the structural beam members in target beam member set #2, different AoAs were used for data collection in $\beta = 10°$ increments as listed in Table 3.4. Data from the $N_{FSR} = 18$ individual FSRs, limit switches and motor encoder were recorded for further analysis.

The data collection procedure consisted of the following steps:

1) Attaching the angle measurement tool to a beam member using an interchangeable 3D printed beam holder insert,

2) Manually positioning the gripper to a desired AoA for data collection and locking the linear actuator base into the angle measurement tool by using the alignment holes,

3) Driving the linear actuator back and forth to open and close the gripper $N_g = 10$ times. Data from the $N_{FSR} = 18$ individual FSRs, limit switches and the motor encoder was recorded for each *haptic glance* at the end of the linear actuator stroke length, defined by either the high limit switch being triggered or the motor current limit (user defined at 325 mA).

4) Manually shifting the gripper by $\beta = 10°$ and repeating the above steps for each of the AoAs listed in Table 3.4 for target beam member set #2. Figure 3.24 shows the AoA definitions for the beam cross-sectional shapes of target beam member set #2.
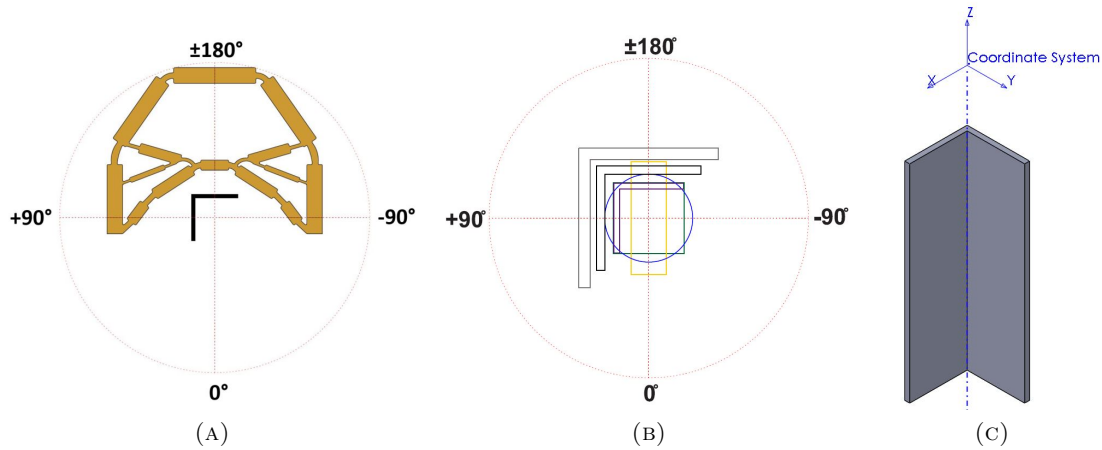
FIGURE 3.24: AoA definitions for target beam member set #2: (A) "L" shaped beam members, (B) All beam members in target beam member set #2, (C) Co-ordinate frame for orientations—only consider rotations about the z-axis i.e. gripper yaw.

To ensure a consistent experiment setup and to control the parameters during data collection, the gripper was positioned to always approach beam members perpendicularly (i.e. as shown in Figure 3.23) and at a set linear distance from the centre of the beam member, but with variable angular positioning around the beam member. The centre is denoted by the centroid of the structural member and is marked by the intersection of the two dotted
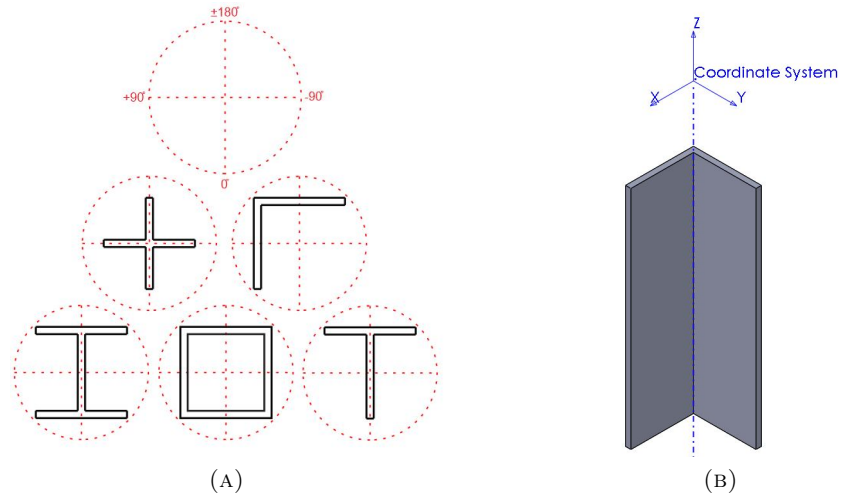
FIGURE 3.25: AoA definitions for target beam member set #3: (A) All beam members in target beam member set #3, (B) Co-ordinate frame for orientations—only consider rotations about the z-axis i.e. gripper yaw.

red lines in Figure 3.24 and 3.25. It should be noted that the gripper also sagged due to gravity, which was uncorrected during grasping. Due to the gripper sag, some shear forces were observed during the experiments, which the FSRs used in this gripper are incapable of measuring.

The set distance from the centre of the target beam member was selected by considering climbing in the practical application environment, where power grasps [54] are ideal. Executing power (or enclosure) grasps typically results in strong and reliable grasps, with sufficient data for feature extraction since the gripper can make significant contact with the beam member surface/s. Increasing or decreasing the set distance would result in precision (pinch) grasps [54] at either the distal or proximal phalanges respectively. Precision grasps are not desirable for the practical application environment as they are not sufficient for supporting the weight of a climbing robot. Additionally, precision grasps involve contacting a beam member at two points, which would not provide sufficient data for beam member recognition—which is the main purpose of the data collection.

3.4.2.4   Experiment 2

Experiment 2 was performed to further test the data collection procedure on a set of beam members with similar cross-sectional shape, that is, the structural beam members in target beam member set #3. The data collection procedure described in Section 3.4.2.3 was repeated, to collect data for the structural beam members included in target beam member set #3. Data from the $N_{FSR} = 18$ individual FSRs, limit switches and motor encoder were recorded for further analysis. The grasping AoAs for the beam members of target beam member set #3 are defined in Figure 3.25.

Depending on the symmetry of the beam members, different AoAs were used for data collection in $\beta = 10°$ increments. For symmetrical members, fewer AoAs were used for data collection, due to repetition, as listed in Table 3.4.

3.4.3   Results

3.4.3.1   Simulation 1

By scaling up the gripper design domain by 250% to produce gripper #5, the linear actuation stroke length required to achieve contact at the gripper's fingertips would be expected to be 250% × 60.91 mm = 152.28 mm. This results in an excessively large gripper being produced. To alleviate this issue, the gripper design domain was compressed to produce gripper #6. By compressing the gripper design, the required stroke length to perform an empty grasp (i.e. achieve full closure of the grippers fingers to meet at their tips) was reduced to 107.2 mm as shown in Figure 3.26a. As Figure 3.26b shows, the total input stroke length of the motor was 125 mm, however, the required input force increases significantly after the gripper's fingers meet at 107.2 mm. Furthermore, the output force also increases from zero, due to the contact of the two fingers.

3.4.3.2   Simulation 2

Gripper #6 was then simulated to grasp each of the 250% scaled structural beam members from target beam member set #1 to observe the adaptability to the various cross-sectional

(A)

(B)
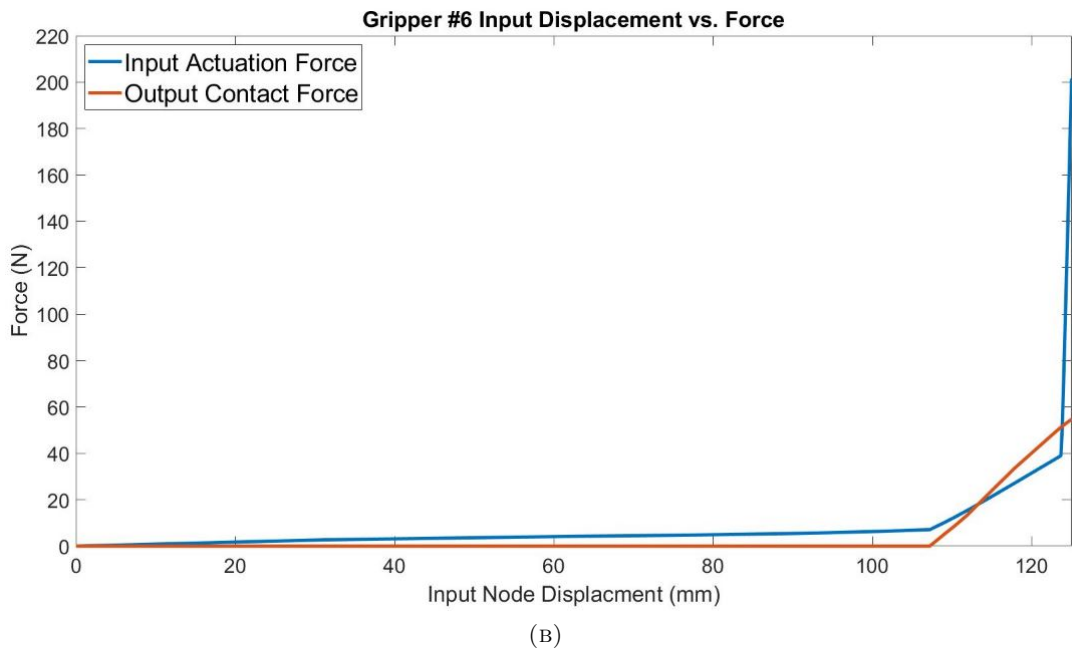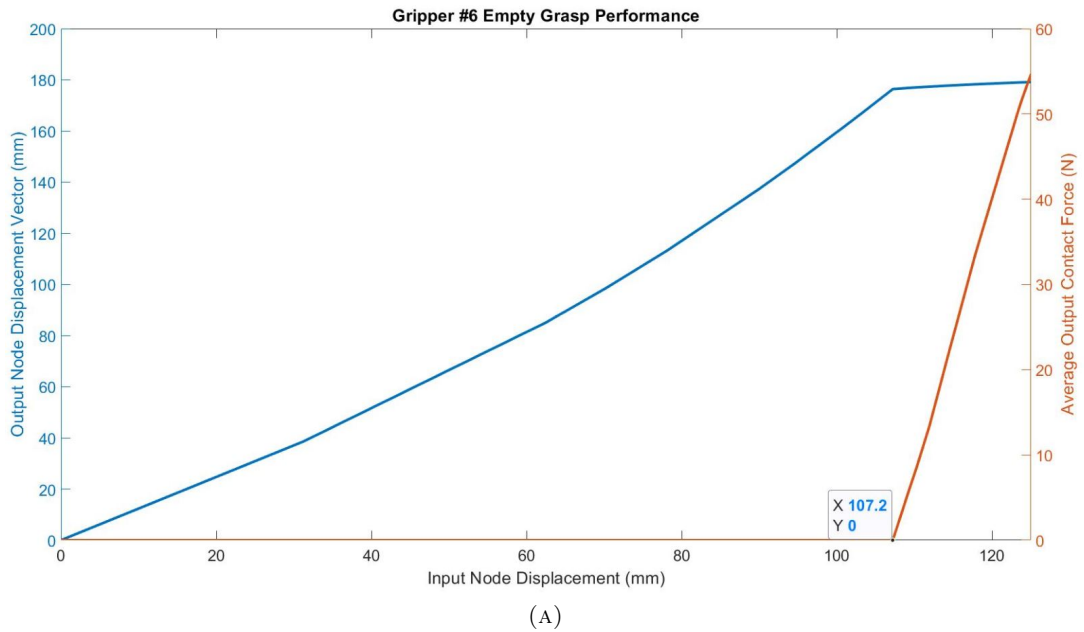
FIGURE 3.26: Gripper #6 empty grasp results: (A) Input displacement vs output displacement vector and average output contact force, (B) Input displacement vs input actuation force and output contact force.

shapes. The results of this qualitative study can be observed in Appendix A, Section A.1.4, where the gripper is seen to proficiently grasp each of the cross-sectional shapes of structural beam members with sufficient surface contact.

3.4.3.3   Experiment 1

To evaluate the gripper design for meeting the sensing requirement, the collected *haptic glance* sensor data was analysed to verify the gripper's adaptability to various target beam members. The raw data is briefly analysed in this chapter, with Chapter 4 detailing a more extensive evaluation. Chapter 4 covers a brief analysis of the sensor arrangement, which is assessed by verifying that the collected grasping data was sufficient for recognising a structural beam member and its properties.

For all of the beam members in target beam member set #2, the averaged raw FSR data (shown in Figure 3.27) across all of the AoAs showed that sensors 1–3 and 10–12 were almost redundant, except for when grasping the larger structural beam members in the target beam member set. Cross-referencing this data with the sensor arrangement shown in Figure 3.21, it can be seen that these somewhat redundant sensors are all located on the distal phalanges of the gripper. The remainder of the sensors were typically making contact with the structural beam members across all AoAs.

Figure 3.28 shows the gripper at two time instances (fully open and fully closed states) during data collection at -40° for an "L" shaped beam member.

For the beam members grasped in this experiment, generally, unique *tactile patterns* were collected for each of the AoAs used for data collection. Figure 3.29 shows an example of averaged raw data from the $N_g = 10$ repeated grasps performed at AoAs from -10° to -90° in β =10° increments for two of the "L" shaped beam members from target beam member set #2 (75×75 mm and 100×100 mm). For each of the AoAs shown, unique *tactile patterns* can be observed. This observation generally extends to the remaining AoAs to beam members from target beam member set #2, with the exception of the problematic AoAs discussed below.

Upon analysis of the experimental data, similarities in the FSR and encoder readings were detected. One such example occurred when grasping at the AoAs of -100° and -140° to the 50×50 mm "L" shaped beam member and the AoAs of -10°, -170° and ±0° to the 81×25 mm rectangular shaped beam member. At these AoAs, the linear actuator reached the extremity of its stroke length and the gripper's fingers were not contacting any surfaces of

(A)

(B)
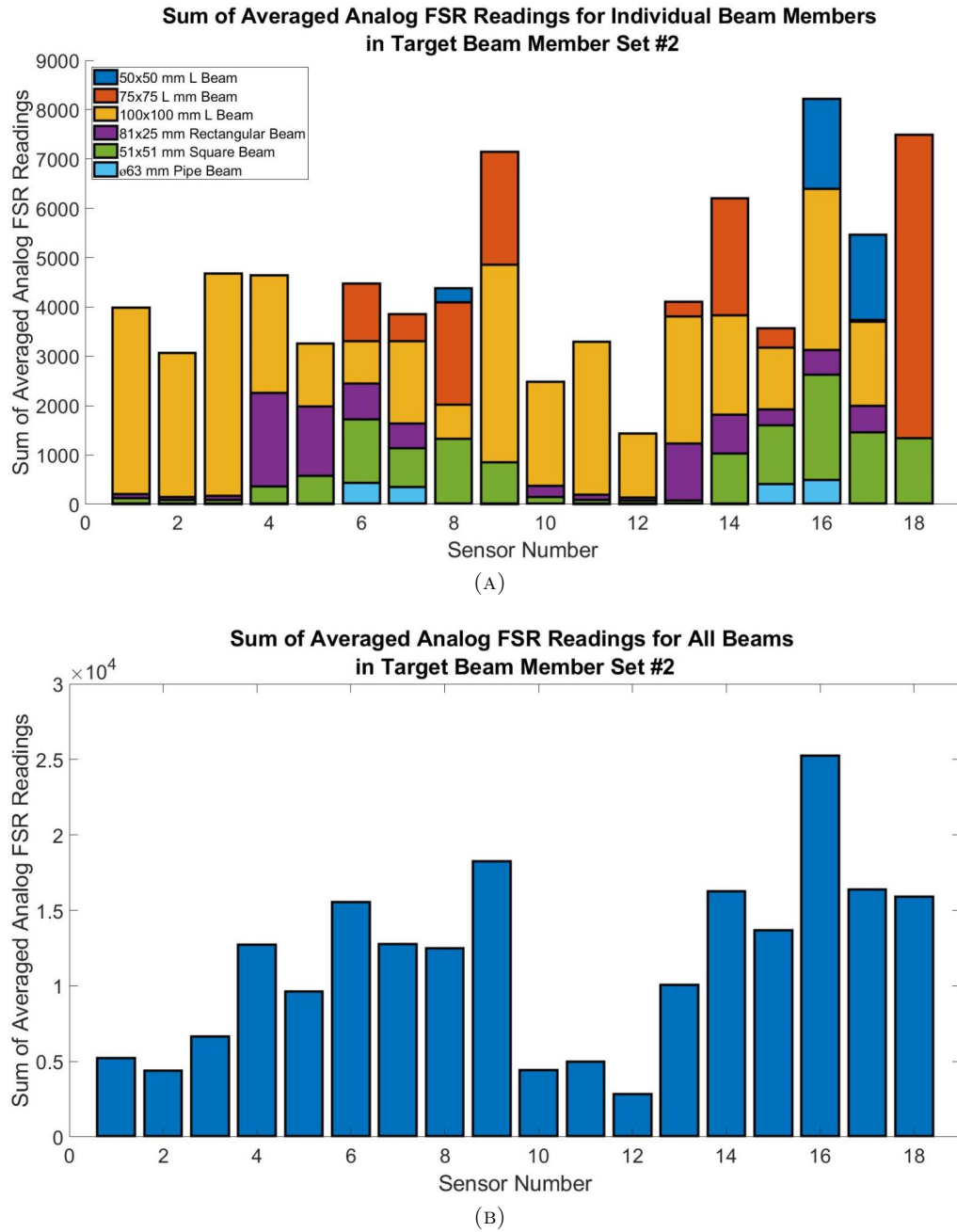
FIGURE 3.27: Sum of raw analog FSR readings for each of the AoAs used for data collection for target beam member set #2: (A) Individual structural beam members, (B) All structural beam members.

the target beam members. Figure 3.30 shows the averaged FSR data and encoder readings for these low data AoAs.

Certain AoAs for different target beam members were also observed to have yielded very similar FSR and motor encoder distance readings. This was expected to occur when
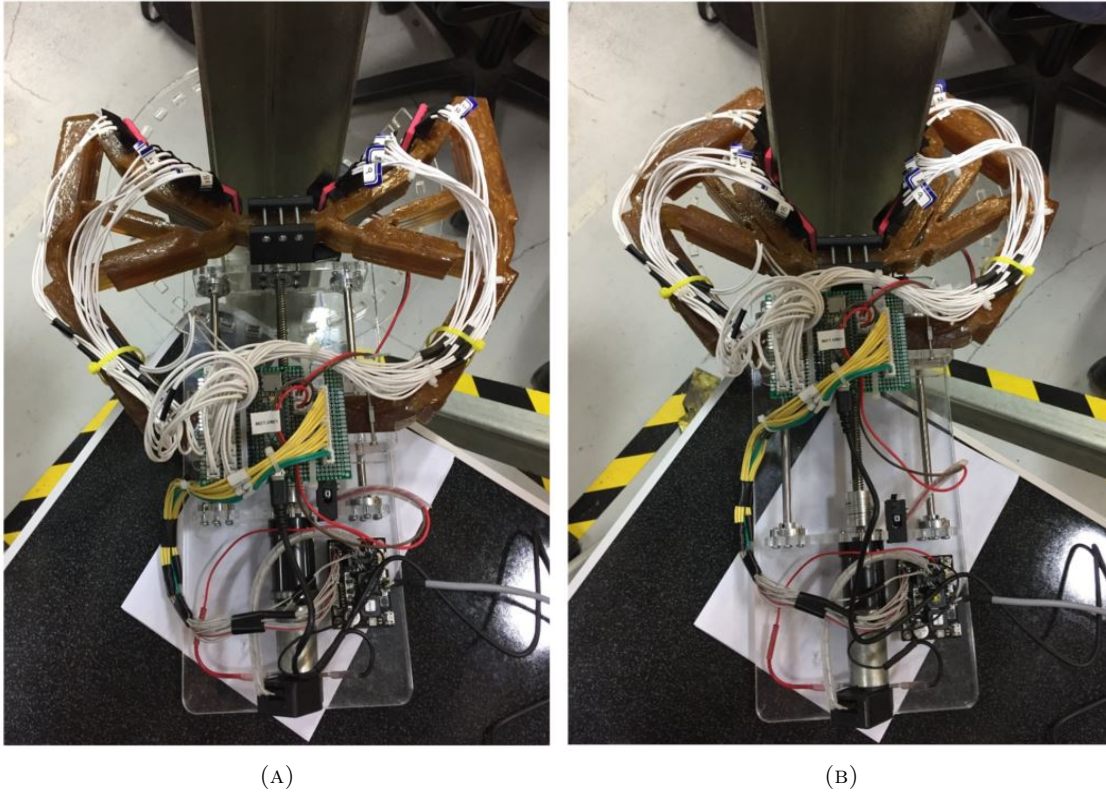
FIGURE 3.28: Gripper pose during data collection, positioned at -40° on a 75 × 75 mm "L" shaped beam member: (A) Fully opened, (B) Fully closed.

grasping "L" shaped beam members at the orientations of +90° and ±180°, since at these AoAs, the gripper was grasping at two edges, equidistant from the axis of symmetry of the gripper. However, due to one edge having a greater surface area than the other, unique *tactile patterns* were generally recorded, and the *tactile patterns* of +90° and ±180° were simply mirror images of each other. In some cases, due to slight misalignment in the AoA, the *tactile patterns* on both fingers appeared identical. Another scenario with limited data was observed when a major edge of a target beam member fell between the proximal and distal finger sections (where no sensors were located) during a grasp.

3.4.3.4   Experiment 2

Similar to the results of experiment 1, for all of the beam members in target beam member set #3, the averaged raw FSR data (shown in Figure 3.31) across all of the AoAs showed that, sensors 1–3 and 10–12 were almost redundant. Once again, this can be attributed

(A)

(B)
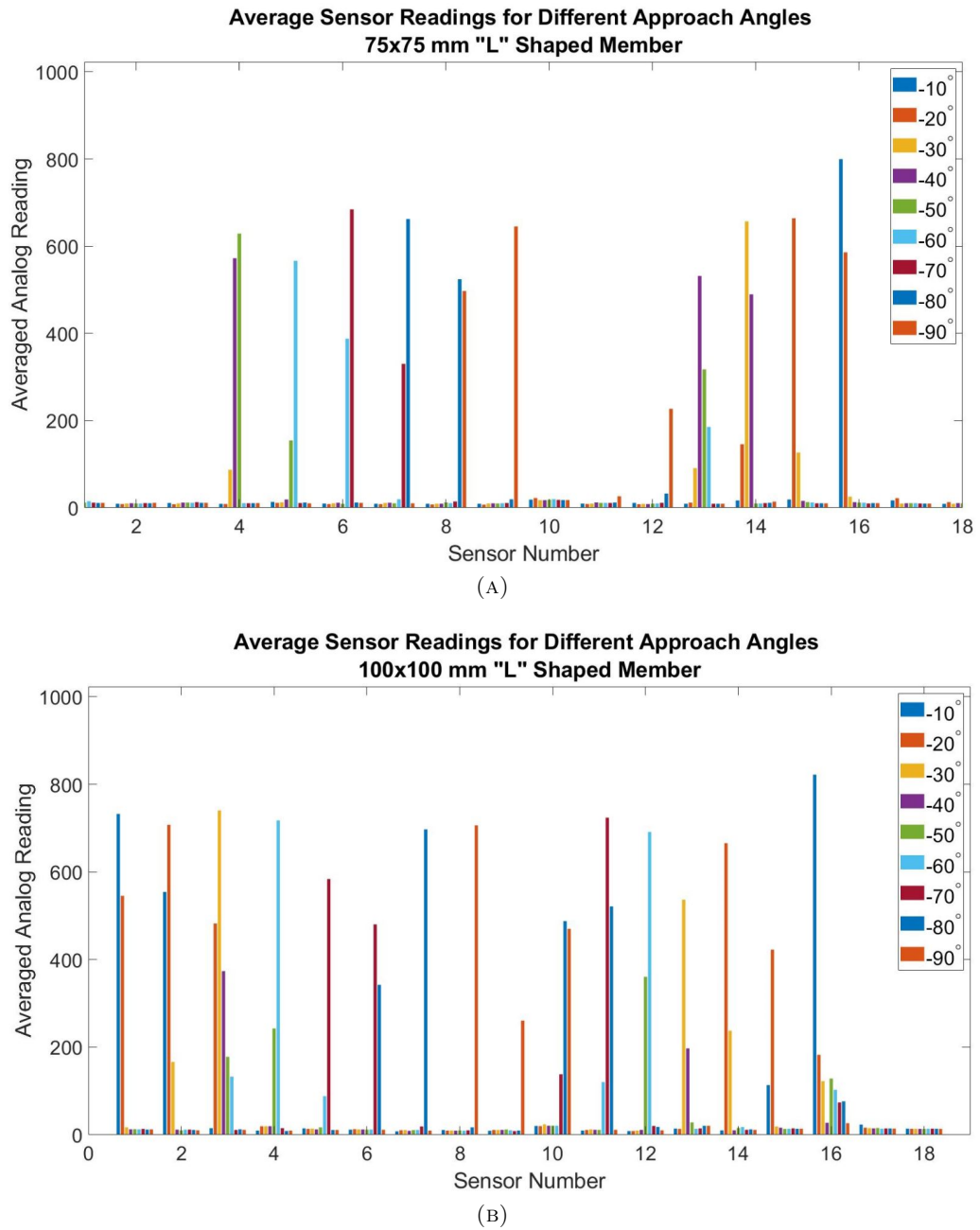
FIGURE 3.29: Averaged raw FSR readings (from $N_g = 10$ repeated grasps) across 9 AoAs (-10° to -90° in $\beta =$10° increments) for two beam members from target beam member set #2 and #3: (A) 75×75 mm "L" shaped beam member, (B) 100×100 mm "L" shaped beam member.

to the overall size of the structural beam members in the target beam member set. The remainder of the sensors were typically making contact with the structural beam members across all AoAs, with the exception of the 50×50 "+" shaped beam member, where minimal contact points were made throughout grasping at all of the data collection AoAs.

(A)

(B)
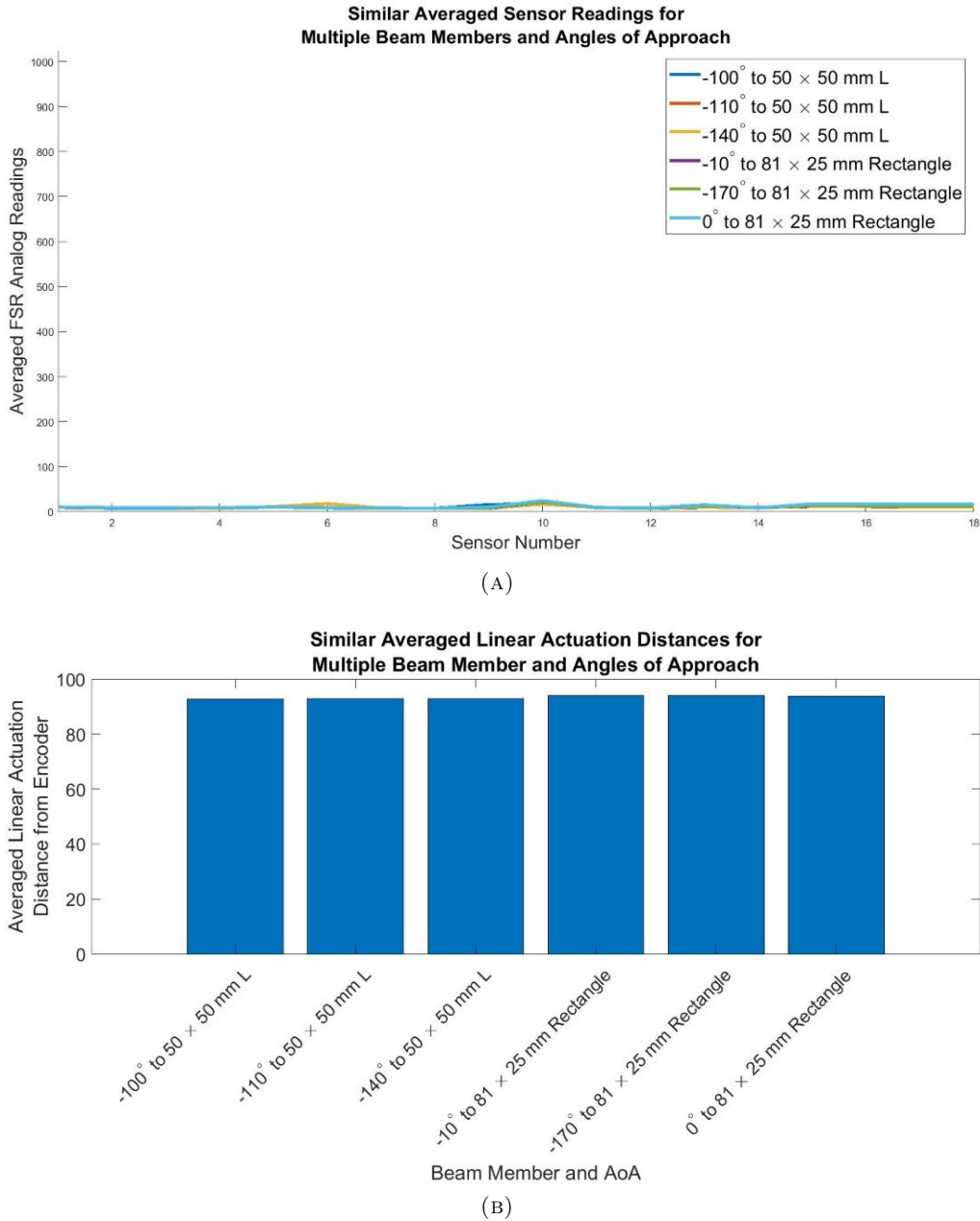
FIGURE 3.30: Similar sensor readings for AoAs to multiple target beam members: (A) Averaged FSR data for low data AoAs, (B) Averaged linear actuation distance for low data AoAs.

By introducing beam members of similar cross-sectional shape into the target beam member set, increased overlap in *tactile patterns* was observed at particular AoAs. In some identified cases, similar data existed between multiple beam members, particularly those of identical sizes or between different AoAs to a single beam member. Further analysis revealed that repeated AoAs (for symmetrical cross-sectional shapes), or similar *tactile*

(A)

(B)
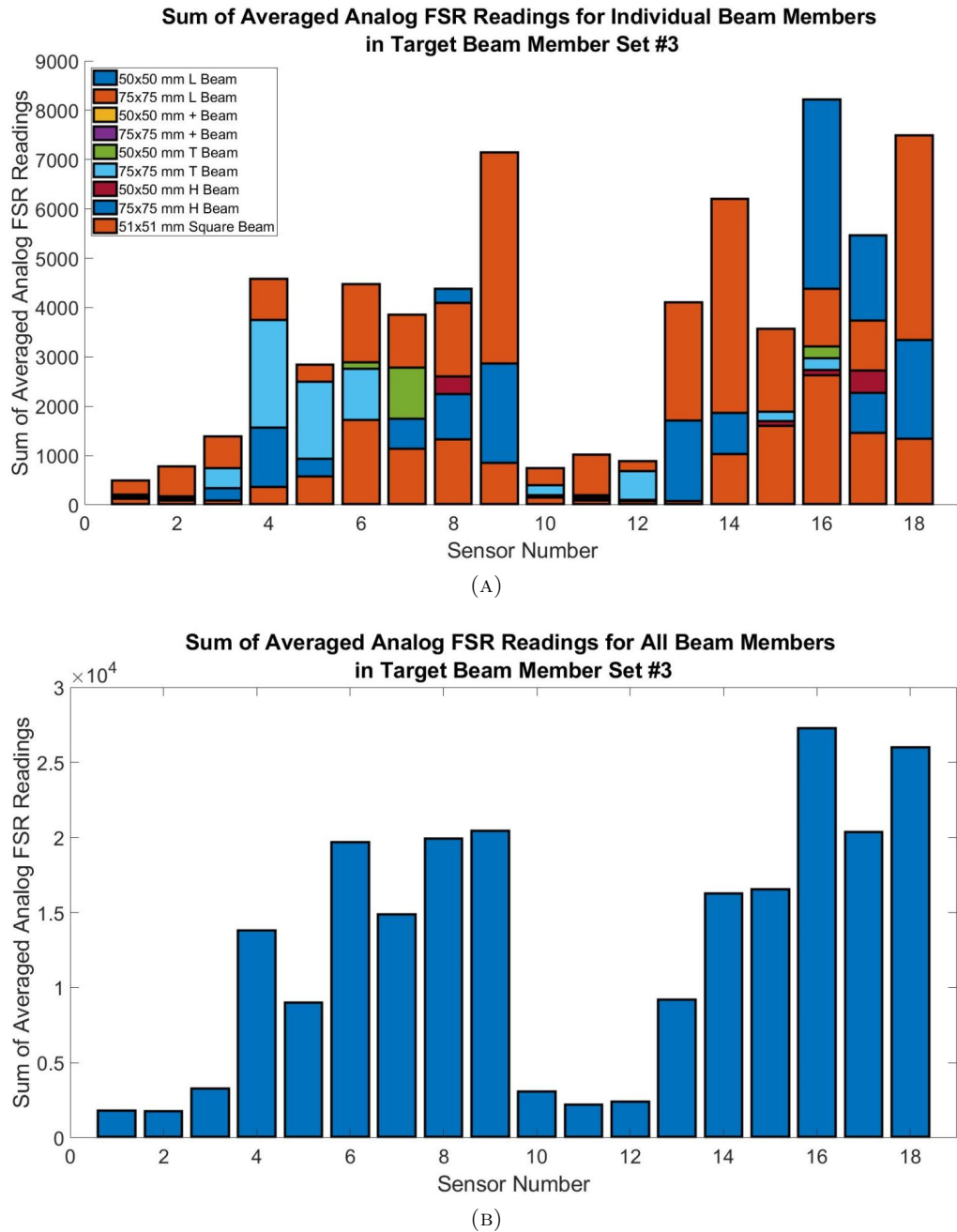
FIGURE 3.31: Sum of raw analog FSR readings for each of the AoAs used for data collection for target beam member set #3: (A) Individual structural beam members, (B) All structural beam members.

patterns for given AoAs are the two main cases resulting in the collection of similar *tactile patterns*. In these cases, the gripper either:

- could not make adequate contact with the beam member during a grasp. Example data for these AoAs are shown in Figure 3.32a, or

- was grasping a portion of a beam member with identical cross-sectional shape and size to another beam member. Example data for these AoAs are shown in Figure 3.32b, and Figure 3.33 shows the gripper points of contact to the beam members which yield this data.

3.5   Discussion

3.5.1   Verification of Stiffness Constrained Topology Optimisation Method

In Section 3.3, the stiffness constrained topology optimisation method was verified through evaluating the performance of three gripper designs in simulation. The results showed that suitable structures for soft grippers were generated to meet the requirement of adaptiveness to varying cross-sectional shapes of beam members, regardless of stiffness constraints being applied. However, gripper #2 far exceeded the capabilities of gripper #1 and gripper #3 when considering the design requirement for strengthened grasping. The data presented in this verification study therefore indicates that gripper #2 is the most effective gripper out of the three presented, considering the adaptability in grasping, input-to-output displacement and force ratios. The stiffness constrained topology optimisation method has therefore proved viable for strengthening discrete elements in regions of the design domain to effectively increase the grasping strength.

In order to be a practical gripper, it is essential that the structure of the grasping mechanism can effectively elastically deform to produce the desired output motions and forces. The required input forces also need to be within reasonable bounds for practical actuation methods. The strength and compliancy of the gripper can be affected by a number of factors relating to the implementation of stiffness constraints in the optimisation model.

In this verification study, an arbitrary value of the stiffness multiplier, α, was applied to the stiffness constrained elements in the design domains for grippers #2 and #3. Further

Averaged FSR Data for AoAs with Poor Beam Member Contact

(A)

Averaged FSR Data for AoAs to Similar Cross-sectional Object Shapes

(B)
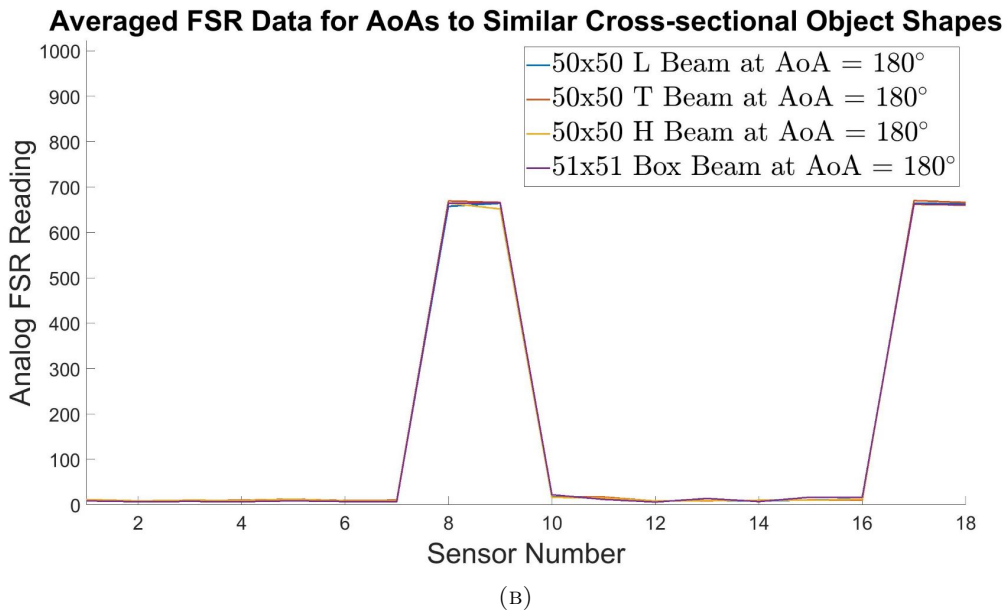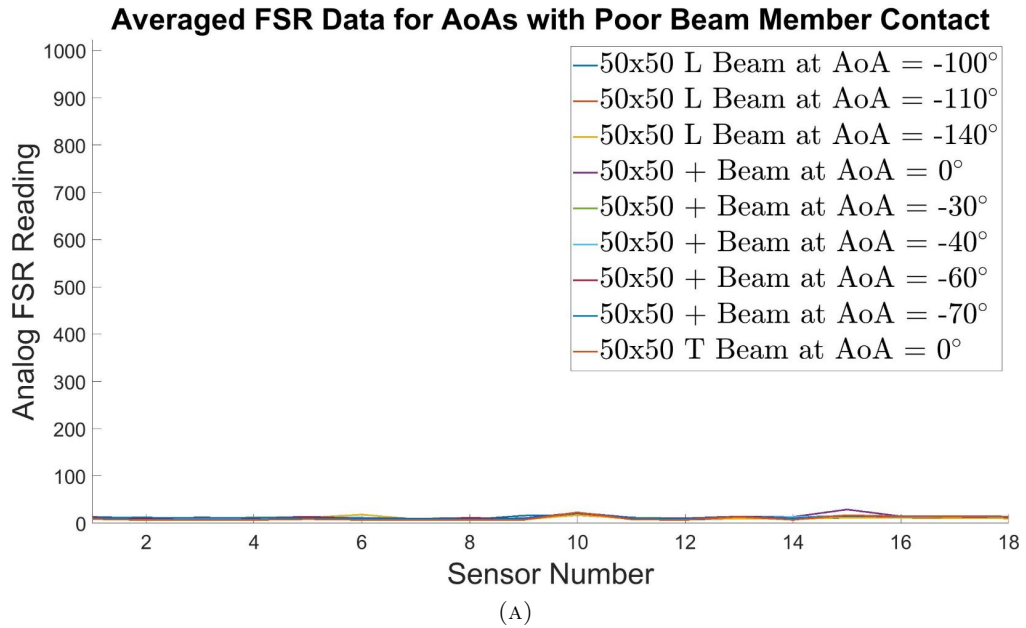
FIGURE 3.32: Similar *tactile patterns* due to: (A) Insufficient contact with the beam member during a grasp, (B) Grasping a portion of a beam member with identical cross-sectional shape to other beam members at particular AoAs.

verification of the stiffness constrained topology optimisation method should conduct a closer study into the selection of this constraint value and its effect on the gripper topology. Ideally, the stiffness multiplier, α, should be optimised to achieve the required grasp strength of the soft gripper, without negatively impacting the flexibility and compliancy of the structure.
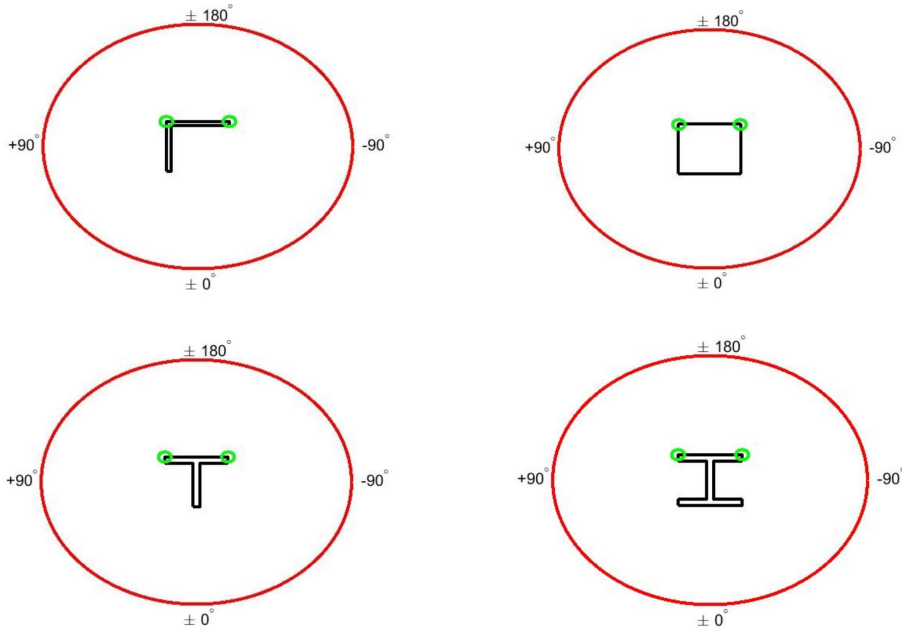
FIGURE 3.33: Gripper points of contact when grasping beam members of similar cross-sectional shape at 180°.

When implementing the stiffness constraints in the design domains of grippers #2 and #3, the number and location of stiffness constrained elements were selected based on the desired output structure of the gripper. As mentioned in Section 3.3.1, as a guideline, the stiffness constrained elements should be located in a region as close to the output force location as possible, and along the path where it is expected that the material will be distributed in the optimisation procedure. In this verification study, the stiffness constraints were applied to elements in an arbitrarily dimensioned region of the design domain. Ideally, optimisation could also be performed to determine the number and location of elements in the design domain which require stiffness constraints. This would eliminate the need for human intuition to select the strategic positions for strengthening.

The structure of the gripper produced by the stiffness constrained topology optimisation method was physically large and required significant linear input displacement to actuate the gripper from the completely open to the completely closed position. Ideally, the gripper structure would be smaller in size, but still able to achieve an enclosing grasp of the beam members in target beam member set #1. Furthermore, actuation of the manufactured prototype gripper #2 required high input forces to enable sufficient deformation of the

gripper around the cross-sectional shape being grasped. Two solutions were identified to alleviate the effects of these issues; reduce the stiffness of the grasping surfaces of the gripper in the model, and/or use a lower Shore Hardness of polyurethane (or other hyperelastic) material.

One of these solutions was implemented in prototyping, where the design of gripper #2 was modified to create gripper #4 by having more defined distal and proximal phalanges, with flexible joints located between them. By reducing the stiffness of the grasping surfaces of the gripper, the physical grasping required lower input actuation forces. Furthermore, for gripper #6, by reducing the distance between pin 1 and the input location, the required linear actuation distance was significantly reduced, although the gripper still is physically large in size, which limits its practicality. It should, however, be noted that the gripper size is highly dependent on the dimensions of the structural beam members in the target beam member set.

3.5.2 Verification of a Prototype Soft Gripper

In Section 3.4.1.4, gripper #6 was designed for the practical application of grasping structural beam members in a power transmission tower. As such, the soft gripper was fitted with simple tactile sensors for the collection of *tactile patterns* during grasping. The gripper design which was based on the topology optimised structure of gripper #5 showed increased compliancy, as a lower input force was required to actuate the gripper from the completely open to the completely closed position. Increased compliancy in the structure resulted in increased surface contact and therefore points of contact for data collection during grasping.

The general purpose of a grasp is to achieve maximum coverage of a beam member, resulting in the maximum number of sensors in contact. However, it is difficult to choose a distance that will result in power grasps being performed for all of the beam members in target beam member sets #2 and #3. When grasping the larger beam members, some precision grasps were executed, which resulted in the collection of data from only two points of contact. For similarly shaped and sized structural beam members, particularly

from target beam member set #3, there were several grasping AoAs across single and multiple beam members which resulted in similar *tactile patterns* being collected.

As extensive grasping was performed with the actuated grasping platform utilising gripper #6, a number of issues which didn't appear in simulation were encountered. Both of the manufactured grippers (#2 and #6) suffered from sag due to gravity which was uncorrected during grasping. This can be attributed to the physical size of the grippers and therefore the physical volume of elastomeric material used. Gripper #2, being smaller in size than gripper #6, was less affected by gravity as its extremities were closer to the rigidly mounted points in the linear actuator rig. A stiffer choice of material (for example Polyurethane with a higher Shore A Hardness) or a deeper extrusion (> 22.5 mm) of the existing material, could lessen the effects of the deflection. However, care must be taken to make these choices, as these changes cause the topology to no longer be optimised, thus the adaptability and compliancy of the grasping structure could be negatively impacted.

3.5.2.1   Actuation

Key components of the actuation platform for gripper #6 deteriorated as a result of extensive repeated grasping for data collection. The main components which experienced noticeable damage were the lead screw and nut. With each grasp, the linear actuator (located at an offset in the z-axis from the gripper input port in simulation) was used to drive the gripper open and closed. As the gripper was actuated into the closed position, an elastic restoring force from the soft gripper was generated and thus a moment was generated in the lead screw nut (see Figure 3.34). This caused misalignment and grinding of the nut against the lead screw. This grinding effect intensified as the gripper was towards the end of its linear actuation stroke length, as the required actuation force increased (according to the force plots shown in Figure 3.26b).

Wear on these key components resulted in elongated stroke lengths being recorded by the motor encoder as more grasping actions were undertaken and wear worsened. The effects of this wear could have been less severe, if additional linear actuation guide rails or lead screws were added above the gripper to prevent excessive torques from being applied to the overall structure. Alternatively, if the lead screw could be mounted directly at the input
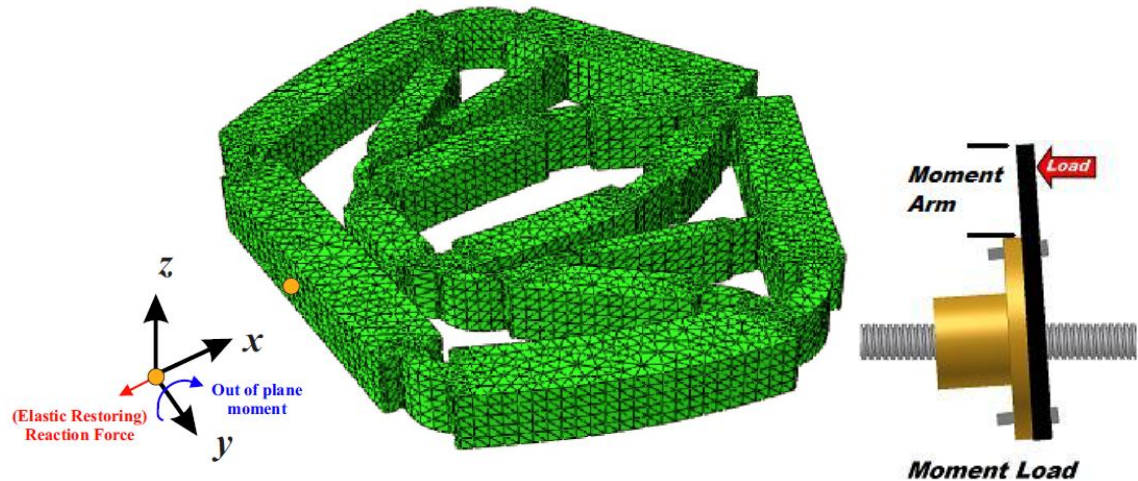
FIGURE 3.34: Engineering issues caused by offset of the linear actuation platform.

port (as was simulated), the generated torques would be heavily reduced, if not entirely eliminated. A ball screw could also be used as a substitute for the lead screw and would eliminate grinding effects; however, since ball screws are backdrivable, a brake would be required on the motor to enable secure grasping. Ball screws, however, can handle higher axial loads and torques and have faster actuation speeds than lead screws. Any future designs would take these options and improvements into careful consideration to improve the repeatability of the grasping rig.

3.5.2.2 Sensing

During grasping, the array of FSRs located on the grippers inner finger surfaces suffered from certain scenarios which could have limited the accuracy and reliability of the sensor readings. For example, despite efforts to ensure that the grasping AoA was consistent for all repeated grasps, slight misalignments in the rig components could have introduced variance in FSR readings and hence the recorded *tactile patterns*. One scenario which resulted in limited grasping data being collected was observed when a major edge of a structural beam member fell between the proximal and distal finger sections (where no sensors were located).

Depending on the target beam member set, a selection of sensors were subject to repetitive forces from edges of the beam members during data collection. Some of these sensors

degraded significantly in their sensitivity and needed replacement. This is a potential factor that has reduced the precision of the overall data collected. Calibration was not performed to take this into consideration, since it was expected there would be some variance and fluctuation in the sensor readings regardless.

Selection of appropriate buffer materials to distribute the grasping forces across several sensors was challenging, due to the memory effect of the foam material. A trade-off was required between foam material thickness and sensing sensitivity. Thicker foam resulted in a larger memory effect, however the sensors were not as sensitive to light touch. Additionally, some fluctuation in sensor readings was experienced when the sensor pads slipped during grasping, applying a shear force to the sensor assembly and causing delamination of the sensors.

Sensor drift over time can affect the reliability of the sensor readings; however, due to the short time period in which the data collection took place, this drift offset was not considered. For more precise results over longer periods of time, sensor drift should be considered. Sensor data could have also been recorded both at the start and end of the grasp action, and the difference recorded as the raw sensor reading. This would eliminate any erroneous or inconsistent readings across multiple grasps due to sensor drift or sensors which were replaced.

Future designs would investigate the viability of embedding the FSRs directly within the polyurethane material, with a rigid backing surface such as a 3D printed section. By embedding sensors directly within the gripper material, sensor delamination should be eliminated, as no shear force could be directly applied to the sensors surface. It is then possible that further sensors could be used, to increase the density of the sensing elements in the gripper and achieve better coverage of grasping surfaces. The sensitivity of such a setup, however, and the cable management strategy would need to be carefully considered.

Chapter 4

Comparative Study of Machine Learning Classifiers for Beam Member Recognition

This chapter presents a comparative study of commonly used machine learning classifiers for beam member recognition using the prototype soft gripper presented in Section 3.4.1.4 and the grasping data collected in Sections 3.4.2.3 and 3.4.2.4. Compared to the object identification and recognition problems discussed in Section 2.3.2, the beam member recognition problem discussed in this chapter has many challenging aspects.

Object recognition problems discussed in recent literature have focussed on grasping and recognising objects from a set of common household items, often using machine learning classifiers. These objects are typically small in size and have unique, distinguishing features which permit rapid and accurate recognition, using data from a single grasp. For the structural beam member recognition problem discussed in this chapter, similarities in the cross-sectional shape and size of different beam members can be a source of confusion, thus decreasing the accuracy and rate of recognition with a single grasp.

Furthermore, depending on the cross-sectional shape of a beam member, its distinct edges can be spaced at significant distances from one another. Then, depending on the grasping AoA, sparse sensory data might be collected, due to minimal points of contact during a

grasp. Additionally, depending on the grasping AoA to a beam member, similar tactile readings may be collected, resulting in erroneous classifications. In this chapter, a beam member can be recognised using data from a single grasp through the classification of three properties: (1) cross-sectional shape, (2) size (dimensions), and (3) grasping AoA.

4.1 Overview

For classification of the cross-sectional shape, size and grasping AoA of a beam member, sufficient data needs to be collected **during grasping**. An efficient method identified for feature extraction in human *haptic perception* is the *haptic glance* (enclosure grasping), which is adopted in this research.

Using the data collected during grasping, methods for recognising a beam member and its properties need to be developed. With rigid grippers, where the kinematics of the grasping mechanism are known and joint position sensors (amongst others) are reliable, the recognition is somewhat trivial. With soft grippers, however, knowing the exact configuration of the gripper as it interacts with beam members is highly complex. For example, unpredictable deformations can arise during grasping, and a lack of accurate position sensing methods can be a source of further complications.

As discussed in Chapter 2, object recognition methods for soft grippers in the literature have mostly focussed on the use of COTS sensing solutions and their integration with soft grippers. Existing methods of object recognition using soft grippers use either proprioceptive (pneumatic pressure, stretch or bend) sensors and/or a single force sensor for contact detection (usually in the fingertips). Methods combining proprioceptive and exteroceptive force sensing can be limited by a lack of informative data across different grasping scenarios. For example, due to object size or grasping angles, a fingertip sensor might not always make contact with a target object [168]. Few soft grippers have been designed with only force sensors for object recognition, as proprioception has been the major focus of sensing for soft grippers. Even fewer approaches to sensing in soft grippers have used an **array** of tactile sensors distributed along the grippers fingers [171].

Due to the sparseness of data collected with soft grippers and a lack of kinematic models, approaches to object identification and recognition using soft and underactuated grippers have utilised machine learning methods. Typically, machine learning **classifiers** are trained for object recognition. In this research, the use of machine learning classifiers for beam member recognition can be assessed across four metrics:

1) Training time (s)

2) Classification time (s)

3) 10 Fold Cross-validation Accuracy (%), or Out-of-bag (OOB) Accuracy for Random Forest (RF) (%)

4) Test Data Classification Accuracy (%)

By selecting the classifier with high classification accuracy and classification speed, a structural beam member and its properties can be recognised with tactile data from a single or a few *haptic glance/s*.

In this chapter, classification results from several commonly used machine learning classifiers are analysed. In this analysis, two target beam member sets are considered, where the beam members are unique (target beam member set #2) and similar (target beam member set #3) in cross-sectional shape and size. Furthermore, the classifier performance is compared by both including and excluding the motor encoder readings from the data sets. Combinations of settings for the classifier evaluation across the two target beam member sets are summarised by Figure 4.1.

The results are analysed, the limitations of beam member recognition using data from a single *haptic glance* are discussed and conclusions are drawn.

4.2 Classification Algorithms

The commonly used classifiers which are evaluated in this chapter are: k-Nearest Neighbours (k-NN), Linear Discriminant Analysis (LDA), Multiclass Support Vector Machine
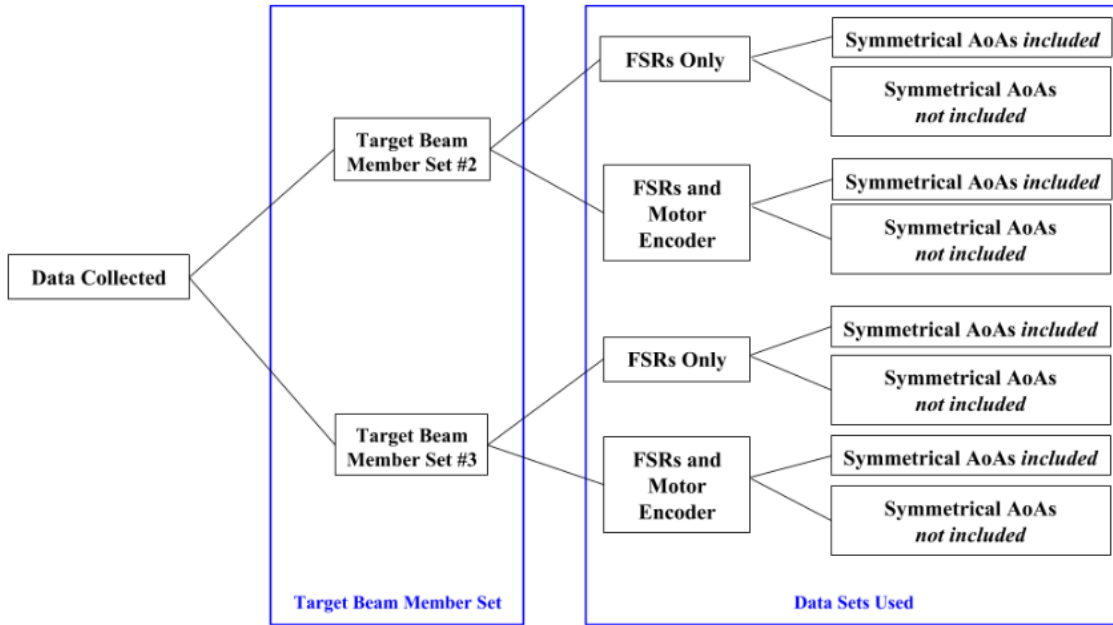
FIGURE 4.1: Classifier training settings for the two target beam member sets.

(SVM), Naïve Bayes and Random Forest (RF). These classifiers were selected, based on object recognition machine learning methods used in recent literature [166, 168–171].

These classifiers were trained in MATLAB R2018b using the statistics and machine learning toolbox. Unless otherwise stated, all input arguments to train the classifiers in MATLAB use the default settings. The results presented in this chapter are averaged over 1000 rounds of classifier training and testing using the parallel computing toolbox, with 12 workers in the parallel pool.

The overall machine learning method can be summarised by the following: Given a set of N training examples of the form $(x_1, y_1), \ldots, (x_N, y_N)$ such that x_i is the feature vector of the ith example and y_i is its class, a learning algorithm seeks a function $g : X \rightarrow Y$, where X is the input space and Y is the output space. The function g is an element of some space of possible functions G.

The goal of the classification during grasping was to recognise, from a defined target beam member set, a structural beam member and its properties of cross-sectional shape, size and the gripper's grasping AoA. For each case study, classifiers were trained both with and without including the symmetrical data from repeated AoAs as well as with and without

the motor encoder readings (see Figure 4.1). The symmetrical data from repeated AoAs refers to the symmetrical structural members, which, when grasped from AoAs separated by 90° or 180°, (depending on the number of axes of symmetry) can yield identical tactile patterns. By analysing the results of each combination, the most suitable combination permitting high classification accuracy and classification speed can be determined.

The data sets for classification (listed in Table 4.1) consist of beam members (Bm) in the target beam member set, and their associated AoAs (N_{AoA}, as defined in Table 3.4), or

$$N_{ba} = \sum_{i=1}^{Bm} N_{AoA,i} \tag{4.1}$$

beam-angle pairs (N_{ba}). The data used in MATLAB for training and testing of the classifiers was comprised of tables with $N_g \times N_{ba}$ rows (of observations) and $N_{FSR} + N_{enc} + 1$ columns (of predictor variables), where N_{enc} was either 1 or 0 and the additional column provided the classifier response data (beam member cross-sectional shape, size and grasping AoA). The number of predictor variables used by the classifiers were therefore either 18 or 19, depending on the inclusion of the encoder data.

TABLE 4.1: Data set descriptions for target beam member sets #2 and #3.

Target Beam Member Set #	Number of Beam Members in Set (Bm)	Number of Beam-Angle Pairs (N_{ba}) with symmetrical AoAs *not included*	Number of Beam-Angle Pairs (N_{ba}) with symmetrical AoAs *included*
2	6	136	216
3	9	207	324

To calculate a classifier's accuracy, one common technique is to split the training set by using two-thirds for training and the other third for estimating performance [153]. In this thesis, to evaluate the effectiveness of each classifier, the data sets (corresponding to a target beam member set) were split into training data (60%) and test data (40%). The training data was used to fit the classification model for each learning algorithm, and the test data was used to provide an unbiased evaluation of the model's fit on the training data set. The MATLAB function, `cvpartition`, was used to divide the data such that the response classes were represented in approximately the same proportion in each partition.

4.2.1   k-Nearest Neighbours (k-NN)

The k-NN classifier is an instance-based, or "lazy-learning" algorithm. As Figure 4.2 shows, k-NN classifiers operate on the simple idea that a new sample can be categorised according to known samples that are 'similar', based on their proximity to one another (using a distance metric). For this to be possible, the algorithm stores all of the training data, which can be computationally expensive. Using the training data as a representation, the classifier does not learn any model and makes predictions based on the similarity between an input sample and each training instance.

The k-NN classifier can be powerful, however, some features such as their large storage requirements, sensitivity to the distance metric used, and unintuitive method for selecting 'k' limit the effectiveness of such instance-based classifiers. Furthermore, the k-NN classification accuracy can be easily affected by the selection of the training data and distance metric, as well as localised anomalies in the feature space. To obtain more accurate results, weighting schemes can be used to alter the distance measurements and voting influence of each instance in the feature space [153].

A disadvantage of this classifier is therefore the lack of generalisation, since a model is not trained. For this reason, the classification can also be sensitive to irrelevant features and the scale of the data. One advantage of this method is that it is not necessary to make any assumptions about the underlying distribution of the data. Typically, this classifier is fast to train and predict (times $\propto$ (Data Size)^2), with a small memory overhead. As the data size increases, however, the prediction stage can become slower and higher memory overheads are required.

Equation 4.2 describes the Euclidean distance metric, defining the distance between instances x and y.

$$D(x,y) = \left(\sum_{i=1}^{m} |x_i - y_i|^2 \right)^{1/2} \tag{4.2}$$

To fit data to this model in MATLAB using the `fitcknn` function, there are three parameters which need to be defined:
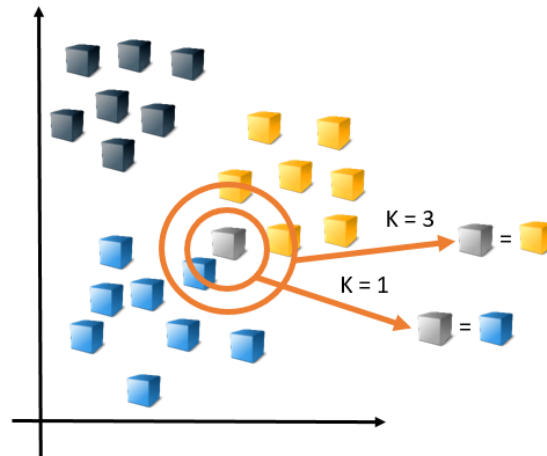
FIGURE 4.2: Example of k-NN classification with $K = 1$ and $K = 3$ neighbours. Source: [183].

1) The number of neighbours used for classification (`NumNeighbors`),

2) The metric used for calculating the distances between neighbours (`Distance`), and

3) The weighting given to different neighbours (`DistanceWeight`).

In this study, several combinations of settings were tested and the best classification accuracies were achieved by training the k-NN classifiers with two neighbours, an Euclidean distance metric and an inverse distance weight.

4.2.2 Linear Discriminant Analysis (LDA)

LDA is a simple method used to find the linear combination of features which best separate two or more classes of objects [184], and works when the measurements made on each observation are continuous quantities [153]. In LDA, the covariance for each response class is assumed to be the same, which results in linear boundaries between classes as shown in Figure 4.3. LDA commonly works well for data sets which contain more predictors than observations. Typically, this classifier is fast to train and predict (times $\propto$ Data Size), with a small memory overhead ($\propto$ Number of Predictors).

For each class, the LDA model estimates the mean and variance. The prediction output from LDA is based on estimating the probability that a new set of inputs belongs to each
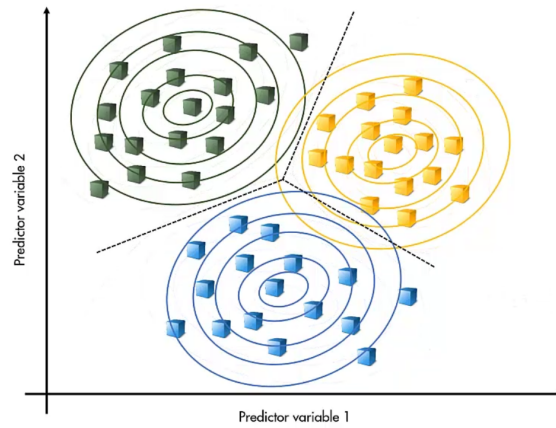
FIGURE 4.3: Example of LDA classification. Source: [183].

class. Then, the class with the highest probability is the output class and the outcome of the prediction.

The model uses Bayes Theorem to estimate the probabilities. This is represented by estimating the probability of the output class given the input using the probability of each class and the probability of the data belonging to each class.

To fit data to this model in MATLAB using the `fitcdiscr` function, first, the type of boundary used is set to linear by defining `DiscrimType = 'linear'`. There are then two remaining parameters which need to be defined:

1) Coefficient threshold for including predictors in a linear boundary (`Delta`).

2) Regularization to use when estimating the covariance matrix for LDA (`Gamma`).

In this study, the best results were achieved by setting both `Gamma` and `Delta` to zero.

4.2.3 Multiclass Support Vector Machine (SVM)

SVMs use the concept of a "margin" which falls on either side of a hyperplane separating **two** data classes. By maximising the margin, the largest possible distance between the hyperplane and the instances on either side has proven to reduce an upper bound on the expected generalisation error [153]. If the training data is linearly separable, then a pair $(\mathbf{w}, b)$ exists such that

$$\mathbf{w}^T\mathbf{x}_i + b \geq 1, \text{for all } \mathbf{x}_i \in P$$

$$\mathbf{w}^T\mathbf{x}_i + b \leq -1, \text{for all } \mathbf{x}_i \in N$$

with the decision rule given by $f_{\mathbf{w},b}(\mathbf{x}) = \text{sgn}(\mathbf{w}^T\mathbf{x} + b)$ where $\mathbf{w}$ is termed the weight factor and b the bias (or $-b$ is termed the threshold).

When it is possible to linearly separate two classes, an optimum separating hyperplane can be found by minimizing the squared norm of the separating hyperplane. The minimization can be set up as a convex quadratic programming problem:

$$\underset{\mathbf{w},b}{\text{minimise}} \ \mathbf{\Phi}(\mathbf{w}) = \frac{1}{2} \parallel \mathbf{w} \parallel^2$$

$$\text{subject to } y_i(\mathbf{w}^T\mathbf{x}_i + b) \geq 1,$$

$$i = 1, \dots, l.$$

For linearly separable data, once the optimum hyperplane is found, the data points lying on its margin are called the support vector points. The solution is represented as a linear combination of only these support vector points, with all other data points being ignored.

Consequently, the model complexity of an SVM is not affected by number of training data features. Therefore, SVMs perform well when the data contains a large number of features, with respect to the number of training instances.

These underlying calculations for classification with SVMs are binary in nature, therefore restricting their usage. However, multiclass classification with SVMs can be achieved by creating an Error-Correcting Output Codes (ECOC) classifier. If there are multiple classes in the data, the ECOC model reduces with model down to multiple binary classifiers using a one-vs-one design. Multiclass predictions are then achieved through the combination of the individual classifiers as shown by Figure 4.4.
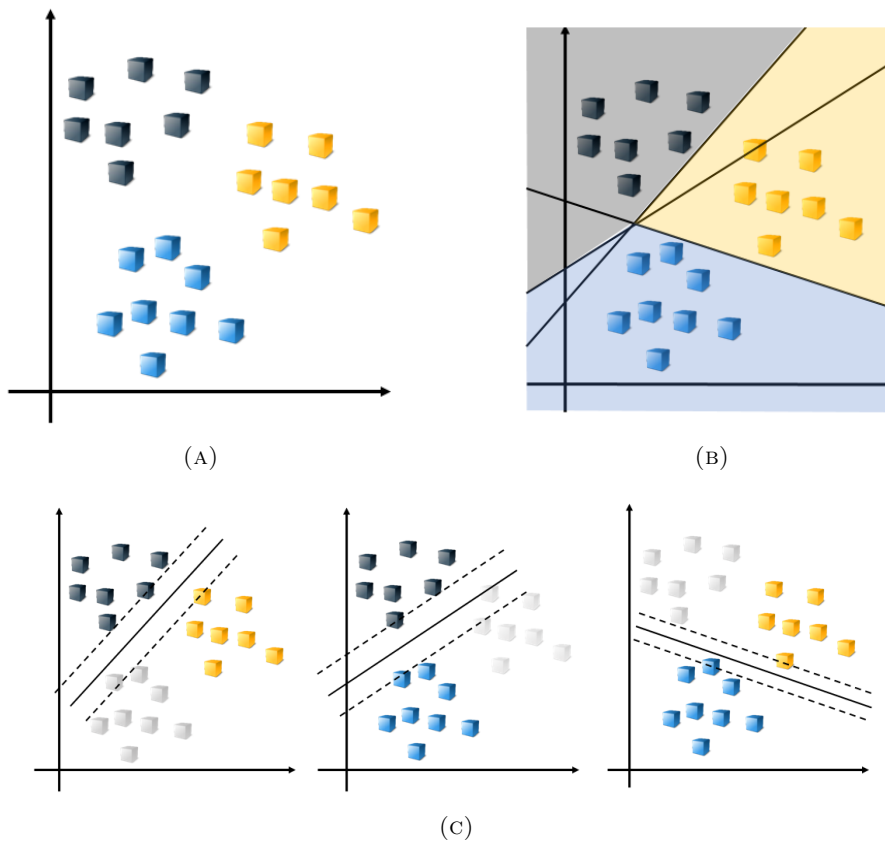
FIGURE 4.4: Example of Multiclass SVM classification [183]: (A) Complete data set containing three classes, (B) Resultant multi class classification, (C) Individual binary SVM classifiers. Source: [183].

To fit data to this model in MATLAB using the `fitecoc` function, first a template needs to be defined using the `templateSVM` function. In this study, the Multiclass SVM was trained using several different Kernel types, with Gaussian producing the best results.

4.2.4 Naïve Bayes

A Naïve Bayes classifier assumes the independence of the predictors within each class (see Figure 4.5). By assuming that data comes from a certain underlying distribution, it can be treated as a statistical sample, which can reduce the influence of outliers in the model.

Naïve Bayesian networks are simple Bayesian networks comprised of directed acyclic graphs with only one parent (representing the unobserved node) and several children (observed

nodes) with a strong assumption of independence among child nodes in the context of their parent [185]. The independence model (Naïve Bayes) is then based on estimating:

$$R = \frac{P(i|X)}{P(j|X)} = \frac{P(i)P(X|i)}{P(j)P(X|j)} = \frac{P(i)\prod P(X_r|i)}{P(j)\prod P(X_r|j)}$$

Comparing the two probabilities, the larger probability indicates the class label value that is more likely to be the actual label (if $R > 1$: predict i, else predict j) [153].

One major advantage of the Naïve Bayes classifier is its short computational time for training, since only a single pass of the data is required to either count frequencies (discrete variables) or to compute the normal probability distribution function (continuous variables, under normality assumptions) [153]. This classifier is a good choice for relatively simple problems or when there is a significant amount of missing data. However, this algorithm is considered to have a high bias, because it assumes that the dataset comes from a single probability distribution, and that this model can be used to discriminate between the classes.
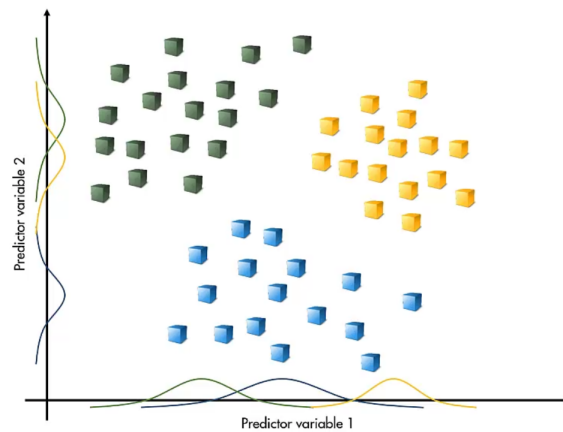
FIGURE 4.5: Example of Naïve Bayes classification. Source: [183].

To fit data to this model in MATLAB using the `fitcnb` function, a distribution type which is used to calculate probabilities must be defined. In this study, a kernel smoothing density estimate was fitted by setting the `'DistributionNames'` property to `'kernel'`. A Gaussian kernel smoother, set by the input name-value pair `'Kernel'`, `'normal'` in the `fitcnb` function achieved the best results. Model fitting and prediction times for kernel distributions are slow, however and require a moderate to large memory overhead.

4.2.5 Bagged Trees Ensemble (Random Forests (RFs))
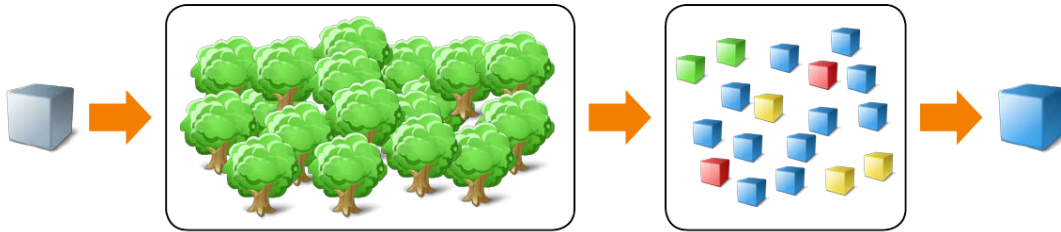
FIGURE 4.6: Example of Trees Ensemble classification. Source: [183].

Decision trees, like k-NN, do not make any assumptions about the data. Using the MAT-LAB function `fitctree`, models can be fitted at speeds $\propto$ Data Size, predictions can be fast and at the cost of only a small memory overhead.
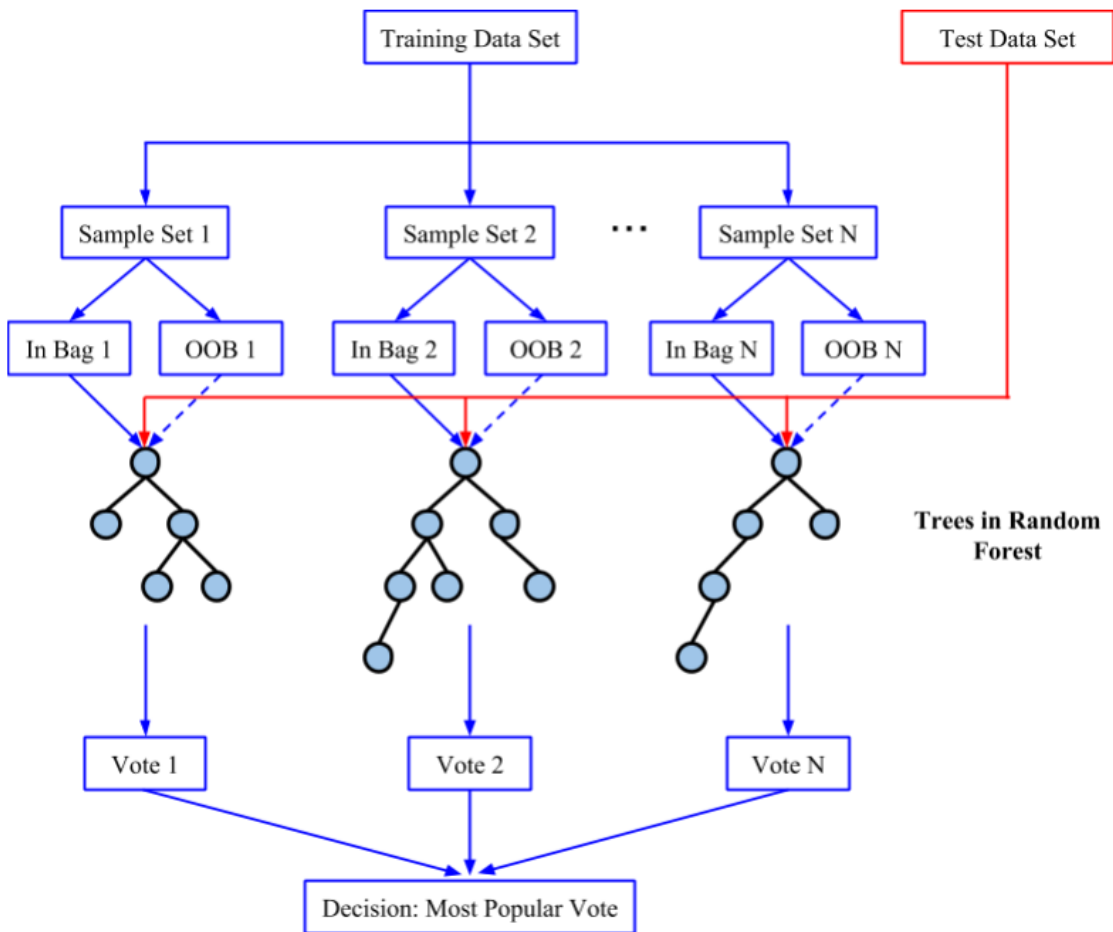
FIGURE 4.7: Simplified representation of RF classification.

However, classification trees are considered weak learners as they are highly sensitive to the training data used. Consequently, two slightly different training data sets can produce two entirely different trees, resulting in different predictions. To improve upon the weaknesses of individual trees, an ensemble (or a forest) of trees can be "grown" to strengthen the classification capabilities. By using a forest of trees, new observations can be applied and the resulting predictions can be compared and the majority vote can be counted as the classification output (as shown in Figure 4.6).

Two main ensemble-aggregation methods exist for creating ensembles; boosting, or bootstrap aggregating (bagging). Random Forests are ensembles of bagged trees, where each tree in the ensemble is grown on an independently-drawn bootstrap replica of input data. The observations not included in this replica are called OOB and can be used to estimate the prediction error of the bagged ensemble (see Figure 4.7). This method of bootstrap aggregation reduces the effects of overfitting (because of the Law of Large Numbers) and improves generalisation due to the randomness [154].

More formally, a Random Forest is a classifier consisting of a collection of tree-structured classifiers $\{h(\mathbf{x}, \Theta_k), k = 1, \ldots\}$ where the $\{\Theta_k\}$ are independent identically distributed random vectors and each tree casts a unit vote for the most popular class at input $\mathbf{x}$ [154].

In this study, the `TreeBagger` function was used to create bagged ensembles of weak decision tree learners. For evaluation, RFs were trained with 10, 100 and 1000 trees to determine the forest size which would provide a suitable trade-off between accuracy, computational power and speed. The output variables of `'OOBPredictorImportance'`,`'OOBVarImp'` and `'OOBPrediction'` were all set to `'On'` to monitor the OOB error with each additional tree grown in the forest. The predictor importance can be used to determine redundant predictors in the classification. By identifying these, the number of inputs can be evaluated and a reduced feature space data set can be used to train the classifier, with minimal impact on classification accuracy.

4.3 Results

This section analyses the results from the classifiers in recognising a structural beam member and its properties (cross-sectional shape, size and grasping AoA) from the two individual target beam member sets (#2 and #3). Each of the classifiers are assessed across a number of metrics, including classifier training time, classification time (test time), 10-fold cross-validation accuracy (or OOB accuracy for Random Forest (RF)), and classification accuracy (using the test data sets).

This section focuses on analysing the classification results of the data sets which **do not include** the repeated AoAs from symmetrical beam members. By limiting the data set, analysis of excessive misclassifications due to known circumstances are avoided. The full detailed results (both including and not including repeated AoAs from symmetrical structural beam members) can be found in Appendix B.

4.3.1 Target Beam Member Set #2: Beam Members of Unique Cross-sectional Shapes and Sizes

Overall, the results in Figure 4.8 show that relatively high classification accuracies were achieved by all of the evaluated classifiers. This can be attributed to the unique cross-sectional shape and size of the structural beam members in the target beam member set. It can be observed that typically, very minor improvements in the classification accuracies were achieved by including the motor encoder data in the training model. Furthermore, by including the motor encoder data, the average classifier training and classification times increased. It can therefore be deduced that for rapid classification using this data set, data from tactile sensors **only** is sufficient and inclusion of the motor encoder data is not necessary.

The classification results can be further analysed by observation of the individual classifier confusion matrices. By comparing the confusion matrices for each of the evaluated classifiers, it was found that each classifier generally confused the same beam members and AoAs. Thus, for brevity, a single confusion matrix will be further analysed in this section.
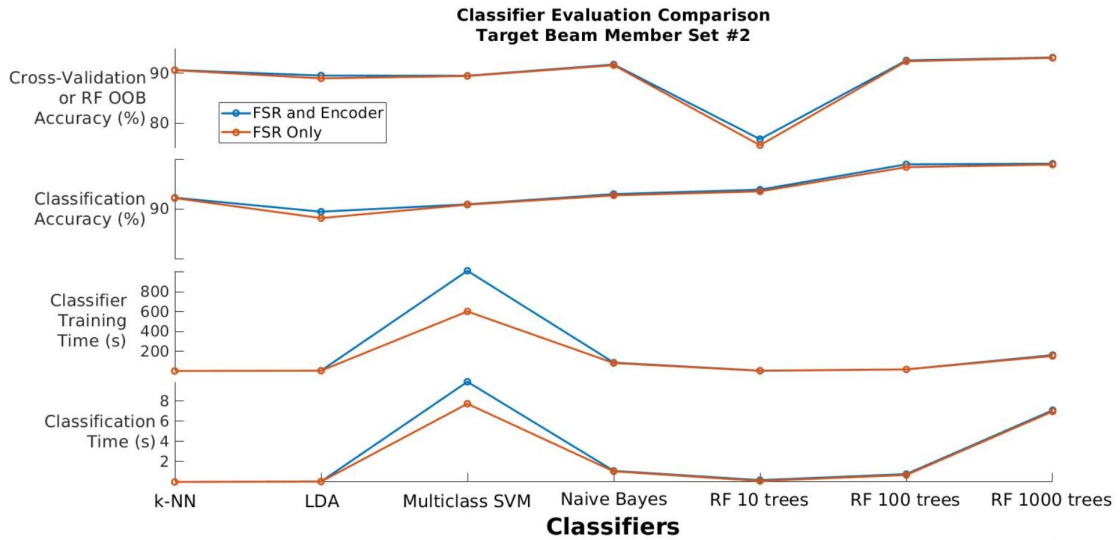
FIGURE 4.8: Target beam member set #2: comparison of commonly used classifiers evaluated against the four metrics.

The k-NN classifier confusion matrix for target beam member set #2 in Figure 4.9 highlights the erroneous classifications, which relate to one of two identified scenarios discussed in Section 3.4.3.3. In this confusion matrix, 4/10 of the grasps at each unique AoA (as laid out in Table 3.4) are classified. The "low data" misclassifications occur with both the 50×50 mm "L" beam member and the 81×25 mm rectangular beam member. The AoAs for these target beam members are either self-misclassified (i.e. the true AoA is mistaken for another AoA of the same beam member—see red and dark blue boxes in Figure 4.9), or misclassified with another beam member (i.e. the true AoA may be correct, but the beam member is mistaken, or both AoA and beam member are incorrect—see purple box in Figure 4.9).

Similarities in the 50×50 mm "L" beam member and the 51×51 mm square beam member from particular grasping AoAs also resulted in erroneous classifications—see light blue and green boxes in Figure 4.9. The misclassification of beam members is more clearly represented in the confusion matrix for beam members and their dimensions (not individual AoAs) from target beam member set #2, as shown in Figure 4.10.

There are several advantages and disadvantages to each of the classifiers evaluated for the beam member recognition problem with target beam member set #2. When selecting a classifier for the practical application, understanding the functionality of a classifier

is of high importance. The requirements should be prioritised and the advantages and disadvantages carefully evaluated, especially when considering the potential for expansion of the target beam member set. For example, the inclusion of similar beam members in a target beam member set may result in the collection of further *tactile patterns* which can be easily confused by a classifier. The following paragraphs delve into the performance of each individual classifier, given **only** the tactile grasping data from target beam member set #2, and their suitability for generalising to other data sets. This analysis will be continued in Section 4.3.2, through analysis of the classifier performance for the beam member recognition problem with target beam member set #3.

FIGURE 4.9: Confusion matrix for one trained k-NN classifier for target beam member set #2. Highlighted boxes show sources of confusion in the classification.

FIGURE 4.10: Confusion matrix for one trained k-NN classifier, classifying individual beam member cross-sectional shapes and sizes, not individual AoAs from target beam member set #2.

The k-NN classifier achieved the fastest training and classification times out of all of the evaluated classifiers, as well as one of the highest classification accuracies. These rapid training and classification times can be attributed to the fact that the classifier doesn't learn any model from the training data, but makes predictions based on the similarity between the input test sample and training instances. The grasping data collected at each AoA for the beam members of target beam member set #2 was typically unique, resulting in well defined classes within the feature space and therefore resulting in accurate classifications. Whilst the training and classification times would not increase dramatically with the addition of further beam members to the target beam member set, the advantage of the high classification accuracy is directly dependent on the collection of unique *tactile patterns* during grasping. Therefore, it is expected that with the collected *tactile patterns* from target beam member set #3, there will be a decrease in the classification accuracy. The results of this classification will be discussed further in Section 4.3.2.

The LDA classifier achieved one of the fastest training and classification times, since the size of the tactile data set is relatively small. However, the classification accuracy was the lowest out of all of the evaluated classifiers. This could be related to the underlying

assumption that the covariance for each response class is assumed to be the same. If this was true, then the defined linear boundaries between classes would accurately describe the feature space. Since there are multiple "low data" AoAs or AoAs with similar collected *tactile patterns*, this boundary assumption does not hold true, therefore affecting the classification accuracy. With an increase in similar *tactile patterns* across multiple beam members, a decrease in the classification accuracy would be expected.

The Multiclass SVM classifier achieved the slowest training and classification times amongst all of the evaluated classifiers. This can be attributed to the large number of response classes in the feature space and the need for the ECOC model to reduce the total model down into a number of binary classifiers using a one-vs-one design (see Section 4.2.3). Additionally, these slow training and classification times could be due to the choice of a kernel distribution, as discussed in Section 4.2.4. Similar to the LDA classifier, overlap of *tactile patterns* in the feature space can result in the classifier model failing to set up distinct boundaries in the feature space for classification, which in turn affects the classification accuracy.

The Naïve Bayes classifier achieved slow training and classification times. This classifier assumes that the data comes from a certain underlying distribution. In the case of the unique *tactile patterns* collected from grasping beam members from target beam member set #2, this results in high classification accuracies. However, it is not necessarily true that this high classification accuracy and the assumptions made about the data extend to other target beam member sets where different *tactile patterns* may be collected.

Ensemble classifiers, such as RFs which use the method of bootstrap aggregation can achieve good classification results, with models that generalise well and do not overfit the data. Therefore, the remainder of this section will focus on a more detailed discussion of the results using an RF classifier.

4.3.1.1   Random Forests

With RF classifiers, there are two main input settings that can be adjusted to alter the classification accuracy, training and classification times: (1) the number of trees grown

in the forest, and (2) the number of predictors in the feature space. To determine a suitable number of trees, the OOB error for a given size of RF can be analysed with each additional tree grown in the forest. Ideally, the number of trees grown in the forest should be optimised to achieve the highest reduction in the OOB error. By increasing the number of trees in the forest, the OOB error can be drastically reduced, and the classification accuracy improved, however, this comes at the cost of increasing the training and classification times.

To select the number of predictors, the predictor importance can be extracted for each trained RF. By analysing the predictor importance and selecting a threshold value for the importance, for example by selecting the predictors which fall within the top 80% of the predictor importance values, a reduced feature space model can be developed. Depending on the threshold value set, similar classification accuracies can be achieved to the full feature space model, but with the advantage of faster training and classification times. Another method of feature space dimensionality reduction is to use an iterative sequential feature selection, whereby predictors are added and removed in turn, evaluating the effect on the quality of the model. In this section, the two settings of selecting the number of trees grown in the forest, and the number of predictors selected in the feature space based on the predictor importance values will be further analysed.

For the RF classifiers, growing at least 100 trees in the forest (regardless of the inclusion of motor encoder data, as shown in Figure 4.11) provided an acceptable trade-off between classification accuracy and computational effort. As shown in the listing of results in Table 4.2, it is possible that even fewer than 100 trees could be grown in the forest to achieve similar classification accuracies.

TABLE 4.2: Target beam member set #2 classification accuracy and OOB error for between 10 and 100 trees grown in the RF using the FSR only data set.

Number of Trees	10	20	30	40	50	60	70	80	90	100
OOB Error (%)	24.38	13.26	10.44	9.33	8.46	8.35	7.94	7.87	7.67	7.61
Classification Accuracy (%)	91.78	93.21	93.84	93.96	94.04	94.13	94.15	94.20	94.22	94.33

To determine the number of predictors required for the classification model, Figure 4.12 can be analysed. Figure 4.12a shows the average predictor importance over 1000 trained RF classifiers grown with 100 trees. Overlaid on this plot is the weighted sum of averaged raw FSR data for all of the beam members in the target beam member set. It is evident by the data trends in this plot that the importance of the predictors is related to the number of times a particular tactile sensor has been activated during grasping.

Intuitively, by excluding the tactile data from FSRs 1–3 and 10–12 (sensors with the lowest sum of averaged data *and* predictor importance) in the training phase, an increase in classification speed would be expected, with little to no impact on the classification accuracy. However, in making this decision to eliminate a large portion of the predictors (1/3), it is overlooked that these sensors, whilst not always in contact with the target beam member during grasping, provide distinguishing *tactile patterns* required for classification of the larger beam members in the target beam member set (see Figure 3.27a). Therefore, removing these low importance predictors from the feature space without proper analysis of the data can in fact result in a reduction in the classification accuracy.

Reducing the feature space based on the importance of the predictors (without any further
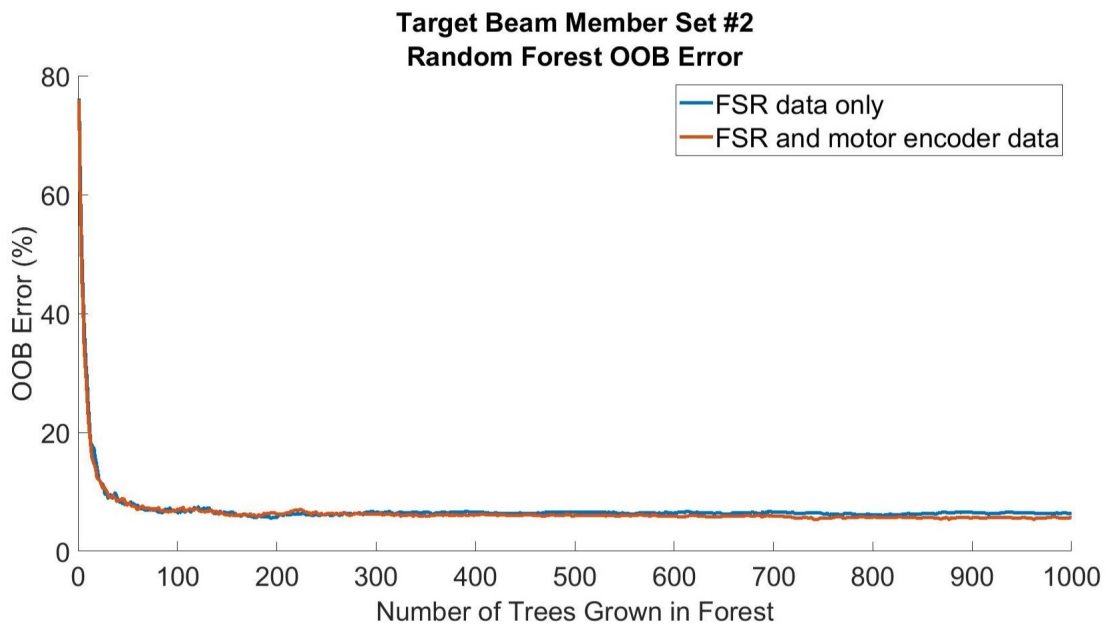
FIGURE 4.11: Target beam member set #2: RF OOB error with increasing number of trees grown in the forest.

(A)

(B)
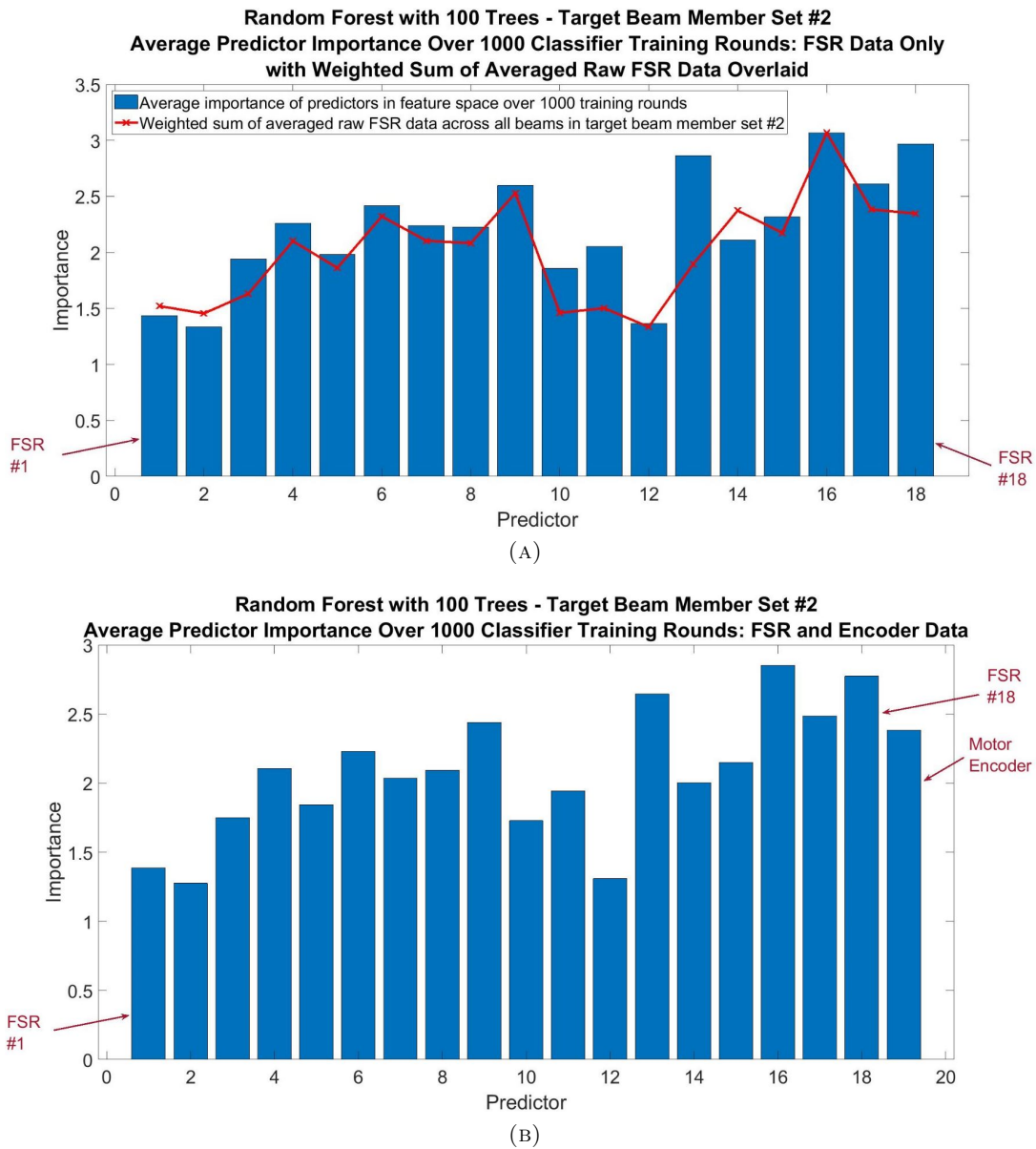
FIGURE 4.12: RF with 100 trees. Average importance of predictors in feature space for target beam member set #2: (A) Trained using only FSR data (plot overlaid with weighted sum of averaged raw FSR data for all beam members in the target beam member set), (B) Trained using FSR and motor encoder data.

analysis) is therefore infeasible, particularly when considering future grasping applications with a wider range of cross-sectional shapes, sizes and grasping AoAs to target beam members. Since this study only includes a subset of beam members and AoAs that may be found in a truss structure such as a power transmission tower, it may be considered critical to keep all current tactile sensors as predictors in the feature space.

An analysis for reduction of the feature space is therefore focussed on the effectiveness of including a form of proprioceptive data in the classification model. In this study, proprioceptive sensing in the form of a motor encoder coupled to the linear actuator— which controls the grasping motions of the gripper—is used. As previously discussed, and shown in Figure 4.8, only very minor improvements in the classification accuracy across all of the classifiers was achieved by including the motor encoder data in the trained models. The motor encoder predictor importance is shown in Figure 4.12b; in this plot, the motor encoder predictor has an importance value in the upper 25% of the predictors.

4.3.2 Target Beam Member Set #3: Beam Members of Similar Cross-Sectional Shapes and Sizes
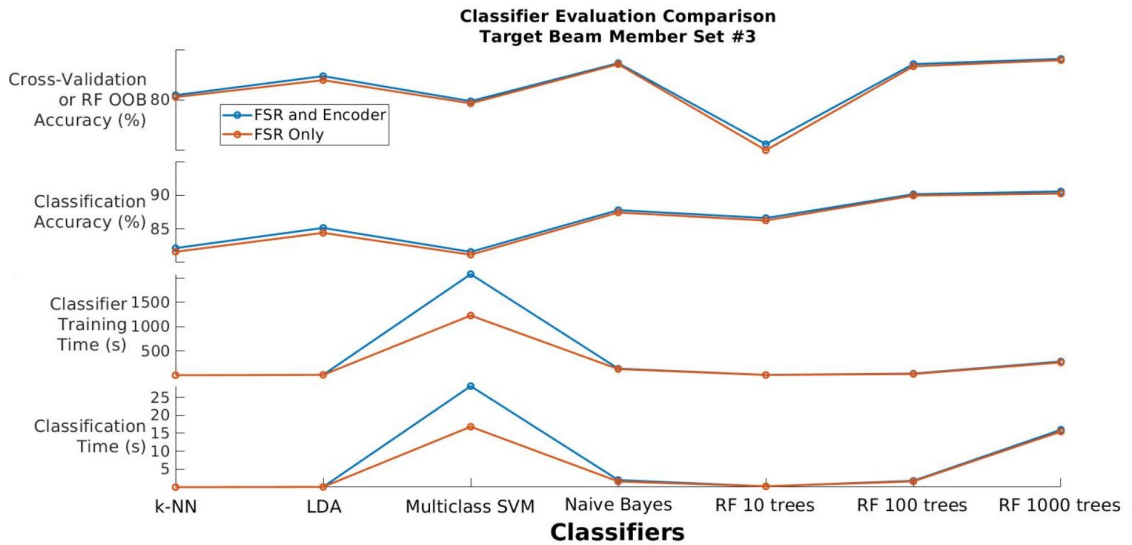
FIGURE 4.13: Target beam member set #3: comparison of commonly used classifiers evaluated against the four metrics.

Overall, the results in Figure 4.13 show similar trends to the classification accuracies for target beam member set #2. However, due to the increased similarities in the collected data—caused by the inclusion of beam members of similar cross-sectional shapes and sizes—a decrease in the average classification accuracy is observed. As with target beam member set #2, marginal improvements in the classification accuracy, at the expense of training and classification times can be achieved by including the motor encoder data in the classifier models. It can therefore be deduced that for rapid classification using this

data set, data from tactile sensors **only** is sufficient and inclusion of the motor encoder data is not necessary.

By introducing additional beam members of similar cross-sectional shape and identical dimensions into the target beam member set, a significant decrease in the classification accuracy, and therefore increase in misclassifications was observed for target beam member set #3. Despite an increase in AoA misclassifications being observed in Figure 4.14, the majority of AoAs still lie along the diagonal of the confusion matrix.

FIGURE 4.14: Confusion matrix for one trained k-NN classifier for target beam member set #3. Highlighted boxes show sources of confusion in the classification.

As with target beam member set #2, the source of confusion stemmed from some "low data" *tactile patterns* from grasping AoAs to the 50×50 mm "L" beam, 50×50 mm "+" beam and 50×50 mm "T" beam. However, similar non-zero *tactile patterns* were more commonly collected, due to the similarities in structural beam member cross-sectional shapes and sizes. Similar non-zero *tactile patterns* were most frequently collected during grasping where the portion of the beam member being grasped appeared identical in shape to other beam members in the target beam member set.

The drastic increase in confusion can be seen in the example k-NN confusion matrix in Figure 4.14. Due to the large number of misclassified AoAs, the confusion between structural beam members can be observed more clearly in Figure 4.15. In this figure, it is clear that erroneous classifications arise as a result of similarities in the cross-sectional shapes sizes of the structural beam members. In these cases, due to identical dimensions, adding the motor encoder data as a predictor in the classifier does not have a noticeable effect on improving the classification accuracy, as the actuation distance readings would be identical.

k-NN Classifier Confusion Matrix
Target Beam Member Set #3: FSRs and Motor Encoder Data
Classification of Cross-Sectional Shape and Dimension

Actual Class \ Predicted Class	75x75 mm "T" Beam	75x75 mm "T" Beam	75x75 mm "+" Beam	50x50 mm "T" Beam	50x50 mm "T" Beam	50x50 mm "+" Beam	51x51 mm Square Beam	75x75 mm "L" Beam	50x50 mm "L" Beam
50x50 mm "L" Beam	0	1	0	2	7	1	9	0	124
75x75 mm "L" Beam	10	2	0	0	0	0	0	131	1
51x51 mm Square Beam	0	0	0	0	5	0	19	0	12
50x50 mm "+" Beam	0	0	0	4	0	29	0	0	3
50x50 mm "I" Beam	0	0	0	1	55	0	3	0	13
50x50 mm "T" Beam	0	1	0	131	3	1	1	0	7
75x75 mm "+" Beam	0	0	36	0	0	0	0	0	0
75x75 mm "T" Beam	2	129	0	5	0	0	0	8	0
75x75 mm "I" Beam	54	3	0	0	0	0	0	15	0

FIGURE 4.15: Confusion matrix for one trained k-NN classifier, classifying individual beam member cross-sectional shapes and sizes, not individual AoAs from target beam member set #3.

The advantages and disadvantages of each of the individual classifiers for the beam member recognition problem—using tactile data **only** with target beam member set #3—are discussed below. With this target beam member set, the effects of similarities in the feature space are clearly evident through the deteriorating performance of the majority of the classifiers. This further demonstrates the effectiveness and suitability of particular classifiers for the practical application problem.

The k-NN classifier was able to maintain the fast training and classification times observed with target beam member set #2. However, the increased size of the data set and feature space—where the response classes are more clustered due to similarities in the beam member cross-sectional shapes and sizes—causes a significant decrease in the classification accuracy, compared to the other evaluated classifiers. With more similar *tactile patterns* in the feature space, classification using the same number of neighbours as target beam member set #2 evidently increases the classification confusion. This clearly demonstrates the poor ability of this classifier to generalise to new data sets with increased similarity in the feature space predictors.

The LDA classifier had a relatively slow training time, however it maintained the fast classification time previously observed. When compared to the results of classification for target beam member set #2, both of these times increased in duration, aligning with the general statement in Section 4.2.2 that the times are proportional to the size of the data. The LDA classifier was able to achieve a higher classification accuracy with target beam member set #3, relative to the other evaluated classifiers, whose results across the two target beam member sets showed similar trends. However, as predicted in Section 4.3.1, a decrease in the classification accuracy overall is observed.

As observed with target beam member set #2, the Multiclass SVM classifier achieved the slowest training and classification times amongst all of the evaluated classifiers for target beam member set #3. Compared to the classification for target beam member set #2, these times increased in proportion with the increased number of response classes. Despite the lengthy training and classification times, the classifier also achieves the lowest classification accuracy. These features are clearly undesirable, especially when considering

that many other classifiers with faster training and classification times could be used for the beam recognition problem, with higher accuracies.

Similar to the classification results with target beam member set #2, the Naïve Bayes classifier achieved slow training and classification times. Additionally, high classification accuracies were observed for the beam recognition problem with target beam member set #3. This classifier assumes that the data comes from an underlying distribution, with independence of the predictors within each class. This statement must hold true for a significant proportion of the feature space, otherwise significantly lower classification accuracies would be observed. The decrease in classification accuracy from target beam member set #2 to #3 can be attributed to a decrease in the number of response classes with independent predictors. Across the two target beam member sets, the Naïve Bayes classifier performs consistently. A question that remains to be answered, is how the classifier performance will deteriorate with increased similarities in the feature space predictors and response classes.

Similar to the analysis conducted in Section 4.3.1.1, the remainder of this section will focus on a more detailed discussion of the results using an RF classifier.

4.3.2.1 Random Forests

In this section, the results of the RF classifiers with varying input settings are analysed. In particular, the effects of varying the number of trees grown in the forest and the number of predictors in the feature space are investigated.

As Figure 4.16 shows, similar to target beam member set #2, growing at least 100 trees in the forest (regardless of the inclusion of motor encoder data) provides an acceptable trade-off between classification and computational effort. Unlike target beam member set #2, by growing more than 300 trees in the RF, a lower percentage of OOB error is achieved with the data set only comprised of FSR data. Across the two data sets, similar OOB errors were observed with fewer than 300 trees grown in the RF. As shown in the listing of results in Table 4.3, it is possible that even fewer than 100 trees could be grown in the forest to achieve similar classification accuracies.

Determining the number of predictors required for the efficient functionality of the classification model can be achieved by analysing the averaged predictor importance values in Figure 4.17. Figure 4.17a shows the average predictor importance over 1000 trained RF classifiers grown with 100 trees. Overlaid on this plot is the weighted sum of averaged raw FSR data for all of the beam members in the target beam member set. Similar to the data presented in the analysis of target beam member set #2, it can be seen that there is a direct relation between the predictor importance and the number of times a particular tactile sensor was activated during grasping. In this plot, the lowest importance predictors corresponded to tactile sensors 1–3 and 10–12. Since target beam member set #3 is comprised of some members from target beam member set #2, the previous analysis holds true for this target beam member set also, where it is not necessarily productive to greedily reduce the feature space based on predictor importance alone.

As shown in Figure 4.17b, the 19th predictor which corresponds to the motor encoder reading has a higher importance than a significant portion of the FSR predictors; however, the results in Figure 4.16 have shown that lower OOB error is typically achieved by using only the FSR data set. Therefore, considering that this target beam member set is representative of only a subset of structural beam members that could be found in a truss
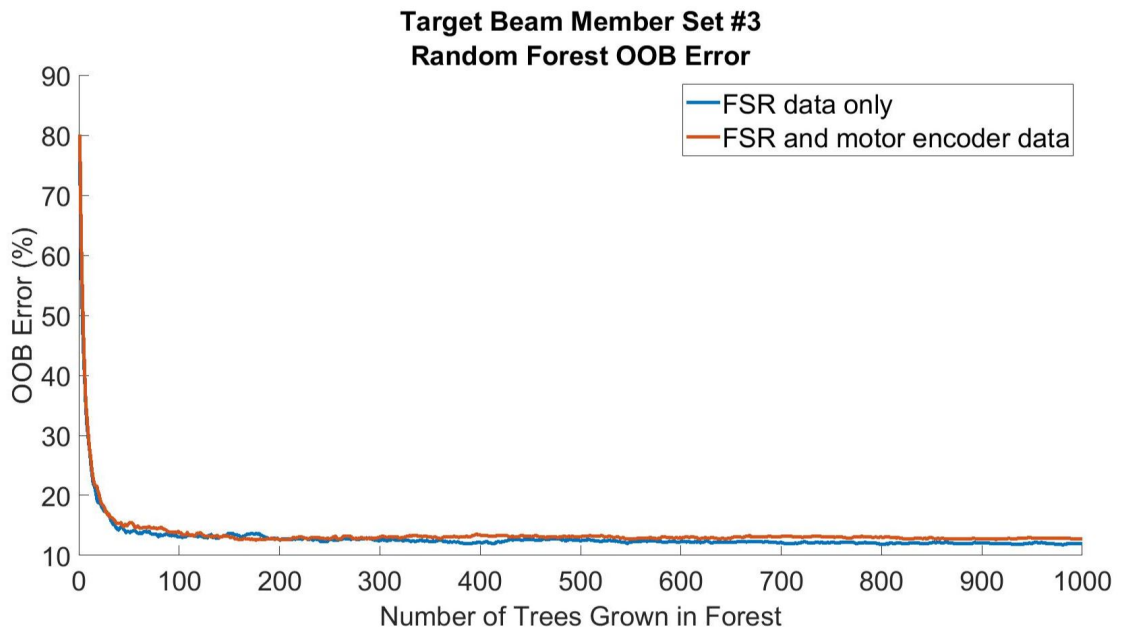
FIGURE 4.16: Target beam member set #3: RF OOB error with increasing number of trees grown in the forest.

TABLE 4.3: Target beam member set #3 classification accuracy and OOB error for between 10 and 100 trees grown in the RF using the FSR only data set.

Number of Trees	10	20	30	40	50	60	70	80	90	100
OOB Error (%)	29.93	19.74	16.64	15.40	14.6	14.05	13.79	13.7	13.39	13.32
Classification Accuracy (%)	86.24	88.05	88.94	89.25	89.49	89.62	89.74	89.82	89.91	89.94

structure, it can be determined that the FSRs are critical sensing components, with the current layout providing sufficient data for beam member recognition.

4.4 Discussion

In this chapter, a range of commonly used machine learning classifiers were compared for the task of beam member recognition in a truss structure. The tactile data collected in Sections 3.4.2.3 and 3.4.2.4 was used to train and evaluate the chosen classifiers for recognising structural beam members from beam member sets #2 and #3. Overall, the evaluated classifiers achieved good classification results, with similar classification accuracies, however, with varying training and classification times. For the two target beam member sets analysed, regardless of the classifier, minor improvements in the classification accuracies were observed when the data sets included data from the motor encoder. However, by including this data, slight increases in the classifier training and classification times were also recorded. It was therefore deduced that the use of **only** tactile data was sufficient for recognition of a structural beam member from the target beam member sets (#2 and #3).

Whilst the classification results were promising overall, some limitations to the accuracies of the classifiers became evident, depending on the data set used for training and evaluation. For example, the average classification accuracy of target beam member set #3 was lower than that of set #2. This was attributed to the similarities in the cross-sectional shapes and sizes of the beam members in target beam member set #3, causing similar *tactile patterns* to be collected during grasping, and therefore clustered response classes in the feature space. Since the classifiers directly use this raw tactile data to classify the
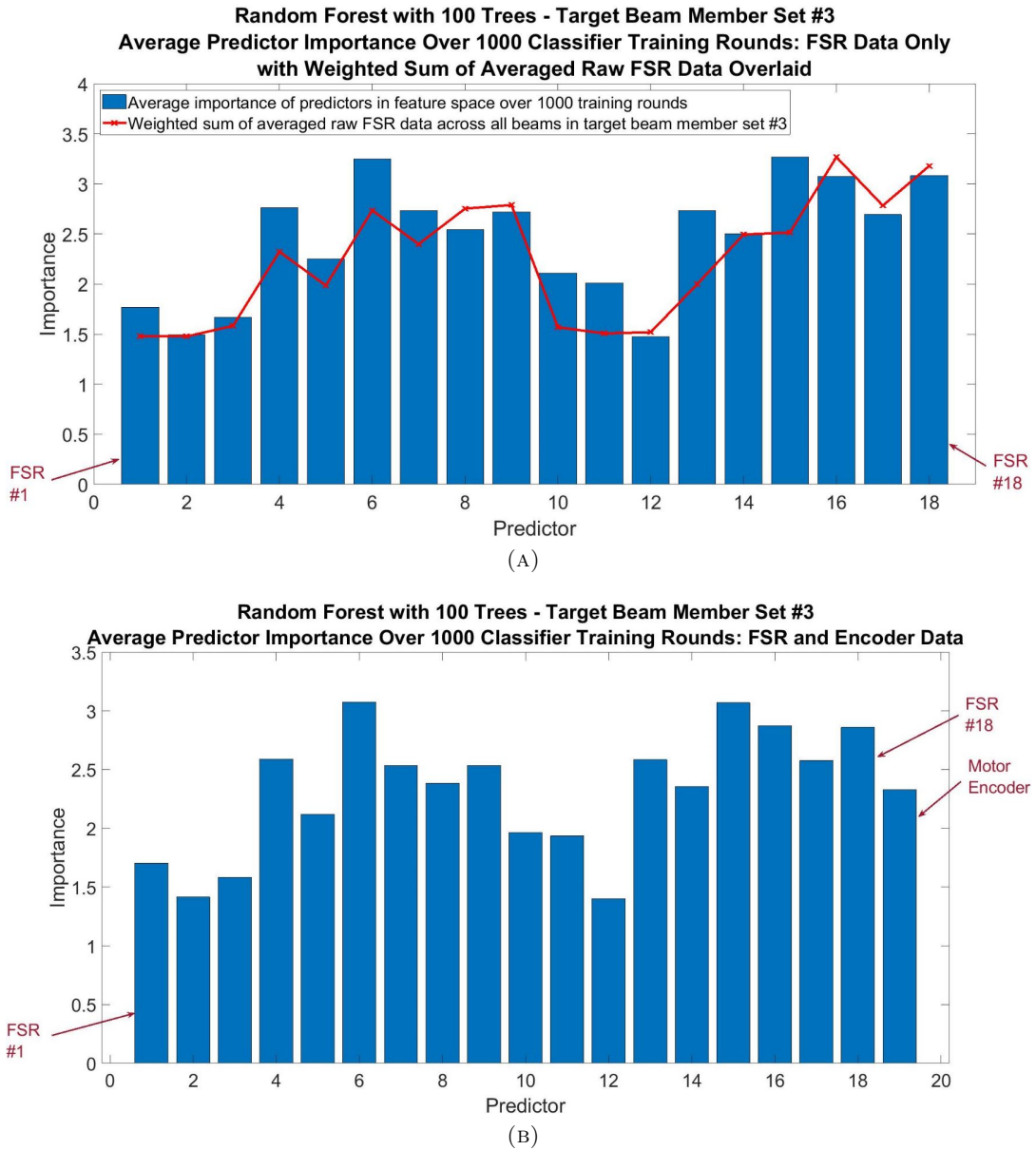
FIGURE 4.17: RF with 100 trees. Average importance of predictors in feature space for target beam member set #3: (A) Trained using only FSR data (plot overlaid with weighted sum of averaged raw FSR data for all beam members in the target beam member set), (B) Trained using FSR and motor encoder data.

beam member being grasped, the classification results were expected to be erroneous for particular beam members and AoAs.

Considering the requirements for the practical application environment—where beam member recognition would ideally be performed during climbing—the classifiers with excessive classification times (Multiclass SVM and RF with 1000 trees) are not considered

as practical candidates. Furthermore, some of the classifiers evaluated (LDA and Naïve Bayes) function on the assumption that the data comes from a certain underlying distribution. Considering future work with an expanded data set, this continued assumption may result in an increase in erroneous classifications. With the scope of future work in consideration, it is therefore preferable to select a classifier that does not make any assumptions about the data.

The two evaluated classifiers which do not make any assumptions about the data used are the k-NN and RF classifiers. An RF grown with 100 trees was consistently able to achieve the second highest classification accuracy (after an RF with 1000 trees) across the two target beam member sets. The RF classifier with 100 trees was slow to train and classify, compared to the k-NN classifier, but had the advantage of a consistently higher classification accuracy (∼3% higher for target beam member set #2 and ∼8% higher for target beam member set #3).

As outlined in Section 4.2.1, there are several limitations to the effectiveness of a k-NN classifier in practical application settings. For example, if the target beam member set was to increase substantially in size, classifier training and test times would be negatively impacted. Additionally, the classifier may suffer from a reduction in classification accuracy, as the model can become more sensitive given the scale of the data and the features comprising the feature space.

The results presented in this chapter must take into consideration expansion of the data sets (for the practical application) to include more structural beam members of similar cross-sectional shapes and sizes. Despite the high classification accuracies of the k-NN classifier for target beam member set #2, this accuracy did not scale with the increased size of target beam member set #3. Therefore, despite the short training and classification times of the k-NN classifier, the classifier is not considered as reliable for the practical application.

Based on the four metrics in the evaluation criteria, it can be concluded that the RF classifier grown with at least 100 trees produced favourable classification results across the two evaluated target beam member sets. The RF classifier performed consistently, with high classification accuracies and relatively fast training and classification times, as compared to the other classifiers.

Chapter 5

An Information-Based Method for Selecting the Next Best Grasping Angle-of-Approach

The research presented in Chapters 3 and 4 showed that a single *haptic glance* is broadly sufficient for beam member recognition using a soft gripper retrofitted with FSRs. Recognition was achieved through the use of machine learning methods to classify the cross-sectional shape, size and grasping AoA of a structural beam member, based on tactile data collected during grasping. Considering the target beam member set containing beam members of unique cross-sectional shapes and sizes (set #2), classification accuracies ranging from approximately 89% to 94% were achieved. These classification accuracies were related to the uniqueness of the structural beam members in the target beam member set, where unique *tactile patterns* were typically collected.

An increase in erroneous classifications was observed in Chapter 4 when classifying structural beam members of similar cross-sectional shapes and sizes (from target beam member set #3). With this target beam member set, classification accuracies ranging from approximately 81% to 90% were achieved with a single *haptic glance*. Strategically performing further *haptic glances* can result in more useful data for classifying a structural beam member and its properties (i.e. cross-sectional shape, size and grasping AoA). Exhaustively

grasping a structural beam member at all possible AoAs for data collection would be both time consuming and impractical. Ideally, a simple strategy to minimise the number of *haptic glances* and maximise the amount of information that can be collected would be developed. Naturally, the question that needs to be answered is how to select the next best grasping AoA to permit rapid recognition of the structural beam members.

In this chapter, this question is answered by developing an information-based method which uses raw FSR readings to select the next best grasping AoA for recognising a structural beam member and its properties. Based on the classification results presented in Chapter 4, a RF classifier grown with 100 trees is used as the basis for developing the proposed method. The focus of this research is on recognising beam members from a beam member set (target beam member set #3) which have similar (or even identical) cross-sectional shapes at certain AoAs. Similarities in the structural beam members at particular AoAs increases the difficulty of the recognition problem and leads to confusion in beam member recognition.

5.1 Overview

Based on the results presented in Chapter 4, several limitations to the beam member recognition approach using a single *haptic glance* were identified. These limitations were mainly related to the collection of similar *tactile patterns* during grasping; either due to similarities in the structural beam members, or due to scenarios where the gripper could not make adequate points of contact during grasping for data collection. In both of these cases, similar tactile data resulted in erroneous classifications of a beam member and its properties. In order to address these limitations, a strategy is required to select the next best grasping AoA, at which to perform a *haptic glance* to quickly collect useful data for recognising a beam member.

Several strategies exist to minimise the number of required touches or grasps for data collection to gain enough confidence in the classification or recognition of a target object. The general approach to the problem of where to touch next in object recognition has relied

on selecting an action to maximise the expected information gain (calculated probabilistically by Kullback Leibler Divergence (KLD), Bhattacharyya distance or an alternative histogram comparison method) from a set of viable candidate actions. By maximising the information gained from each grasp, a minimum number of grasps is inherently achieved.

These described methods have been developed for rigid grippers, with strategies for soft grippers yet to emerge. Object recognition methods using soft grippers, however, have predominantly focused on the use of proprioceptive sensors, rather than exteroceptive tactile sensors. In this chapter, based on the results in Chapter 4, an array of simple force sensors (FSRs) is used as the main sensory input for beam member recognition.

This chapter presents a simple information-based method for soft or adaptive grippers to select the next best grasping AoA in recognising beam members with similar cross-sectional shapes and sizes. Common approaches to information-based methods utilise probabilistic measures of information such as Shannon's entropy or Fisher information. However, the information-based method presented in this research uses a simple, non-probabilistic method for calculating information, similar to [186] and [187]. In this research, information is calculated based on the sum of the variance of collected tactile sensor data for a known set of structural beam members at known, discrete, angular displacements and set linear positions. The next best AoA is then selected based information calculated for candidate grasping AoAs.

A trained RF classifier [154] with 100 trees is used to provide an initial state estimate, i.e. perceived beam member cross-sectional shape, size and grasping AoA, after executing a single *haptic glance*. If the result of the classification is inconclusive, stipulated by multiple votes existing above a user defined threshold value (%), then the information-based method is used to select the next best grasping AoA. Based on the current predictions, candidate AoAs are generated and the next best AoA is determined as the candidate AoA where the predicted *tactile patterns* from the array of FSRs have the highest sum of variance, defined as the information value.

The proposed method is verified by performing simulations with data collected using a soft gripper retrofitted with FSRs. This method is not limited to a specific case of robotic manipulation and can be used for other adaptive robotic gripper designs fitted with suitable tactile sensors.

5.2 Information-based Method

This section details an information-based method for selecting the next best grasping AoA. In the context of the truss structure application environment there are two main scenarios where ambiguity arises in the classification of a structural beam member from a single *haptic glance*:

1) Multiple beam members can have similar cross-sectional shapes at certain AoAs, making it difficult to determine the true beam member shape e.g. disambiguating between a "T" beam and an "I" beam, and

2) Certain AoAs to a single beam member may also be similar, making it difficult to determine the true AoA of the gripper to the beam member e.g. due to symmetry, or other similarities in beam member shapes from different AoAs.

The state space of the problem of selecting the next best grasping AoA consists of all possible beam members (Bm) and AoAs (N_{AoA}), or $N_{ba} = Bm \times N_{AoA}$ beam-angle pairs. Before execution of the first *haptic glance*, all N_{ba} beam-angle pairs are considered as possible candidates for beam member recognition. After each executed *haptic glance* and based on the votes cast by the RF classifier, a number of beam-angle pairs may be eliminated from the set of candidates. The most informative grasping AoA is the one which has the highest probability of eliminating the most beam-angle pairs from the set of candidates.

The information-based method is illustrated by Figure 5.1. An initial grasp provides FSR data (a *tactile pattern*) which is used to make predictions about the beam member using a RF classifier. Votes cast by the RF classifier are sorted in descending order for analysis. If a single vote exists above a user defined threshold (classification accuracy), τ, then this
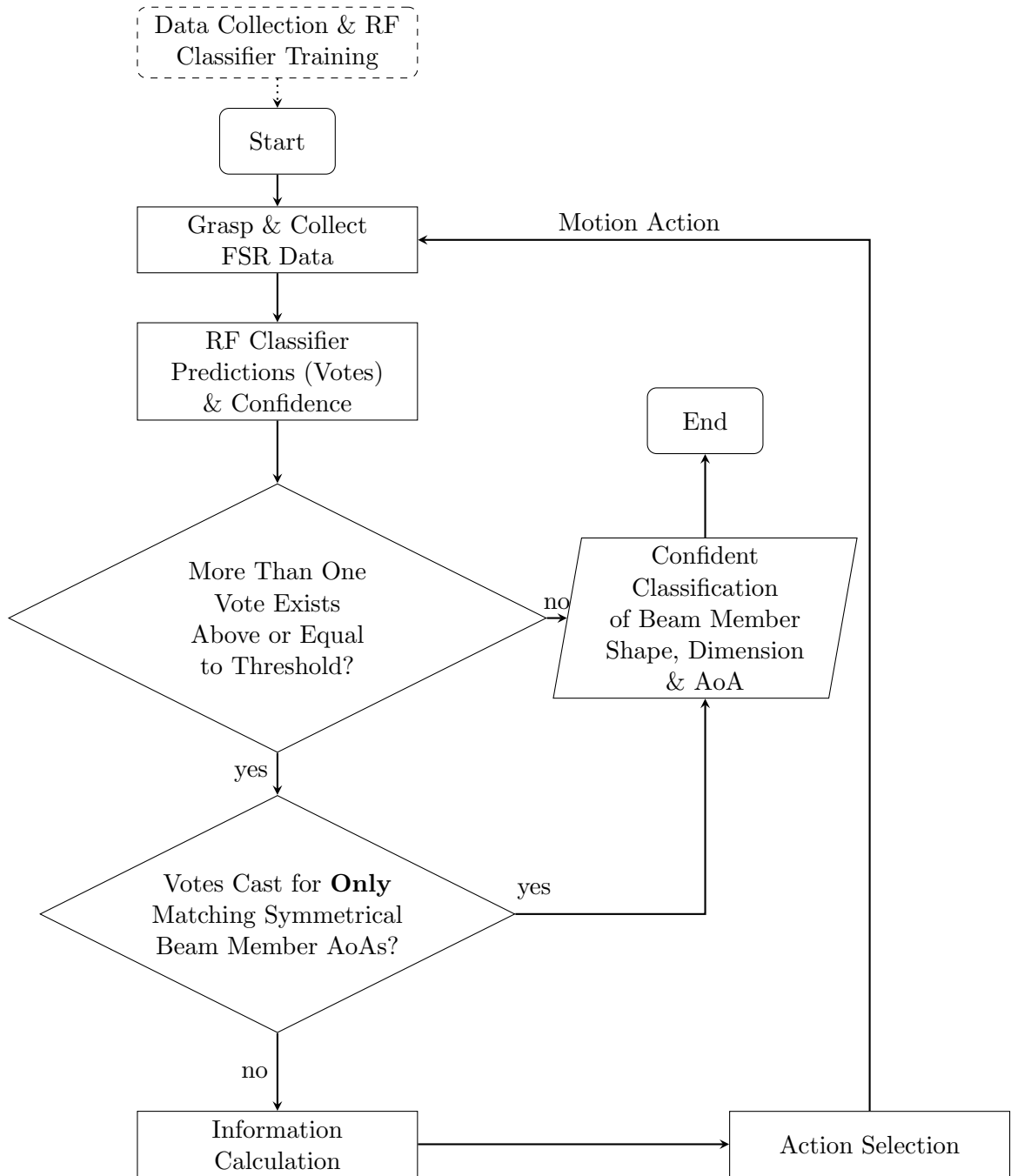
FIGURE 5.1: Flow chart of the information-based method.

vote dominates the classification, the RF classifier is confident and only one *haptic glance* is requithis process repeats, incrementing the number of grasps performed,red to recognise the beam member and its properties. The user defined threshold must be defined based on the performance of the classifier for a given data set. For the data obtained in this

thesis, the selection of the user defined threshold is further detailed in Section 5.3.2, with reference to Table 5.2.

If multiple votes exist above the threshold, then there *may* be confusion in the classification. A possible case where multiple votes may exist above the threshold and result in confident classification is when the beam member being grasped is symmetrical. Symmetrical beam members contain repeated AoAs, i.e. where the data obtained from a given AoA is identical to another AoA shifted by a number of degrees, depending on the axis or axes of symmetry. If all votes cast above the threshold are for only matching symmetrical beam member AoAs, then no further grasping actions could be undertaken to disambiguate the AoAs. If there is confusion in the classification, i.e. votes for non-repeated AoAs, then additional *haptic glances* are required to collect further data for recognition of the structural beam member. At this step in the process, information for candidate AoAs is calculated.

Information is calculated by comparing the expected *tactile patterns* across $N_{AoA} - N_{grasps}$ candidate AoAs (i.e. excluding any previously grasped AoAs including the current perceived AoA). The expected *tactile patterns* for candidate AoAs are taken as the average of data from the number of grasps (N_g) in the data collection phase—conducted offline. The candidate AoA i.e. the AoA shift with the highest overall variance in the individual FSR readings (the next best AoA) is expected to provide the best possible data for unambiguous recognition of the beam member and its properties. An action is selected based on the calculated next best AoA, and another grasp is executed. This process repeats, incrementing the number of grasps performed, N_{grasps}, until a single vote dominates the classification output, i.e. only one vote exists above the threshold and the beam member and AoA can be recognised. In this process, with each additional grasp performed, the candidate beam member and AoA set is reduced.

Candidate AoAs for a grasping action are comprised of angle shifts in increments of β degrees from the current predicted beam member AoAs, where β degrees refers to the angular increments in the AoAs during data collection. Therefore, to calculate information for candidate AoAs, the input matrix, F, of the FSR data differs, and is directly dependent on the initial votes cast by the RF classifier above the threshold.

Information is calculated (Equations 5.1, 5.2, 5.3) for the $N_{AoA} - N_{grasps}$ candidate AoAs (i.e. excluding any previously grasped AoAs including the current perceived AoA, $I = [I_1, I_2, ..., I_{N_{AoA}-N_{grasps}}]$). Information for a candidate AoA, I_a, is calculated by the sum of the variance (σ^2) in the $N = N_{FSR}$ individual FSR readings for the n predicted beam member AoAs.

$$\mu_i = \frac{1}{n} \sum_{j=1}^{n} F_{ij} \tag{5.1}$$

$$\sigma_i^2 = \frac{1}{n} \sum_{j=1}^{n} (F_{ij} - \mu_i)^2 \tag{5.2}$$

$$I_a = \sum_{i=1}^{N} \sigma_i^2 \tag{5.3}$$

The aim of the action selection is to choose the most favourable AoA for grasping, i.e. the AoA corresponding to $\max(I)$, which can provide sufficient data to unambiguously recognise a beam member and its properties.

5.2.1   Classifier Training

The results presented in Chapter 4 demonstrated that all of the commonly used classifiers evaluated had similar performance outcomes, with the major differentiating factors being the classifier training and classification times. For classification of structural beam members in target beam member set #3, the variety of commonly used classifiers evaluated, including k-NN, LDA, Multiclass SVM, Naïve Bayes and RF were all suitable candidates resulting in relatively high classification accuracies.

Theoretically, any of the evaluated classifiers could be used to provide classifier predictions in the information-based method presented. However, from all of the classifiers trained and tested, a RF classifier with 100 trees provided one of the highest classification accuracies, with a suitable trade-off between training time and classification time. This classifier also performed with consistently high performance in classification accuracy across the two

target beam member sets. As briefly addressed in Chapter 4, in future work, the predictor importance can also be examined to determine the effectiveness of any changes to the sensor density and placement on the gripper. The gripper design can then be modified based on the results of this analysis.

Following the data collection procedure described in Section 3.4.2.4, FSR data was collected at discrete $\beta = 10°$ increments to each of the beam members in target beam member set #3. The collected dataset, as summarised by Table 4.1, is comprised of the $Bm = 9$ beam members from target beam member set #3, with AoAs defined in Table 3.4, totalling 207 unique beam-angle pairs. The complete dataset (populating the repeated AoAs for symmetrical beam members) is comprised of a total of $Bm = 9$ beams with $N_{AoA} = 36$ ($360°/\beta$) AoAs, therefore $N_{ba} = 324$ beam-angle pairs.
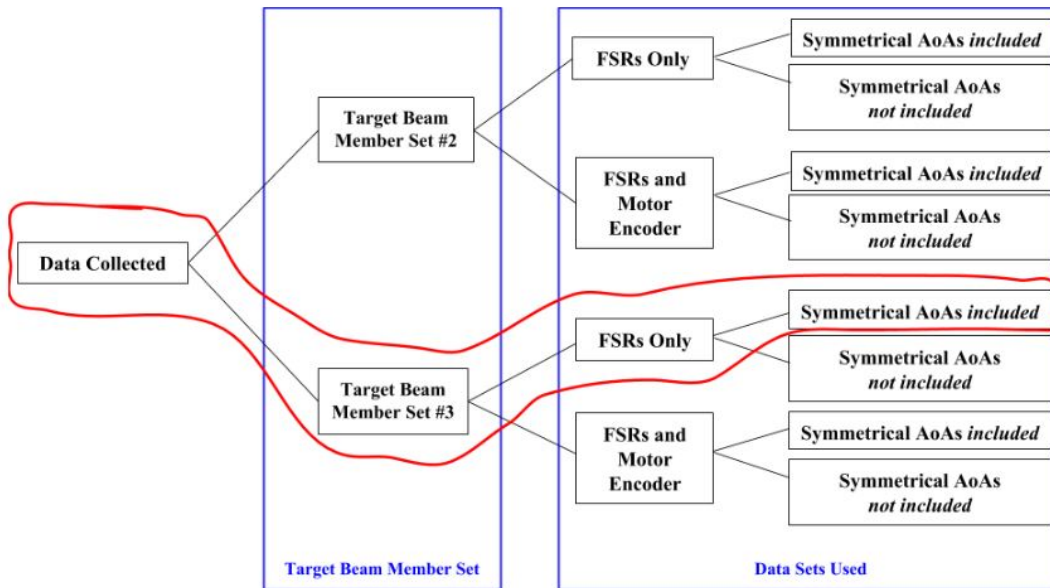
FIGURE 5.2: Classifier training settings for the information based method—An RF classifier is trained with 100 trees, with a 90:10 data split for training and test data respectively.

Regardless of symmetrical beam members, the goal of the classification stage in the information-based method is to recognise the structural beam member being grasped, including the grasping AoA. Therefore, all beam-angle pairs from target beam member set #3, including the symmetrical AoAs must be used in the classifier training phase, as shown in Figure 5.2. For training the RF classifier with 100 trees, the data set containing only FSR data was used, for reasons previously discussed in Chapter 4. The complete

data set was partitioned, with 90% of the data for training the classifier and 10% for testing the classifier. Since the RF classifier with 100 trees had already been evaluated with a 60:40 data split in the classifier analysis presented in Chapter 4, the 90:10 data split was implemented to allow for a single dataset from each individual AoA to be used as simulated *haptic glance* data.

5.3 Results

5.3.1 Beam Recognition Using a Single Haptic Glance

Since the votes cast by the RF classifier dictate if the information-based method is required, the results of classification using the RF classifier alone are first analysed. This analysis reveals the misclassified AoAs (see Figure 5.3), therefore providing insight into the AoAs which will provide interesting case studies using the information-based method.

5.3.1.1 Classification with the RF Classifier Only

High classification accuracies are expected when the beam members being grasped significantly differ in size and/or cross-sectional shape, such as the structural beam members in target beam member set #2. However, the structural beam members of target beam member set #3 consists of beam members with identical dimension and similar cross-sectional shape at certain AoAs.

The confusion matrix in Figure 5.3 shows the RF classifier accuracy for all of the possible $N_{AoA} = 36$ AoAs to each of the $Bm = 9$ beam members (324 beam-angle pairs) using a single *haptic glance*. It can be seen that confusion exists between multiple beam members, particularly those of identical dimension or between different AoAs to a single beam member.

Upon removal of the repeated AoAs for the symmetrical beam members, the dataset could be reduced to 207 unique AoAs as listed in Table 3.4. The classification accuracy with this reduced dataset is shown in the confusion matrix in Figure 5.4. Comparing Figures
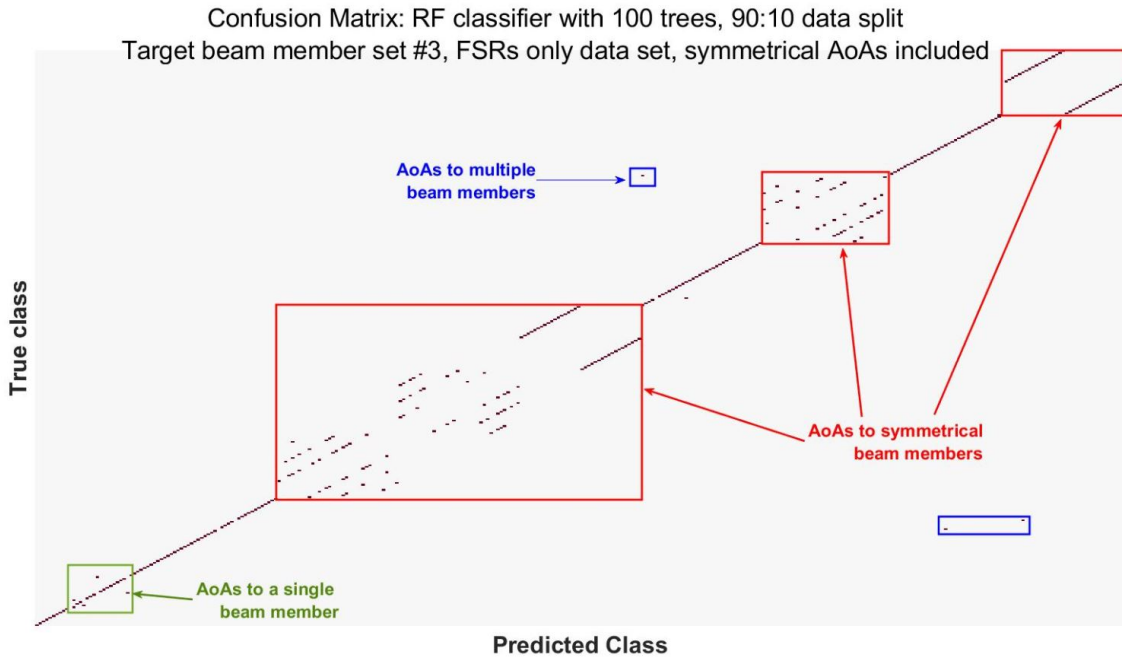
FIGURE 5.3: Confusion matrix from the RF classifier trained with 100 trees on 90% of the complete dataset (training set) for target beam member set #3. Results shown are the classifications of the remaining 10% of the complete data **including** symmetrical AoAs (test set) using input data from FSRs only.

5.3 and 5.4, a drastic reduction in the confused AoAs can be observed, however a number of confused AoAs remain, where the beam member cannot be recognised by using a single *haptic glance.*

The averaged classifier performance is summarised by Table 5.1, for RF classifiers trained with 100 trees and both including and excluding data from symmetrical AoAs. Analysis of the RF classification results show that the classification output alone cannot be wholly trusted. By definition, the most frequent vote cast by each of the trees in the RF is the classification output. The classification result therefore simply needs to be higher in confidence than all other votes cast. In many cases, multiple AoAs may receive a significant portion of the votes, making the classification decision very close. For these problematic "low information" AoAs, additional grasps would be required to recognise the beam member and its properties.
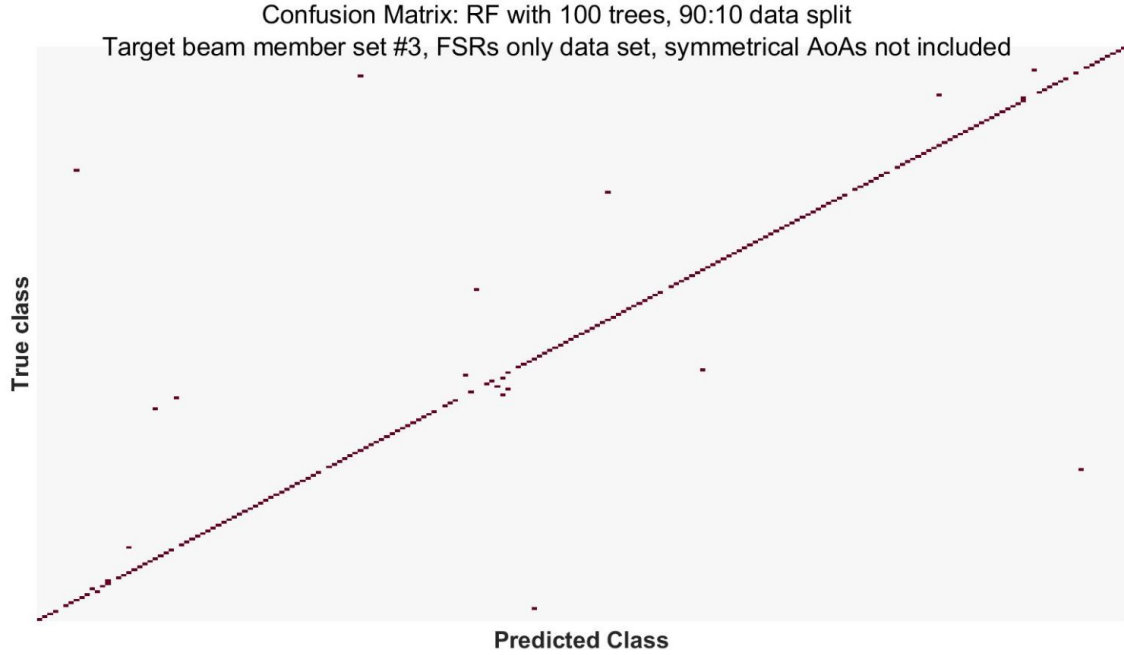
FIGURE 5.4: Confusion matrix from the RF classifier trained with 100 trees on 90% of the complete dataset (training set) for target beam member set #3. Results shown are the classifications of the remaining 10% of the reduced data **not including** symmetrical AoAs (test set) using input data from FSRs only.

5.3.1.2 Classification with the Proposed Information-based Method

The remainder of this section discusses results using the information-based method, using a single RF classifier trained with 100 trees. Similar to the RF classifier alone, using the information-based method still results in the majority of AoAs (82.4% – 96.6%, depending on threshold value) being classified with a single *haptic glance* (see Table 5.2). In these cases, a single *haptic glance* provided unique *tactile patterns* for rapid recognition of a beam member and its properties. However, it is important to have a confident perception of a beam member and its properties, which is not always possible to obtain by executing a single *haptic glance*.

TABLE 5.1: Averaged RF results over 1000 classifier training rounds for the information-based method—grasping AoAs for target beam member set #3.

Symmetrical AoAs Included? (Y/N)	Average OOB Accuracy (%)	Average Classification Accuracy (%)	Average Classifier Training Time (s)	Average Classification Time (s)
Y	41.63	42.61	75.02	1.51
N	88.99	90.77	35.13	1.10

The RF classifier outputs the highest vote as the classification result, regardless of the number of votes cast and their confidence ratings. The information-based method, however, is used to analyse the individual RF classifier votes and assess whether or not the RF classifier output will be sufficient for unambiguous classification overall. This allows for any ambiguous AoAs to be flagged before they are classified (either correctly or incorrectly) and for further *haptic glances* to be selected. It is therefore possible that further ambiguous AoAs would arise from using the information-based method, depending on the threshold value (τ) chosen.

An example of this can be observed by inputting the *tactile pattern* from the AoA of -120° to the 50x50 "T" shaped beam member into the RF classifier. The three highest votes cast by the RF classifier are:

1) **31%** for -120° 50× 50 "T"

2) **30%** for -30° 50× 50 "T"

3) **11%** for -120° 50× 50 "L"

Whilst the RF classifier has correctly classified the AoA, the margin of victory was only 1%, meaning that the AoA was very close to being incorrectly classified. Assuming that the threshold, τ, is set to at most 18%, the information-based method will flag this as an ambiguous AoA, as two votes would exist above the threshold. This AoA, however, is not considered ambiguous by the RF classifier alone, since it was correctly classified and would appear along the diagonal of the confusion matrix.

A similar case which demonstrates a "low data" *tactile pattern* resulting in misclassification by the RF classifier is the AoA of -140° to the 50 × 50 "L" shaped beam member. The three highest votes cast by the RF classifier are as follows:

1) **21%** for -110° 50× 50 "L"

2) **19%** for -140° 50× 50 "L"

3) **11%** for -100° 50× 50 "L"

For both of the AoA cases stated above, the information-based method will flag these cases as ambiguous and decide to select further strategic *haptic glances* to collect more data to ensure that the beam member and its properties can be correctly recognised. As shown by the results in Table 5.2, in order to flag these ambiguous AoA cases, a threshold value must be selected appropriately.

5.3.2 Beam Recognition using Multiple Haptic Glances

Table 5.2 summarises the results of the information-based method across all of the 324 AoAs in the dataset, with varying threshold values (τ). It can be clearly seen that the majority of beam member AoAs could be classified with a single *haptic glance*, regardless of the threshold value. For the remaining AoAs where more than one *haptic glance* was required, typically the beam member and AoA could be recognised with fewer than four *haptic glances*.

TABLE 5.2: Results of beam member recognition using the information-based method across the 324 unique AoAs with varying threshold values.

τ	Number of *Haptic Glances* Required For Correct Classification					Misclassified AoAs	AoAs with All Votes $< \tau$
	1	2	3	4	5		
10%	267 (82.41%)	36	6	12	3	0	0
15%	283 (87.35%)	30	4	6	1	0	0
16%	284 (87.65%)	29	4	6	1	0	0
17%	288 (88.89%)	30	4	2	0	0	0
18%	293 (90.43%)	26	3	2	0	0	0
19%	295 (91.05%)	23	3	2	0	0	1
20%	297 (91.67%)	20	3	2	0	1	1
25%	305 (94.14%)	14	1	0	0	1	3
30%	313 (96.60%)	3	0	0	0	4	4

Based on the presented results for target beam member set #3, the ideal threshold value to achieve the lowest number of *haptic glances*, without misclassifying the structural beam members and their properties, was $\tau = 18\%$. Therefore, the remainder of this section will further analyse and discuss the results obtained with this threshold value.

When using the information-based method for beam member cross-sectional shape and AoA recognition, the 31 (9.57%) grasps which could not be classified using a single *haptic glance* could be classified with more than 1, but typically fewer than 4 *haptic glances*. Across the complete data set, an average of 1.12 *haptic glances* were required for recognition of the beam member and its properties.

The cases where more than two *haptic glances* were required for recognition were examined carefully to determine if excessive grasping actions were executed as a result of the selection of the next best grasping AoA by the information-based method. In most of these cases, by choosing the AoA with the **highest** calculated information, an ambiguous AoA was selected, therefore requiring additional *haptic glance/s* to recognise the beam member AoA.

5.3.3   Case Studies

The results are further examined in this section by analysing the two cases identified in Section 3.4.3.4 where a single *haptic glance* was not sufficient for the recognition of a beam member and its properties. The first case study covers example cases of disambiguation between multiple beam member cross-sectional shapes, where multiple AoAs to multiple beam members may receive votes above the threshold. The second case study covers example cases of disambiguation between multiple AoAs to a single beam member cross-sectional shape, where multiple AoAs to a single beam member may receive votes above the threshold.

5.3.3.1   Disambiguating Between Beam Members with Differing Cross-sectional Shapes and/or Sizes

Disambiguating between beam members with differing cross-sectional shapes refers to the case identified by Figure 3.32b and Figure 3.33, where votes may be cast by the RF classifier for multiple beam member cross-sectional shapes and AoAs. The goal of the action selection is to choose the next best AoA that will narrow down the true beam member and AoA from the list of potential beams after any *haptic glance*.

In this section, the results of selecting two threshold values ($\tau = 15\%$ and $\tau = 18\%$) will be analysed for comparison. Along with the overall number of grasps required for beam member recognition, the selection of the threshold value, τ can directly affect the next best grasping AoA calculated by the information based method. This change in calculated next best grasping AoA is evident in the case study of executing a primary *haptic glance* at $\pm 180°$ to the 50×50 "T" beam member.

By selecting a threshold value of $\tau = 15\%$, the RF classifier casts votes (greater than or equal to the threshold value) for many different beam member cross-sectional shapes and AoAs:

1) **31%** for 180° 50×50 "T"

2) **21%** for 180° 50×50 "L"

3) **19.67%** for 0° 50×50 "H"

4) **15%** for 90° 50×50 "L"

Upon initial confusion in the beam member cross-sectional shape from the first *haptic glance*, the information-based method is used to calculate (using Equations 5.1, 5.2 and 5.3) the information for each candidate angle shift from the original grasped AoA. The results of this calculation reveal that the AoA located at an angle shift of 90° CCW has the highest information. By navigating to this AoA, there is a high probability of eliminating the largest number of beam member cross-sectional shapes and AoAs from the list of possibilities. The information-based method also calculates that the AoA with the lowest information is located at a 10° shift CW. Examples of these calculations are summarised below.

Since the original votes cast above the threshold were for four possible AoAs, information is calculated using FSR data (from 18 sensors) for each of these four possible AoAs. The data is then a 4×18 array, consisting of four rows of the possible AoAs, and 18 columns consisting of the FSR data for each of these corresponding AoAs. For each of the n sensors, the average is calculated on a column wise basis.

FIGURE 5.5: Information-based method (with $\tau = 15\%$) for grasping at the initial AoA of 180° to the 50×50 "T" beam member.

As shown in Figure 5.5, the data from sensor 8 for the high information AoA shift of 90° CCW from grasp 1, across each of the four possible AoAs consists of the following raw FSR data:

$$
\begin{bmatrix}
20.0 \\
669.2 \\
668.1 \\
7.6
\end{bmatrix}
$$

Using Equation 5.1, the average for sensor 8, where $i = 8$ is calculated as:

$$
\begin{aligned}
\mu_i &= \frac{1}{n} \sum_{j=1}^{n} F_{ij} \\
&= \frac{1}{4}(20 + 669.2 + 668.1 + 7.6) \\
&= 341.225
\end{aligned}
$$

Using Equation 5.2, the variance for sensor 8, where $i = 8$ is calculated as:

$$\sigma_i^2 = \frac{1}{n} \sum_{j=1}^{n} (F_{ij} - \mu_i)^2$$

$$= \frac{1}{4}[(20 - 341.225)^2 + (669.2 - 341.225)^2$$

$$+ (668.1 - 341.225)^2 + (7.6 - 341.225)^2]$$

$$= 1.0723 \text{x} 10^5$$

Performing the above calculations for the remaining 17 sensor values and performing the sum of the variance across each of these N total sensors, the information for the given angle shift of a degrees, I_a, is calculated as $3.8037 \text{x} 10^5$.

As shown in Figure 5.5, the data from sensor 8 for the low information AoA shift of 10° CW from grasp 1, across each of the four possible AoAs consists of the following raw FSR data:

$$\begin{bmatrix} 602.8 \\ 620.7 \\ 717.5 \\ 637.5 \end{bmatrix}$$

Using Equation 5.1, the average for sensor 8, where $i = 8$ is calculated as:

$$\mu_i = \frac{1}{n} \sum_{j=1}^{n} F_{ij}$$

$$= \frac{1}{4}(602.8 + 620.7 + 717.5 + 637.5)$$

$$= 644.625$$

Using Equation 5.2, the variance for sensor 8, where $i = 8$ is calculated as:

$$\sigma_i^2 = \frac{1}{n} \sum_{j=1}^{n} (F_{ij} - \mu_i)^2$$

$$= \frac{1}{4}[(602.8 - 644.625)^2 + (620.7 - 644.625)^2$$

$$+ (717.5 - 644.625)^2 + (637.5 - 644.625)^2]$$

$$= 1.9208\text{x}10^3$$

Performing the above calculations for the remaining 17 sensor values and performing the sum of the variance across each of these N total sensors, the information for the given angle shift of a degrees, I_a, is calculated as $3.8154\text{x}10^4$.

Performing the above calculations for the remaining 33 candidate AoA shifts from the original grasping AoA, the information for the candidate AoAs is summarised by Figure 5.6. Figure 5.6 shows that the candidate AoA with the highest information across the possible 35 angle shifts of 10° increments from the original grasped AoA is at 90° CCW. Conversely, the candidate AoA with the lowest information is located at 350° CCW (or 10° CW) from the original grasped AoA.

As summarised by Figure 5.5, by implementing the information-based method to select the next best grasping AoA, the potential beam member cross-sectional shapes and AoAs are eliminated with one additional grasp. After the second *haptic glance* has been executed, the beam member and its properties are recognised (with 83% confidence, all other votes are less than or equal to 3% each) and no further *haptic glances* are required for classification.

Selecting a higher threshold value, $\tau = 18\%$, the fourth vote (15% for 90° 50× 50 "L") is excluded from the analysis. Consequently, the information calculation process is conducted on three possible *tactile patterns*, rather than four. Then, upon initial confusion in the beam member cross-sectional shape from the first *haptic glance*, the information-based method calculates that the AoA located at an angle shift of 180° CCW (or CW) has the highest information. By navigating to this AoA, there is a high probability of eliminating the largest number of beam member cross-sectional shapes and AoAs from the list of
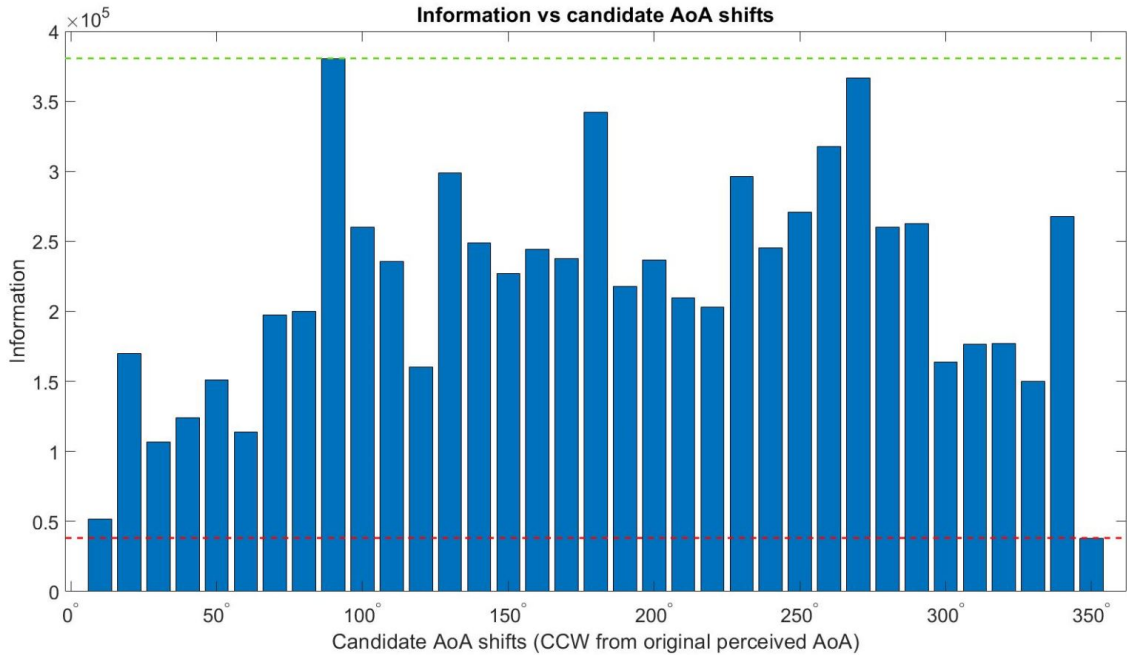
FIGURE 5.6: Information vs. candidate AoA shifts for the original perceived AoA of $\pm 180°$ to the 50×50 "T" shaped beam member.

possibilities. As with the threshold value of $\tau = 15\%$, the information-based method also calculates that the AoA with the lowest information is located at a 10° shift CW.

As summarised by Figure 5.7, by implementing the information-based method to select the next best grasping AoA, the potential beam member cross-sectional shapes and AoAs are eliminated with one additional grasp. After the second *haptic glance* has been executed, the RF classifier casts the following votes:

1) **39%** for -20° 75×75 "T"

2) **35%** for 0° 50×50 "T"

3) **23%** for -10° 75×75 "T"

Despite three votes existing above or equal to the confidence threshold, from the initial grasp, the only possible beam members that remained in the candidate pool were the 50×50 "T", "L" and "H" beams. From the RF predictions using the *tactile patterns* obtained during the second grasp, it is evidently more likely that the beam being grasped
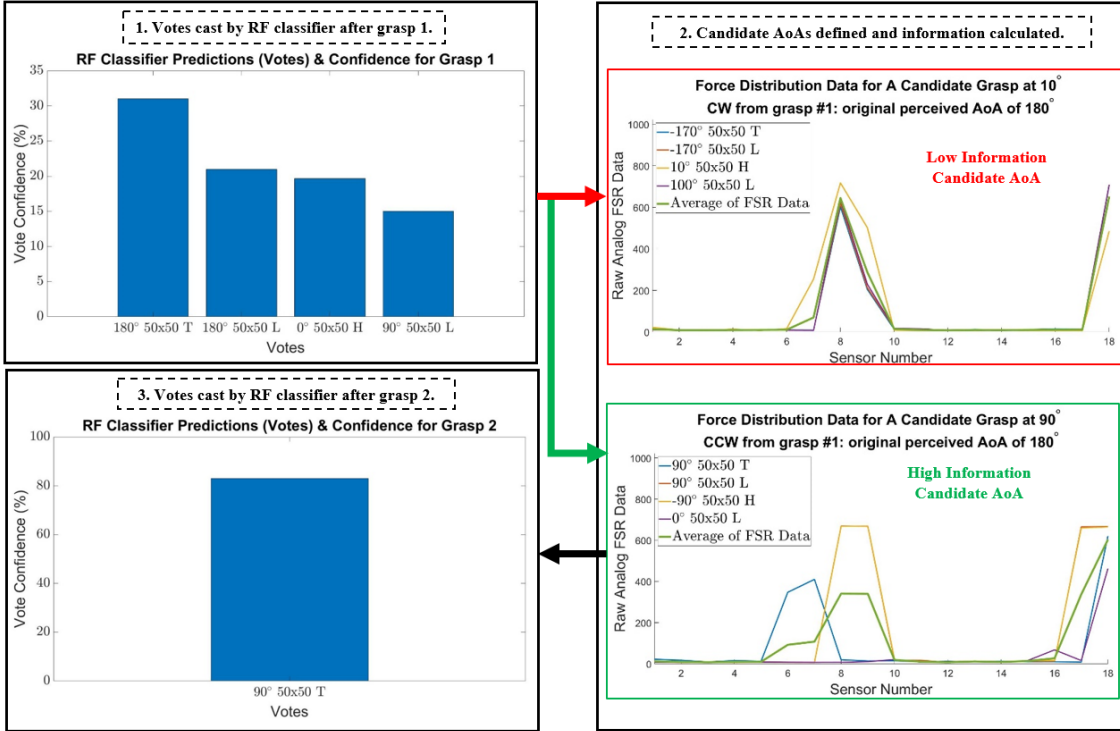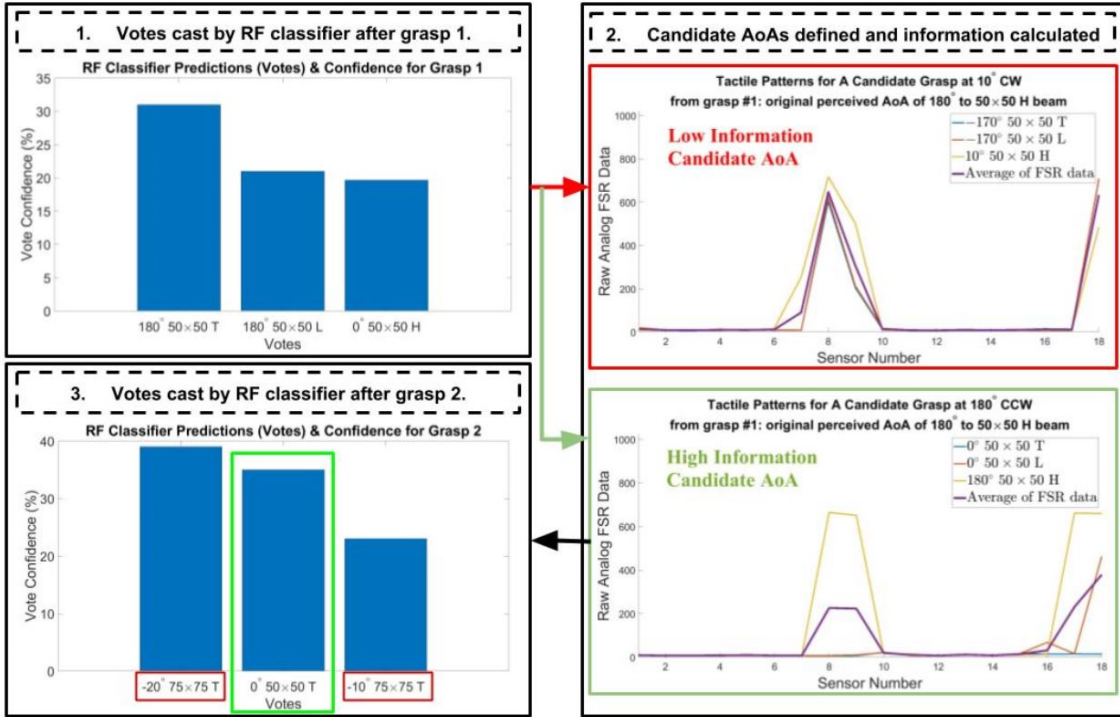
FIGURE 5.7: Information-based method (with $\tau = 18\%$) for grasping at the initial AoA of 180° to the 50×50 "T" beam member.

is a 75×75 "T" beam at either -20° or -10° (votes highlighted in red in step 3 of Figure 5.7). However, since this beam member shape and size was eliminated from the candidate pool based on the predictions made from grasp 1, the only remaining vote was for the 50×50 "T" beam at 0° (highlighted in green in step 3 of Figure 5.7). Based on these votes, two *haptic glances* were required to recognise the beam member and its properties, and no further *haptic glances* are required for classification.

There are many examples of grasping AoAs in target beam member set #3, where changing this threshold value from $\tau = 15\%$ to $\tau = 18\%$ has no effect on the overall result of the information-based method. One example of this can be observed when executing a primary *haptic glance* at the grasping AoA of -120° to the 75×75 "L" shaped beam member. At this grasping AoA, the following votes are cast by the RF classifier:

1) **53%** for -120° 75×75 "L"

2) **20%** for -130° 75×75 "T"

It can be seen that changing the threshold value, τ, from 15% to 18% would have no effect on the information calculation procedure for selecting the next best grasping AoA. If a threshold value, τ, greater than 20% was defined, however, no further grasps would be required for beam member recognition.

Another example of this can be observed when executing a primary *haptic glance* at the grasping AoA of -10° to the 75×75 "T" shaped beam member. Based on the *tactile patterns* obtained from grasping at this AoA, the votes cast by the RF classifier are as follows:

1) **43%** for 0° 50×50 "T"

2) **28%** for -10° 75×75 "T"

3) **28%** for -20° 75×75 "T"

For the result of this beam member recognition to be affected, a threshold value, τ, of greater than 28% would need to be defined. In this case, increasing the threshold value to this level is clearly not ideal, since this change would result in misclassification of both the beam member and AoA.

5.3.3.2 Disambiguating Between Multiple AoAs to a Single Cross-sectional Shape and Size of Beam Member

Disambiguating between multiple beam member AoAs refers to the case identified by Figure 3.32a, where votes may be cast by the RF classifier for multiple AoAs to a single cross-sectional shape of beam member, e.g. -100°, -110°, -140° to the 50 × 50 "L" shaped beam member. The goal of the action selection is to choose the next best AoA that will narrow down the true beam member AoA from the list of potential beam AoAs after any *haptic glance*.

In this section, the results of selecting two threshold values ($\tau = 15\%$ and $\tau = 18\%$) will be analysed for comparison. Similar to the previous section, changing the threshold value can not only affect the number of grasps required for classification, but also the calculation of the next best grasping AoA. This change in calculated next best grasping AoA is evident

in the case study of executing a primary *haptic glance* at -40° to the 50×50 "L" shaped beam member.

Based on the *tactile patterns* obtained from grasping at this AoA, the votes cast by the RF classifier (with the threshold value, τ, set to 15%) are as follows:

1) **58%** for -40° 50×50 "L"

2) **16%** for 140° 50×50 "L"

From the votes and confidence levels shown above, it can be deduced that at least one additional *haptic glance* would be required before the beam member and its properties can be recognised. In fact, in this case, **four** *haptic glances* are required to be executed (as shown in Table 5.3 and Figure 5.8). Setting the threshold value higher (to $\tau =$18%, for example), results in recognition by performing a single *haptic glance*.

TABLE 5.3: Information-based method calculation process, for an initial *haptic glance* performed at -40° to the 50×50 "L" beam.

Grasp Number	Votes	Confidence (%)	Perceived Beam & AoA	Ambiguity in Perceived Beam? (Y/N)	Motion Required to Reach Next Best AoA	Expected AoA Reached After Motion Action
1	-40° 50×50 "L" +140° 50×50 "L"	58 16	-40° 50×50 "L"	Y	140° CCW	± 180°
2	+90° 50×50 "L" ± 180° 50×50 "L"	52 24	+90° 50×50 "L"	Y	90° CCW	+90°
3	+90° 50×50 "L" ± 180° 50×50 "T" ± 180° 50×50 "L"	40 29 21	+90° 50×50 "L"	Y	90° CCW	± 0°
4	± 0° 50×50 "L"	96	± 0° 50×50 "L"	N	N/A	N/A

In Figure 5.8, the outcomes of each *haptic glance*, and the motion action required to navigate to the next best grasping AoA are displayed. The current perceived AoA is shown by a blue cross on the circumference of the red circle, which represents the highest vote cast by the RF classifier for the current grasp. The black arrow pointing towards the red circle indicates the true AoA. Therefore, the error between the actual and perceived AoA can be seen by comparing the position of the black arrow and blue cross for each grasp.

It is important to note that the motion action is always measured from the reference point of the current perceived grasping AoA. For example, the perceived AoA after grasp 1
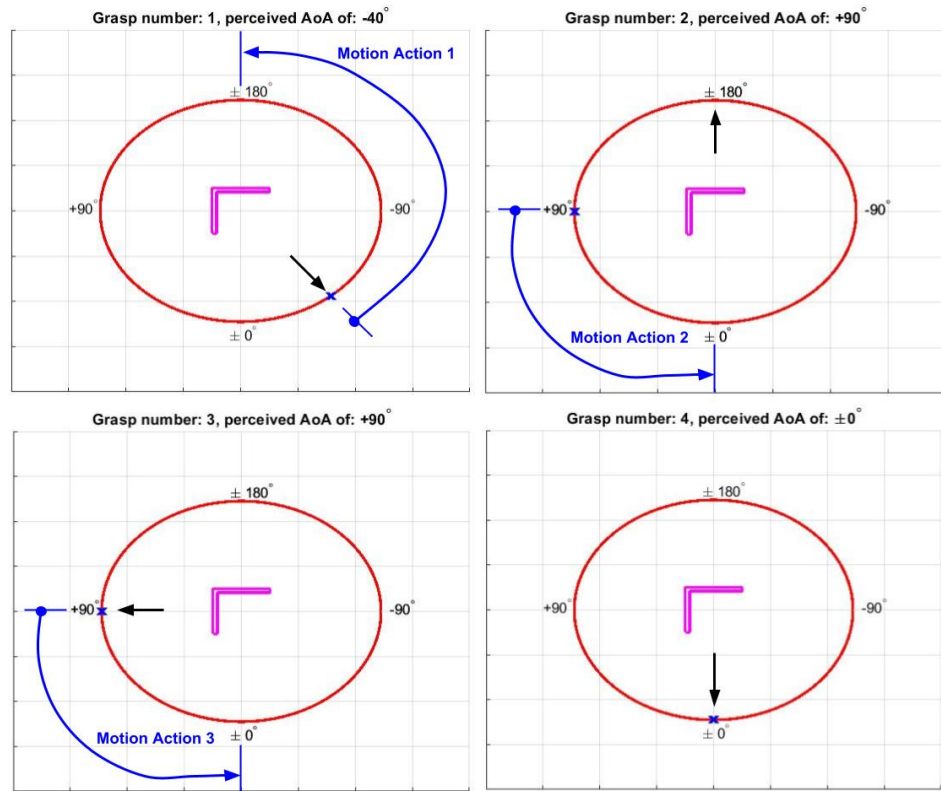
FIGURE 5.8: Information-based method implemented with $\tau = 15\%$ for grasping at the initial AoA of -40° to the 50×50 "L" beam member. Four grasping and three motion actions are shown, relating to the information in Table 5.3.

is -40°. Based on this perceived AoA, the next best AoA was calculated at a 140° shift CCW. A motion action of 140° CCW would result in an expected new grasping AoA of $\pm$ 180°. However, as can be seen in grasp 2, the perceived AoA is +90°, which is caused by similar *tactile patterns* existing between the AoAs of $\pm$180° and +90° for the 50×50 "L" shaped beam member. The grasping AoA of +90° is then used as the reference point for calculating the next best grasping AoA shift, instead of the expected (and actual) AoA of $\pm$ 180°.

Contrary to the example above, there are many examples of grasping AoAs in target beam member set #3, where changing the threshold value, τ, from 15% to 18% has no effect on the overall result of the information-based method. An example of this is the initial grasping AoA of $\pm$-100° to the 50× 50 "L" beam member. At this grasping AoA, the number of grasps required and the calculated next best grasping AoA are unaltered with changing τ values.

Figure 5.9a shows the votes cast by the RF classifier at the first grasping AoA of -100° to the 50× 50 "L" shaped beam member. In this problem, the information-based method is seeking to disambiguate between the AoAs of -100° and -140° after the first *haptic glance.* The remaining sub figures in column 1 of Figure 5.9 show the votes cast by the RF classifier after performing *haptic glances* at the high information AoAs shown in column 2 of Figure 5.9. In column 1, it can be clearly seen that all of the votes cast by the RF classifier have confidence levels above 18%.

The high information cases for candidate grasps 3 and 4 show identical *tactile patterns.* After grasp 2 has been executed, the votes cast are separated by 90°. When rotating by 90° to navigate to the high information AoA for grasp 3, the votes are still separated by 90° and the information-based method is now seeking to disambiguate between 0° and 90°. It should be noted that since only the 50×50 "L" beam is being considered for AoA disambiguation, that the vote cast for the 50×50 "T" beam is discounted in grasp 3.

Finally, by rotating a further 90° to reach the high information AoA shown by the *tactile patterns* in Figure 5.9f, the RF classifier is once again seeking to disambiguate between 0° and 90°, however with this additional rotation, the RF classifier now has absolute confidence in the identity of the beam member AoA. Thus, no further *haptic glances* are required to determine the beam member and its properties.

One further example of increasing the threshold value, τ, from 15% to 18% which has no effect on the information-based method calculation is the initial grasping AoA of 10° to the 75×75 "T" shaped beam member. At this grasping AoA, the following votes are cast by the RF classifier:

1) **61%** for 10° 75×75 "T"

2) **39%** for 20° 75×75 "T"

At this grasping AoA, a threshold value change from 15% to 18% would have no effect on the information calculation procedure for selecting the next best grasping AoA. However, if a threshold value, τ, greater than 39% were defined, then no further grasps would be required for beam member recognition. As will be discussed further in the following section, the threshold value needs to be carefully selected.

(A)

(B)

(C)

(D)

(E)

(F)

(G)

No further grasping actions required. Beam member and AoA confidently identified after 4 grasps.

(H)
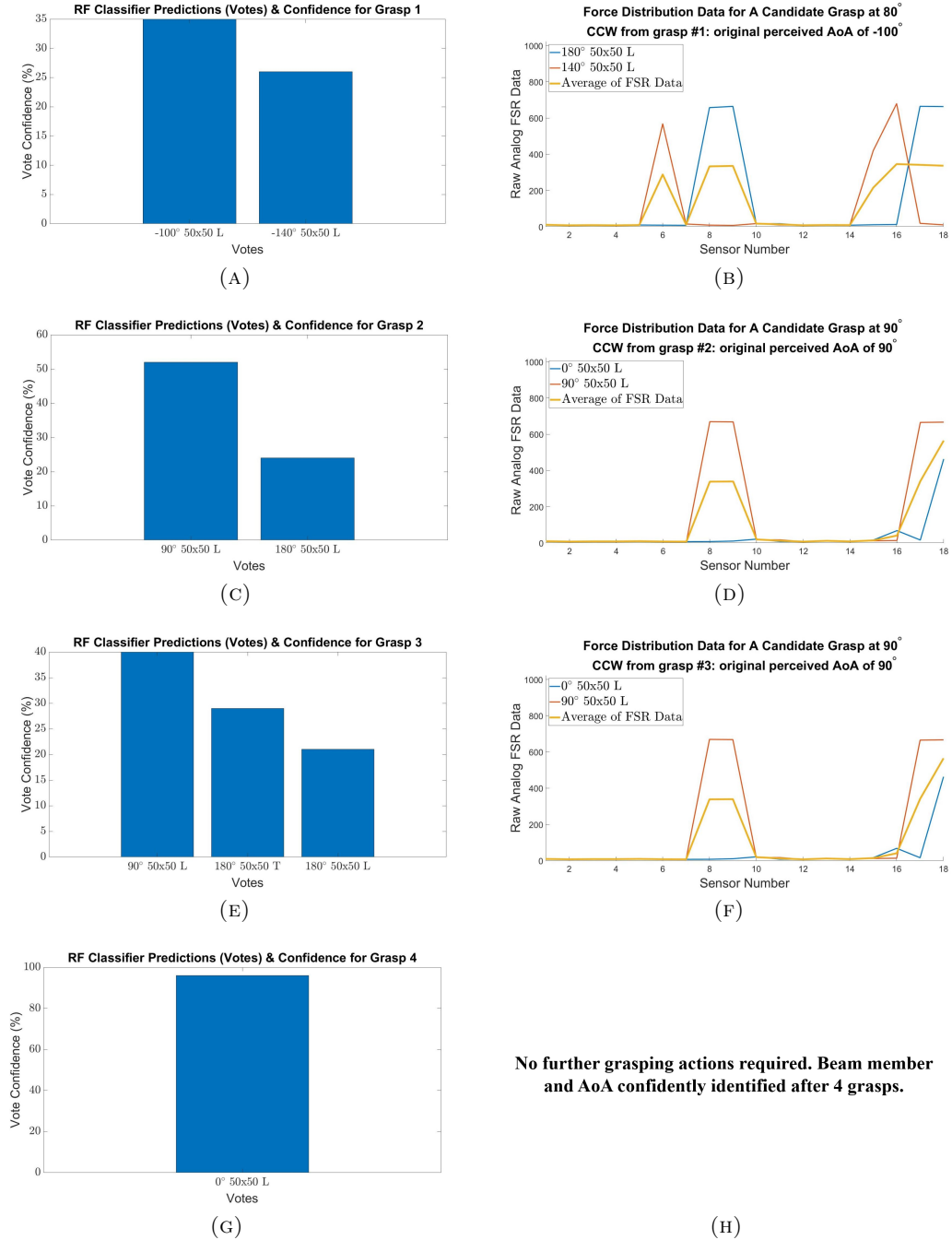
FIGURE 5.9: Information-based method process for an initial grasping AoA of -100° to the 50× 50 "L" shaped beam member. **Column 1:** RF classifier votes above threshold ($\tau = 18\%$) for grasps 1–4. *(A):* Original grasping AoA of -100° to the 50×50 "L" beam member. *(C),(E),(G):* High information grasping AoAs shown in column 2. **Column 2:** High information candidate AoAs, based on $\beta = 10°$ incremental angle shifts from the initial grasp data obtained at the AoA of -100° to the 50×50 "L" beam member. *(B),(D),(F):* High information candidate AoAs based on the classifications for grasps 1–3. *(G):* Beam member and AoA are correctly recognised, no further grasps required.

5.4 Discussion

In this chapter, an information-based method was presented for selecting the next best grasping AoA, with the aim of achieving rapid recognition of a structural beam member and its properties i.e. cross-sectional shape, size and grasping AoA. The method was tested and evaluated by using *tactile patterns* collected from grasping beam members of varying cross-sectional shapes and sizes (target beam member set #3) with the soft gripper presented in Chapter 3.

This method was evaluated using controlled simulations, whereby the data from first grasping location was contained within the existing dataset. For the future deployment of this method, the first grasp will be random and unknown. The first grasp will always contain the most information about a possible structural beam member (i.e. provide the highest information gain). However, depending on the outcome of the classification for the first grasp, the information-based method may not always be required. Since the information is calculated to select the next best grasping AoA, the information calculated in this method is not the same as the information gained from the initial grasp.

The information-based method was designed to address some of the limitations of the structural beam member recognition methods discussed in Chapter 4. The complexity of the structural beam member recognition problem is caused by a number of factors, including (1) similarities in the cross-sectional shape and size of different beam members, (2) the collection of sparse sensory data, where minimal points of contact are achieved during grasping, and (3) the collection of similar tactile readings. By implementing the proposed information-based method, it was found that for ambiguous AoAs in the target beam member set, typically fewer than 4 *haptic glances* were required to correctly recognise a structural beam member and its properties.

Overall, the proposed method has been shown to perform well for the given target beam member set, and a minimum number of *haptic glances* are executed to reduce the number of candidate beam members and AoAs from the candidates. There are several limitations to this method, which warrant further discussion in Chapter 6.

Chapter 6

Conclusions

This thesis has addressed three questions relating to grasping and touch based perception of beam members in truss structures. (1) Methods for designing adaptive grippers for grasping structural beam members with different cross-sectional shapes and sizes; (2) Sensing for data collection and methods for classifying structural beam member properties; and (3) Efficient methods for selecting the next best grasping action to confidently recognise a structural beam member and its properties.

First, a stiffness constraint based topology optimisation method was presented. Three grippers were designed and a comparison of their grasping capabilities was performed to verify the design method. A prototype gripper was manufactured. This design incorporated sensors for tactile data collection during grasping of structural beam members.

Next, the prototype soft gripper was used to collect data during grasping of structural beam members with varying cross-sectional shapes and sizes. Using the collected data, machine learning classifiers were compared for beam member recognition. Each of the classifiers was found to have particular advantages and disadvantages, considering the sensor readings collected from grasping similarly shaped and sized beam members, with limited contact points. Each of the evaluated classifiers was able to achieve similar classification accuracies with tactile data from a single *haptic glance*. From the evaluated classifiers, considering the practical application and given the available grasping data sets, a Random Forest (RF) classifier was found to perform reliably.

Despite promising beam member recognition results using tactile data from a single grasp, or *haptic glance*, cases existed where insufficient tactile data was collected for unambiguous beam member recognition. To address this limitation, an information-based method was developed for a soft gripper to select the next best grasping AoA to gather sufficient tactile data for recognition of beam members. The information-based method was designed to select the next best grasping AoA in a 2D plane for recognising a structural beam member and its properties using data from simple tactile sensors only.

6.1 Summary of Contributions

6.1.1 A Stiffness Constrained Topology Optimisation Method

A method for the design of a soft gripper for the application of grasping beam members in truss structures such as power transmission towers was developed (Chapter 3). The method was based on a topology optimisation compliant mechanism synthesis design. Stiffness constraints were added in the optimisation model which allows for changing the stiffness of a set of discrete elements in the design domain. The aim of changing the stiffness was to increase the output grasping strength of the gripper, whilst maintaining the features of compliancy and adaptability to varying cross-sectional shapes and sizes of beam members.

To evaluate the proposed method, three gripper designs, each with stiffness constrained elements in different elements in the design domain were analysed. One prototype gripper was manufactured. This gripper incorporated sensors in the form of FSRs and a linear actuator for controlled grasping. This gripper was used to collect data during grasping of a series of structural beam members from the defined target beam member sets.

6.1.2 A Comparative Study of Machine Learning Classifiers for Beam Member Recognition

A comparative study of machine learning classifiers for tactile based beam member recognition in truss structures was conducted (Chapter 4). This comparison was conducted using

grasping data collected using the prototype soft gripper. Five commonly used machine learning classifiers were trained with data from grasping data sets, with beam members of both unique and similar cross-sectional shapes and sizes. Data from a single *haptic glance* was used for training and evaluation. Simulation results were presented and evaluated. The metrics used for comparison included training and classification times, classification accuracies and confusion matrices.

Based on the results from the specific data sets, the advantages and disadvantages of each classifier were analysed. Several factors affecting the accuracy of the beam member recognition were also highlighted through this analysis. Some sources of confusion in the classification were attributed to (1) similarities in the cross-sectional shapes and sizes of the structural beam members, (2) sparse sensory data collected during grasping with the soft gripper and (3) limited points of contact between the gripper and target beam member during grasping. The classifiers were able to achieve similar classification accuracies, given the data sets used in this research.

6.1.3 An Information-based Method for Selecting the Next Best Grasping Angle-of-Approach

To address the erroneous classifications of beam members from a single *haptic glance*, an information-based method for selecting the next best grasping AoA for confident recognition of beam members with similar cross-sectional shapes and sizes was presented (Chapter 5). In this method, the gripper was assumed to collect data during grasping at discrete AoAs to beam members from a specified target beam member set.

For ambiguous grasping AoAs, the information-based method was required to recognise a beam member and its properties through execution of further *haptic glances*. The AoA with the highest calculated information was chosen by the method, resulting in the beam member being recognised efficiently, with a minimised number of grasping actions. For the available data sets and based on the simulation results presented, fewer than four grasps were typically needed for recognition of a beam member and its properties.

6.2   Discussion of Limitations and Future Work

There are a number of practical limitations to the methods developed in this thesis. In this section, some of the limitations encountered in this research are discussed. Possible future work is then proposed.

6.2.1   About the Stiffness Constrained Topology Optimisation Method

Many challenges remain in designing a gripper capable of reliable adhesion to structural beam members of varying cross-sectional shapes and sizes. The overarching issue faced in this gripper design problem is the adaptability of the gripper to provide sufficient points of contact during grasping. For practical applications of the gripper in a climbing robot system, grasping strength is also a critical feature. This thesis did not extensively analyse the grasping strength of the soft gripper. It was assumed that the grasping strength required for the climbing robot would be provided by a rigid mechanical exoskeletal frame of the gripper, which was identified as outside of the scope of this thesis. Realising a gripper design capable of both adaptability and grasping strength would facilitate realistic future gripper research for a truss structure climbing robot.

Considering the stiffness constrained topology optimisation design method presented in this thesis, there are limiting factors requiring careful consideration for future work. As outlined in Section 3.5.1, there are three variables that need to be appropriately selected in the stiffness constrained topology optimisation method:

- Stiffness multiplier value, α,

- The number of stiffness constrained elements in the design domain, and

- The location of stiffness constrained elements in the design domain.

Future work proposed for this gripper design method involves optimisation of these variables, to ensure that the gripper can effectively adapt to structural beam members, with sufficient grasping strength for some applications. Further verification studies would be required to analyse the effect of these variables on the gripper topology. Future work in

the area of topology optimised gripper design could also consider the use of multiple input actuation locations, as opposed to a single input actuation.

Furthermore, the role of symmetry in the design domain should be further explored. For example, the current assumption of symmetrical dummy pins which simulate the contact points during grasping is not representative of a true application of the gripper, since the contacts may not be symmetrical for different AoAs to different structural beam members. The effect of changing the location of these dummy pins requires further investigation and analysis.

Another interesting area of further study would consider the stiffness of any sensors embedded within the gripper structure as part of the optimisation procedure. In this thesis, the gripper was designed first, then sensors were retrofitted to its grasping surfaces. This approach was taken, since achieving a certain stiffness of the overall gripper was not the goal of the optimisation. Considering future designs, the stiffness of the gripper may be significantly affected, depending on the size and location of any sensors embedded within the gripper. Therefore, the stiffnesses of the sensors used should be added into the topology optimisation procedure, to ensure that the topology optimised gripper is representative of any manufactured prototype with integrated sensors.

To meet the requirement of firm grasping, an alternative gripper design which better exploits the 3D design domain in the stiffness constrained topology optimisation method could be produced. For example, a gripper comprised of several fingers offset from each other in the z-axis of the design domain (see Figure 6.1) could provide firmer, more stable grasps due to increased points of contact across multiple fingers during interaction with beam members. This type of grasp provides more reliable grasps than the two fingered gripper designs. By using the 3D design domain as opposed to creating a 2D topology which is extruded, a 3D optimised structure can be achieved. Such a gripper would still be simple to control, with a single actuation input and a fixed central pin.

Should the gripper produced from this 3D topology optimisation require any further design adjustments, the ability to generalise and parameterise these design changes would be beneficial. A closer study of the modifications undertaken to produce gripper #4 from gripper #2 would be useful in this case. A formal comparative study regarding the physical

grasping results of grippers #2 and #4 should also be conducted, to further verify the design changes and increases in compliancy.
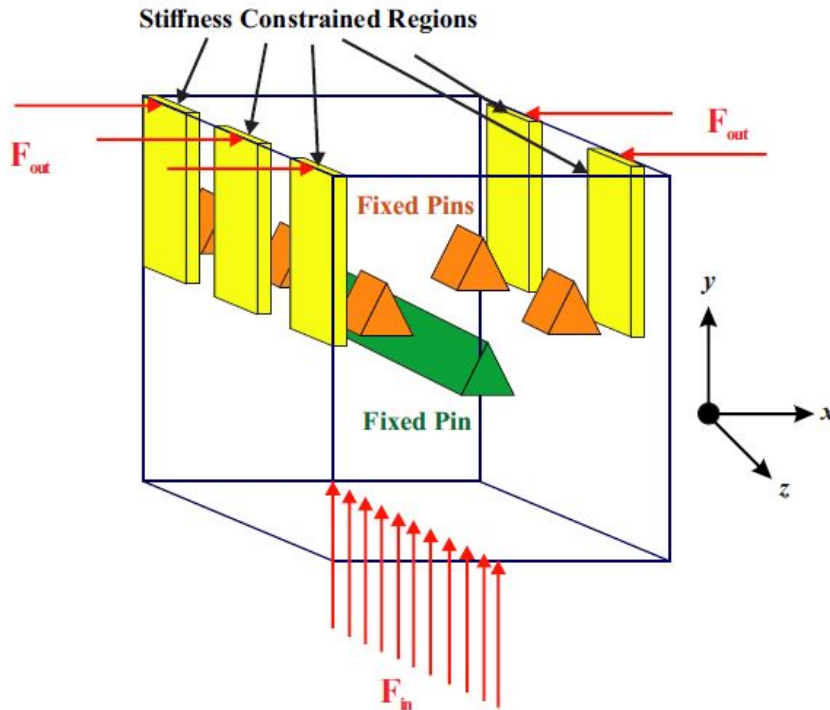
FIGURE 6.1: An example of a multi fingered hand design domain.

In terms of the practical application of the gripper, future work could involve aspects related to the prototype gripper design. Several interesting areas of potential future work include the selection and evaluation of alternative soft prototyping materials, as well as the selection and integration of sensors and actuators in the grasping platform.

The design of a rigid exoskeletal frame—which was identified as being outside the scope of this research—is important when considering the grasping strength requirement for supporting the weight of a climbing robot. Future work in the area of gripper design can consider the direction of developing a hybrid rigid/soft gripper. Such a design would need to carefully consider the possible points of contact of the compliant inner surfaces of the gripper, since the points of contact directly affect the topological structure of the gripper, when using the topology optimisation approach. Integrating a rigid exoskeletal frame with a soft gripper could bring about many interesting research challenges, and is an area of robotics that has not received much attention in the literature.

6.2.2 Comparative Study of Machine Learning Classifiers for Beam Member Recognition

The comparative study of machine learning classifiers showed that the evaluated classifiers were able to achieve similar classification accuracies, with particular classifiers having advantageous features over others.

Whilst the classification results were promising overall, there were some limitations in the overall classification accuracies, depending on the target beam member set and data set used for training and classification. There were two main grasping scenarios which resulted in the collection of similar *tactile patterns*, which can considerably limit the classification accuracy with a single *haptic glance*. Since the classifiers directly interpret the raw data to perform classifications, the results of this recognition process are expected to be erroneous. Additionally, sensing implementation issues described in Section 3.5.2.2 can limit the repeatability of the collected *tactile patterns* across multiple grasps at a given AoA.

Two possible solutions to increase the recognition accuracy of a structural beam member and its properties have been identified. The first solution relates to the hardware setup, where the density and layout of the tactile sensing array can be altered, whilst the second solution involves executing further *haptic glances* which can provide unique and distinguishing *tactile patterns*.

As highlighted in Section 3.5.2.2, some grasping AoAs resulted in limited tactile data being collected. In particular, limited data was collected when beam member contacts fell between the proximal and distal phalanges (where no FSRs were located) during grasping. To overcome this issue, a solution considered for future work would be to distribute FSRs in this area of the gripper. However, since this portion of the gripper is a flexible hinge, false positive sensor readings might result when the gripper is actuated and the hinge bends.

Another solution might be to increase the density of the tactile array to cover a greater surface area of the grippers phalanges. It is expected that this approach may result in the collection of more detailed *tactile patterns* for classification. By increasing the density of the tactile array, however, a careful analysis of the predictors in the classification

model would need to be performed to confirm their favourable impact on the classification accuracy.

Based on the grasping experiments conducted and the data collected, the selected FSRs were determined to be a feasible sensing option for the application. However, further analysis should be conducted regarding the sensitivity of the sensors and the relationship between the location of the sensors and their sensing accuracy. For the practical application, where shear forces are expected to be encountered, it would be beneficial to use alternative sensors which are be able to measure such forces. Having access to this data could be used to train the classifier help in determining the grippers AoA and the beam member orientation.

Considering future work for the practical application scenario, since the classifiers are trained offline for given data sets, the classifier training time is not the most critical requirement. Future work, considering the practical application scenario would include progressive learning techniques for multi-class classification, whereby new classes can be learned as they are encountered, instead of completely re-training the classifier. This capability will enable the classifier to be more robust.

6.2.3 About the Information-based Method for Selecting the Next Best Grasping Angle-of-Approach

Since the RF classifier has been trained only with data from rotations about the z-axis in increments of β degrees, the information-based method is currently limited to a single axis for selecting the next best grasping AoA. Further to this point, the current data sets are comprised of data which has been collected using the soft gripper with uncorrected positioning as it was affected by sag due to gravity. In other words, in the data collection grasping actions, the gripper might not approach a target beam member at exactly 90°. The true effects of this gravitational sag on the information-based method are unknown, as no comparative data has been collected for alternate grasping AoAs where the gripper pitch is altered.

One direction of future work includes further expanding the target beam member set to cover more structural beam members (i.e. to increase Bm). The data collected could then be used to more rigorously test the information-based method in a practical setting, and a threshold value (τ) could be appropriately selected. It is possible that with an expanded data set, multiple votes may still exist above the threshold, but the beam member AoA can still be considered as recognised. In this case, an upper threshold value may also need to be defined to ensure that excessive grasping actions are not undertaken.

The case studies presented in Section 5.3.3 highlight the importance of selecting an appropriate threshold value, specific to the target beam member set. As shown in Table 5.2, the threshold value is a key factor in the accuracy and efficiency of the information-based method. Setting this value too low can result in excessive grasping actions. Setting this value too high can result in erroneous classifications, or the information-based method failing to function at particular AoAs where all votes may be cast below the threshold value, τ. Depending on the target beam member set and the *tactile patterns* obtained during grasping, an appropriate threshold value needs to be selected. This value can be selected by analysing the classification performance using a classifier only and observing the votes cast by the classifier for all misclassified AoAs. This threshold value will therefore need to be assessed and selected based on the results of any conducted experiments. It can be a challenge to select the optimal value for the threshold, since there are parameters that are application dependent.

An algorithm to run all test cases (all possible grasping AoAs for all beam members in a target beam member set) and calculate the optimal threshold value for the application could be developed and implemented. This would result in more reliable results with the chosen threshold value/s, since manual selection of the threshold value is prone to human error.

In future work, it is envisaged that the gripper described in this thesis can be attached to a robot arm. This would allow for the information-based method to be extensively tested on a physical system. Considering the practical implementation in a robotic system, some other limitations arise relating to the work envelope of the robot arm and its reachability,

particularly in a truss structure environment such as a power transmission tower. Considering these factors, including the travel cost in the information-based method—specifically in the action selection decision phase—can be critical to the efficient functionality of the robot. Some poses for candidate grasping AoAs may require lengthy joint motions, therefore increasing the travel time. If this was ignored in a practical system, the results may be undesirable, as the motion action required to complete a grasp may be too time consuming to be practically implemented.

Further work with this integrated gripper-arm system would include an adaptation to the information-based method, where multiple strategic *haptic glances* could be executed to recognise the structural beam member and its orientation about the z-axis, as well as its properties. Since the experiments conducted in this thesis were tightly controlled, testing and data collection would also be conducted to determine the effects of varying the gripper AoA in the x and y axes (gripper roll and pitch). Due to the wide variety of possible gripper deformations, a deeper study into the resultant amplitudes of forces due to different force contact locations should be conducted. By collecting grasping data through testing with combinations and variations of AoAs in the x, y and z axes, an adapted information-based method which is not limited to AoAs in discrete increments about a single axis of a structural beam member could be developed.

Related to this future work is taking into consideration the more complex nature of the truss structure application environment, where structural beam members are located at many different angles relative to one another, throughout the structure. Grasping these structural members during climbing can introduce shear forces and increase the adverse effects of gravity on the grasping system. To realise a fully functioning climbing robot system which utilises the information-based method described in this thesis, significant further development is required, which takes into consideration all aspects and possible grasping scenarios during climbing.

Furthermore, using this data to fit a regression model, as opposed to a classification model, is also a potential topic for further investigation. This adapted information-based method would make the grasping system and decision making process more realistic, and simply appropriated to the application of a climbing robot in a truss structure.

Using the data obtained to determine the identity of a structural beam member and the gripper's grasping AoA, it would then be possible to select a grasping AoA which would result in stable, reliable grasping. This is important when considering the practical application of the system for a climbing robot. For the structural beam members in the target beam member set, some cross-sectional shapes would have more desirable grasping AoAs where sufficient points of contact can be made to prevent slip and increase grasp stability. Future work, once a beam member is recognised, would be to determine the best grasping AoA for climbing.

For a stable grasp to be executed, the gripper presented in this thesis would also need to be supported by a rigid mechanism capable of providing the required grasping strength to support the weight of a climbing robot. With this system in place, further work would involve a study of the contact points and how they correlate with the strength of a grasp and the information obtained about a beam member.

During data collection with the gripper, the rig positioning assumes that the gripper is always positioned at a consistent distance from the centre of the structural beam member. In practice, without prior knowledge of the beam member being grasped there is no way to consistently position the gripper at the desired distance for data collection. A consequence of this in the real-world application is that the classification in the information-based method is expected to be less effective when grasping at different distances from the structural beam members, since the training data could not correlate with the collected tactile data. To investigate the effect of varying the linear distance between the gripper and the structural member during grasping, further data collection and analysis would be required.

A data set representative of the application environment is a key component of the information-based method. Being able to update or add to this database quickly and efficiently—especially considering additional grasping AoA cases where variations in gripper roll and pitch are also present—is important for the information-based method. Currently, the data collection requires a user to manually position the grasping rig at a set distance and grasping AoA, which can be time consuming and prone to human positioning errors. There are two proposed methods to improve this process: 1) automate the gripper

positioning by adding additional actuators to the grasping rig or by attaching the gripper to a robot arm; or 2) grow the data base in simulation using a model of the gripper and sensor layout. Should option two be chosen, it is essential to compare the results of the simulated grasping data with a ground truth of physically obtained grasping data using the gripper rig.

Appendix A

Grasping Simulation Results

This appendix presents the detailed results of the grasping simulations performed for the grippers #1 – #3 from Section 3.3 and gripper #6 from Section 3.4 in Chapter 3.

A.1 Grasping Structural Beam Members from Target Beam Member Set #1

A.1.1 Gripper #1

Figure A.1 shows the grasping performance of gripper #1 for each of the structural beam members in target beam member set #1.

FIGURE A.1: Gripper #1 grasping each of the beam members in target beam member set #1: (A) Pipe Beam, (B) "+" Beam, (C) "T" Beam, (D) "I" Beam, (E) Box Beam, (F) "L" Beam.

A.1.2   Gripper #2

Figure A.2 shows the grasping performance of gripper #2 for each of the structural beam members in target beam member set #1.

<table>
<tr><td>(A)</td><td>(B)</td><td>(C)</td></tr>
<tr><td>(D)</td><td>(E)</td><td>(F)</td></tr>
</table>
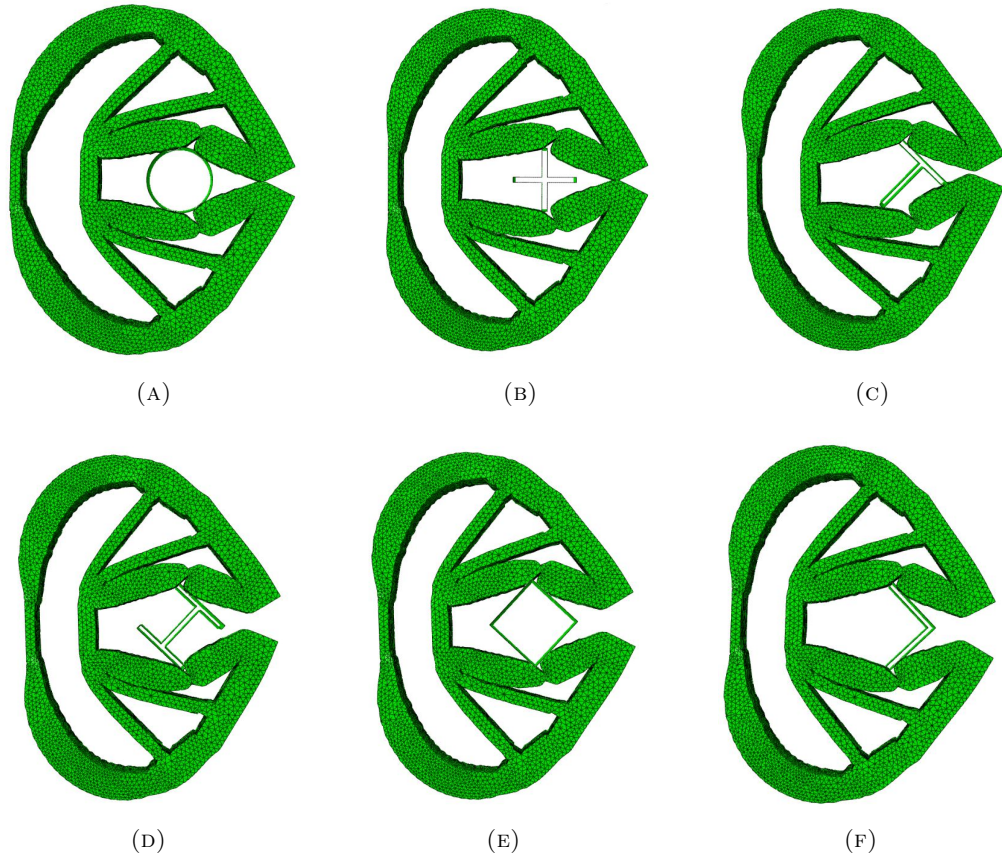
FIGURE A.2: Gripper #2 grasping each of the beam members in target beam member set #1: (A) Pipe Beam, (B) "+" Beam, (C) "T" Beam, (D) "I" Beam, (E) Box Beam, (F) "L" Beam.

Figure A.3 shows the grasping performance of gripper #2, grasping the 30×30 "L" shaped structural beam member of target beam member set #1 at varying AoAs.
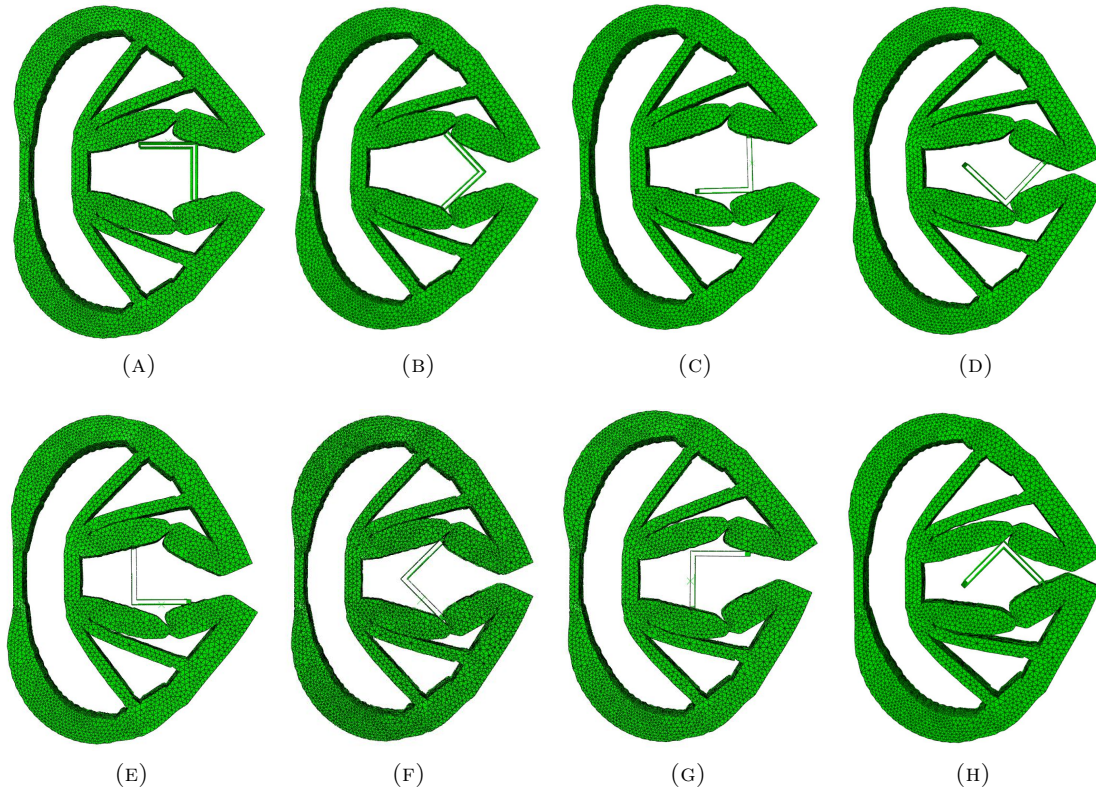
FIGURE A.3: Gripper #2 grasping "L" shaped beam member from target beam member set #1 at various AoAs and positions: (A) $\pm 0°$, (B) -45°, (C) -90°, (D) -135°, (E) $\pm 180°$, (F) +135°, (G) +90°, (H) +45°.

A.1.3 Gripper #3

Figure A.4 shows the grasping performance of gripper #3 for each of the structural beam members in target beam member set #1.
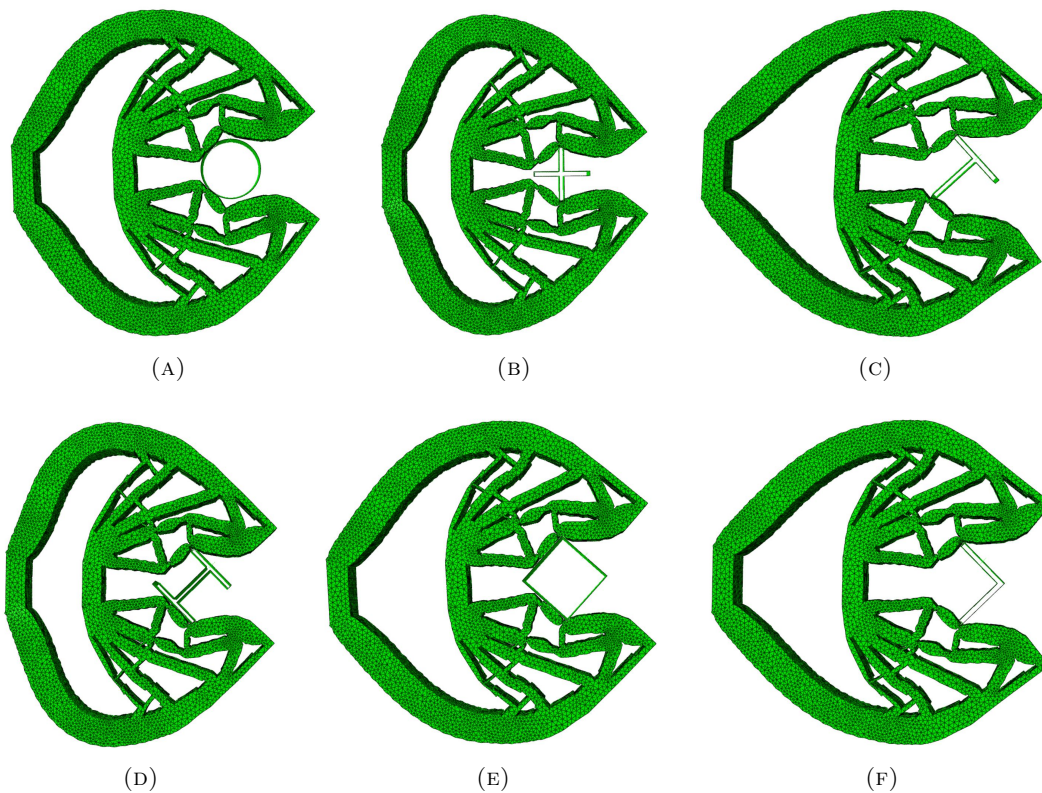

(A) (B) (C)

(D) (E) (F)
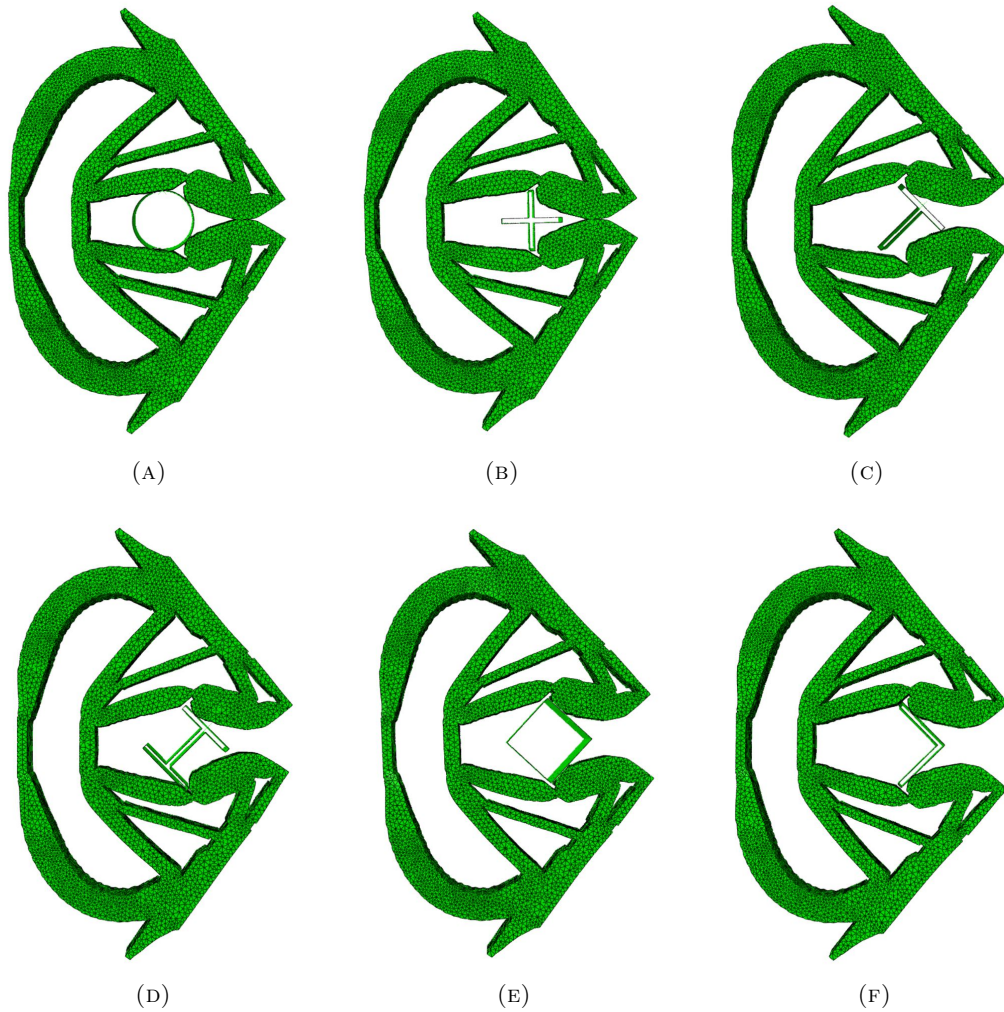
FIGURE A.4: Gripper #3 grasping each of the beam members in target beam member set #1: (A) Pipe Beam, (B) "+" Beam, (C) "T" Beam, (D) "I" Beam, (E) Box Beam, (F) "L" Beam.

A.1.4 Grasping 250% Scaled Structural Beam Members from Target Beam Member Set #1

A.1.4.1 Gripper #6

Figure A.5 shows the grasping results of gripper #6 for grasping the scaled ($250\% \times 30$ mm = 75 mm) structural beam members from target beam member set #1.
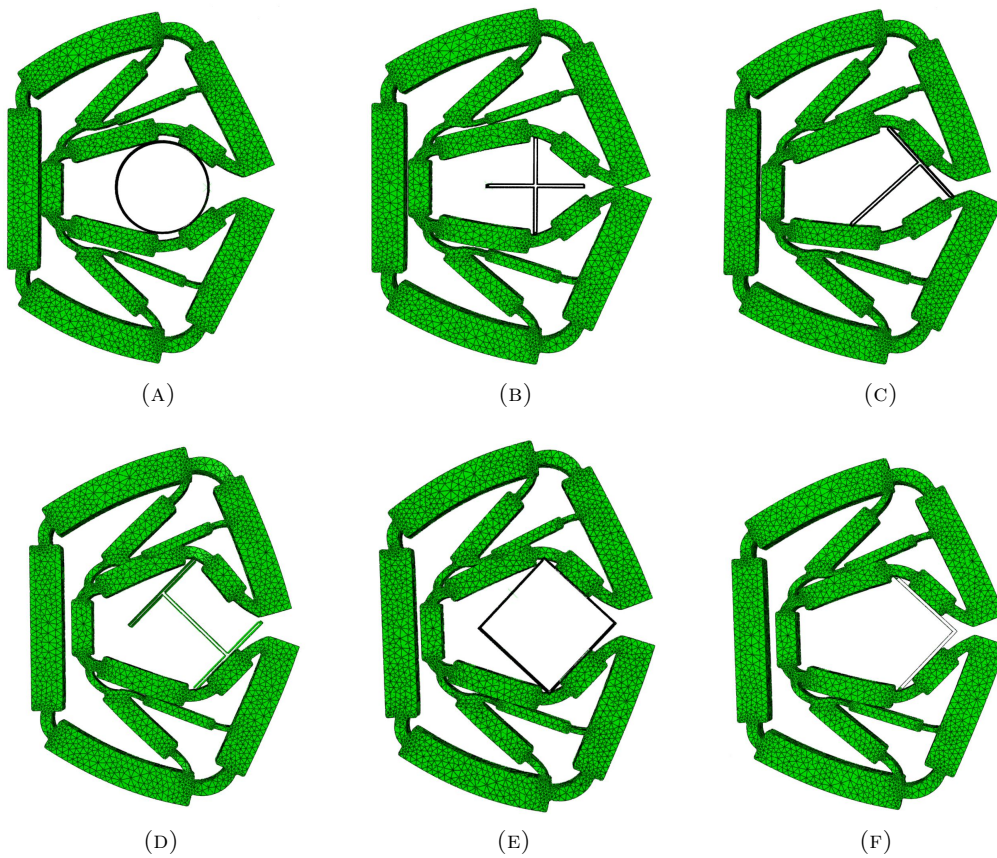
FIGURE A.5: Gripper #6 grasping each of the scaled (250%) sizes of beam members in target beam member set #1 (A) Pipe Beam, (B) "+" Beam, (C) "T" Beam, (D) "I" Beam, (E) Box Beam, (F) "L" Beam.

Appendix B

Classifier Comparison: Results

This appendix presents the complete classification training and test results across the two target beam member sets (#2 and #3) used for collecting experimental grasping data, as summarised by Table 3.4. Results shown are for the data combinations as summarised by Figure 4.1.

B.1 Target Beam Member Set # 2

TABLE B.1: Commonly used classifier results—grasping AoAs for target beam member set #2, not including repeated AoAs from symmetrical beam members.

Classifier	Average 10-fold Cross-validation Accuracy (%)		Average Classification Accuracy (%)		Average Classifier Training Time (s)		Average Classification Time (s)	
Dataset Used	FSRs & Encoder	FSRs Only	FSRs & Encoder	FSRs Only	FSRs & Encoder	FSRs Only	FSRs & Encoder	FSRs Only
k-NN	90.63	90.59	91.15	91.11	0.23	0.20	0.0070	0.0061
LDA	89.53	88.97	89.75	89.11	3.19	3.14	0.046	0.040
Multiclass SVM	89.49	89.44	90.49	90.45	1013	602.01	9.89	7.72
Naïve Bayes	91.74	91.60	91.51	91.38	84.98	80.07	1.10	1.05

TABLE B.2: RF results—grasping AoAs for target beam member set #2, not including repeated AoAs from symmetrical beam members.

Number of Trees in RF	Average OOB Error (%)		Average Classification Accuracy (%)		Average Classifier Training Time (s)		Average Classification Time (s)	
Dataset Used	FSRs & Encoder	FSRs Only	FSRs & Encoder	FSRs Only	FSRs & Encoder	FSRs Only	FSRs & Encoder	FSRs Only
10	23.17	24.38	91.95	91.78	3.49	1.85	0.18	0.099
100	7.45	7.61	94.48	94.20	15.86	15.70	0.78	0.69
1000	6.86	6.94	94.54	94.45	160.53	151.77	7.08	6.96

TABLE B.3: Commonly used classifier results—grasping AoAs for target beam member set #2, including repeated AoAs from symmetrical beam members.

Classifier	Average 10-fold Cross-validation Accuracy (%)		Average Classification Accuracy (%)		Average Classifier Training Time (s)		Average Classification Time (s)	
Dataset Used	FSRs & Encoder	FSRs Only	FSRs & Encoder	FSRs Only	FSRs & Encoder	FSRs Only	FSRs & Encoder	FSRs Only
k-NN	49.53	49.52	49.42	49.38	0.36	0.34	0.014	0.014
LDA	52.30	52.03	52.02	51.55	7.44	7.40	0.083	0.077
Multiclass SVM	49.01	48.98	49.05	49.03	1880.1	1889.8	39.42	29.70
Naïve Bayes	50.01	49.74	48.77	48.90	144.29	135.40	2.10	2.030

TABLE B.4: RF results—grasping AoAs for target beam member set #2, including repeated AoAs from symmetrical beam members.

Number of Trees in RF	Average OOB Error (%)		Average Classification Accuracy (%)		Average Classifier Training Time (s)		Average Classification Time (s)	
Dataset Used	FSRs & Encoder	FSRs Only	FSRs & Encoder	FSRs Only	FSRs & Encoder	FSRs Only	FSRs & Encoder	FSRs Only
10	57.86	58.37	49.89	49.91	6.91	5.82	0.26	0.23
100	51.04	51.15	50.88	50.85	68.52	63.58	2.22	1.75
1000	51.18	51.22	51.01	51.00	280.43	271.33	16.58	16.43

B.2 Target Beam Member Set # 3

TABLE B.5: Commonly used classifier results—grasping AoAs for target beam member set #3, not including repeated AoAs from symmetrical beam members.

Classifier	Average 10-fold Cross-validation Accuracy (%)		Average Classification Accuracy (%)		Average Classifier Training Time (s)		Average Classification Time (s)	
Dataset Used	FSRs & Encoder	FSRs Only	FSRs & Encoder	FSRs Only	FSRs & Encoder	FSRs Only	FSRs & Encoder	FSRs Only
k-NN	80.97	80.59	82.14	81.60	0.37	0.35	0.014	0.013
LDA	84.74	83.94	85.14	84.41	7.21	7.14	0.080	0.080
Multiclass SVM	79.78	79.35	81.58	81.16	2079.4	1228.8	28.16	16.85
Naïve Bayes	87.31	87.10	87.78	87.43	134.95	126.20	1.99	1.60

TABLE B.6: RF results—grasping AoAs for target beam member set #3, not including repeated AoAs from symmetrical beam members.

Number of Trees in RF	Average OOB Error (%)		Average Classification Accuracy (%)		Average Classifier Training Time (s)		Average Classification Time (s)	
Dataset Used	FSRs & Encoder	FSRs Only	FSRs & Encoder	FSRs Only	FSRs & Encoder	FSRs Only	FSRs & Encoder	FSRs Only
10	28.73	29.93	86.60	86.24	6.28	5.59	0.23	0.25
100	12.88	13.32	90.14	89.94	33.35	25.72	1.778	1.62
1000	11.85	12.10	90.55	90.24	282.11	262.68	16.00	15.51

TABLE B.7: Commonly used classifier results—grasping AoAs for target beam member set #3, including repeated AoAs from symmetrical beam members.

Classifier	Average 10-fold Cross-validation Accuracy (%)		Average Classification Accuracy (%)		Average Classifier Training Time (s)		Average Classification Time (s)	
Dataset Used	FSRs & Encoder	FSRs Only	FSRs & Encoder	FSRs Only	FSRs & Encoder	FSRs Only	FSRs & Encoder	FSRs Only
k-NN	42.29	41.95	42.29	41.97	0.60	0.58	0.030	0.030
LDA	47.99	47.23	47.29	46.83	16.04	16.21	0.17	0.16
Multiclass SVM	41.70	41.48	41.92	41.65	7400	4748.5	153.48	115.94
Naïve Bayes	44.58	44.33	43.94	43.79	228.58	198.99	3.52	3.59

TABLE B.8: RF results—grasping AoAs for target beam member set #3, including repeated AoAs from symmetrical beam members.

Number of Trees in RF	Average OOB Error (%)		Average Classification Accuracy (%)		Average Classifier Training Time (s)		Average Classification Time (s)	
Dataset Used	FSRs & Encoder	FSRs Only	FSRs & Encoder	FSRs Only	FSRs & Encoder	FSRs Only	FSRs & Encoder	FSRs Only
10	63.21	63.82	44.28	44.05	7.35	7.52	0.43	0.47
100	56.97	57.18	45.60	45.54	61.65	52.38	3.78	3.36
1000	56.92	57.09	45.79	45.73	676.55	607.40	33.72	34.54

Bibliography

[1] Erik Brynjolfsson and Andrew Mcafee. *Machine, Platform, Crowd: Harnessing Our Digital Future*. WW Norton & Co, 2017.

[2] Leila Takayama, Wendy Ju, and Clifford Nass. Beyond dirty, dangerous and dull: What everyday people think robots should do. In *Proceedings of the 3rd ACM/IEEE International Conference on Human-Robot Interaction (HRI)*, pages 25–32, 2008.

[3] Wei Wang, Yingying Wang, Kun Wang, Houxiang Zhang, and Jianwei Zhang. Analysis of the kinematics of module climbing caterpillar robots. In *Proceedings of IEEE/ASME International Conference on Advanced Intelligent Mechatronics (AIM)*, pages 84–89, 2008.

[4] Simon Kalouche, Nick Wiltsie, Hai-Jun Su, and Aaron Parness. Inchworm style gecko adhesive climbing robot. In *Proceedings of IEEE/RSJ International Conference on Intelligent Robots and Systems (IROS)*, pages 2319–2324, 2014.

[5] Keith D. Kotay and Daniela L. Rus. Navigating 3D steel web structures with an inchworm robot. In *Proceedings of IEEE/RSJ International Conference on Intelligent Robots and Systems (IROS)*, pages 368–375, 1996.

[6] B.L. Luk, A.A. Collie, and J. Billingsley. Robug II: An intelligent wall climbing robot. In *Proceedings of IEEE International Conference on Robotics and Automation (ICRA)*, pages 2342–2347, 1991.

[7] Mahmoud Tavakoli, Carlos Viegas, Lino Marques, J. Norberto Pires, and Aníbal T. de Almeida. OmniClimbers: Omni-directional magnetic wheeled climbing robots for

inspection of ferromagnetic structures. *Robotics and Autonomous Systems*, 61(9): 997–1007, 2013.

[8] Ran Liang, Meteb Altaf, Eball Ahmad, Rong Liu, and Ke Wang. A low-cost, light-weight climbing robot for inspection of class curtains. *International Journal of Advanced Robotic Systems*, 11(7):106, 2014.

[9] Juan Carlos Grieco, Manuel Prieto, Manuel Armada, and Pablo Gonzalez de Santos. A six-legged climbing robot for high payloads. In *Proceedings of IEEE International Conference on Control Applications (Cat. No.98CH36104)*, pages 446–450, 1998.

[10] Marc Osswald and Fumiya Iida. Design and control of a climbing robot based on hot melt adhesion. *Robotics and Autonomous Systems*, 61(6):616–625, 2013.

[11] William R. Provancher, Samuel I. Jensen-Segal, and Mark A. Fehlberg. ROCR: An energy-efficient dynamic wall-climbing robot. *IEEE/ASME Transactions on Mechatronics*, 16(5):897–906, 2011.

[12] Tim Bretl, Stephen Rock, Jean-Claude Latombe, Brett Kennedy, and Hrand Aghazarian. *Free-Climbing with a Multi-Use Robot*, pages 449–458. Springer Tracts in Advanced Robotics. Springer, 2006.

[13] Yisheng Guan, Li Jiang, Haifei Zhu, Xuefeng Zhou, Chuanwu Cai, Wenqiang Wu, Zhanchu Li, Hong Zhang, and Xianmin Zhang. Climbot: A modular bio-inspired biped climbing robot. In *Proceedings of IEEE/RSJ International Conference on Intelligent Robots and Systems (IROS)*, pages 1473–1478, 2011.

[14] M.I. Nor Faizal, W.A.F.W. Othman, and S.S.N.A. Syed Hassan. Development of pole-like tree climbing robot. In *Proceedings of IEEE International Conference on Control System, Computing and Engineering (ICCSCE)*, pages 224–229, 2015.

[15] Zahra Bakhtiar Khalid, Md. Hasib Ullah, Razu Ahmed, Zakir Hasan Choudhury, Imrul Kaish, and Md. Khalilur Rhaman. Electrical pole climbing robot: For wiring and repairing distribution lines. In *Proceedings of 18th International Conference on Computer and Information Technology (ICCIT)*, pages 368–372, 2015.

[16] G. Clark Haynes, Alex Khripin, Goran Lynch, Jonathan Amory, Aaron Saunders, Alfred A. Rizzi, and Daniel E. Koditschek. Rapid pole climbing with a quadrupedal robot. In *Proceedings of IEEE International Conference on Robotics and Automation (ICRA)*, pages 2767–2772, 2009.

[17] Tin Lun Lam and Yangsheng Xu. A flexible tree climbing robot: Treebot - design and implementation. In *Proceedings of IEEE International Conference on Robotics and Automation (ICRA)*, pages 5849–5854, 2011.

[18] C. Balaguer, A. Gimenez, and A. Jardon. Climbing robots' mobility for inspection and maintenance of 3D complex environments. *Autonomous Robots*, 18(2):157–169, 2005.

[19] Yeoreum Yoon and Daniela Rus. Shady3D: A robot that climbs 3D trusses. In *Proceedings of IEEE International Conference on Robotics and Automation (ICRA)*, pages 4071–4076, 2007.

[20] Jorg Mampel, Kurt Gerlach, Cornelius Schilling, and Hartmut Witte. A modular robot climbing on pipe-like structures. In *Proceedings of 4th International Conference on Autonomous Robots and Agents*, pages 87–91, 2009.

[21] Mahmoud Tavakoli, Ali Marjovi, Lino Marques, and Aníbal T. de Almeida. 3DCLIMBER: A climbing robot for inspection of 3D human made structures. In *Proceedings of IEEE/RSJ International Conference on Intelligent Robots and Systems (IROS)*, pages 4130–4135, 2008.

[22] Bing L. Luk, David S. Cooke, Stuart Galt, Arthur A. Collie, and Sheng Chen. Intelligent legged climbing service robot for remote maintenance applications in hazardous environments. *Robotics and Autonomous Systems*, 53(2):142–152, 2005.

[23] Daniel Schmidt and Karsten Berns. Climbing robots for maintenance and inspections of vertical structures - a survey of design aspects and technologies. *Robotics and Autonomous Systems*, 61(12):1288–1305, 2013.

[24] Australian Energy Regulator. Electricity Transmission, 2009. URL https://www.aer.gov.au/system/files/Chapter%205%20%20Electricity%20transmission%202009.pdf.

[25] Andrew Ledovskikh. IBISWorld Industry Report D2620 Electricity Transmission in Australia, 2018.

[26] Tokyo Electric Power Company (TEPCO). Power Transmission Lines, 2018. URL https://www7.tepco.co.jp/pg/supply/facility/power-e.html.

[27] Transpower. Towers and Poles Fleet Strategy, 2013. URL https://www.transpower.co.nz/sites/default/files/uncontrolled_docs/Fleet%20Strategy%20-%20TL%20Towers%20and%20Poles.pdf.

[28] PPG Protective & Marine Coatings. Transmission tower maintenance bottom line savings through active maintenance, 2015. URL http://pacificsouthwest.net/wp-content/uploads/2015/02/Transmission-Tower-WhitePaper-Final.pdf.

[29] ElectraNet. Information Sheet: Capital Expenditure Program, 2017. URL https://www.electranet.com.au/wp-content/uploads/resource/2017/04/ElectraNet-Revenue-Proposal-Overview-2019-2023-Capex-factsheet.pdf.

[30] TBS Group. TBS Group, 2018. URL https://www.tbsgroup.co.nz/.

[31] Tower Power Group. Tower Power Group, 2018. URL http://towerpowergroup.com/.

[32] Harriet Arkell. They get a real buzz out of their job: Pylon painters work 165ft in the air just inches away from 400,000-volt electricity cables, 2012. URL http://www.dailymail.co.uk/news/article-2240980/Meet-men-paint-pylons-just-inches-away-400-000-volt-electricity-cables.html.

[33] Rebecca Puddy. Electranet 'was warned' of tower risk long ago, 2016. URL https://www.theaustralian.com.au/news/nation/electranet-was-warned-of-tower-risk-long-ago/news-story/abc21f33acf2b752e6ec3e6fcb6e1999.

[34] Tom Fedorowytsch. Collapsed electricity pylon, 2016. URL http://www.abc.net.au/news/2016-09-29/collapsed-electricity-pylon/7888408.

[35] Binhai Wang, Xiguang Chen, Qian Wang, Liang Liu, Hailong Zhang, and Bingqiang Li. Power line inspection with a flying robot. In *Proceedings of 1st International Conference on Applied Robotics for the Power Industry (CARPI)*, pages 1–6, 2010.

[36] Xiaolong Hui, Jiang Bian, Yongjia Yu, Xiaoguang Zhao, and Min Tan. A novel autonomous navigation approach for UAV power line inspection. In *Proceedings of IEEE International Conference on Robotics and Biomimetics (ROBIO)*, 2017.

[37] Hyeoncheol Baik and Jorge Valenzuela. Unmanned aircraft system path planning for visually inspecting electric transmission towers. *Journal of Intelligent & Robotic Systems*, pages 1–15, 2018.

[38] Flyability. ELIOS - Inspect & Explore Indoor and Confined Spaces, 2018. URL https://www.flyability.com/elios/.

[39] Paulo Debenest, Michele Guarnieri, Kensuke Takita, Edwardo F. Fukushima, Shigeo Hirose, Kiyoshi Tamura, Akihiro Kimura, Hiroshi Kubokawa, Narumi Iwama, and Fuminori Shiga. Expliner - robot for inspection of transmission lines. In *Proceedings of IEEE International Conference on Robotics and Automation (ICRA)*, pages 3978–3984, 2008.

[40] Andrew Phillips, Eric Engdahl, Drew McGuire, Mark Major, and Glynn Bartlett. Autonomous overhead transmission line inspection robot (TI) development and demonstration. In *Proceedings of 2nd International Conference on Applied Robotics for the Power Industry (CARPI)*, pages 94–95, 2012.

[41] Nicolas Pouliot, Pierre-Luc Richard, and Serge Montambault. Linescout technology opens the way to robotic inspection and maintenance of high-voltage power lines. *IEEE Power and Energy Technology Systems Journal*, 2(1):1–11, 2015.

[42] George ElKoura and Karan Singh. Handrix: Animating the human hand. In *Proceedings of ACM SIGGRAPH/Eurographics Symposium on Computer Animation*, pages 110–119, 2003.

[43] Dr George McGavin. The incredible human hand and foot, 2014. URL https://www.bbc.com/news/science-environment-26224631.

[44] Carmel Majidi. Soft robotics: A perspective - current trends and prospects for the future. *Soft Robotics*, 1(1):5–11, 2014.

[45] Rocket Seals. What is the durometer of an o-ring, 2019. URL https://www.rocketseals.com/blog/2015/10/20/what-is-the-durometer-of-an-o-ring/.

[46] Josie Hughes, Utku Culha, Fabio Giardina, Fabian Guenther, Andre Rosendo, and Fumiya Iida. Soft manipulators and grippers: A review. *Frontiers in Robotics and AI*, 3(69):1–12, 2016.

[47] Goran Lundström. Industrial robot grippers. *Industrial Robot: An International Journal*, 1(2):72–82, 1974.

[48] Festo. Parallel grippers, 2018. URL https://www.festo.com/cat/en-au_au/products_010804.

[49] Festo. Vacuum grippers, 2018. URL https://www.festo.com/cat/en-au_au/products_040000.

[50] Robotiq. Adaptive grippers, 2018. URL https://robotiq.com/products/adaptive-grippers.

[51] Soft Robotics Inc. Superpick, 2018. URL https://www.softroboticsinc.com/.

[52] Festo. Bionictripod with fingripper, 2018. URL https://www.festo.com/cms/en_corp/9779.htm.

[53] Eric Brown, Nicholas Rodenberg, John Amend, Annan Mozeika, Erik Steltz, Mitchell R. Zakin, Hod Lipson, and Heinrich M. Jaeger. Universal robotic gripper based on the jamming of granular material. *Proceedings of the National Academy of Sciences*, 107(44):18809–18814, 2010.

[54] Mark R. Cutkosky. On grasp choice, grasp models, and the design of hands for manufacturing tasks. *IEEE Transactions on Robotics and Automation*, 5(3):269–279, 1989.

[55] G. Robinson and J.B.C. Davies. Continuum robots - a state of the art. In *Proceedings of IEEE International Conference on Robotics and Automation (ICRA)*, pages 2849–2854, 1991.

[56] Shigeo Hirose and Yoji Umetani. The development of soft gripper for the versatile robot hand. *Mechanism and Machine Theory*, 13(3):351–359, 1978.

[57] Matei Ciocarlie, Fernando Mier Hicks, Robert Holmberg, Jeffrey Hawke, Michael Schlicht, Jeff Gee, Scott Stanford, and Ryan Bahadur. The velo gripper: A versatile single-actuator design for enveloping, parallel and fingertip grasps. *The International Journal of Robotics Research*, 33(5):753–767, 2014.

[58] Spencer B. Backus and Aaron M. Dollar. An adaptive three-fingered prismatic gripper with passive rotational joints. *IEEE Robotics and Automation Letters*, 1(2): 668–675, 2016.

[59] Lael U. Odhner, Leif P. Jentoft, Mark R. Claffee, Nicholas Corson, Yaroslav Tenzer, Raymond R. Ma, Martin Buehler, Robert Kohout, Robert D. Howe, and Aaron M. Dollar. A compliant, underactuated hand for robust manipulation. *The International Journal of Robotics Research*, 33(5):736–752, 2014.

[60] Aaron M. Dollar and Robert D. Howe. The highly adaptive SDM hand: Design and performance evaluation. *The International Journal of Robotics Research*, 29(5): 585–597, 2010.

[61] Mahmoud Tavakoli, Lino Marques, and Aníbal T. de Almeida. Flexirigid, a novel two phase flexible gripper. In *Proceedings of IEEE/RSJ International Conference on Intelligent Robots and Systems (IROS)*, pages 5046–5051, 2013.

[62] Raphael Deimel and Oliver Brock. A compliant hand based on a novel pneumatic actuator. In *Proceedings of IEEE International Conference on Robotics and Automation (ICRA)*, pages 2047–2053, 2013.

[63] Raphael Deimel and Oliver Brock. A novel type of compliant and underactuated robotic hand for dexterous grasping. *The International Journal of Robotics Research*, 35:161–185, 2015.

[64] Dalibor Petković, Nenad D. Pavlović, Shahaboddin Shamshirband, and Nor Badrul Anuar. Development of a new type of passively adaptive compliant gripper. *Industrial Robot*, 40(6):610–623, 2013.

[65] M. E. Giannaccini, I. Georgilas, I. Horsfield, B. H. P. M. Peiris, A. Lenz, A. G. Pipe, and S. Dogramadzi. A variable compliance, soft gripper. *Autonomous Robots*, 36 (1-2):93–107, 2013.

[66] Kevin C. Galloway, Kaitlyn P. Becker, Brennan Phillips, Jordan Kirby, Stephen Licht, Dan Tchernov, Robert J. Wood, and David F. Gruber. Soft robotic grippers for biological sampling on deep reefs. *Soft Robotics*, 3(1):23–33, 2016.

[67] Ying Wei, Yonghua Chen, Tao Ren, Qiao Chen, Changxin Yan, Yang Yang, and Yingtian Li. A novel, variable stiffness robotic gripper based on integrated soft actuating and particle jamming. *Soft Robotics*, 3(3):134–143, 2016.

[68] Ashlih Dameitry and Hideyuki Tsukagoshi. Lightweight underactuated pneumatic fingers capable of grasping various objects. In *Proceedings of IEEE International Conference on Robotics and Automation (ICRA)*, pages 2009–2014, 2016.

[69] Mariangela Manti, Taimoor Hassan, Giovanni Passetti, Nicolò D'Elia, Cecilia Laschi, and Matteo Cianchetti. A bioinspired soft robotic gripper for adaptable and effective grasping. *Soft Robotics*, 2(3):107–116, 2015.

[70] Dalibor Petković and Nenad D. Pavlović. Compliant multi-fingered passively adaptive robotic gripper. *Multidiscipline Modeling in Materials and Structures*, 9(4): 538–547, 2013.

[71] S. Arimoto. Intelligent control of multi-fingered hands. *Annual Reviews in Control*, 28(1):75–85, 2004.

[72] L. Birglen. The kinematic preshaping of triggered self-adaptive linkage-driven robotic fingers. *Mechanical Sciences*, 2(1):41–49, 2011.

[73] Chih-Hsing Liu, Ta-Lun Chen, Chen-Hua Chiu, Mao-Cheng Hsu, Yang Chen, Tzu-Yang Pai, Wei-Geng Peng, and Yen-Pin Chiang. Optimal design of a soft robotic gripper for grasping unknown objects. *Soft Robotics*, 5(4):452–465, 2018.

[74] Matteo Cianchetti, Tommaso Ranzani, Giada Gerboni, Iris De Falco, Cecilia Laschi, and Arianna Menciassi. STIFF-FLOP surgical manipulator: Mechanical design and experimental characterization of the single module. In *Proceedings of IEEE/RSJ*

International Conference on Intelligent Robots and Systems (IROS), pages 3576–3581, 2013.

[75] Yingtian Li, Yonghua Chen, Yang Yang, and Ying Wei. Passive particle jamming and its stiffening of soft robotic grippers. *IEEE Transactions on Robotics*, 33(2): 446–455, 2017.

[76] Kaori Mizushima, Takumi Oku, Yosuke Suzuki, Tokuo Tsuji, and Tetsuyou Watanabe. Multi-fingered robotic hand based on hybrid mechanism of tendon-driven and jamming transition. In *Proceedings of IEEE International Conference on Soft Robotics (RoboSoft)*, pages 376–381, 2018.

[77] Amir Mohammadi Nasab, Amin Sabzehzar, Milad Tatari, Carmel Majidi, and Wanliang Shan. A soft gripper with rigidity tunable elastomer strips as ligaments. *Soft Robotics*, 4(4):411–420, 2017.

[78] Yaohui Chen, Fang Wan, Tong Wu, and Chaoyang Song. Soft-rigid interaction mechanism towards a lobster-inspired hybrid actuator. *Journal of Micromechanics and Microengineering*, 28(1):014007, 2017.

[79] Wookeun Park, Seongmin Seo, and Joonbum Bae. A hybrid gripper with soft material and rigid structures. *IEEE Robotics and Automation Letters*, 4(1):65–72, 2018.

[80] Panagiotis Polygerinos, Nikolaus Correll, Stephen A. Morin, Bobak Mosadegh, Cagdas D. Onal, Kirstin Petersen, Matteo Cianchetti, Michael T. Tolley, and Robert F. Shepherd. Soft robotics: Review of fluid-driven intrinsically soft devices; manufacturing, sensing, control, and applications in human-robot interaction. *Advanced Engineering Materials*, 19(12):1700016, 2017.

[81] Andrew D. Marchese, Konrad Komorowski, Cagdas D. Onal, and Daniela Rus. Design and control of a soft and continuously deformable 2D robotic manipulation system. In *Proceedings of IEEE International Conference on Robotics and Automation (ICRA)*, pages 2189–2196, 2014.

[82] Andrew D. Marchese, Robert K. Katzschmann, and Daniela Rus. Whole arm planning for a soft and highly compliant 2D robotic manipulator. In *Proceedings of*

IEEE/RSJ International Conference on Intelligent Robots and Systems (IROS), pages 554–560, 2014.

[83] Andrew D. Marchese, Russ Tedrake, and Daniela Rus. Dynamics and trajectory optimization for a soft spatial fluidic elastomer manipulator. In *Proceedings of IEEE International Conference on Robotics and Automation (ICRA)*, pages 2528–2535, 2015.

[84] Weiting Liu, Fei Li, Cesare Stefanini, Dajing Chen, and Paolo Dario. Biomimetic flexible/compliant sensors for a soft-body lamprey-like robot. *Robotics and Autonomous Systems*, 58(10):1138–1148, 2010.

[85] Kenji Kure, Takefumi Kanda, Koichi Suzumori, and Shuichi Wakimoto. Flexible displacement sensor using injected conductive paste. *Sensors and Actuators A: Physical*, 143(2):272–278, 2008.

[86] John Ulmen and Mark Cutkosky. A robust, low-cost and low-noise artificial skin for human-friendly robots. In *Proceedings of IEEE International Conference on Robotics and Automation (ICRA)*, pages 4836–4841, 2010.

[87] Alexandre Girard, Jean-Philippe Lucking Bigué, Benjamin M. O'Brien, Todd A. Gisby, Iain A. Anderson, and Jean-Sébastien Plante. Soft two-degree-of-freedom dielectric elastomer position sensor exhibiting linear behavior. *IEEE/ASME Transactions on Mechatronics*, 20(1):105–114, 2015.

[88] Hongying Zhang, Michael Yu Wang, Jisen Li, and Jian Zhu. A soft compressive sensor using dielectric elastomers. *Smart Materials and Structures*, 25(3):035045, 2016.

[89] Francis Thérien and Jean-Sébastien Plante. Design and calibration of a soft multiple degree of freedom motion sensor system based on dielectric elastomers. *Soft Robotics*, 3(2):45–53, 2016.

[90] Hongying Zhang and Michael Yu Wang. Multi-axis soft sensors based on dielectric elastomer. *Soft Robotics*, 3(1):3–12, 2016.

[91] Yong-Lae Park, Bor-Rong Chen, and R. J. Wood. Design and fabrication of soft artificial skin using embedded microchannels and liquid conductors. *IEEE Sensors Journal*, 12(8):2711–2718, 2012.

[92] Joseph T. Muth, Daniel M. Vogt, Ryan L. Truby, Yiğit Mengüç, David B. Kolesky, Robert J. Wood, and Jennifer A. Lewis. Embedded 3D printing of strain sensors within highly stretchable elastomers. *Advanced Materials*, 26(36):6307–6312, 2014.

[93] Tong Lu, Lauren Finkenauer, James Wissman, and Carmel Majidi. Rapid prototyping for soft-matter electronics. *Advanced Functional Materials*, 24(22):3351–3356, 2014.

[94] Edward L. White, Jennifer C. Case, and Rebecca K. Kramer. Multi-mode strain and curvature sensors for soft robotic applications. *Sensors and Actuators A: Physical*, 253:188–197, 2017.

[95] Rebecca K. Kramer, Carmel Majidi, and Robert J. Wood. Masked deposition of gallium-indium alloys for liquid-embedded elastomer conductors. *Advanced Functional Materials*, 23(42):5292–5296, 2013.

[96] C Majidi, R Kramer, and R J Wood. A non-differential elastomer curvature sensor for softer-than-skin electronics. *Smart Materials and Structures*, 20(10):105017, 2011.

[97] Helge A. Wurdemann, Sina Sareh, Ali Shafti, Yohan Noh, Angela Faragasso, Damith S. Chathuranga, Hongbin Liu, Shinichi Hirai, and Kaspar Althoefer. Embedded electro-conductive yarn for shape sensing of soft robotic manipulators. In *Proceedings of 37th Annual International Conference of the IEEE Engineering in Medicine and Biology Society (EMBC)*, pages 8026–8029, 2015.

[98] Yong-Lae Park and Robert J. Wood. Smart pneumatic artificial muscle actuator with embedded microfluidic sensing. In *Proceedings of IEEE SENSORS*, 2013.

[99] Wyatt Felt and C. David Remy. Smart braid: Air muscles that measure force and displacement. In *Proceedings of IEEE/RSJ International Conference on Intelligent Robots and Systems (IROS)*, pages 2821–2826, 2014.

[100] Ryan L. Truby, Michael Wehner, Abigail K. Grosskopf, Daniel M. Vogt, Sebastien G. M. Uzel, Robert J. Wood, and Jennifer A. Lewis. Soft somatosensitive actuators via embedded 3D printing. *Advanced Materials*, 30(15):1706383, 2018.

[101] Tekscan. Products for pressure mapping and force measurements, 2018. URL https://www.tekscan.com/products-solutions.

[102] Spectra Symbol. Products, 2018. URL http://www.spectrasymbol.com/products/.

[103] Interlink Electronics. Standard products, 2018. URL https://www.interlinkelectronics.com/standard-products.

[104] Pressure Profile Systems. General tactile sensor instrumentation catalog, 2018. URL https://pressureprofile.com/general-sensor-catalog.

[105] Paolo Dario and Danilo De Rossi. Tactile sensors and the gripping challenge: Increasing the performance of sensors over a wide range of force is a first step toward robotry that can hold and manipulate objects as humans do. *IEEE Spectrum*, 22 (8):46–53, 1985.

[106] Robert D. Howe and Mark R. Cutkosky. Sensing skin acceleration for slip and texture perception. In *Proceedings of IEEE International Conference on Robotics and Automation (ICRA)*, pages 145–150, 1989.

[107] TakkTile. Takktile sensors, 2018. URL https://www.labs.righthandrobotics.com/takktile-sensors.

[108] Leif P. Jentoft, Yaroslav Tenzer, Daniel Vogt, Jia Liu, Robert J. Wood, and Robert D. Howe. Flexible, stretchable tactile arrays from MEMS barometers. In *Proceedings of 16th International Conference on Advanced Robotics (ICAR)*, 2013.

[109] Yaroslav Tenzer, Leif P. Jentoft, and Robert D. Howe. The feel of MEMS barometers: Inexpensive and easily customized tactile array sensors. *IEEE Robotics & Automation Magazine*, 21(3):89–95, 2014.

[110] SynTouch. Sensor technology: Biotac technologies, 2018. URL https://www.syntouchinc.com/en/sensor-technology/.

[111] Jeremy A. Fishel and Gerald E. Loeb. Bayesian exploration for intelligent identification of textures. *Frontiers in Neurorobotics*, 6(4):1–20, 2012.

[112] Craig Chorley, Chris Melhuish, Tony Pipe, and Jonathan Rossiter. Development of a tactile sensor based on biologically inspired edge encoding. In *Proceedings of International Conference on Advanced Robotics*, 2009.

[113] Luke Cramphorn, Benjamin Ward-Cherrier, and Nathan F. Lepora. Tactile manipulation with biomimetic active touch. In *Proceedings of IEEE International Conference on Robotics and Automation (ICRA)*, pages 123–129, 2016.

[114] Nathan F. Lepora, Kirsty Aquilina, and Luke Cramphorn. Exploratory tactile servoing with active touch. *IEEE Robotics and Automation Letters*, 2(2):1156–1163, 2017.

[115] Andrew N. Iwaniuk and Ian Q. Whishaw. How skilled are the skilled limb movements of the raccoon (procyon lotor)? *Behavioural Brain Research*, 99(1):35–44, 1999.

[116] K. C. Catania. A nose that looks like a hand and acts like an eye: the unusual mechanosensory system of the star-nosed mole. *Journal of Comparative Physiology A: Sensory, Neural, and Behavioral Physiology*, 185(4):367–372, 1999.

[117] Abdulmotaleb El Saddik, Mauricio Orozco, Mohamad Eid, and Jongeun Cha. *Haptics: General Principles*, pages 1–20. Springer, 2011.

[118] Susan J. Lederman and Roberta L. Klatzky. Hand movements: A window into haptic object recognition. *Cognitive Psychology*, 19(3):342–368, 1987.

[119] S.J. Lederman and R.L. Klatzky. Haptic perception: A tutorial. *Attention, Perception, & Psychophysics*, 71(7):1439–1459, 2009.

[120] Roberta L. Klatzky and Susan J. Lederman. Identifying objects from a haptic glance. *Perception & Psychophysics*, 57(8):1111–1123, 1995.

[121] R. Klatzky, R. Bajcsy, and S. Lederman. Object exploration in one and two fingered robots. In *Proceedings of IEEE International Conference on Robotics and Automation (ICRA)*, pages 1806–1809, 1987.

[122] Allison M. Okamura and Mark R. Cutkosky. Feature detection for haptic exploration with robotic fingers. *The International Journal of Robotics Research*, 20(12):925–938, 2001.

[123] Paolo Dario and Giorgio Buttazzo. An anthropomorphic robot finger for investigating artificial tactile perception. *The International Journal of Robotics Research*, 6 (3):25–48, 1987.

[124] Ruzena Bajcsy. Active perception. *Proceedings of the IEEE*, 76(8):966–1005, 1988.

[125] S.A. Stansfield. A robotic perceptual system utilizing passive vision and active touch. *The International Journal of Robotics Research*, 7(6):138–161, 1988.

[126] S.A. Stansfield. Robotic grasping of unknown objects: A knowledge-based approach. *The International Journal of Robotics Research*, 10(4):314–326, 1991.

[127] Peter K. Allen and Kenneth S. Roberts. Haptic object recognition using a multi-fingered dextrous hand. In *Proceedings of IEEE International Conference on Robotics and Automation (ICRA)*, pages 342–347, 1989.

[128] Giorgio Buttazzo, Paolo Dario, and Ruzena Bajcsy. Finger based explorations. In *Proceedings of SPIE 0726 Intelligent Robots and Computer Vision*, 1987.

[129] A. Bicchi, P. Dario, and P. C. Pinotti. *On the Control of a Sensorized Artificial Finger for Tactile Exploration of Objects*, pages 251–256. IFAC Proceedings Series, vol.9. Pergamon Press Books, 1986.

[130] Kenneth S. Roberts. Robot active touch exploration: Constraints and strategies. In *Proceedings of IEEE International Conference on Robotics and Automation (ICRA)*, pages 980–985, 1990.

[131] G. Buttazzo, A. Bicchi, and P. Dario. Robot tactile perception. In *Sensor-Based Robots: Algorithms and Architectures*, pages 25–40. Springer, 1991.

[132] Peter K. Allen. Integrating vision and touch for object recognition tasks. *The International Journal of Robotics Research*, 7(6):15–33, 1988.

[133] A. M. Okamura, M. L. Turner, and M. R. Cutkosky. Haptic exploration of objects with rolling and sliding. In *Proceedings of IEEE International Conference on Robotics and Automation (ICRA)*, pages 2485–2490, 1997.

[134] Jivko Sinapov and Alexander Stoytchev. Object category recognition by a humanoid robot using behavior-grounded relational learning. In *Proceedings of IEEE International Conference on Robotics and Automation (ICRA)*, pages 184–190, 2011.

[135] Ruben D. Ponce Wong, Randall B. Hellman, and Veronica J. Santos. Haptic exploration of fingertip-sized geometric features using a multimodal tactile sensor. *Next-Generation Robots and Systems*, 9116:911605, 2014.

[136] Mårten Björkman, Yasemin Bekiroglu, Virgile Högman, and Danica Kragic. Enhancing visual perception of shape through tactile glances. In *Proceedings of IEEE/RSJ International Conference on Intelligent Robots and Systems (IROS)*, pages 3180–3186, 2013.

[137] Vivian Chu, Ian McMahon, Lorenzo Riano, Craig G. McDonald, Qin He, Jorge Martinez Perez-Tejada, Michael Arrigo, Naomi Fitter, John C. Nappo, Trevor Darrell, and Katherine J. Kuchenbecker. Using robotic exploratory procedures to learn the meaning of haptic adjectives. In *Proceedings of IEEE International Conference on Robotics and Automation (ICRA)*, pages 3048–3055, 2013.

[138] Bertrand Higy, Carlo Ciliberto, Lorenzo Rosasco, and Lorenzo Natale. Combining sensory modalities and exploratory procedures to improve haptic object recognition in robotics. In *Proceedings of IEEE-RAS 16th International Conference on Humanoid Robots (Humanoids)*, pages 117–124, 2016.

[139] Nicolas Sommer and Aude Billard. Multi-contact haptic exploration and grasping with tactile sensors. *Robotics and Autonomous Systems*, 85:48–61, 2016.

[140] Uriel Martinez-Hernandez, Tony J. Dodd, Lorenzo Natale, Giorgio Metta, Tony J. Prescott, and Nathan F. Lepora. Active contour following to explore object shape with robot touch. In *Proceedings of World Haptics Conference (WHC)*, pages 341–346, 2013.

[141] Robin A. Russell. Object recognition by a 'smart' tactile sensor. In *Proceedings of Australian Conference on Robotics and Automation (ACRA)*, pages 93–98, 2000.

[142] Gunther Heidemann and Matthia Schöpfer. Dynamic tactile sensing for object identification. In *Proceedings of IEEE International Conference on Robotics and Automation (ICRA)*, pages 813–818, 2004.

[143] Zachary Pezzementi, Erion Plaku, Caitlin Reyda, and Gregory D. Hager. Tactile-object recognition from appearance information. *IEEE Transactions on Robotics*, 27(3):473–487, 2011.

[144] Hongbin Liu, Xiaojing Song, Thrishantha Nanayakkara, Lakmal D. Seneviratne, and Kaspar Althoefer. A computationally fast algorithm for local contact shape and pose classification using a tactile array sensor. In *Proceedings of IEEE International Conference on Robotics and Automation (ICRA)*, pages 1410–1415, 2012.

[145] Shan Luo, Wenxuan Mou, Kaspar Althoefer, and Hongbin Liu. Novel tactile-SIFT descriptor for object shape recognition. *IEEE Sensors Journal*, 15(9):5001–5009, 2015.

[146] Tadeo Corradi, Peter Hall, and Pejman Iravani. Bayesian tactile object recognition: Learning and recognising objects using a new inexpensive tactile sensor. In *Proceedings of IEEE International Conference on Robotics and Automation (ICRA)*, pages 3909–3914, 2015.

[147] G. Vezzani, N. Jamali, U. Pattacini, G. Battistelli, L. Chisci, and L. Natale. A novel bayesian filtering approach to tactile object recognition. In *Proceedings of IEEE-RAS 16th International Conference on Humanoid Robots (Humanoids)*, pages 256–263. IEEE, 2016.

[148] Stefano Caselli, Corrado Magnanini, and Francesco Zanichelli. Haptic object recognition with a dextrous hand based on volumetric shape representations. In *Proceedings of IEEE International Conference on Multisensor Fusion and Integration for Intelligent Systems (MFI)*, pages 280–287, 1994.

[149] Magnus Johnsson and Christian Balkenius. Experiments with proprioception in a self-organizing system for haptic perception. In *Towards Autonomous Robotic Systems*, 2007.

[150] Shinya Takamuku, Atsushi Fukuda, and Koh Hosoda. Repetitive grasping with anthropomorphic skin-covered hand enables robust haptic recognition. In *Proceedings of IEEE/RSJ International Conference on Intelligent Robots and Systems (IROS)*, pages 3212–3217, 2008.

[151] Nicolas Gorges, Stefan Escaida Navarro, Dirk Göger, and Heinz Wörn. Haptic object recognition using passive joints and haptic key features. In *Proceedings of IEEE International Conference on Robotics and Automation (ICRA)*, pages 2349–2355, 2010.

[152] Harold Soh and Yiannis Demiris. Incrementally learning objects by touch: Online discriminative and generative models for tactile-based recognition. *IEEE Transactions on Haptics*, 7(4):512–525, 2014.

[153] S. B. Kotsiantis. Supervised machine learning: A review of classification techniques. In *Proceedings of Emerging Artificial Intelligence Applications in Computer Engineering*, pages 3–24, 2007.

[154] Leo Breiman. Random forests. *Machine Learning*, 45(1):5–32, 2001.

[155] Michael W. Hannan and Ian D. Walker. Kinematics and the implementation of an elephant's trunk manipulator and other continuum style robots. *Journal of Robotic Systems*, 20(2):45–63, 2003.

[156] Robert J. Webster and Bryan A. Jones. Design and kinematic modeling of constant curvature continuum robots: A review. *The International Journal of Robotics Research*, 29(13):1661–1683, 2010.

[157] R. Adam Bilodeau, Edward L. White, and Rebecca K. Kramer. Monolithic fabrication of sensors and actuators in a soft robotic gripper. In *Proceedings of IEEE/RSJ International Conference on Intelligent Robots and Systems (IROS)*, pages 2324–2329, 2015.

[158] Nicholas Farrow and Nikolaus Correll. A soft pneumatic actuator that can sense grasp and touch. In *Proceedings of IEEE/RSJ International Conference on Intelligent Robots and Systems (IROS)*, pages 2317–2323, 2015.

[159] John Morrow, Hee-Sup Shin, Calder Phillips-Grafflin, Sung-Hwan Jang, Jacob Torrey, Riley Larkins, Steven Dang, Yong-Lae Park, and Dmitry Berenson. Improving soft pneumatic actuator fingers through integration of soft sensors, position and force control, and rigid fingernails. In *Proceedings of IEEE International Conference on Robotics and Automation (ICRA)*, pages 5024–5031, 2016.

[160] Mirna Issa, Dalibor Petković, Nenad D. Pavlović, and Lena Zentner. Sensor elements made of conductive silicone rubber for passively compliant gripper. *The International Journal of Advanced Manufacturing Technology*, 69(5-8):1527–1536, 2013.

[161] Yang Yang and Yonghua Chen. Innovative design of embedded pressure and position sensors for soft actuators. *IEEE Robotics and Automation Letters*, 3(2):656–663, 2018.

[162] Rui Pedro Rocha, Pedro Alhais Lopes, Aníbal T. de Almeida, Mahmoud Tavakoli, and Carmel Majidi. Fabrication and characterization of bending and pressure sensors for a soft prosthetic hand. *Journal of Micromechanics and Microengineering*, 28(3): 034001, 2018.

[163] Zhongkui Wang and Shinichi Hirai. A 3D printed soft gripper integrated with curvature sensor for studying soft grasping. In *Proceedings of IEEE/SICE International Symposium on System Integration (SII)*, pages 629–633, 2016.

[164] Khaled Elgeneidy, Niels Lohse, and Michael Jackson. Bending angle prediction and control of soft pneumatic actuators with embedded flex sensors – a data-driven approach. *Mechatronics*, 50:234–247, 2018.

[165] Yang Chen, Shaofei Guo, Cunfeng Li, Hui Yang, and Lina Hao. Size recognition and adaptive grasping using an integration of actuating and sensing soft pneumatic gripper. *Robotics and Autonomous Systems*, 104:14–24, 2018.

[166] Bianca S. Homberg, Robert K. Katzschmann, Mehmet R. Dogar, and Daniela Rus. Haptic identification of objects using a modular soft robotic gripper. In *Proceedings*

of IEEE/RSJ International Conference on Intelligent Robots and Systems (IROS), pages 1698–1705, 2015.

[167] Benjamin Shih, Dylan Drotman, Caleb Christianson, Zhaoyuan Huo, Ruffin White, Henrik I. Christensen, and Michael T. Tolley. Custom soft robotic gripper sensor skins for haptic object visualization. In *Proceedings of IEEE/RSJ International Conference on Intelligent Robots and Systems (IROS)*, pages 494–501, 2017.

[168] Bianca S. Homberg, Robert K. Katzschmann, Mehmet R. Dogar, and Daniela Rus. Robust proprioceptive grasping with a soft robot hand. *Autonomous Robots*, 43(3): 681–696, 2018.

[169] John Nassour, Vishal Ghadiya, Vincent Hugel, and Fred H. Hamker. Design of new sensory soft hand: Combining air-pump actuation with superimposed curvature and pressure sensors. In *Proceedings of IEEE International Conference on Soft Robotics (RoboSoft)*, pages 164–169, 2018.

[170] Adam J. Spiers, Minas V. Liarokapis, Berk Calli, and Aaron M. Dollar. Single-grasp object classification and feature extraction with simple robot hands and tactile sensors. *IEEE Transactions on Haptics*, 9(2):207–220, 2016.

[171] Juan Gandarias, Jesús Gómez de Gabriel, and Alfonso García-Cerezo. Enhancing perception with tactile object recognition in adaptive grippers for human-robot interaction. *Sensors*, 18(3):1–20, 2018.

[172] Alexander Schneider, Jurgen Sturm, Cyrill Stachniss, Marco Reisert, Hans Burkhardt, and Wolfram Burgard. Object identification with tactile sensors using bag-of-features. In *Proceedings of IEEE/RSJ International Conference on Intelligent Robots and Systems (IROS)*, pages 243–248, 2009.

[173] Uriel Martinez-Hernandez, Tony J. Dodd, and Tony J. Prescott. Feeling the shape: Active exploration behaviors for object recognition with a robotic hand. *IEEE Transactions on Systems, Man, and Cybernetics: Systems*, 48(12):2339–2348, 2017.

[174] Paul Hebert, Thomas Howard, Nicolas Hudson, Jeremy Ma, and Joel W. Burdick. The next best touch for model-based localization. In *Proceedings of IEEE International Conference on Robotics and Automation (ICRA)*, pages 99–106, 2013.

[175] Niccolo Tosi, Olivier David, and Herman Bruyninckx. Action selection for touch-based localisation trading off information gain and execution time. In *Proceedings of IEEE International Conference on Robotics and Automation (ICRA)*, pages 2270–2275, 2014.

[176] Tyler E. Bruns and Daniel A. Tortorelli. Topology optimization of non-linear elastic structures and compliant mechanisms. *Computer Methods in Applied Mechanics and Engineering*, 190(26–27):3443–3459, 2001.

[177] Kai Liu and Andrés Tovar. An efficient 3D topology optimization code written in matlab. *Structural and Multidisciplinary Optimization*, 50(6):1175–1196, 2014.

[178] Ole Sigmund. Design of material structures using topology optimization, 1994.

[179] Albert A. Groenwold and L. F. P. Etman. A quadratic approximation for structural topology optimization. *International Journal for Numerical Methods in Engineering*, 82(4):505–524, 2009.

[180] Martin P. Bendsøe. *Optimization of Structural Topology, Shape, and Material.* Springer, 1995.

[181] Blaise Bourdin. Filters in topology optimization. *International Journal for Numerical Methods in Engineering*, 50(9):2143–2158, 2001.

[182] Interlink Electronics. Fsr force sensing resistor integration guide and evaluation parts catalog, 2010. URL https://www.sparkfun.com/datasheets/Sensors/Pressure/fsrguide.pdf.

[183] MATLAB. Machine learning with matlab, 2018. URL https://matlabacademy.mathworks.com/.

[184] Jerome H. Friedman. Regularized discriminant analysis. *Journal of the American Statistical Association*, 84(405):165–175, 1989.

[185] I.J. Good. *Probability and the Weighing of Evidence.* Charles Griffin, 1950.

[186] Phillip Quin, Gavin Paul, Alen Alempijevic, Dikai Liu, and Gamini Dissanayake. Efficient neighbourhood-based information gain approach for exploration of complex

3D environments. In *Proceedings of IEEE International Conference on Robotics and Automation (ICRA)*, pages 1343–1348, 2013.

[187] Stefan Isler, Reza Sabzevari, Jeffrey Delmerico, and Davide Scaramuzza. An information gain formulation for active volumetric 3D reconstruction. In *Proceedings of IEEE International Conference on Robotics and Automation (ICRA)*, pages 3477–3484, 2016.